



National Library
of Canada

Acquisitions and
Bibliographic Services Branch

395 Wellington Street
Ottawa, Ontario
K1A 0N4

Bibliothèque nationale
du Canada

Direction des acquisitions et
des services bibliographiques

395, rue Wellington
Ottawa (Ontario)
K1A 0N4

Number of microfiches

Number of microfiches

NOTICE

The quality of this microform is heavily dependent upon the quality of the original thesis submitted for microfilming. Every effort has been made to ensure the highest quality of reproduction possible.

If pages are missing, contact the university which granted the degree.

Some pages may have indistinct print especially if the original pages were typed with a poor typewriter ribbon or if the university sent us an inferior photocopy.

Reproduction in full or in part of this microform is governed by the Canadian Copyright Act, R.S.C. 1970, c. C-30, and subsequent amendments.

AVIS

La qualité de cette microforme dépend grandement de la qualité de la thèse soumise au microfilmage. Nous avons tout fait pour assurer une qualité supérieure de reproduction.

S'il manque des pages, veuillez communiquer avec l'université qui a conféré le grade.

La qualité d'impression de certaines pages peut laisser à désirer, surtout si les pages originales ont été dactylographiées à l'aide d'un ruban usé ou si l'université nous a fait parvenir une photocopie de qualité inférieure.

La reproduction, même partielle, de cette microforme est soumise à la Loi canadienne sur le droit d'auteur, SRC 1970, c. C-30, et ses amendements subséquents.

UNIVERSITY OF ALBERTA

**THE EFFECTS OF FINES CONTENT ON THE MONOTONIC
TRIAxIAL TESTING OF COHESIONLESS SOILS FOR
EVALUATION OF IN-SITU STATE**

BY

ROGER KEVIN SKIRROW

**A THESIS SUBMITTED TO THE FACULTY OF GRADUATE STUDIES AND
RESEARCH IN PARTIAL FULFILLMENT OF THE REQUIREMENTS FOR THE
DEGREE OF MASTERS OF SCIENCE.**

IN

**GEOTECHNICAL ENGINEERING
DEPARTMENT OF CIVIL ENGINEERING
EDMONTON, ALBERTA**

SPRING, 1996



National Library
of Canada

Acquisitions and
Bibliographic Services Branch

395 Wellington Street
Ottawa, Ontario
K1A 0N4

Bibliothèque nationale
du Canada

Direction des acquisitions et
des services bibliographiques

395, rue Wellington
Ottawa (Ontario)
K1A 0N4

Author - Auteur

Author - Auteur

The author has granted an irrevocable non-exclusive licence allowing the National Library of Canada to reproduce, loan, distribute or sell copies of his/her thesis by any means and in any form or format, making this thesis available to interested persons.

L'auteur a accordé une licence irrévocable et non exclusive permettant à la Bibliothèque nationale du Canada de reproduire, prêter, distribuer ou vendre des copies de sa thèse de quelque manière et sous quelque forme que ce soit pour mettre des exemplaires de cette thèse à la disposition des personnes intéressées.

The author retains ownership of the copyright in his/her thesis. Neither the thesis nor substantial extracts from it may be printed or otherwise reproduced without his/her permission.

L'auteur conserve la propriété du droit d'auteur qui protège sa thèse. Ni la thèse ni des extraits substantiels de celle-ci ne doivent être imprimés ou autrement reproduits sans son autorisation.

ISBN 0-612-10758-2

Canada

University of Alberta

Library Release Form

Name of Author: Roger Kevin Skirrow

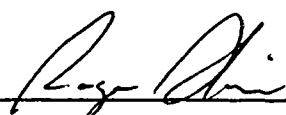
Title of Thesis: **The Effects of Fines Content on the Monotonic Triaxial Testing of Cohesionless Soils for Evaluation of In-Situ State**

Degree: Masters of Science

Year this Degree Granted: 1996

Permission is hereby granted to the University of Alberta Library to reproduce single copies of the thesis and to lend or sell such copies for private, scholarly or scientific research purposes only.

The author reserves all other publication and other rights in association with the copyright of the thesis, and except as hereinbefore provided, neither the thesis nor any substantial portion thereof may be printed or otherwise reproduced in any material form whatever without the author's prior written permission.



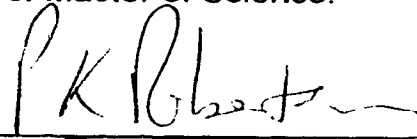
Roger Kevin Skirrow
9620-75 Street
Edmonton, Alberta
T6C 2H9

Dated: March 31, 1996

University of Alberta

Faculty of Graduate Studies and Research

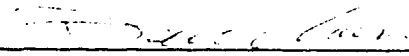
The undersigned certify that they have read, and recommended to the Faculty of Graduate Studies and Research for acceptance, a thesis entitled The Effects of Fines Content on the Monotonic Triaxial Testing of Cohesionless Soils for Evaluation of In-Situ State submitted by Roger Kevin Skirrow in partial fulfillment of the requirements for the degree of Master of Science.



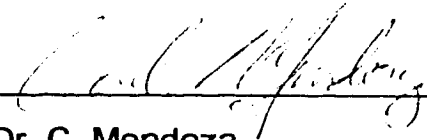
Dr. P.K. Robertson (Supervisor)



Dr. D.C. Sego (Co-supervisor)



Dr. D.C. Chan



Dr. C. Mendoza

Dated: March 31, 1996

To Kim

for her support, patience and encouragement throughout the years.

To Jen and Rob

for their unique perspective on education, for sharing the computer, and for being themselves

"An expert is a man who has made all the mistakes which can be made in a very narrow field."

Neils Bohr

"Genius lasts longer than Beauty. That accounts for the fact that we all take such pains to over-educate ourselves."

Oscar Wilde

ABSTRACT

The influence of fines content on the undrained monotonic response of sand has been reported by Been and Jefferies (1985) and Hird and Hassona (1990). Pitman (1994) illustrated the influence of various types of fines on the undrained monotonic response of Ottawa sand at one stress level. A test methodology developed by Sasitharan (1994) was used to determine the steady state lines for Ottawa sand with from 0 to 20 percent Kaolinite fines content. This involved monotonic triaxial compression testing of various sand/fines mixtures at varying levels of isotropic consolidation. The triaxial test results indicated a rotation and shift in the steady state line as fines increased. The slope of the steady state line increased with added fines as did the slope of the isotropic consolidation line. The sample compressibility increased as fines were added. The shift in steady state line was noted with the addition of as little as 5% fines. Been and Jefferies (1985) showed a shift with as little as 2% fines addition.

Sasitharan (1994) and Cunning (1994) used bender element technology to measure shear wave velocity in triaxial samples. The shear wave measurements, and corresponding state conditions were used to develop a framework for estimating the in-situ state of Ottawa sand with varying fines content. A single relationship between shear wave velocity and void ratio was found to describe reasonably well both compressible and incompressible sands, with and without fines content. The undrained shear strength at steady state may be determined for both contractive and dilative conditions.

Acknowledgments

This thesis was the product of several phases of work, including, but by no means limited to, laboratory testing, interpretation of results, and writing. I would like to thank several individuals who helped me to complete my research.

I thank Gerry Cyre and Steve Gamble for their expertise and support during the laboratory work, particularly in the maintenance of bender element, and assistance with triaxial equipment. I shared the lab for many months with John Cunning and I thank John for his humor and energy while we toiled away.

An especially appreciative thank you is reserved for Dr. Robertson, who was supportive and provided guidance throughout. His insights into, and obvious enthusiasm for, liquefaction studies and geotechnical engineering have always amazed me.

I thank AGRA Earth & Environmental for the support and patience during my studies.

TABLE OF CONTENTS

LIST OF TABLES

LIST OF FIGURES

NOTATIONS

ABBREVIATIONS

SYMBOLS

1. INTRODUCTION	1
1.1 OVERVIEW	1
1.2 PURPOSE	2
1.3 THESIS ORGANIZATION	3
2. BACKGROUND	5
2.1 CRITICAL STATE AND STEADY STATE SOIL MECHANICS THEORY	5
2.1.1 CRITICAL STATE AND STEADY STATE SOIL MECHANICS AND AS A FRAMEWORK FOR MODELING THE BEHAVIOR OF COHESIONLESS SOIL	5
2.1.2 HISTORICAL DEVELOPMENT OF CRITICAL STATE AND STEADY STATE SOIL MECHANICS	6
2.2 PARAMETERS USED IN USS AND CSSM ANALYSIS	7
2.2.1 STATE PARAMETER	7
2.2.2 OTHER PARAMETERS	8
2.3 MONOTONIC UNDRAINED RESPONSE OF SATURATED SANDS	8
2.3.1 SUMMARY	8
2.3.2 STRAIN SOFTENING	9
2.3.3 LIMITED STRAIN SOFTENING	10
2.3.4 STRAIN HARDENING	10

2.3.5	LIQUEFACTION	11
2.3.5.1	Liquefaction Phenomena and Terminology	11
2.3.5.2	Flow Liquefaction	11
2.3.5.3	Cyclic Liquefaction and Cyclic Mobility	12
2.3.5.4	Historical Liquefaction Studies	12
2.3.5.5	Models	13
2.3.5.6	Sample Preparation	13
2.3.6	RESEARCH ON FINES CONTENT AND RELATED FABRIC CONCEPTS	15
2.3.6.1	Compressibility and Fines Content	15
2.3.6.2	Fabric and Anisotropy	16
2.3.7	SHEAR WAVE VELOCITY MEASUREMENTS FOR LIQUEFACTION ASSESSMENT	18
2.3.7.1	Historical overview	18
2.3.7.2	Shear Wave Velocity	20
3.	TESTING PROGRAM	31
3.1	MATERIAL TESTED	31
3.1.1	SAND	31
3.1.2	FINES	31
3.1.3	OTHER SANDS DISCUSSED IN THIS STUDY	32
3.1.3.1	Koyguk Sand (Been and Jefferies, 1985)	32
3.1.3.2	Leighton Buzzard Sand—LBS [(Hird and Hassona, 1990), (Sladen et al, 1985), and (Arthur and Menzies, 1972)]	32
3.1.3.3	Hong Kong Pearl River Sand (Robertson and Skirrow, 1994)	32
3.2	SIEVE ANALYSIS	32
3.3	TRIAXIAL TESTING	33
3.3.1	TEST NOMENCLATURE	33
3.3.2	TEST APPARATUS	33
3.3.2.1	Modifications to Conventional Triaxial Apparatus	33
3.3.2.1.1	Loading Frame	33
3.3.2.1.2	Triaxial Cell	34
3.3.2.2	Bender Elements	34
3.3.3	SAMPLE PREPARATION	34
3.3.4	CALCULATION OF VOID RATIO	35
3.3.5	SATURATION PHASE	36
3.3.6	CONSOLIDATION PHASE	37

3.3.7	SHEAR WAVE VELOCITY MEASUREMENTS	37
3.3.8	SHEARING PHASE	38
3.4	PROBLEMS OBSERVED DURING THE TEST PROGRAM	38
4. RESULTS		47
4.1	SIEVE ANALYSIS	47
4.2	VOID RATIO	47
4.3	TRIAXIAL TEST	47
4.3.1	DEVIATOR STRESS - STRAIN	48
4.3.2	PORE PRESSURE - STRAIN	48
4.3.3	DEVIATOR STRESS - MEAN EFFECTIVE PRESSURE STRESS PATHS	49
4.3.4	NORMALIZED DEVIATOR STRESS - NORMALIZED MEAN EFFECTIVE PRESSURE	49
4.3.5	VOID RATIO - MEAN EFFECTIVE PRESSURE	49
4.4	SHEAR WAVE VELOCITY RESULTS	50
5. DISCUSSION		87
5.1	SIEVE ANALYSIS	87
5.2	VOID RATIO	87
5.2.1	INTERGRANULAR VOID RATIO	87
5.2.2	MINIMUM VOID RATIO (DENSEST STATE ATTAINED)	88
5.2.3	MAXIMUM VOID RATIO (LOOSEST STATE ATTAINED)	88
5.2.4	COMPRESSIBILITY	89
5.3	TRIAXIAL TEST	89
5.3.1	DEVIATOR STRESS - STRAIN	90
5.3.1.1	Comparison of Deviator Stress versus Strain curves	90
5.3.1.2	Use of Brittleness Index to Compare Deviator Stress - Strain Responses	90
5.3.2	PORE PRESSURE - STRAIN	91
5.3.2.1	Comparison of Pore Pressure - Strain Curves	91

5.3.3	DEVIATOR STRESS - MEAN EFFECTIVE PRESSURE	92
5.3.3.1	Comparison of Deviator Stress - Mean Effective Pressure Curves	92
5.3.3.2	Comparison of Normalized Deviator Stress - Mean Effective Pressure Curves	93
5.3.4	VOID RATIO - MEAN EFFECTIVE PRESSURE	94
5.3.5	STEADY STATE CONDITIONS	94
5.3.5.1	Steady State Conditions - This Study	94
5.3.5.2	Steady State Conditions - Other Studies	95
5.3.6	STATE PARAMETER, Ψ	96
5.3.6.1	State Parameter Related to Mean Effective Stress	96
5.3.6.2	State Parameter Related to Brittleness Index	96
5.3.6.3	State Parameter Related to Unconfined Shear Stress	97
5.4	Shear Wave Velocity Results	98
5.4.1	SHEAR WAVE VELOCITY - VOID RATIO	98
5.4.2	NORMALIZED SHEAR WAVE VELOCITY - VOID RATIO	98
5.4.3	SHEAR WAVE - VOID RATIO - MEAN EFFECTIVE STRESS RELATIONSHIP	98
5.4.3.1	Shear Wave Velocity Contours	99
5.4.4	MEAN EFFECTIVE STRESS - VOID RATIO - SHEAR WAVE VELOCITY RELATIONSHIP FOR OTHER SANDS	100
5.4.5	SHEAR WAVE VELOCITY - VERTICAL EFFECTIVE STRESS	101
5.4.6	SPT RELATIONSHIPS	101
5.4.7	CPT RELATIONSHIPS	102
5.5	Testing Limitations	103
5.5.1	REPEATABILITY	104
<u>6. SUMMARY AND CONCLUSIONS</u>		<u>153</u>
6.1	Undrained Monotonic Triaxial Compression Tests	153
6.2	Shear Wave Velocity Relationships	154
6.3	Practical Application	154
6.4	Further Study	156
<u>REFERENCES</u>		<u>157</u>

LIST OF TABLES

Table 2.1	Shear Wave Velocity Relationships	21
Table 2.2	Steady State Parameters	22
Table 2.3	Shear Wave Parameters	22
Table 3.1	Void Ratio Monitoring Procedure	40
Table 4.1	Representative Sieve Analysis Results	51
Table 4.2	D ₁₀ , D ₆₀ And C _u Results	51
Table 4.3	Void Ratio Calculations	52
Table 4.4	Summary Of Void Ratio Showing Loosest And Densest State Attained	53
Table 4.5	Summary Of Test Conditions	54
Table 4.6	Excess Pore Pressures Developed During Triaxial Testing	55
Table 4.7	Shear Wave Velocity Measurements	56
Table 5.1	Brittleness Indices	105
Table 5.2	Summary Of Normalized p'-q Parameters	106
Table 5.3	Steady State Parameters	106
Table 5.4	Initial State Parameters	107
Table 5.5	Shear Wave And Steady State Parameters	108

LIST OF FIGURES

Figure 2.1	Soil Collapse Boundary in $e - q - p'$ Space (after Sasitharan, 1994)	24
Figure 2.2	USS Parameters in $e - \log p'$ Showing Definition of Γ and λ	25
Figure 2.3	USS Parameters in Normalized Stress Path Space Showing Definition of M, s and β	25
Figure 2.4	Relationship Between RSR and Ψ in $e - \log p'$ Space	26
Figure 2.5	Behavior of Cohesionless Soil Under Undrained Monotonic Loading (after Robertson, 1994)	27
Figure 2.6	Stress Paths in $q - p'$ Space	28
Figure 2.7	Flow Chart for Liquefaction (after Robertson, 1994)	29
Figure 2.8	Grain Size Liquefaction Boundaries (after Seed et al, 1976)	30
Figure 3.1	Schematic of Laboratory Set-Up	41
Figure 3.2	Schematic of Modifications To Triaxial Cell Base	42
Figure 3.3	Schematic of Modifications To Triaxial Cell Cap	43
Figure 3.4	Schematic of Assembled Triaxial Cell	44
Figure 3.5	Schematic of Half-Section of Loading Portion of Triaxial Cell With Shear Wave Bender Assembly	45
Figure 3.6	Schematic of Protruding Bender Element Assembly and Details	46
Figure 4.1	Selected Grain Size Distribution Results	57
Figure 4.2	Deviator Stress Versus Strain For 5% Fines, All Tests	58
Figure 4.3	Deviator Stress Versus Strain For 7.5% Fines, All Tests	59
Figure 4.4	Deviator Stress Versus Strain For 10% Fines, All Tests	60
Figure 4.5	Deviator Stress Versus Strain For 5% Fines, Loose Tests	61
Figure 4.6	Deviator Stress Versus Strain For 7.5% Fines, Loose Tests	62
Figure 4.7	Deviator Stress Versus Strain For 10% Fines, Loose Tests	63
Figure 4.8	Excess Pore Pressure Versus Strain For 5% Fines, All Tests	64
Figure 4.9	Excess Pore Pressure Versus Strain For 7.5% Fines, All Tests	65

Figure 4.10	Excess Pore Pressure Versus Strain For 10% Fines, All Tests	66
Figure 4.11	Excess Pore Pressure Versus Strain For 5% Fines, Loose Tests	67
Figure 4.12	Excess Pore Pressure Versus Strain For 7.5% Fines, Loose Tests	68
Figure 4.13	Excess Pore Pressure Versus Strain For 10% Fines, Loose Tests	69
Figure 4.14	Stress Path in p'-q Space for 5% Fines, All Tests	70
Figure 4.15	Stress Path in p'-q Space for 7.5% Fines, All Tests	71
Figure 4.16	Stress Path in p'-q Space for 10% Fines, All Tests	72
Figure 4.17	Stress Path in p'-q Space for 5% Fines, Loose Tests	73
Figure 4.18	Stress Path in p'-q Space for 7.5% Fines, Loose Tests	74
Figure 4.19	Stress Path in p'-q Space for 10% Fines, Loose Tests	75
Figure 4.20	Normalized Stress Path for 5% Fines	76
Figure 4.21	Normalized Stress Path for 7.5% Fines	77
Figure 4.22	Normalized Stress Path for 10% Fines	78
Figure 4.23	Void Ratio - Log Mean Effective Stress For 5% Fines	79
Figure 4.24	Void Ratio - Log Mean Effective Stress For 7.5% Fines	80
Figure 4.25	Void Ratio - Log Mean Effective Stress For 10% Fines	81
Figure 4.26	Maximum, Minimum And Steady State Lines For 5% Fines	82
Figure 4.27	Maximum, Minimum And Steady State Lines For 7.5% Fines	83
Figure 4.28	Maximum, Minimum And Steady State Lines For 10% Fines	84
Figure 4.29	Typical Shear Wave Response Plot	85
Figure 4.30	Shear Wave Velocity versus Void Ratio, All Test Results.	86
Figure 5.1	Grain Size Distribution Superimposed On Seed <i>et al</i> (1976) Boundaries For Liquefiable Soil	109
Figure 5.2	Change in Intergranular Void Ratio With Increasing Fines Content	110
Figure 5.3	State Lines Defining e_{min} in $e - \log p'$ Space	111
Figure 5.4	State Lines Defining e_{max} in $e - \log p'$ Space	112
Figure 5.5	Compressibility ($e_{max} - e_{min}$) Versus $\log p'$	113
Figure 5.6	Brittleness Index Versus p'/p'_{ss}	114

Figure 5.7	Brittleness Index Versus p'/p'_{ss} Showing Other Researchers Data	115
Figure 5.8	Normalized p'-q Diagrams With "m", "s" And "β" Lines For 5% Fines	116
Figure 5.9	Normalized p'-q Diagrams With "m", "s" And "β" Lines For 7.5% Fines	117
Figure 5.10	Normalized p'-q Diagrams With "m", "s" And "β" Lines For 10% Fines	118
Figure 5.11	Change in I_B With Increased Fines Content For Several Researchers	119
Figure 5.12	Change in I_B With Increased Fines Content	120
Figure 5.13	Rotation of Steady State Lines With Increased Fines Content	121
Figure 5.14	Steady State Lines, e_{min} And e_{max} Lines For Various Fines Content	122
Figure 5.15	State Lines for Kogyuk (Been and Jefferies, 1985)	123
Figure 5.16	State Lines for Leighton Buzzard Sand (Hird and Hassona, 1990)	124
Figure 5.17	State Lines For Ottawa Sand, Leighton Buzzard Sand And Kogyuk Sand With 10% Fines Content	125
Figure 5.18	State Lines For Several Sands And Fines Contents	126
Figure 5.19	Steady State Line for Hong Kong Pearl River Sand	127
Figure 5.20	Change in Ψ With Mean Effective Stress	128
Figure 5.21	Normalized p'-q Plots at Ψ Values of 0.05 and 0.10	129
Figure 5.22	Brittleness Index Versus Ψ	130
Figure 5.23	Ratio Of S_u/p'_o Versus Ψ Value For Samples For $\Psi > 0$	131
Figure 5.24	Ratio Of S_u/p'_o Versus Ψ Value For All Samples	132
Figure 5.25	Normalized Shear Wave Velocity Versus Void Ratio	133
Figure 5.26	Shear Wave Velocity Versus Mean Effective Stress	134
Figure 5.27	Calculated Shear Wave Velocity Versus Measured Shear Wave Velocity	135
Figure 5.28	Contours Of Shear Wave Velocity Plotted on Graph of Void Ratio Versus Mean Effective Pressure	136
Figure 5.29	Contours Of Shear Wave Velocity Plotted on Graph of Void Ratio Versus Mean Effective Pressure With Measure Shear Wave Values	137
Figure 5.30	Normalized V_s Versus Void Ratio For A Wide Variety Of Sands	138
Figure 5.31	V_s Versus Vertical Effective Stress For $K_o = 0.4$, and $\Psi = 0$ For Ottawa Sand	139

Figure 5.32	Vs Versus Vertical Effective Stress For $K_o = 0.4$, and $\Psi = 0$ For Leighton Buzzard Sand	140
Figure 5.33	Vs Versus Vertical Effective Stress For $K_o = 0.4$, and $\Psi = 0.1$	141
Figure 5.34	Vs Versus Vertical Effective Stress For $K_o = 1.0$, and $\Psi = 0.1$	142
Figure 5.35	Comparison Of Vs - σ_v Lines For Clean Sand and 10% Fines at Corresponding K_o Values Of 0.4 and 1.0 , With $\Psi = 0$	143
Figure 5.36	Comparison Of Vs - σ_v Lines For Clean Sand and 10% Fines at Corresponding K_o Values Of 0.4 and 1.0 , With $\Psi = 0.1$	144
Figure 5.37	N_{60} Versus Vertical Effective Stress For Ottawa Sand With Various Fines Contents For $K_o = 0.4$, at $\Psi = 0$	145
Figure 5.38	N_{60} Versus Vertical Effective Stress For Leighton Buzzard Sand With Various Fines Contents For $K_o = 0.4$, at $\Psi = 0$	146
Figure 5.39	N_{60} - σ'_v Lines For Various Fines Content For $K_o = 1.0$, at $\Psi = 0$	147
Figure 5.40	Change in N_{60} as Fines Content Increases For Steady State Conditions	148
Figure 5.41	CPT q_c - σ'_v Lines For Ottawa Sand at $K_o = 0.4$, $\Psi = 0$	149
Figure 5.42	CPT q_c - σ'_v Lines For Leighton Buzzard Sand at $K_o = 0.4$, $\Psi = 0$	150
Figure 5.43	CPT q_c - σ'_v Lines At For $K_o = 1.0$, $\Psi = 0$	151
Figure 5.44	Change In q_c As Fines Content Increases	152

NOTATIONS

Abbreviations

A	-	Void ratio(e) = 0 intercept of V_{s1} - e line
A_{max}	-	Maximum ground acceleration
A_s	-	Surface area of sample covered by membrane
ASCE	-	American Society of Civil Engineers
ASTM	-	American Society for Testing and Materials
B	-	Slope of V_{s1} - e line
b	-	Length of bender element protrusion into sample
CANLEX	-	Canadian Liquefaction Experiment
CPT	-	Cone Penetration Test
CSR	-	Critical Stress Ratio
CSSM	-	Critical State Soil Mechanics
CVRL	-	Critical Void Ratio Line
C_u	-	Coefficient of uniformity
d	-	Sample diameter
D_r	-	Relative density
e	-	Void ratio
e_g	-	Intergranular void ratio
e_{mc}	-	Void ratio corrected for membrane penetration
e_{min}	-	Minimum void ratio
e_{max}	-	Maximum void ratio
e_{ss}	-	Void ratio at steady state
fc	-	Fines fraction of sample expressed as a decimal ratio
G	-	Shear modulus
H_c	-	Current sample height
K_o	-	Coefficient of lateral earth pressure at rest
LSS	-	Limited strain softening
L_t	-	Length of travel of shear wave
LVDT	-	linear voltage displacement transducer
M	-	Value of q_{ss}/p'_{ss}
m_1, m_2	-	Constants
Mf	-	Mass of fines
Ms	-	Mass of sand

MT	-	Moist tamping
n	-	Stress exponent, constant
N	-	Standard Penetration Test blow count
(N₁)₆₀	-	Standard Penetration Test blow count, corrected to 1 atm. pressure and 60% efficiency
OS	-	Ottawa sand
P_a	-	Reference pressure, taken as 100 kPa
PMT	-	Pressuremeter Test
p'_c	-	Mean effective pressure, or first stress invariant of the stress tensor
p'_{ss}	-	Mean effective pressure at steady state
q	-	Deviator stress, or the second invariant of the stress deviator tensor
q_c	-	CPT tip resistance
q_{ss}	-	Deviator stress at steady state
r²	-	Standard deviation regression coefficient
RSR	-	Reference State Ratio
s	-	Slope of collapse surface in the stress path plot
SCPT	-	Seismic Cone Penetration Test
SEM	-	Scanning Electron Microscope
SH	-	Strain hardening
SPT	-	Standard Penetration Test
SS	-	Strain softening
Δt	-	Shear wave travel time
Δu	-	Excess pore pressure
V_i	-	Sample volume at beginning of consolidation phase
ΔV	-	Change in volume
ΔV_m	-	Volume correction due to membrane penetration
ΔV_{H2O}	-	Volume change during saturation
V_p	-	Velocity of compression wave
V_s	-	Velocity of shear wave
V_{s1}	-	Normalized shear wave velocity
(V_s)_{ψ=0}	-	V_s at steady state
w	-	Moisture content

Symbols

ϵ_a	-	Axial strain
ϵ_{um}	-	Unit membrane penetration
ϵ_{pt}	-	Strain at phase transformation
ϵ_r	-	Radial strain
ϵ_v	-	Volumetric strain
ϕ	-	Mobilized friction angle
ϕ_{csr}	-	Friction angle mobilized at peak shear stress
ϕ_{pt}	-	Friction angle mobilized at phase transformation
ϕ_{uss}	-	Friction angle mobilized at ultimate steady state
ϕ_{cv}	-	friction angle at constant volume
γ_f	-	Specific gravity of fines particles
γ_s	-	Specific gravity of sand particles
λ	-	slope of the steady state line in e-log p' space
Γ	-	Intercept of the SSL in e-log p' space at p'=1 kPa
μ	-	Poisson's ratio
ρ	-	Soil mass density
ρ_w	-	Density of water
σ'_1	-	Effective major principal stress
σ'_3	-	Effective minor principal stress
σ'_a	-	Effective stress in direction of wave propagation
σ'_b	-	Effective stress in direction of particle motion
σ'_c	-	Effective stress in direction perpendicular to a and b
σ'_{dp}	-	Effective peak deviator stress
σ'_h	-	Effective stress in horizontal direction
σ'_p	-	Effective stress in direction perpendicular to axis
σ'_v	-	Effective stress in vertical direction
τ/σ'	-	Resistance ratio
ψ	-	State parameter

1. INTRODUCTION

1.1 Overview

The liquefaction behavior of cohesionless soils is an active area of research in many countries. The conditions under which liquefaction of cohesionless materials can occur are now fairly well established. In situ testing, consisting of the Standard Penetration Testing (SPT) and the Cone Penetration Test (CPT), and more recently, the seismic cone penetration test (SCPT) characterize cohesionless soil deposits, and provide an empirical base for the evaluation of liquefaction susceptibility. In situ shear wave velocity measurements provide a more detailed delineation of potential liquefaction zones than SPT or CPT tests since the shear wave velocity measurements are more responsive to changes in soil state which are predictive of liquefaction conditions (Tokimatsu and Hosaka, 1986). Laboratory testing, consisting of monotonic and cyclic triaxial, and rotational shear tests, are used to estimate the liquefaction potential and steady state parameters for reconstituted samples, and undisturbed frozen core samples of cohesionless soils (Yoshimi *et al.*, 1989).

The laboratory results determined from reconstituted samples are often viewed with some skepticism since it is difficult to produce laboratory samples that accurately replicate or maintain the in situ soil fabric, fines content and fines distribution, void ratio and stress conditions found under field conditions. Prior to shear wave velocity measurement techniques it was difficult to physically assess the quality of samples without the use of a scanning electron microscope or other techniques. Representative undisturbed samples of saturated sands have historically been difficult to obtain and test results are subjected to varying degrees of manipulation (Tokimatsu and Hosaka, 1986) however, recent advances in in-situ ground freezing techniques are now available to retrieve high quality undisturbed samples of saturated sand. Provided sufficient controls are in place during the freezing and thawing process, the samples retrieved will maintain the in situ fabric and stress conditions (Yoshimi *et al.*, 1978, and Yoshimi *et al.* 1984). Such samples are normally retrieved in a frozen state and trimmed and thawed prior to testing for steady state parameters and for assessing liquefaction potential.

Studies utilizing shear wave velocity (V_s) measurements done in situ and on retrieved frozen samples have concluded that shear wave velocity measurements provide a methodology by which the sample integrity can be verified between the in situ state and the prepared thawed sample. Soil fabric and void ratio are reasonably well maintained during controlled freeze-thaw sampling and testing (Sasitharan, 1994) . The use of CPT and pressuremeter testing (PMT) devices can provide a reasonably accurate assessment of the in situ stress and pore pressure conditions. It is therefore possible to undertake a field testing and laboratory testing program to

determine the liquefaction potential of real soils under stresses accurately modeling real conditions using shear wave velocity measurements as both a quality assurance and predictive tool.

There is a relatively high level of confidence in the assessment of liquefaction potential using the above methodology. The retrieval of in situ frozen samples, particularly at significant depths, is both time consuming and expensive. The expense for such testing is likely only justified for major projects or where the damage due to a liquefaction event would be great. An alternative to recovery of high quality in situ samples is to utilize reconstituted samples of disturbed soils retrieved from conventional methods such as SPT or tube sampling. Shear wave velocity measurements may be used to qualitatively verify that reconstituted samples are prepared in such a way as to model the natural soil formation process. Reconstituted samples can be consolidated to a desired void ratio to match the in situ case. Stress and pore pressure conditions are also easily reproduced and manipulated in triaxial testing. Reconstituted soil samples prepared to simulate field void ratio and stress condition may be expected to behave in a similar manner to undisturbed samples if the shear wave velocities could be matched prior to shearing. Relatively inexpensive sampling and conventional testing means can be used to measure laboratory shear wave velocities at various void ratio and imposed stress conditions which can be subsequently matched to in situ measurements of the V_s to provide a framework for assessing the field liquefaction potential and steady state strength appropriate for design.

Several researchers have investigated the influence of fines on the collapse response of sands (Troncoso and Verdugo 1985, Kuerbis 1989, Kuerbis and Vaid 1989, Pitman 1993, Sasitharan 1994). An increase in fines content has been shown to change the steady state response of several sands. This change is more pronounced for the addition of plastic fines, as opposed to nonplastic silts. There has been limited study into the effect that increasing fines content has on the V_s and associated V_s - steady state parameter relationships. This research investigates the change in steady state conditions which occur upon the addition of small percentages of plastic fines to Ottawa sand. Triaxial test were undertaken at several initial confining stress levels and at several void ratios for each degree of added fines. Relationships between the void ratio, mean effective stress and V_s for each fines content were developed.

1.2 Purpose

Previous research at the University of Alberta by Sasitharan (1994) provided a framework for the determination of a collapse surface observed through a variety of stress paths, and also provided some initial investigation into the use of V_s to determine liquefaction behavior. Additional research at the University of Alberta by Pitman (1993) undertook steady state testing

of Ottawa sand at varying fines content. Pitman investigated the response of the collapse surface resulting from the addition of three types of fines, Kaolinite, crushed Silica fines, and fine Silica sand. Pitman clearly showed that changes in the collapse surface and steady state conditions occurred, and that the nature of the change depended on the percentage and plasticity of the added fines. A limitation to this work was that all testing was carried out at a single mean effective stress, 350 kPa, and as such no steady state relationships between the void ratio and mean effective stress could be determined.

Recent research at the University of Alberta by Cunning (1994) showed V_s measurements could be used to evaluate the in situ state of saturated cohesionless soils over a wide range of void ratio and stress conditions. Shear wave velocity and laboratory stress conditions were combined to produce plots of V_s against effective vertical pressure and contours of V_s on a void ratio - mean effective pressure plot. Comparison with field V_s determined from SCPT tests results provides a basis for assessing the liquefaction potential of in situ cohesionless deposits.

The above researchers have provided a framework by which the V_s and steady state parameters could be determined for a given sand deposit. The objective of this research is to determine the effect that increasing fines content has on the steady state conditions, V_s and the relationship between these parameters.

In order to achieve this objective a series of isotropically consolidated, monotonically loaded, undrained triaxial tests were undertaken on samples of Ottawa sand prepared with no fines, 5, 7.5, 10 and 20 percent fines. Kaolinite was used for the fines for all tests. These results were compiled and a steady state line determined for each fines content level. Shear wave velocity measurements were determined along the consolidation lines for the densest and loosest states for each of the 5, 7.5 and 10 percent fines tests. Relationships were determined between the V_s and void ratio and mean effective pressures. Graphs showing V_s contours on the void ratio - mean effective pressure were produced for each fines content and for the combined testing program. Results of past research at the University of Alberta on Ottawa sand, Syncrude tailings sand, Hong Kong Pearl River Sand, and from other sources is compared to provide a basis for assessing the implications of increased fines content on the steady state and V_s relationships for a given sand.

1.3 Thesis Organization

Chapter 1 provides an introduction for the thesis, the purpose of the investigation a summary of content in each chapter.

Chapter 2 introduces concepts from critical state soil mechanics and liquefaction theory and discusses the basic assumptions and theory concerning the effects of fines on these two concepts. A discussion of compressibility and shear strength concepts is provided wherein the inter-relationship of these two phenomena follows. Shear wave theory and the relationship to undrained shear strength values are also presented.

Chapter 3 outlines the testing apparatus and testing program undertaken. Descriptions of the soil used in this research and those used by others and incorporated into this work are provided. A summary of the monotonic triaxial test and shear wave measurements are also presented. Representative sieve analysis, void ratio determination and tabulated results are also presented.

Chapter 4 presents the laboratory test results and a discussion of the various graphs and charts produced.

Chapter 5 presents a comparison and discussion of the results. The shear wave velocity - mean effective pressure - void ratio concepts as determined through the laboratory test program are presented .

Chapter 6 presents conclusions from the investigation and potential avenues for future study.

2. BACKGROUND

2.1 Critical State and Steady State Soil Mechanics Theory

2.1.1 CRITICAL STATE AND STEADY STATE SOIL MECHANICS AND AS A FRAMEWORK FOR MODELING THE BEHAVIOR OF COHESIONLESS SOIL

Critical state soil mechanics (CSSM) provides a unified model relating the ultimate state of a soil element to the current void ratio and stress conditions existing within the element. A state can be defined which describes the relationship of void ratio - deviation stress - mean effective stress ($e-q-p'$) along a boundary beyond which soil collapse will occur. This is called the critical state surface or state boundary. Figure 2.1 shows a representation of the soil collapse boundary in $e-q-p'$ space (based on Sasitharan, 1994).

State boundary and critical state conditions have been determined for a wide variety of soils. In two dimensional deviator stress - mean effective stress space ($q-p'$) there exists a collapse boundary. As a soil element is undergoes monotonic or cyclic loading, in either drained or undrained conditions, the stress path will eventually reach this ultimate state. Further loading will result in a collapse of the sample to a steady state stress condition. A soil sample at a given initial $e-q-p'$ condition can be taken along any stress path to failure.

A line exists in $e-p'$ space, termed the steady state line or critical state line. Loading of a soil element at a constant void ratio will result in either strain hardening, strain softening or limited strain softening behavior. Soil loaded under drained conditions, i.e. changing void ratio, will eventually reach the same steady state condition defined by undrained conditions. Steady state conditions will also be reached under monotonic or cyclic testing conditions.

Steady state conditions have been described as a state of constant volume, shear stress, mean stress and velocity (Poulos, 1981). Critical state has been described as a state of continued deformation under conditions of constant shear stress, mean effective stress, volume and deformation rate (Roscoe *et al.*, 1958). For saturated sand at large strains the critical and steady state conditions are considered to be interchangeable (Ishihara, 1993). Most of the tests in this study were carried to at least 20% strain, a condition which is considered to have reached both steady state and critical state. Several researchers have identified a condition of limited steady state or quasi steady state (Ishihara, 1993). Since this state persists for only a short time, at moderate strain levels, the use of the term "steady" is misleading. In referring to this condition, the term phase transformation (Vaid and Chem, 1985) will be used in this study.

CSSM and steady state concepts are applied to real world problems through the state parameter, ψ , which relates the current void ratio of a soil element to the steady state void ratio at a given mean effective stress (Been and Jefferies, 1985). If the value of ψ is positive the state of the soil element is above the steady state line in e - p' space and the sample would be expected to contract to reach SS. Negative ψ values predict a dilatant response of the soil to reach SS. SPT, CPT, and more recently in situ V_s measurements are being used to define the in situ state of a given soil element. Once the initial state of void ratio and stress are known it is possible to predict large strain behavior, i.e. the steady state condition. This research has shown that a change in fines content will affect the steady state condition and e - p' relationship. There are subtle changes to the V_s - e and V_s - p' relationships but overall these relationships are shown to be acceptable for a wide variety of sand types and compressibility. A similar analysis technique may be extended to a measure termed RSR (Reference State Ratio) which defines the initial mean effective stress conditions relative to the final state.

2.1.2 HISTORICAL DEVELOPMENT OF CRITICAL STATE AND STEADY STATE SOIL MECHANICS

CSSM was first used by Roscoe *et al* (1958) to describe the behavior of clays in a three dimensional space of void ratio - deviator stress - mean effective stress (e - q - p'). A boundary was described in e - q - p' space that separates states that can and cannot exist, i.e. a state boundary. The authors suggested that a state boundary concept could be used to describe the e - q - p' behavior of cohesionless soils in addition to clay.

The CSSM framework was extended to describe the behavior of sands by Castro (1969) who investigated the strain softening and steady state condition exhibited by loose sands in triaxial loading. Poulos (1981) has defined the steady state of deformation as: "The steady state of deformation for any mass of particles is that state in which the mass is continuously deforming at constant volume, constant normal effective stress, constant shear stress and constant velocity. The state of deformation is achieved only after all particle orientation has reached a static steady state condition and after all particle breakage, if any, is complete, so that the shear stress needed to continue deformation and the velocity of deformation remains constant."

A state parameter, Ψ , was introduced by Been and Jefferies (1985) to describe the relation of the initial void ratio to the void ratio at steady state. They showed that the state parameter can be used to predict the normalized peak undrained strength, the peak angle of shearing resistance, dilation rate, and other soil response. It is therefore possible to predict soil behavior based on the initial state of the soil in e - q - p' space. Although they did not explicitly describe the relationship between the state parameter and the e_{min} or e_{max} line, their work was

based on the concept of parallel steady state and consolidation lines. As discussed later, the state line and the consolidation lines determined in this study were not found to be parallel.

Sladen *et al.* (1985) investigated the behavior of very loose sands used for offshore artificial islands, and proposed that a surface exists in the e - q - p' which defines the collapse surface of very loose sands. The collapse surface was used to analyze flow failures of sand berms on the sea bed.

Hird and Hassona (1990) studied the effects of compressibility on the steady state behavior of sand by varying fines content. They suggested that the severity of liquefaction could be thought of in terms of the horizontal distance from the initial stress and void ratio condition to the final steady state stress in e - p' space. This is represented by the ratio of p'_c/p'_{ss} . This measurement has some advantages over the state parameter since it provides information on the steady state strength which may be a more meaningful design parameter than void ratio.

Further work on the collapse surface was carried out by Alarcon-Guzman *et. al.* (1988) who described the initiation of strain softening behavior within the collapse surface framework proposed by Sladen *et al.* (1985). Ishihara *et. al.* (1991) and Been *et al.* (1991) determined that the collapse surface was invariant for different stress paths and testing condition. The steady state was therefore shown to be identical to the critical state, at least for cohesionless soils. Ishihara *et. al.* (1991) used CSSM to analyze several case studies on the flow liquefaction of sand.

The drained behavior of flow slides was investigated by Eckersly (1990) who showed that collapse could be triggered from a static condition such as a rising the water table. Sasitharan (1994) proved and defined a collapse surface for loose sand in a CSSM framework. A state boundary equation was defined by Sasitharan in terms of e - q - p' parameters.

Konrad (1993) confirmed that the failure envelope for a given sand is unique. He also showed that the peak strength envelope was unique for a given sand prepared by moist tamped methods.

2.2 Parameters used in USS and CSSM analysis

2.2.1 STATE PARAMETER

Been and Jefferies (1985) suggest that the behavior of sand may be characterized in terms of a state parameter and a fabric parameter. The state parameter encompasses the void ratio and stress conditions, and the fabric parameter encompasses the structure of the sand

grains. The concepts of soil fabric is discussed later in this report. Been and Jefferies defined the state parameter as the "void ratio difference between the initial sand state and the steady state conditions at the same mean effective stress." However, they infer this to be the void ratio difference between the steady state line and the initial state line which are commonly shown to be parallel. This research shows that this initial condition is not true for most stress ranges, especially at higher fines contents. Since the lines defining the maximum and minimum void ratios were found to be not parallel to the steady state line, the use of Ψ as a comparison tool between sand or as an indication of compressibility is prone to misinterpretation. Figures are discussed later in this report which show the change in maximum positive and negative state parameters with increased mean effective stress.

2.2.2 OTHER PARAMETERS

The common parameters used in the analysis and discussion of USS and CSSM concepts are shown on the figures noted below. The notations and definitions provided are used throughout this work.

- Figure 2.1 Three Dimensional Representation of State parameter concepts
- Figure 2.2 Void Ratio Against Log p' Showing Definition of Γ and λ
- Figure 2.3 Normalized Stress Path Space Showing Definition of M, s and β
- Figure 2.4 Reference State Ratio, RSR, and State Parameter, Ψ

The CSSM concepts may be defined mathematically using the following relationships:

$$p' = \left(\frac{\sigma'_1 + 2 * \sigma'_3}{3} \right) \tag{2.1}$$

$$q = (\sigma'_1 - \sigma'_3) \tag{2.2}$$

$$M = \frac{6 * \sin(\phi')}{(3 - \sin(\phi'))} = \frac{q_{ss}}{p'_{ss}} \text{ (Constant volume friction angle - } \phi_{cv} \text{)} \tag{2.3}$$

2.3 Monotonic Undrained Response of Saturated Sands

2.3.1 SUMMARY

The monotonic undrained triaxial test response of saturated sands may take one of three distinct paths. These three responses are strain softening (SS), limited strain softening

(LSS), and strain hardening (SH). These responses are shown on Figure 2.5, and are described below. The initial state of a soil sample will determine whether a sample exhibits SS, LSS or SH behavior. Loose sands, as determined by the void ratio, are usually associated with SS behavior, medium dense sands with LSS behavior and dense sands with SH behavior, respectively. However, depending on the initial mean effective stress any of the three behaviors may be associated with any given soil void ratio. The final steady state is dependent only on the initial state and is independent of the stress path.

Typical stress paths in $q - p'$ space are shown in Figure 2.6 for drained and undrained monotonic loading and for undrained cyclic loading. The stress path response of saturated sand subjected to monotonic loading is affected by several factors. These factors include: previous strain history (Ishihara *et al.*, 1980); method of sample preparation (Kuerbis, 1989); stress path and direction of loading (Been *et al.*, 1991); initial state and anisotropy of sample (Georgiannou, 1988). It is generally held that the initial state will determine the steady state conditions (Been *et al.*, 1991), and that a unique steady state exists for a particular sand. Monotonic undrained and drained loading on a given sand has been shown to determine a single collapse surface and unique steady state parameters (Sasitharan, 1994). This investigation has shown this postulate holds for a sand with a given fines content, but does not hold for a sand with varying fines content. Some researchers have applied upper and lower bounds for the steady state line, in response to scatter in steady state data (Konrad, 1990).

2.3.2 STRAIN SOFTENING

Strain softening behavior is characterized by a peak strength followed by a reduction in shear strength. A steady level of shear strength is attained, usually before twenty percent strain has occurred. This post peak steady shear strength is termed the residual or steady state strength. The ratio of the loss in strength to the peak strength is termed the Brittleness Index (Pitman, 1993) and is determined using the following equation:

$$I_B = \frac{q_{\text{peak}} - q_{\text{ss}}}{q_{\text{peak}}} \quad (2.4)$$

Where: I_B is the Brittleness Index;
 q_{peak} is the peak shear strength; and
 q_{ss} is the steady state shear strength.

This equation is only valid for isotropic tests and where there is a well defined peak and steady state value. Values of I_B vary from 0 to 1. The higher the value of I_B the smaller the value of q_{ss} relative to the peak. Significant deformations would be anticipated for materials

exhibiting a high I_B value whereas strain softening of a material with a low I_B value would not be expected to show substantial deformation as it strain softened.

Strain softening behavior is usually associated with loose sands, but may also be associated with dense sands if the confining stress is very high. The behavior of loose sands showing strain softening is typified by large deformation, a distinct "collapse" of the sand as observed through a loss of shear strength and contractant volumetric measurements.

2.3.3 LIMITED STRAIN SOFTENING

Ishihara (1993) describes a quasi steady state condition where the shear strength reaches a peak value followed by a drop off of strength to a post peak low value. The post peak low, known as quasi steady state or the phase transformation (PT), condition is valid for a limited strain after which the shear strength increases. The increase in shear strength commonly continues until the end of the test, about 20% strain. Post PT strength values can exceed the initial peak strength values.

The I_B can be used to describe the initial peak to quasi steady state condition, but is an inappropriate descriptor for post PT strength. Since the value of the PT strength was found to increase beyond the strain level limits of most tests, the choice of a peak post PT strength is arbitrarily determined by the level of strain testing was terminated at, usually 20 to 25% strain.

The limited strain softening response is usually associated with medium dense samples. The stress path behavior of a LSS sand sample is typified by the presence of an elbow in the stress path which may be well defined or only barely discernible, as shown on Figure 2.5.

2.3.4 STRAIN HARDENING

A strain hardening response is characterized an increase in shear strength within the initial two percent strain followed by a gradual, non-uniform increase in shear strength until a peak value is reached. For this study, several tests on very dense samples did not reach a discrete peak shear strength value during the triaxial test, within about 25% strain. The data used to derive the steady state lines excluded all points which did not reach what was considered to be a clear steady state condition. The I_B is not appropriate for describing strain hardening behavior.

A saturated sand, whether it be loose or dense, may exhibit strain hardening behavior if the initial confining stress conditions are low enough, however strain hardening is usually associated with dense sands. Strain hardening results from a tendency for dilation of the sample, whereas strain softening results from a tendency for contraction. Of interest to the

application of CSSM concepts to field materials is the boundary between contractant and dilatant soil behavior at large strains. The steady state line defines this boundary.

2.3.5 LIQUEFACTION

2.3.5.1 Liquefaction Phenomena and Terminology

During monotonic or cyclic loading where SS or LSS behavior is noted, there is a contraction of the soil during loading. This contraction results in an increase in pore pressure and a consequent decrease in effective stress and some deformation of the soil. Flow liquefaction of the soil mass occurs when the soil structure collapses, causing a large rise in pore water pressure which produces a corresponding loss of shear strength. Early studies into liquefaction behavior were initiated in response to the catastrophic damage caused by several earthquakes, which were considered to be the trigger for liquefaction failure. Liquefaction of some soils was noted to occur a short time after the initial earthquake vibrations had subsided, and were also observed to occur several hours after the vibration. Earthquake induced liquefaction phenomena consists of sand boils, large settlements, loss of foundation support, flow failures in embankments, and other associated phenomena. If the in situ static shear stress is greater than the ultimate state shear resistance, then a flow liquefaction is possible and large flow deformations may be expected. If the static shear stress is less than the steady state shear resistance than flow liquefaction is not anticipated, but some deformation is expected.

Castro (1975) recognized two clearly different phenomena, which he termed liquefaction and cyclic mobility. He relates the liquefaction of a sand to the critical state defined by the critical void ratio, i.e. the state of continuous deformation at constant resistance and volume. Cyclic liquefaction, is the accumulation of pore pressure during cyclic loading and the consequent changes in effective stress and void ratio. Small strains produce pore pressure changes which add cumulatively, eventually resulting in a pore pressure equal to the confining pressure, momentarily resulting in zero effective stress and the onset of cyclic liquefaction during which each cycle produces increasingly larger strains. Cyclic mobility is the gradual increase of strains without an accompanying loss of shear strength. Cyclic mobility may occur in loose or dense samples, although the onset of mobility would occur at different levels of cycle repetition.

Robertson (1993) has developed a flow chart by which the liquefaction potential of a cohesionless deposit may be evaluated, this chart has been updated and is reproduced as Figure 2.7. Following the work of Castro (1975), the flow chart divides liquefaction into flow and cyclic phenomena.

2.3.5.2 Flow Liquefaction

Flow liquefaction involves a strain softening response under conditions of undrained shear, with either a static or dynamic trigger mechanism. If in situ shear stresses are greater than the steady state strength then flow liquefaction can occur and large deformations are possible. A stable condition will eventually be reached when the in situ stresses are reduced to the steady state value. Deformations can be expected to continue for an extended period after the triggering event has stopped.

2.3.5.3 Cyclic Liquefaction and Cyclic Mobility

Martin, *et al* (1975) discussed the fundamentals of liquefaction under cyclic loads and described cyclic liquefaction as the condition that exist when pore pressure have built up during cyclic loading such that they equal the confining pressure and produce a condition of zero effective confining pressure. Large deformations are possible only so long as the triggering mechanism is active. Cyclic mobility involves a cyclic trigger mechanism which acts on a deposit which is subject to large initial shear stresses and for which shear stress reversal does not occur. Deformations under cyclic mobility are expected to be limited and only occur so long as the cyclic trigger is active.

2.3.5.4 Historical Liquefaction Studies

Cyclic liquefaction is commonly associated with earthquakes . Numerous case histories document the often severe damage done by cyclic liquefaction of granular soil during major earthquake events. These case histories provide useful background for the study of general liquefaction phenomena.

Idriss and Seed (1967), Donovan (1968) and several others analyzed and discussed soil behavior during the 1964 Niigata earthquake. These investigators provide a wealth of information on the earthquake and soil movements and provided some quantification for the evaluation of the liquefaction phenomena.

Dobry and Alvarez (1967) provide a useful description of the nearly simultaneous failure of several tailings dams in Chile due to the March 28, 1965 Chilean earthquake. However, as discussed by Leps (1968), the paper is limited in scope and application to new designs since it does not provide substantial information on the earthquake peak ground acceleration, frequency of seismic pulses or orientation of the seismic pulses.

The March 3, 1985 Chilean earthquake resulted in the liquefaction failure of two small reservoir embankments and extensive cracking to numerous others. De Alba *et al.* (1988) analyzed these failures and postulated a progressive liquefaction mechanism A portion of the

reservoir embankment which contained a higher percentage of fines, did not liquefy but broke up into small blocks and was carried along by the underlying liquefied soils. This provides a case history in which there is real evidence of the reduction of liquefaction potential due to increased fines content in a sand.

Seed and Silver (1972) described the settlement of sand related to earthquake activity. They note that the vertical settlement due to a series of horizontal shear strain cycles depends only on the number and magnitude of the strain cycles involved. They also note that previous strain history does affect the settlement characteristics of sands.

The October 17, 1989 Loma Prieta earthquake had its epicenter about 50 km from San Francisco yet still caused substantial devastation in the San Francisco area. Shortly after the earthquake occurred, sand boils were observed in sandy materials used to infill an old lagoon. Bardet and Kapuskar (1993) described this liquefaction induced sand boil phenomena.

2.3.5.5 Models

Many analytical models have been developed to study liquefaction behavior. Pastor (1991) modified an isotropic granular soil model to account for sample and anisotropic loading conditions. His model determined the strain hardening or softening response of soil. Jefferies (1993) used a rigid-plastic model called Nor-Sand to describe steady state behavior. Ng and Dobry (1994) used discrete element simulations to model granular soil response to both monotonic and cyclic loading. Gu *et al* (1993) used an undrained elastoplastic model for liquefiable soil to analyze the progressive failure of the Lower San Fernando Dam. Modeling and finite element methods continue to be actively researched and used to study liquefiable soils.

2.3.5.6 Sample Preparation

Many researchers have studied the effects of sample preparation on the liquefaction behavior of sands. Pertinent comments on the research undertaken by these researchers are summarized below.

Mullis *et al.* (1977) studied the effects of sample preparation on the cyclic liquefaction behavior of sand. They noted that the cyclic liquefaction behavior of sand, not the steady state strength, was related to several factors. These factors include: (1) Soil type and gradation; (2) initial effective confining pressure; (3) stress-strain history, and; (4) void ratio or density (and cyclic factors such as duration and number of shaking cycles and intensity of cyclic shear stress). They also noted that the manner in which a sample was prepared (in reconstituted laboratory work) had a major effect on the cyclic liquefaction characteristics.

Mullilis *et al* noted that sample preparation has a major influence on the determination of cyclic liquefaction properties. Their study of different sample preparation techniques clearly showed that: (1) samples formed by pluviation of soil through water were not uniform in section but contained alternating layers of loose and denser materials resulting from segregation; (2) vibrated samples were relatively uniform in density except along a thin layer where the surcharge weight was placed during compaction, and; (3) tamped samples were the most non-uniform in density.

Mullilis *et al* investigated the effects of differing sample preparation techniques on the cyclic liquefaction of sands. They made use of a concept called Formation Factor which is defined as the ratio of the electrical conductivity of the electrolyte to the conductivity of the sand saturated with the electrolyte. This value gives an indication of the anisotropy and particle packing and grouping. In general as the formation factor increases, the dry density and cyclic stress ratio to cause cyclic liquefaction increase. They also determined that the magnitude of the change in liquefaction properties determined from different preparation techniques is a function of the type of sand. The difference in the orientation of the contacts between sand grains and in packing were probably the primary reasons for the observed differences in the dynamic strength of the sand.

DeGregorio (1990) described the effects of different loading systems and sample preparation techniques on the flow liquefaction characteristics of a clean loose sand. He determined that dead load apparatus was able to apply a constant load as flow liquefaction occurred whereas constant strain apparatus was not able to. However, no change was noted for the steady state lines.

Kuerbis and Vaid (1988) compared moist tamping, air pluviation and water pluviation sample preparation techniques. They showed that moist tamping produces the loosest samples and that the samples were metastable even upon saturation. Air pluviated samples were noted to be metastable although some sample disturbance was noted on saturation. Very loose samples could not be made by water pluviation techniques. Water pluviation is best used to make samples from uniform sands, since sample segregation and non-uniformity are observed in non-uniform sand samples.

Hird and Hassona (1990) showed the importance of varying the compaction input to each level in the sample preparation of moist tamped samples. Greater compactive effort is required for the upper layers to contribute a consistent energy input to the sample.

Vaid and Neguessy (1984) showed that wet tamped samples have a more oriented structure than dry pluviated samples and smaller deviations in local void ratio variation, thus

wet tamping produces a more homogeneous fabric. They also showed that specimens prepared by wet tamping have greater resistance to liquefaction than dry pluviated samples.

2.3.6 RESEARCH ON FINES CONTENT AND RELATED FABRIC CONCEPTS

2.3.6.1 Compressibility and Fines Content

The compressibility of a soil sample is related to the compressibility of the individual sand particles, the soil skeleton and any interstitial fines. In most studies the sand particles are assumed to be incompressible and the compressibility of the soil is altered through the addition of compressible fines.

Many researchers have identified the relationship of fines content with liquefaction potential. Seed *et al* (1976) state that fines content must be accounted for in the evaluation of resistance of soil to cyclic loading. Seed *et al* established grain size distribution boundaries to classify soils as potentially liquefiable and most likely to liquefy. These boundaries are shown on Figure 2.8. Liao (1985) found that fines did have an effect on the liquefaction potential of soils and Keubis and Vaid (1988) showed that only plastic fines have a significant effect on the liquefaction resistance. This same conclusion was reached by Pitman (1993).

Been and Jefferies (1985) investigated Kogyuk sand at 4 different silt contents. Large strain triaxial tests were done on a Beaufort Sea sand to develop state parameter concepts. They determined that the state parameter could be a useful design aid while the use of relative density had limited application in design since sands with widely different fines content may have the same density but behave in either contractant or dilatant manners. Hird and Hassona (1990) studied the effects of mica fines on Leighton Buzzard Sand (LBS) and determined that the steady state lines became steeper in $e - \log p$ space as fines were added. The behavior of the LBS was found to be similar to normally consolidated clay at a fines content of about 30 percent. Hird and Hassona also noted that the severity of the liquefaction decreased as the sample compressibility (fines content) increased. They used an expression defined by Ψ/λ_{ss} ($\log p/p_{ss}$ or RSR) as a measure of liquefaction severity.

The issue of soil skeleton compressibility is an issue that should be addressed when dealing with soils composed of a significant portion of fines or compressible particles. De Matos (1988) found that the degree of soil compressibility can be influenced by the grain shape, the grain roughness or texture and the grain size distribution. In the present study the shape, roughness and grain size distribution of the grains of Ottawa sand are assumed to be invariant between samples, thus the change in compressibility of the samples is due to the addition of plastic fines.

The compressibility of the samples can be compared by determining the maximum and minimum void ratio for each level of fines content. This is discussed in Section 5.2.

2.3.6.2 Fabric and Anisotropy

Fabric can represent the spatial arrangement of solid particles and associated voids (Oda, 1972). Oda investigated the initial fabric of granular masses and the relationship of the fabric to mechanical properties of the material. He concluded that the characteristics of the fabric were closely related to particle shape, which he determined using an axial ratio relationship, and by the method of compaction (sample preparation). He also determined that the mechanical property of E (Modulus of Deformation) was dependent on fabric anisotropy and that the fabric of sands have local void ratio variation.

Fabric may refer to microfabric or macrofabric. The importance of macrofabric in relation to the study and interpretation of geotechnical properties is discussed by Rowe (1972). McGown (1980) describes methods of recordings and interpreting macrofabric data based on the nature, form and spatial arrangement of features such as layering and discontinuities in deposits. The microfabric is defined by the orientation of nonspherical particles, known as orientation fabric, and the mutual relation of particles, termed packing (Oda, 1981). Orientation fabric is studied using thin section, X-ray and SEM techniques. Packing conditions may be assessed using the above techniques or by statistically based models. Luo *et al* (1992) describe an automated, computer aided method of particle orientation analysis using a vein and polygonal convex hull analogy.

Arthur and Menzies (1972) concluded that there is an inherent geometrical anisotropy produced by dry pluviation through air that corresponds to a strength anisotropy. He defined two kinds of anisotropy: Inherent anisotropy that is a physical characteristic inherent in the material and entirely independent of the applied strains, and; induced anisotropy that is the physical characteristics due to the strain associated with an applied stress. They note that particle shape and methods of deposition influence the particle orientation of naturally occurring deposits. Layering of the sample may be considered as a third type of anisotropy.

The determination of the anisotropic distribution of the statistical contact normals is crucial in the determination of the anisotropic response. Oda (1981) determined that the initial fabric is well preserved during plane strain tests but is completely lost during triaxial tests where a final fabric is attained irrespective of the initial fabric. All sands tend to show some degree of structural anisotropy. Even uniform spherical glass balls have been shown to arrange in chains when allowed to fall freely under the action of gravity (Kallstenius and Bergau, 1961). Oda (1981) showed the effect of grain shape, as described by an axial ratio relationship, on the minimum and maximum void ratio of sands and spherical glass beads. He showed that as the

axial ratio decreases, the maximum and minimum void ratios attainable both increase. He also showed that strength orientation is present even in samples composed of uniform glass beads.

Rothenberg *et al.* (1986) states that the fabric of sand changes continuously under applied loads and that the dilatant behavior of sand leads to disintegration of fabric manifested by the loss of point contacts. Furthermore, Rothenberg states that the loss of contacts is orientationally non-uniform and that the loss of contacts will be greater in the tensile direction (horizontally in a conventional triaxial test) than in the compressive direction. The number of contacts may initially increase in the compressive direction and then drop off as shearing continues. The development of deviatoric load carrying ability is related to the sum of the anisotropic distribution of contact orientations and directional components of the contact forces by the following equations:

$$\frac{(\sigma_1 - \sigma_2)}{(\sigma_1 + \sigma_2)} = \frac{(a + a_n + a_t)}{2} \quad (2.5)$$

$$S(\theta) = \frac{\{1 + a[\cos(2(\theta - \theta_o))]\}}{2\pi} \quad (2.6)$$

where: a is a coefficient related to anisotropic distribution of contact orientation
 a_n is a coefficient of force anisotropy in normal direction
 a_t is a coefficient of force anisotropy in tangential direction
 $S(\theta)$ is normalized contact orientation distribution
 θ is the angular direction with respect to the horizontal
 θ_o is the direction of anisotropy

These equations may be interpreted to show that the ability of an assembly to carry deviatoric load is dependent on its ability to develop anisotropic distribution of contact orientations ($a > 0$) or to maintain highly directional dependent contact forces ($a_n, a_t > 0$). Tangential forces increase to a point where deformation ceases to be purely elastic at which point a_t drops off as rotation occurs releasing tangential forces. Rothenberg concluded that "...the major characteristic of microstructure that controls macroscopic response of granular materials is the contact orientation distribution." However, Rothenberg did not consider the effect of elastic deformations, particle hardness, pressure sensitivity, fines content or aging.

Yudhbir and Abedenzadeh (1991) conclude that static and cyclic behavior of sand may be explained by its fabric and that application of cyclic shear tends to alter the initial fabric of sands. They showed that a randomly oriented sand mass will tend to orient while regularly arranged sands will tend to destroy its preferred particle orientation.

Mullis *et al.* (1977) showed that moist tamped samples had the highest distribution of interparticle contact normals in the vertical direction (direction of loading) whereas the dry vibratory samples had a distribution the lowest. Moist tamped samples also had the highest dynamic strength. They made use of a concept called Formation Factor which is defined as the ratio of the electrical conductivity of the electrolyte to the conductivity of the sand saturated with the electrolyte. This value indicates the anisotropy and particle packing and grouping. As the formation factor increases, the dry density and cyclic stress ratio to cause initial liquefaction increases. They also determined that the magnitude of the change in liquefaction properties determined from different preparation techniques is a function of the type of sand. The differences in the orientation of the contacts between sand grains and in packing were probably the primary reasons for the observed differences in the dynamic strength of the sand.

Chapuis (1981) studied the internal structure of granular material. He determined that the spatial distribution of the normals to the contact plane act as the internal structural link between stress and strain. He also determined that there is no relationship between the void ratio and the mean number of contacts per grain.

2.3.7 SHEAR WAVE VELOCITY MEASUREMENTS FOR LIQUEFACTION ASSESSMENT

2.3.7.1 Historical overview

The use of bender elements to determine shear wave velocity and the methodology to apply shear wave velocity measurement to the assessment of liquefaction potential has developed rapidly in the past 30 or so years. Early researchers measured shear wave velocity by resonant column techniques and eventually bender element techniques. Shear wave velocities have been used to assess soil state and the tendency for the soil state to contract or dilate. Further correlations have been developed to define a boundary between contractive and dilative states in SPT, or CPT, versus effective vertical stress space have been developed.

Cunning (1994) provides a background describing the historical development and use of shear wave measurements including bender element theory and the use of shear wave velocity to assess liquefaction potential. Pertinent historical details are presented here, although the reader is encouraged to review Cunning's discussion for greater detail.

Early researchers used resonant column technique to determine shear wave and dynamic soil properties, principally small strain elastic moduli, G_{max} , damping properties, and to relate the shear wave velocity to the mean effective stress and associated void ratio. This research was advanced by Ishimoto and Leda (1937), Leda (1938, 1940), Shannon, Yamane, and Deetrich (1959), Willson and Deetrich (1960), Hardin and Richart (1963). Drenivich (1967,

1972) used hollow cylinder sample to maintain constant strain across the sample. Lawrence (1963) used an shear plate transducers to measure shear wave velocity in soils in a triaxial cell apparatus. This development appears to be the earliest predecessor to present day bender element technology.

Shirley (1978) and Shirley and Hampton (1978) helped to pioneer the use of bender elements to measure the shear wave velocity of laboratory prepared samples and unconsolidated marine sediments. Roesler (1979) determined that only the stress in the direction of wave propagation and polarization had any effect on the measured shear wave velocity. Horn (1980) related the use of bender elements and resonant columns to measure the shear wave velocity. Stachan (1981) used bender elements to correlate the shear wave velocity of marine sediment sands to certain dynamic properties. Schultheis (1981) measured shear wave velocity in the laboratory prepared samples of marine sediments using bender elements. Dyvik and Madshus (1985) incorporated bender elements into common geotechnical testing devices including the triaxial cell, oedometer, and the direct simple shear, and found dynamic properties determined by resonant column testing and bender element testing was within 5% of one another. The measurement and use of shear waves in cohesionless media were also developed by Roesler (1979), Know (1984), Yu and Richart (1984), Stokoe et al. (1985) Sasitharan (1994), and Cunning (1994). These researchers determined that the in-situ state of a soil could be evaluated by in-situ shear wave velocity measurements that could be compared to shear wave velocity measurements determined from laboratory samples.

De Alba et al. (1984) measured shear wave velocities in cyclic triaxial tests using bender element techniques. The contractive or dilatant response of saturated sands was directly related to shear wave velocity measurements that thereby provided a method to evaluate the liquefaction potential of saturated sands. The effect of different initial fabric was studied by employing different sample preparation methods

Work by Tokimatsu et. al. (1986) and Tokimatsu and Uchid (1990) related the seismic resistance of a soil to its shear wave velocity. Yoshimi, *et al.* (1989) stated that SPT N value are a better indication of liquefaction potential than relative density when comparing sands of dissimilar geological origins. They state that liquefaction is susceptible to small changes in N. Robertson *et al* (1986) incorporated a seismometer into an electric cone penetrometer and described a SCPT test procedure and methods of analysis. The SCPT was shown to provide a quick and convenient means of profiling a borehole for shear wave measurements. Further research by Robertson et al (1992¹) and (1992²) normalized the shear wave velocity with respect to depth and developed a criteria which separated contractive and dilative responses.

Sasitharan et al. (1992) used bender elements to measure shear wave velocities to measure sample disturbance upon freezing and thawing. This provided a means of assessing sample disturbance, not only during freezing and thawing of samples retrieved from insitu ground freezing techniques, but also a means of comparing the relative state and fabric of reconstituted samples to insitu conditions. Sasitharan et al. (1993) developed a relationship stress to delineate between dilative and contractive response of clean Ottawa sand using shear wave velocity and vertical effective stress measurements. Cuning (1994) analyzed the shear wave response of several sands and showed that a single relationship could be used to relate the shear wave velocity and void ratio for a wide variety of sands. These included incompressible clean Ottawa sand, moderately compressible Syncrude sand with a small percentage of fines, and highly compressible Alaska tailings sand.

The use of protruding bender elements in the determination of shear wave velocity is described in detail by Cuning (1994). Cuning also describes a method by which the shear wave properties of frozen samples may be determined using flush mounted bender elements. These flush mounted bender elements were not used in this research in favor of embedded bender elements that were well tested and had historic success.

2.3.7.2 Shear Wave Velocity

The measured shear wave velocity of an uncemented, unaged sand is determined by such factors as the void ratio, effective stresses, and by the fabric. The large strain response of sand is controlled by the effective stress and void ratio. The shear wave velocity can therefore be used to predict the large strain response of an insitu sand if the vertical effective stress and consolidation state of the sand are known, or can be reasonably estimated. Shear wave measurements taken during triaxial tests on reconstituted samples prepared and consolidated to be representative of insitu conditions can be used to predict a boundary for contractive and dilative behavior.

Through the use of different correlations, the shear wave, SPT, or CPT profiles determined from a field test program can be used to predict the contractive or dilative response of soils under large strain conditions, and thereby predict the potential for gravitational flow liquefaction. Yoshimi, *et al.* (1989) stated that SPT N values are a better indication of liquefaction potential than relative density when comparing sands of dissimilar geological origins. The use of shear wave velocity to produce a dilative/contractive boundary for SPT values is therefore a valuable tool in predicting the liquefaction potential of dissimilar sands.

Several correlations between the shear wave velocity and various physical and state parameters are listed below in Table 2.1. Typical values for Γ , λ and M are shown on Table 2.2. Typical values for A , B and n are shown on Table 2.3.

TABLE 2.1
SHEAR WAVE VELOCITY RELATIONSHIPS

Relationship	Source
$V_s = 133(D^{0.27})$	Bates(1989) - Red Wharf Bay Sand
$V_s = 128(D^{0.28})$	Hamiloun (1976) - Various sands
$G = \rho(V_s^2)$	Robertson, et al (1986), based on SCPT
$V_s = (m_1 - m_2 e)(p')^{0.25}$	Hardin and Richart (1963)
$V_s = (A - Be) \left(\frac{\sigma'_s}{P_a} \right)^{na} \left(\frac{\sigma'_p}{P_a} \right)^{nb}, \quad A = m_1 (P_a)^{na+nb}$ $B = m_2 (P_a)^{na+nb}, \quad na = nb = 0.125 \text{ (typically)}$	Roesler (1979)
$V_s = sa^{0.149} * sb^{0.107} * sc^0, \quad \Sigma powers = 0.256$	
$V_{s1} = V_s \left(\frac{P_a}{\sigma'_v} \right)^{na} \left(\frac{P_a}{\sigma'_h} \right)^{nb}, \quad V_{s1} = V_s \left(\frac{P_a}{\sigma'_v} \right)^{0.25} \left(\frac{1}{K_o} \right)^{0.125}$ $V_{s1} = A - Be$	Robertson (1992)
$e = \frac{A}{B} - \frac{V_s (P_a)^{na+nb}}{B (\sigma'_s)^{na} (\sigma'_p)^{nb}}, \quad \Psi = \left(\frac{A}{B} - \Gamma \right) - V_{s\Psi}$ $V_{s\Psi} = \left(\frac{V_s (P_a)^{na+nb}}{B (\sigma'_s)^{na} (\sigma'_p)^{nb}} - \lambda_{\ln} \ln(p') \right)$ $\Psi = \left(\frac{A}{B} - \Gamma \right) - \left(\frac{V_s (P_a)^{na+nb}}{B (\sigma'_v)^{na+nb} (K_o)^{na}} - \lambda_{\ln} \ln \left[\frac{\sigma'_v}{3} (1 + 2K_o) \right] \right)$	Sasitharan (1994)

TABLE 2.2						
STEADY STATE PARAMETERS						
Material	Fines Content % (<74 μm)	Γ	λ_m	M	Applicable Stress Range (kPa)	Reference
Hong Kong Pearl River Sand	5	1.019	0.056	1.23	10 - 1000	Robertson and Skirrow (1994)
Ottawa Sand	0	0.926	0.032	1.20	10 - 800	Sasitharan (1994)
Alaska Thane Sand	31.7	1.485	0.117	1.48		Cunning (1994)
Syncrude Sand	12.5	0.928	0.027	1.31		Cunning (1994)

TABLE 2.3						
SHEAR WAVE PARAMETERS						
Material	Fines Content % (<74μm)	A	B	n	Reference	
Hong Kong Pearl River Sand	5	356	253	0.25	Robertson and Skirrow (1994)	
Ottawa Sand	0	381	259	0.26	Sasitharan (1994)	
Alaska Thane Sand	31.7	307	167	0.26	Cunning (1994)	
Syncrude Sand	12.5	311	188	0.26	Cunning (1994)	

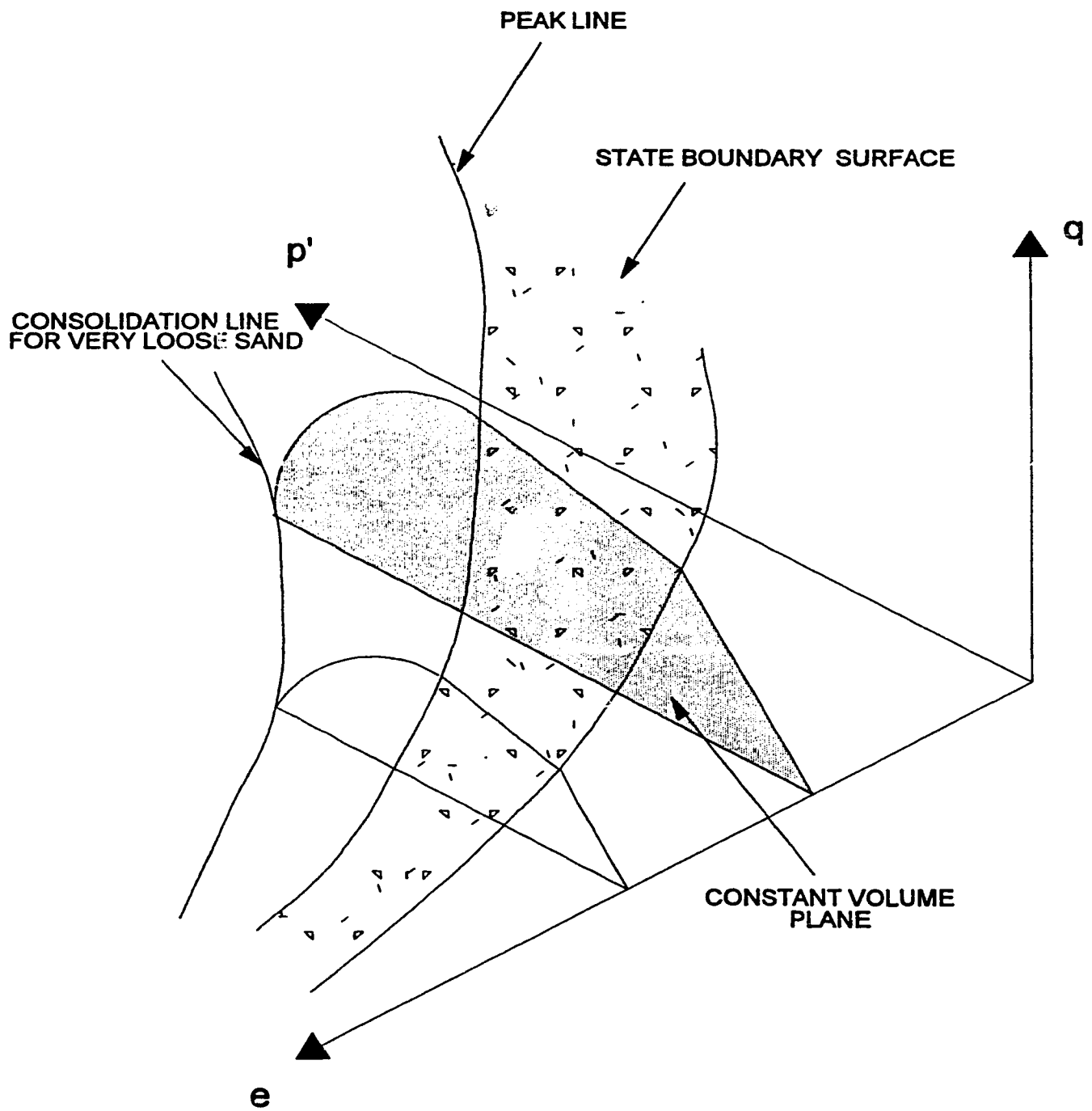


FIGURE 2.1 SCHEMATIC OF STATE RELATIONSHIPS SHOWING THREE DIMENSIONAL $e - q - p'$ SPACE (after Sasitharan, 1994)

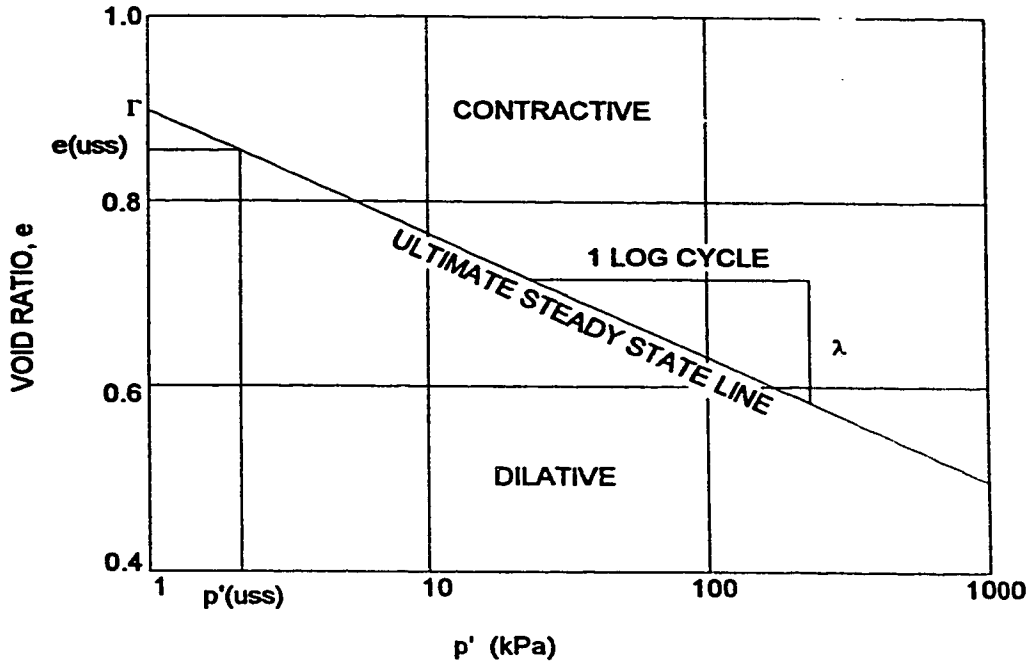


FIGURE 2.2 USS PARAMETERS IN $e - \log p'$ SPACE

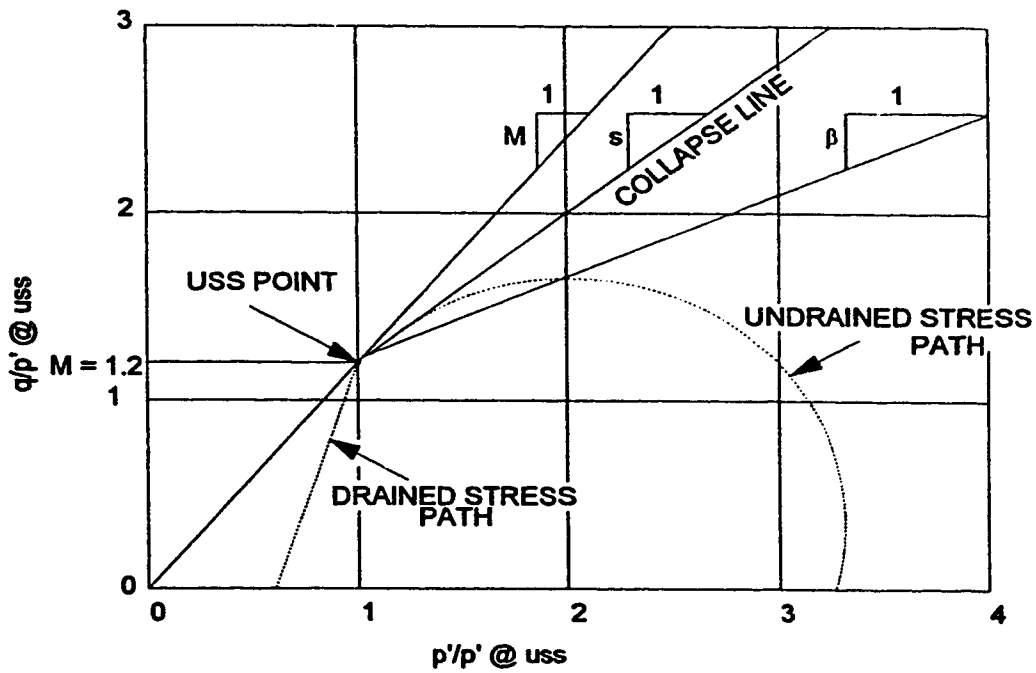


FIGURE 2.3 USS PARAMETERS IN NORMALIZED STRESS PATH SPACE

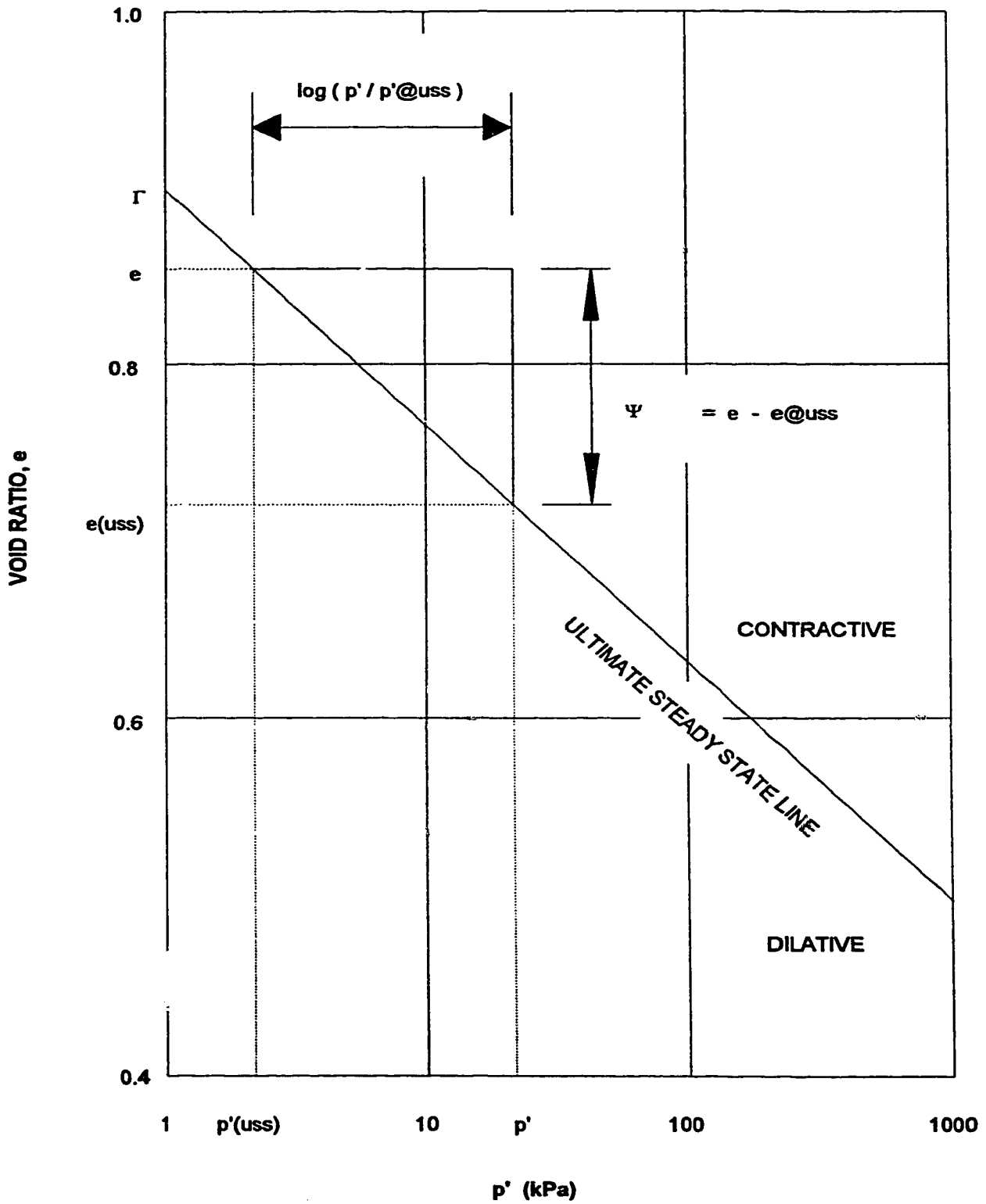


FIGURE 2.4 ADDITIONAL ULTIMATE STEADY STATE PARAMETERS IN $e - \log p'$ SPACE

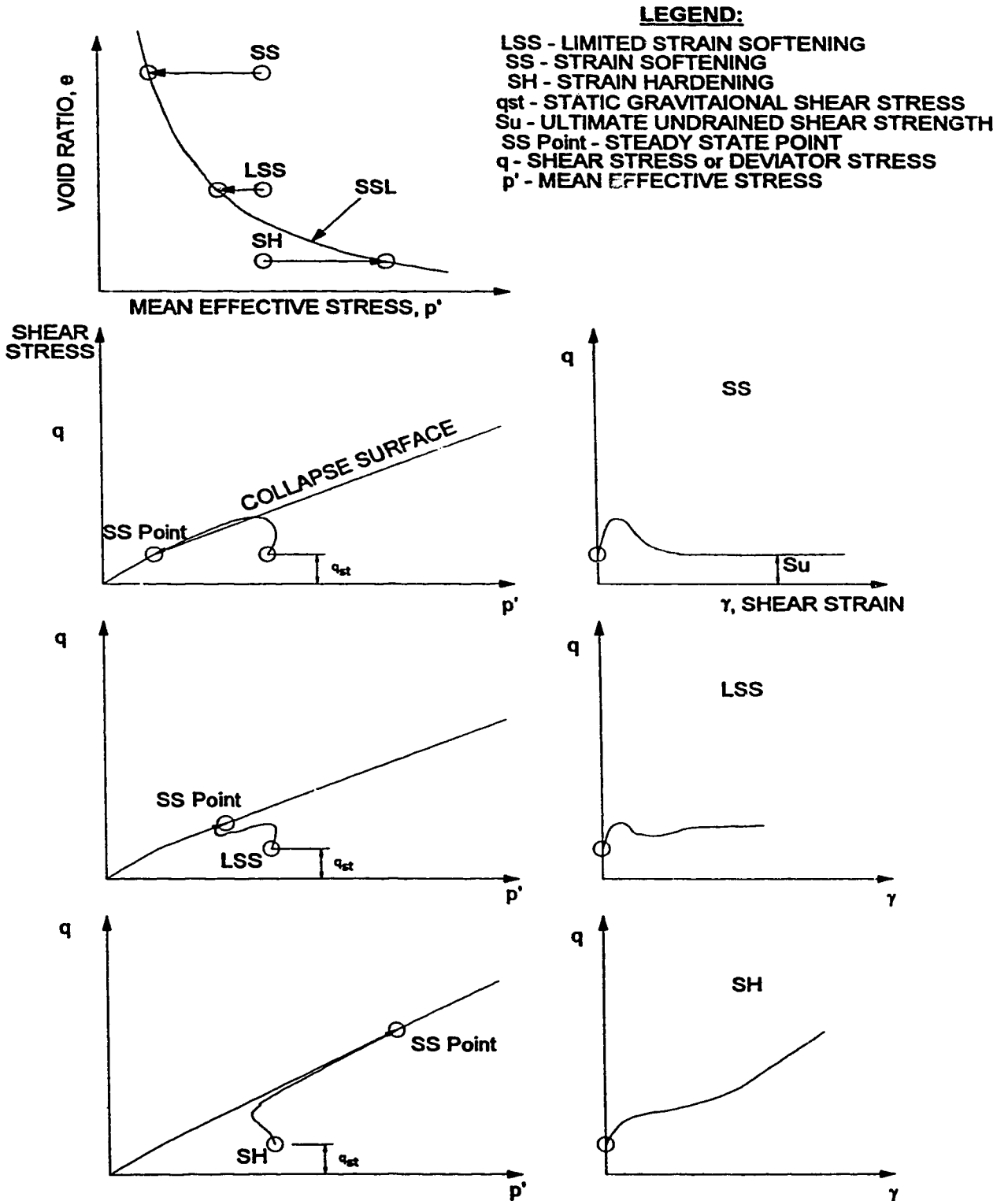


FIGURE 2.5 BEHAVIOR OF COHESIONLESS SOIL UNDER UNDRAINED MONOTONIC LOADING, (after ROBERTSON, 1994)

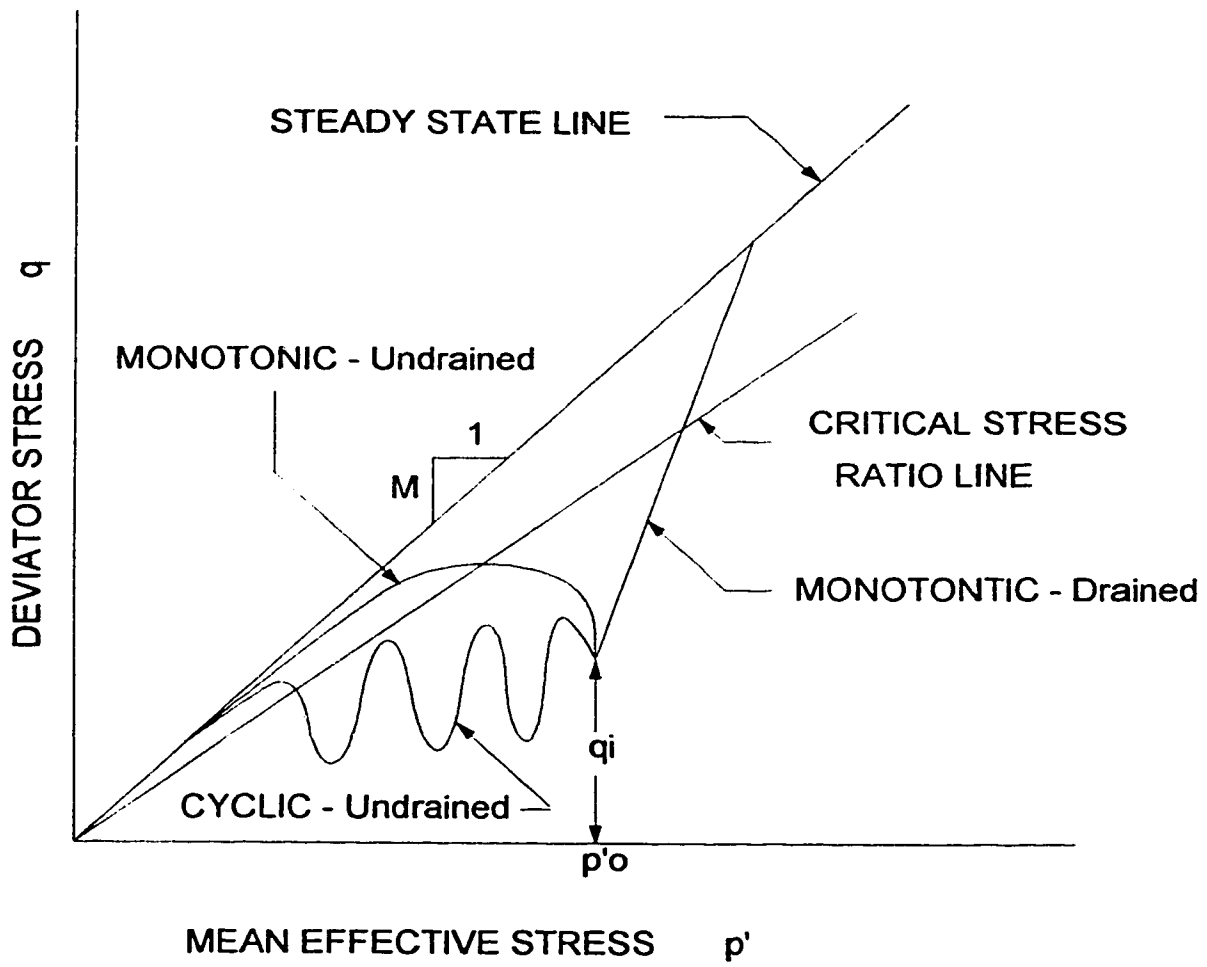


FIGURE 2.6 STRESS PATHS IN $q - p'$ SPACE

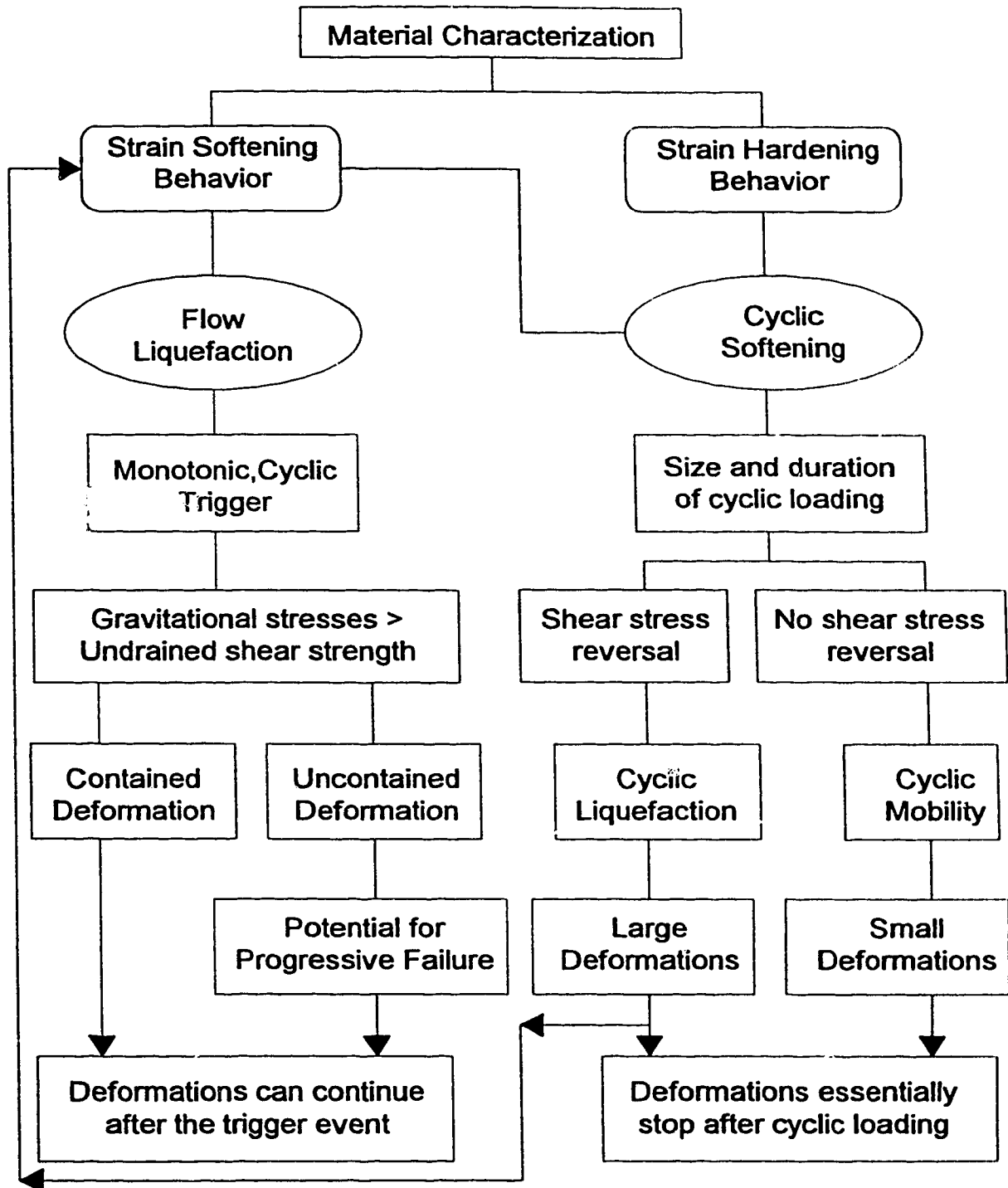
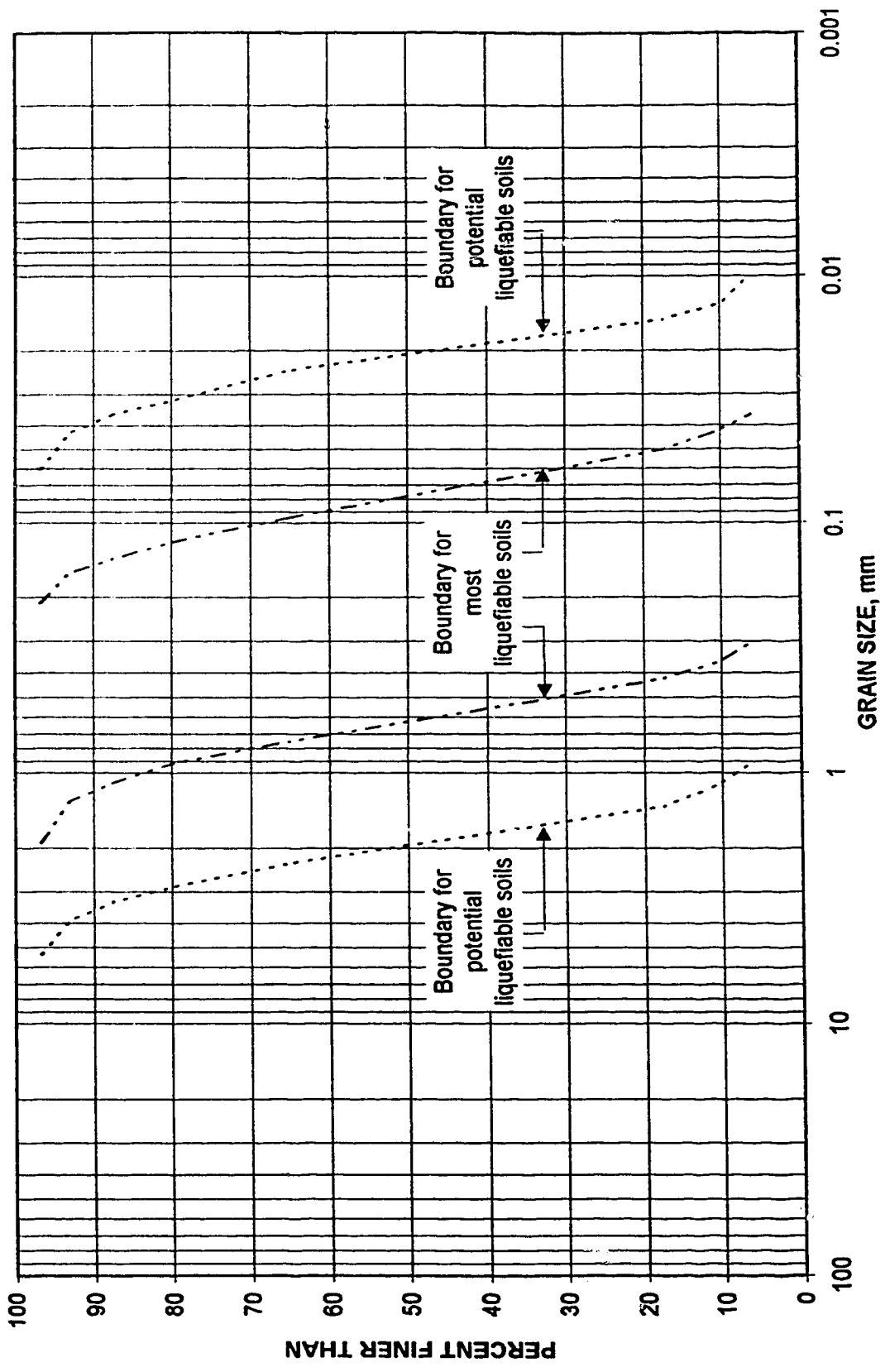


FIGURE 2.7 FLOW CHART FOR LIQUEFACTION (After Robertson, 1994)

FIGURE 2.8 **GRAIN SIZE DISTRIBUTION**
with ZONES OF LIQUEFACTION POTENTIAL
 (after SEED *et. al.*, 1976)



3. TESTING PROGRAM

The testing program undertaken for this investigation consisted of a series of isotropically consolidated, undrained triaxial tests. Shear wave velocity measurements were undertaken at various stages along the consolidation portion of the triaxial test for selected samples. Index tests consisted of sieve analyses tests were done on selected combined sand and fines samples before, and after, triaxial testing to verify the fines content of the sample throughout the triaxial test procedure. The triaxial test and shear wave measurement apparatus and test procedures are described below. Ottawa sand and Kaolinite were used throughout the test program.

3.1 Material Tested

3.1.1 SAND

Ottawa sand, designation C-109, was used for all samples. This sand is the same as that used by other researchers at the University of Alberta (Sasitharan 1994, Pitman 1993, Cuning 1994). The sand is a uniform, sub-rounded quartz sand that is considered to be incompressible in the stress range used for this study. The sand graded between 0.25 to 0.075 mm and contains no fines. Grain size distributions were determined for the Ottawa sand and combined sand and fines samples both before and after triaxial testing. All samples of sand were retrieved from a large batch sample which was kept in an oven set to a constant 60°C to maintain the sand in a dry state.

3.1.2 FINES

Powdered, dry commercially prepared Kaolinite was used as the fines component for all tests. The Kaolinite had a plastic limit of 16% and a liquid limit of 42%. The fines were added to the Ottawa sand, on a percentage by weight of the total sample basis, as determined by the following equation. Using this equation it was possible to maintain a precise fines fraction for each level of percentage fines.

$$W_f = \left(\frac{\%F}{1 - \%F} \right) * W_s \quad (3.1)$$

where: W_f is the weight of fines required to achieve a given percent fines
 $\%F$ is the percent fines required
 W_s is the measured weight of sand.

3.1.3 OTHER SANDS DISCUSSED IN THIS STUDY

3.1.3.1 Koyguk Sand (Been and Jefferies, 1985)

Beaufort Sea dredge sand was tested at several different fines contents. The sand was a uniform, medium grained, quartzite sand with subrounded to subangular particles. The D_{50} was 350 μm . Silt was added to make samples with fines content of 2, 5 and 10%. Variation of the SSL was observed for each level of fines content. Plots of normalized shear stress and drained angle of shearing resistance versus Ψ were produced.

3.1.3.2 Leighton Buzzard Sand—LBS [(Hird and Hassona, 1990), (Sladen et al, 1985), and (Arthur and Menzies, 1972)]

LBS sand was tested and the results compared with the test results for a similar but somewhat finer sand called Banding Sand. In addition the fines content of the LBS was varied to 10, 17 and 30% using mica composed of 80% Muscovite and 20% Kaolinite. The effect of increased sphericity was shown on SSL plots and normalized shear stress - mean effective stress plots.

3.1.3.3 Hong Kong Pearl River Sand (Robertson and Skirrow, 1994)

A well graded, rounded to sub rounded, quartz (88%), feldspar (7%) and calcite (5%) sand was tested to determine shear wave and steady state parameters. The calcite proportion was in the form of angular, friable sea shells that resulted in a moderately compressible sand. The fines content was about 5 percent. Five undrained and seven drained triaxial tests were undertaken, in association with shear wave velocity measurements. The series of tests clearly shows that very loose samples can be prepared at void ratios well above the ASTM or British Standards methods.

3.2 Sieve Analysis

Sieve analyses were carried out on the clean Ottawa sand and selected samples of mixed sand and fines. Sieve tests were done on samples taken from the mix batch and from the triaxial test samples after completion of the triaxial test. Initial trial samples showed that a small portion of the *fines fraction* leached from the triaxial sample during the saturation phase of the test. This loss of fines was plainly visible as a coloring of the pore water discharge. Insertion of filter papers on both the top and bottom of the sample effectively retained the fines fraction of the sample. Sieve analysis done on samples prepared with and without the use of filter papers show that there is only minimal loss of fines content from samples prepared with filter papers.

It is possible that some redistribution of fines occurs during the triaxial test. However, the extent of redistribution was not considered to be significant. A visual inspection of the sample retrieved after shearing did not reveal significant fines redistribution although a thin smear of fines had accumulated on the top filter paper. It was noted that the insertion of filter paper increased the time required to saturate the sample, likely due to the formation of the thin fines smears which impeded drainage. Considering the scanning electron microscope (SEM) work done by Pitman, 1993, it was assumed that the redistribution of fines and potential sample segregation was minimal for the sample preparation and testing techniques used.

3.3 Triaxial Testing

3.3.1 TEST NOMENCLATURE

The test runs were simply labeled with the descriptors r1, r2, etc. Table 4.3 describes the triaxial conditions and percentage fines for each test. Tests were done at 0, 5, 7.5, 10 and 20% fines content. Tests r1 to r6 inclusive were used to refine the test procedure and sample preparation techniques. Tests r7 to r9 were done with clean Ottawa sand only. The no fines content tests were used to confirm the test procedure based on previous investigations done at the University of Alberta (Sasitharan 1994, Pitman 1993, Cunning 1994).

3.3.2 TEST APPARATUS

The triaxial test program undertaken for this investigation used a modified loading frame and modified triaxial cell. The modifications undertaken have been described by Cuning (1994) and are briefly described below:

3.3.2.1 Modifications to Conventional Triaxial Apparatus

3.3.2.1.1 Loading Frame

The triaxial test set up consisted of a modified Wykeham -Farrance loading frame and a modified triaxial cell. The frame and cell were modified to facilitate the set up of very loose sand samples, the use of bender elements, and the use of an internal load cell. The load frame allowed for a compensation load to be placed to facilitate isotropic loading conditions. This modification consisted of the insertion of a load transfer device to allow the wiring from the bender elements and the internal load cell to be accessed. The load frame crossbar rested directly onto the load transfer device. A rod extended through a hole in the crossbar and connected to a loading platen. Weights were placed on the platen to maintain isotropic conditions. These weights were adjusted according to the cell pressure during the back

saturation B_{bar} testing and maintained isotropic loading conditions before shearing. The overall laboratory set-up is shown on Figure 3.1.

3.3.2.1.2 Triaxial Cell

Several modifications were made to a conventional triaxial cell. These modifications included: Extension of the loading ram to allow for strain testing in excess of 20 to 25 percent; Addition of a brass extension above the load cell cap to provide support to the extended load ram; Drilling a hole through the center of the base pedestal and base plate to facilitate the bender element wiring, and; Notching along the base plate of the triaxial cell to protect the bender element wiring from the loading frame base platen.

An internal load cell was used throughout the testing program. The internal load cell was thought to measure more directly and accurately the load applied to the sample. The internal load cell device was constructed in such a way that the application of a hydrostatic pressure produced both extension and compression of the load cell due to elastic strain considerations. Since the load cell calibration factor changed based on the cell pressure it was necessary to apply different calibration factors to the load cell readings based on the cell pressure.

Scale drawings of the triaxial cell base pedestal, top cap and assembled triaxial cell are provided as Figures 3.2, 3.3, and 3.4, respectively. The internal load application portion of the triaxial assembly is detailed in Figure 3.5

3.3.2.2 Bender Elements

The load head and base were modified to incorporate bender elements that were used for the measurement of the shear wave velocity. The bender element consisted of two piezoceramic plates adhered together, sealed with a waterproof sealant and protruded about 1 cm into the sample.. Wiring for the top bender element (receiver) was done in parallel while wiring for the base bender element (transmitter) was done in series. Wires attached to the bender elements were accessed through small holes drilled through the top and bottom sample load platens. The bender elements are shown in detail on Figure 3.6. The bender elements used in this study are similar to those used by Pitman, 1993 and Sasitharan, 1994 and in the initial testing done by Cunning, 1994.

3.3.3 SAMPLE PREPARATION

Sasitharan (1994) showed that samples prepared using a moist tamping procedure were uniform after saturation and consolidation. Vaid and Neguessey (1984) determined that the use of a membrane lined sample former will inhibit the packing of pluviated samples.

Significant fines within the sand will also result in segregation due to differing falling rates and displacement phenomena. For these reasons and since most previous work at the University of Alberta was done using moist tamping techniques, it was decided to use moist tamping sample preparation techniques for all tests.

The moist tamping sample preparation technique used was identical to that used by Cunniff, 1994, with the following exceptions: Filter paper was inserted between the soil sample and porous stones for all samples to minimize the loss of fines during the sample saturation phase. Fines were added to the dry sand and mixed thoroughly before the addition of water.

The rate at which CO₂ and de-aired water were percolated through the sample prior to saturation was closely monitored and regulated. Initial trial samples showed that rapid percolation both segregation and loss on fines was possible. Pitman (1993) also made this observation. The head on de-aired water was maintained at about 1 meter while the CO₂ was applied at about 5 kPa. Using density and void ratio calculations for frozen samples, Pitman showed that samples prepared in this manner did not exhibit significant loss of fines or segregation, and maintained a uniform void ratio throughout the sample.

All sample preparation and triaxial testing was done at an ambient temperature of 22°C.

3.3.4 CALCULATION OF VOID RATIO

An accurate void ratio determination is essential if the triaxial testing and shear wave velocity measurements are to be meaningfully related. The accurate measurement of the sample weight and dimensions before testing is essential if the void ratio is to be accurately determined. It is also necessary to track the void ratio, as calculated immediately after removing the sample mold, throughout the test setup up to the initiation of undrained loading. To do this the measurements and checks listed in Table 3.1, were used. The void ratio was determined using the following relationship that incorporates a volumetric correction for membrane penetration:

$$e = \frac{G_s \left(V_{cd} + \Delta V - 0.0045 \log \left(\frac{CP}{CP_c} \right) (A_s) \right)}{Wg} - 1 \quad (3.2)$$

- where:
- e** = Void Ratio
 - G_s** = Specific gravity of sand (g/cm³)
 - V_{cd}** = Volume at the start of consolidation (cm³)
 - ΔV** = Change in volume during back pressure saturation and consolidation (cm³)
 - 0.0045** = slope of the unit membrane correction versus effective confining pressure for clean Ottawa sand (cm³/cm²/log effective stress)
 - CP** = Base value of effective confining pressure, usually 50 kPa
 - CP_c** = Current effective confining pressure (kPa)
 - A_s** = Surface area of soil covered by membrane (cm²)
 - Wg** = Dry weight of specimen (g)

Vaid and Negussey (1984) suggest a membrane penetration correction factor of 0.0048 cm³/cm² for Ottawa sand with a mean grain size, D₅₀, of 0.35 mm. Sladen and Handford (1987) suggest a membrane penetration factor of 0.0015 cm³/cm² for Syncrude sand with a D₅₀ much smaller than that of Vaid and Negussey's Ottawa sand. A membrane correction factor of 0.0045 was used for all levels of fine content in this study. This value was considered to be somewhat conservative based on calculated D₅₀ values. In any case the correction for membrane penetration is small and affects the calculated void ratio by only ±0.003 for membrane correction factors between 0 and 0.007 cm³/cm² and effective confining pressures below 550 kPa.

3.3.5 SATURATION PHASE

Samples were saturated by first percolating CO₂ through both bottom sample drainage ports for a minimum of 30 minutes each side. This deaired the sample prior to saturation with water. About 5 sample volumes of deaired, deionized water was then trickling through each port under a head of about 10 kPa. Depending on the percentage of fines present this step took from 15 minutes to 4 hours per port. Sample settlement was measured during this phase. Samples with a lower percentage of fines were noted to settle marginally more than higher fines content samples but settlement was not greater than 1 mm in any case.

A series of back saturation B_{bar} tests were then undertaken to ensure that an adequate level of sample saturation was established. This was achieved by alternately increasing the cell

pressure and back pressure by 50 kPa increments and measuring the pore pressure response during each increment. Most samples achieved a minimum B_{bar} value of 0.95 with a cell pressure and back pressure of 500 and 450 kPa respectively. Dense samples required higher cell and back pressure levels to achieve the desired B_{bar} value. This procedure established a starting pre-consolidation p' value of about 50 kPa for each sample.

3.3.6 CONSOLIDATION PHASE

All samples were consolidated in 100 kPa increments to the desired initial mean confining pressure, p'_o from a starting p' value of about 50 kPa. A compensating load was applied simultaneously as the cell pressure was increased. The compensating load was placed to maintain isotropic loading conditions. Consolidation was considered to be complete for each load application if the volume measuring device showed minimal change. The change in volume and height of the sample was used to monitor the void ratio change during each consolidation phase. Consolidation was usually complete within 30 minutes per load increment.

3.3.7 SHEAR WAVE VELOCITY MEASUREMENTS

A bender element is a piezoceramic transducer that is capable of converting electrical signals to mechanical waves as well as mechanical waves into electrical signals. The bender element was developed by Shirley (1978) to determine shear wave velocity. Bender elements and similar concept shear wave measuring devices have been incorporated into many types of geotechnical testing apparatus, such as cone penetrometer, resonant columns, etc. (Ryne and Dyvik(1985), de Alba (1986)). With the bender elements in both the head and the base aligned properly, a shear wave can be generated at the top bender by applying a discrete wave pattern by means of a wave generator. A compression wave and a shear wave are pulsed through the soil from the transmitter to the receiver bender. The received signal is amplified and displayed on a digital oscilloscope from which the arrival of the shear wave can be determined. The height of the sample is known as well as the travel time of the shear wave, thus the shear wave velocity can be determined. The shear wave arrival was interpreted according to the methods described by Brignoli, *et al.* (1994).

Shear wave measurements were taken at the completion of each consolidation phase for selected samples. The sample height and void ratio were calculated at the completion of each consolidation phase to determine the shear wave travel length and sample state. All shear wave measurements were taken using protruding benders as described by Pitman (1993). Trial tests with flush mounted benders, as described by Cuning (1994) were used for shear wave measurements done for the Hong Kong Pearl River Sand. A comparison of the two techniques showed that the protruding benders were somewhat more robust at higher stresses

but produced a slightly more ambiguous wave signal as well. Shear wave measurements were attempted at steady state conditions. However, the signal clarity was inadequate to provide meaningful interpretation of arrival times.

The shear wave velocity was calculated using:

$$V_s = \frac{(H_c - 21.52)}{1000T_t} \quad (3.2)$$

where: V_s = Shear wave velocity [m/s]
 H_c = Current height of the specimen [mm]
 T_t = Arrival time of the shear wave [sec]

3.3.8 SHEARING PHASE

Based on work by Robertson and Skirrow (1994) All samples were tested undrained under constant strain rate controlled conditions. The modified load apparatus ensured that the compensating load was maintained at all time during the shearing phase. A constant strain rate of 0.15 mm/minute was used throughout the test program. The shear testing was continued until steady state was achieved, or until the strain level was considered excessive. Nearly all samples were strained to greater than 20 percent. The pore pressure, cell pressure, back pressure, vertical displacement, and vertical load on the sample area were monitored using electronic pressure transducers LVDT devices. All data was recorded in an IBM XT computer using a Fluke 2400s data logger. The data sampling frequency was rapid during the first 5 percent of strain and periodic thereafter.

3.4 Problems Observed During the Test Program

Several minor problems were encountered during the test program. The first seven tests were abandoned for a variety of reasons, mostly associated with equipment and procedural problems. The problems were resolved through improved procedure checks and equipment maintenance between each test. The main problems that were encountered are listed below:

Lack of vacuum pressure during sample preparation resulting in sample collapse.

Sample disturbance during movement from preparation area to loading frame.

Perforation or tearing of the membrane.

Poor seal of membrane, or cell due to grit or worn "O" rings.

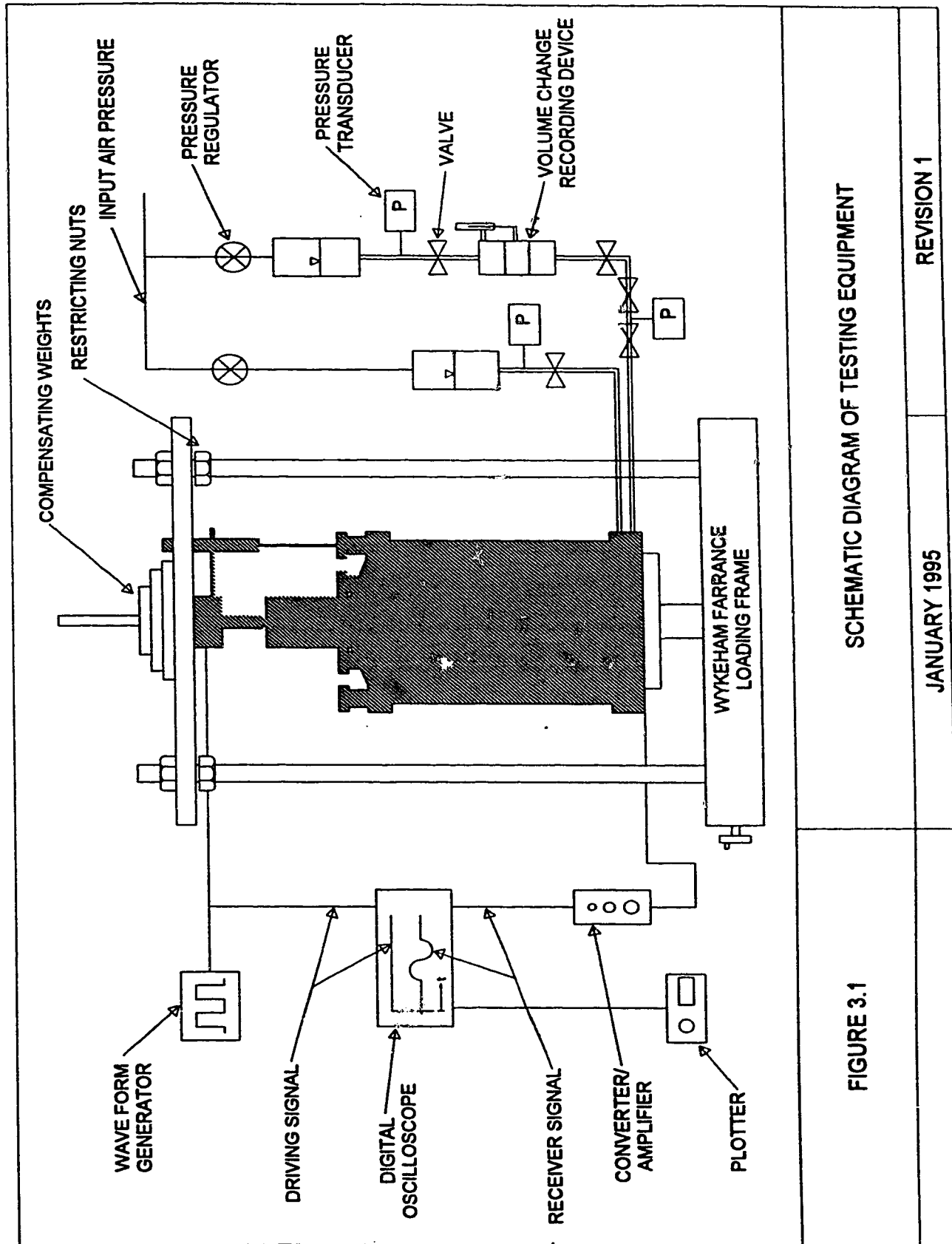
Impact loading of compensation load.

Loss of control board pressure during building maintenance operation.

Jamming of the volume control device preventing egress of consolidation water.

**TABLE 3.1
Procedures Used to Maintain Continuous Void Ratio Tracking**

Step	Procedure
1	<p>Sample preparation</p> <p>Weigh mixed sample before filling triaxial mold sample and after completion of the mold sample. Make sure that there is no spillage during sample construction. Dry retained mixture and calculate weight of sand and fines not used.</p>
2	<p>Sample preparation</p> <p>Measure sample height using dial gauge and reference sample. Measure height of triaxial base, soil sample and load piston assemble. (Dimension H) Measure sample diameter using calipers and sample circumference using tape measurements. The sample diameter & circumference was measured at a minimum of three elevations. Samples with dimensions that deviated more than 1% from the average were remade. Calculate sample volume and initial void ratio.</p>
3	<p>Application of vacuum to sample</p> <p>Measure dimension H before and after switching vacuum pressure from external (mold) to internal (sample). Calculate new sample volume assuming all volume change is associated with a height reduction, that is no circumferential change.</p>
4	<p>Triaxial cell assembly</p> <p>Measure dimension H after assembly of triaxial cell. Setup LVDT and get initial reading relative to dial gauge reading for dimension H</p>
5	<p>Application of cell pressure and discontinuation of vacuum pressure</p> <p>Measure change in height using both dial gauge and LVDT.</p>
6	<p>Saturation Phase</p> <p>Settlement during saturation of the sample was considered to be axial only.</p>
7	<p>Consolidation Phase</p> <p>Changes in volume measured with volume change device, new volume and LVDT readings used to determine current cross section area.</p>
8	<p>Triaxial test</p> <p>Further axial strains were measured using the LVDT. Volumetric strains calculated using elastic theory.</p>

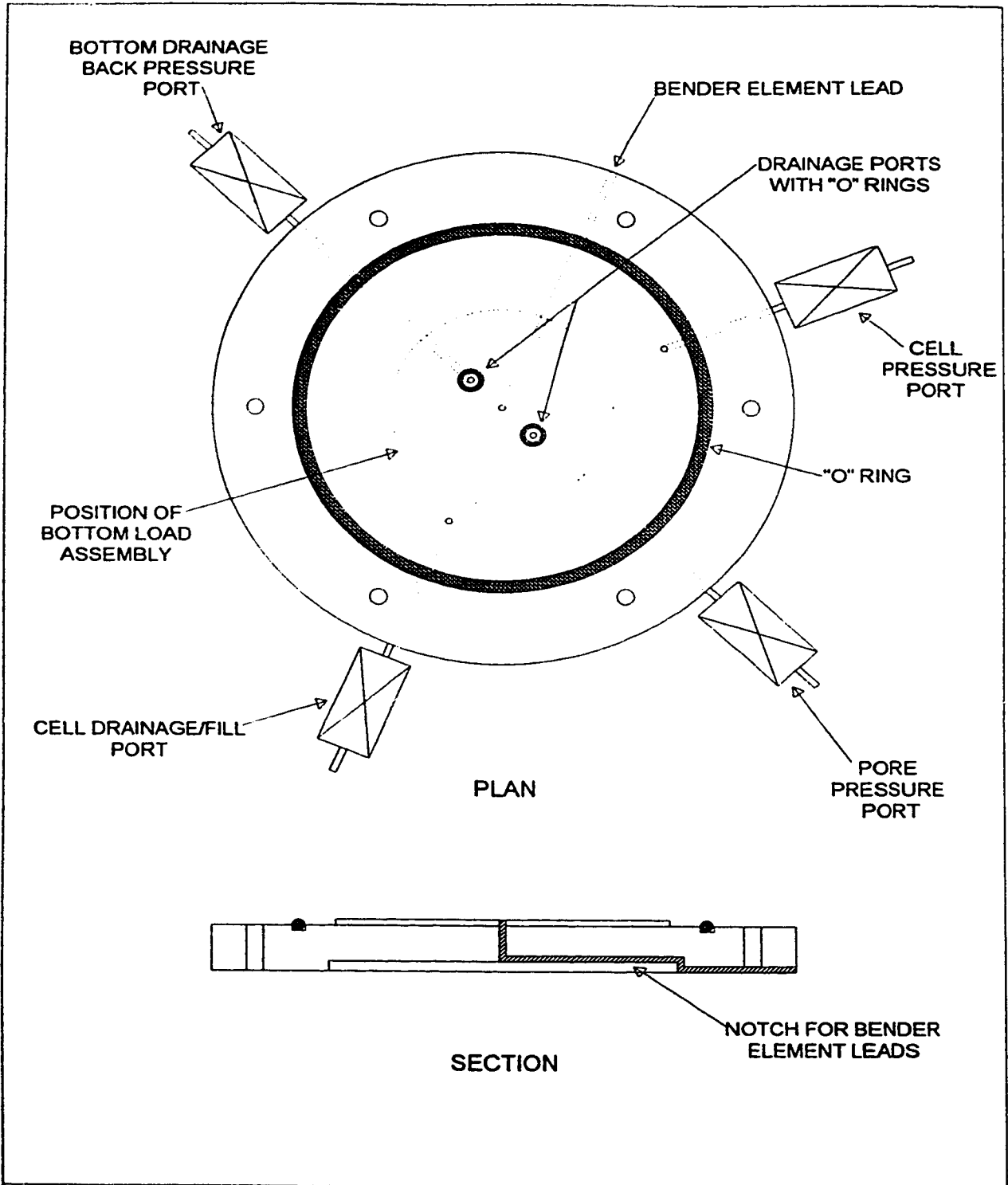


SCHEMATIC DIAGRAM OF TESTING EQUIPMENT

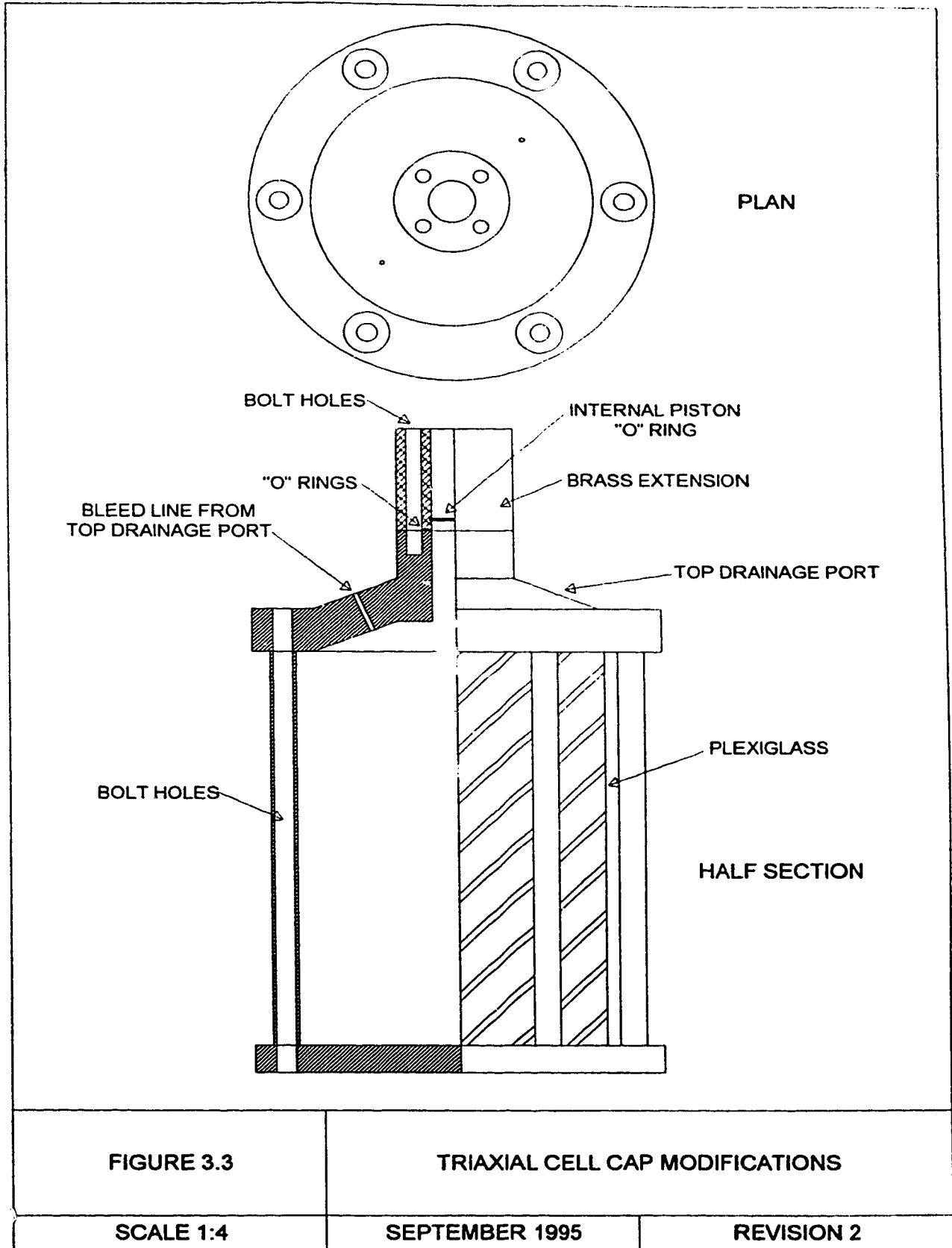
FIGURE 3.1

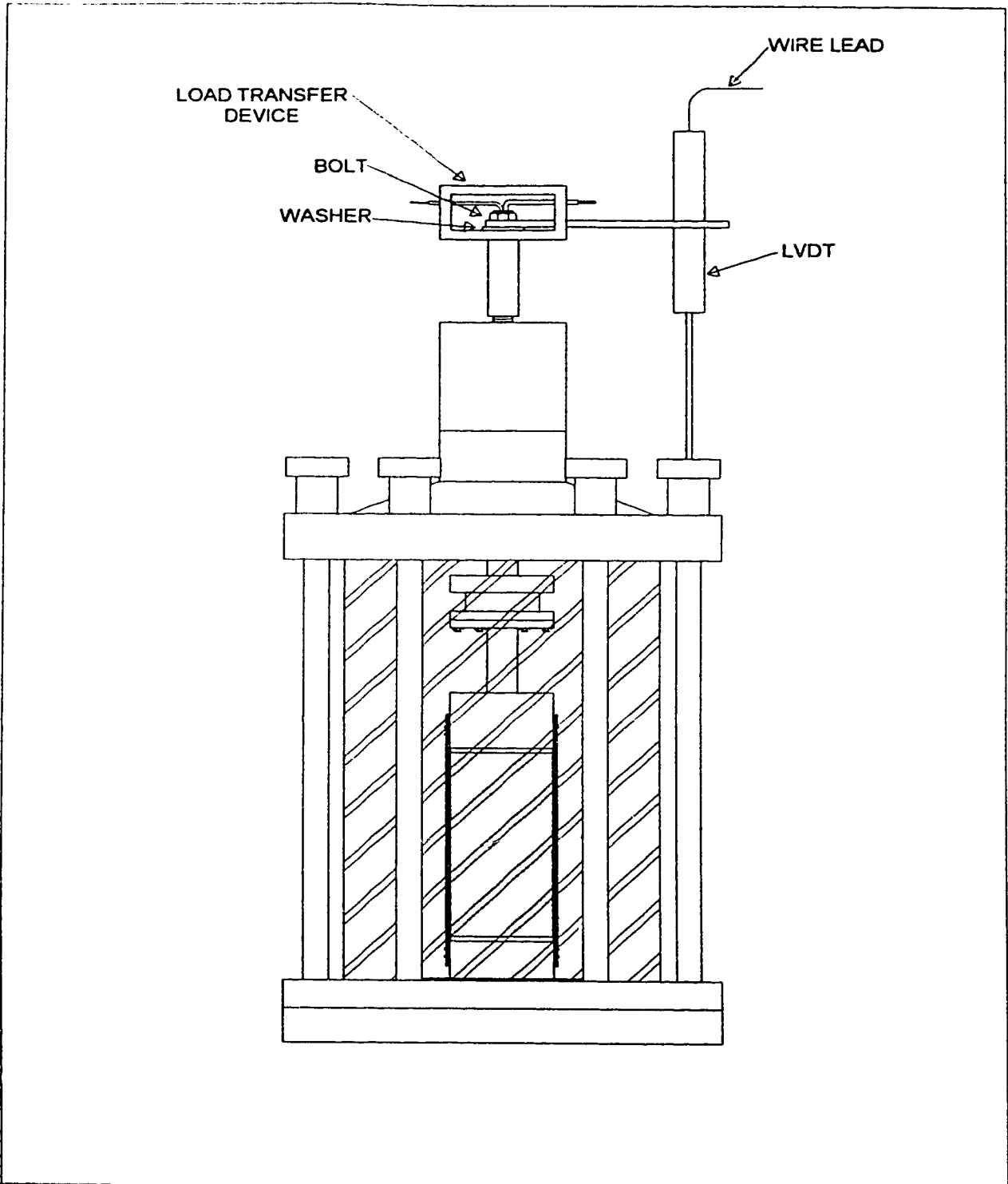
REVISION 1

JANUARY 1995



<p>FIGURE 3.2</p>	<p>TRIAXIAL CELL BASE MODIFICATIONS</p>	
<p>SCALE 1:3</p>	<p>SEPTEMBER 1995</p>	<p>REVISION 2</p>





<p>FIGURE 3.4</p>	<p>ASSEMBLED TRIAXIAL CELL</p>	
<p>SCALE 1:4</p>	<p>SEPTEMBER 1995</p>	<p>REVISION 2</p>

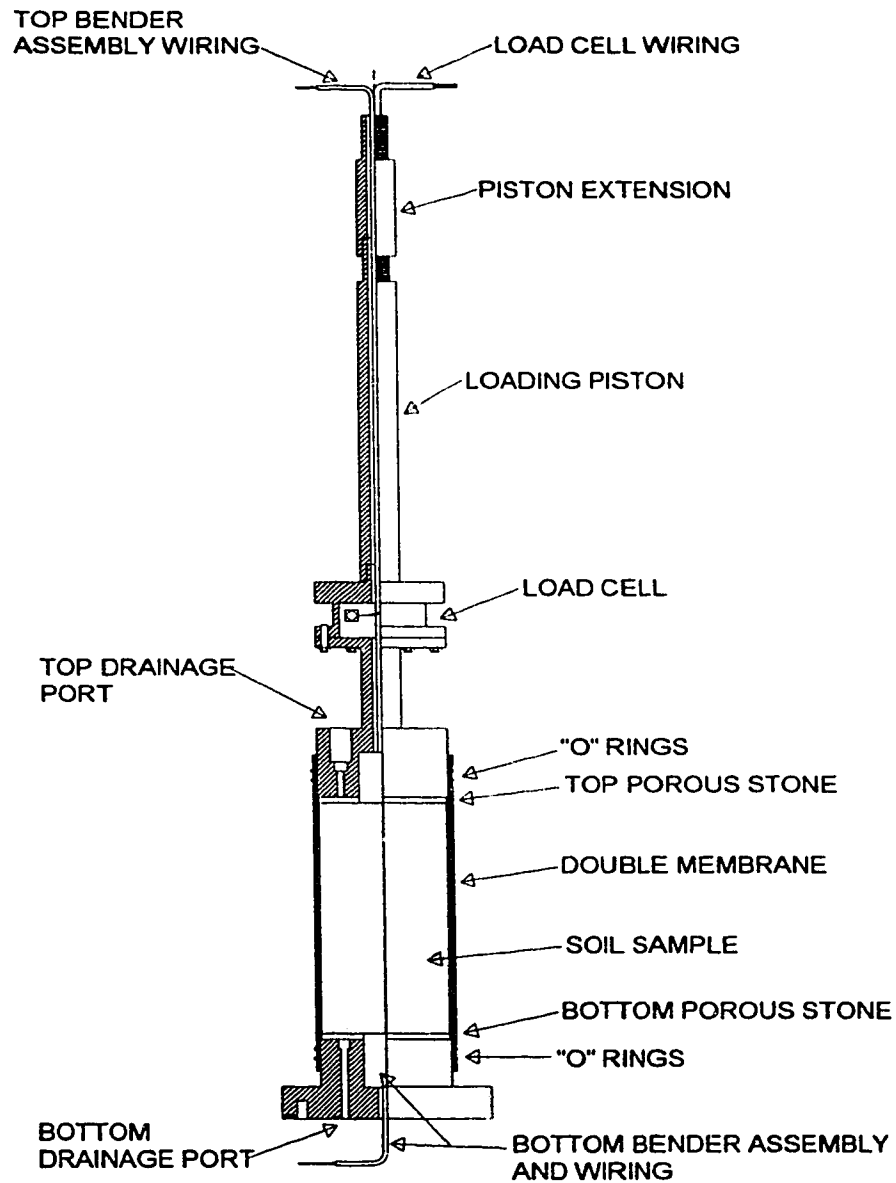


FIGURE 3.5

HALF-SECTION OF LOADING PORTION OF TRIAXIAL CELL WITH SHEAR WAVE BENDER ASSEMBLY

SCALE 1:4

SEPTEMBER 1995

REVISION 2

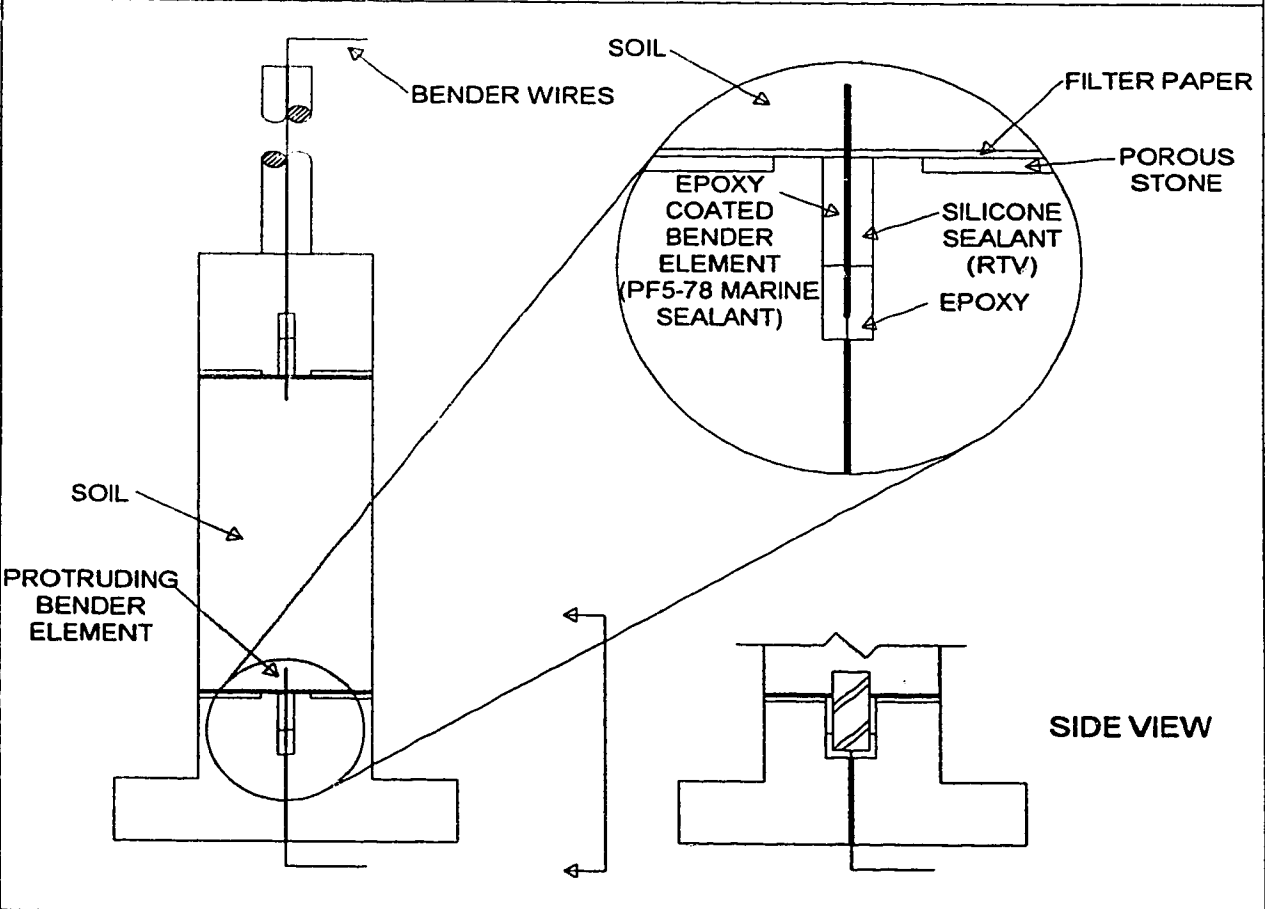
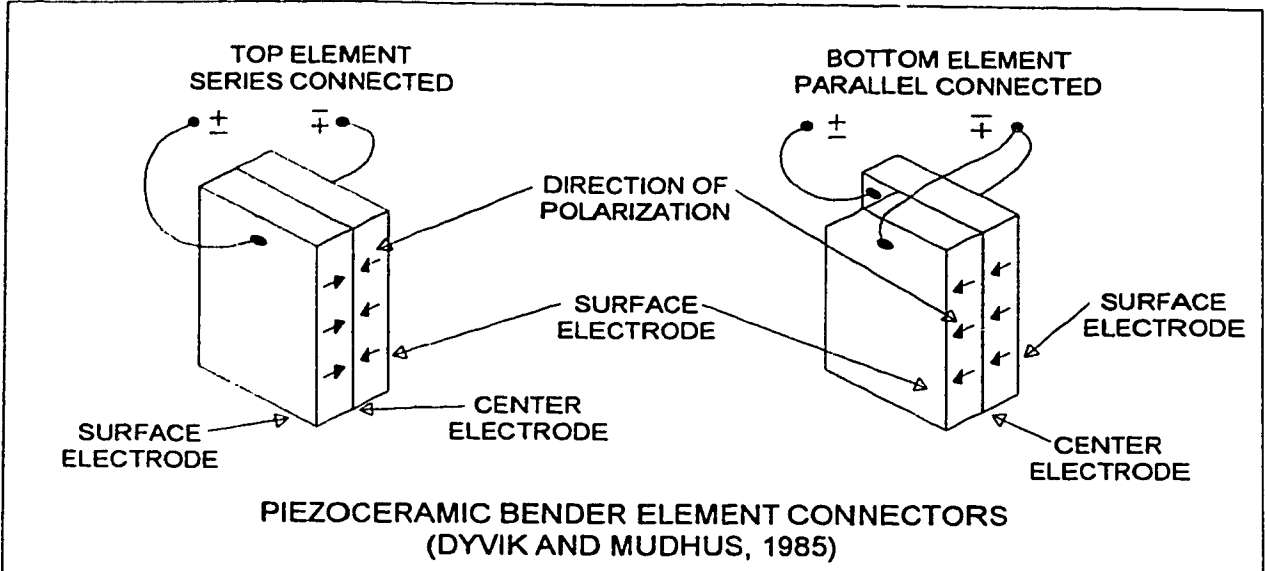


FIGURE 3.6

PROTRUDING BENDER ELEMENT SCHEMATIC WITH DETAILS

SEPTEMBER 1995

REVISION 2

REVISION 2

4. RESULTS

4.1 Sieve Analysis

Selected representative sieve analysis results are presented in Table 4.1. These results are plotted on Figure 4.1. The D_{10} , D_{60} and c_u values determined from the grain size analysis are shown on Table 4.2.

4.2 Void Ratio

The void ratio was determined at each step of the testing sequence. Table 4.3 provides a summary of the calculated void ratios at significant steps during the testing. The void ratio results were further grouped to simplify comparisons and to show the densest and loosest states attained at each percentage of fines added. These results are shown on Table 4.4.

Due to the limitations of the device used to measure the initial sample dimensions, the samples size and mass, and changes in volume, the accuracy of the calculated void ratios was determined to be within $\pm 2\%$ of the calculated void ratio. The accuracy of several measurements, and the associated void ratio accuracy (based on a calculated void ratio of 0.8, typical sample dimensions and 10% fines content) are as follows: Height of sample, ± 0.1 mm (± 0.0012); Diameter of samples, ± 0.1 mm (± 0.0047); Specific gravity of sand, ± 0.01 g/cm³ (0.0062); Specific gravity of fines, ± 0.01 g/cm³ (0.0006); Mass of sand, ± 0.1 g (0.0029); Mass of fines, ± 0.1 g (0.0001); Volume change device measurements, ± 0.01 cc (0.00027). A margin of accuracy of ± 0.016 is thereby determined for a calculated void ratio of 0.800 ($\pm 2\%$).

4.3 Triaxial Test

Twenty-five triaxial tests were undertaken. Nineteen of these tests produced quantitative results. Six tests were terminated due to difficulties during the test. Shear wave measurements were taken during the consolidation portion of six triaxial tests that were consolidated to 450 kPa.

The test conditions are summarized in Table 4.5. The triaxial test samples were isotropically consolidated to the initial mean confining pressures shown on Table 4.5. The minimum \bar{B} was 0.96, with an average \bar{B} value of 0.98. To reach the desired \bar{B} level it was necessary to undertake back pressure saturation cycles to 250 to 750 kPa.

4.3.1 DEVIATOR STRESS - STRAIN

For an undrained compressive triaxial test the deviator stress, denoted as "q", is defined as the load, as recorded by the internal load cell, divided by the corrected cross sectional area of the sample. Figures 4.2, 4.3, 4.4 show the deviator stress plotted against percentage strain for the series of tests done at 5%, 7.5%, and 10% fines, respectively. Figures 4.5, 4.6, and 4.7 show the deviator stress plotted against percentage strain for the loose test only, and exclude the single dense samples at each fines content level.

Figures 4.5, 4.6 and 4.7 show that the maximum deviator stress is developed within 2% strain. Of the 12 tests carried out on loose samples, three tests displayed a quasi steady state or plateau condition as described earlier. For these three tests the post initial peak minimum occurred at 7 to 10% strain. Review of the initial sample preparation void ratio indicates these three tests (r13 - 5% fines at $P'_c = 350$ kPa, r17 - 7.5% fines at $P'_c = 250$ kPa, and r18 - 7.5% fines at 150 kPa) were not prepared at as loose a state as possible. The remaining nine tests shown on Figures 4.5, 4.6 and 4.7 showed a substantial loss of strength after attaining peak stress. Near steady state conditions were reached within about 10% strain with little further reduction in deviator stress beyond 20% strain.

Figures 4.2, 4.3 and 4.4 include the results of the testing carried out on samples prepared to the densest state possible. The deviator stress - strain curves for the dense tests typically reach a peak within about 4% strain, beyond which the deviator stress reduces to a steady state value. The limitation of the testing apparatus and monitoring devices makes for difficulty in assessment of steady state conditions for the dense samples. This was particularly evident for the pore pressure response, as discussed below. A loss of control board pressure during testing for sample r28 (7.5% fines, $P'_c = 450$ kPa) resulted in a dramatic loss of cell pressure before the implementation of corrective measures. The results for this test are included for completeness only and for the shear wave measurements taken during consolidation.

4.3.2 PORE PRESSURE - STRAIN

Figures 4.8, 4.9 and 4.10 show the excess pore pressure developed during the shearing portion of the triaxial test plotted against percentage strain. Figures 4.11, 4.12 and 4.13 show the excess pore pressure developed during testing of very loose samples only. The pore pressure plots were similar for most tests and showed a rapid increase in pore pressure during the first five percent strain after which little change in pore pressures developed. The pore pressure at five percent strain and the maximum excess pore pressure developed are summarized in Table 4.6.

The pore pressure plots for the very dense tests showed an initial increase in pore pressure followed by a rapid decrease in pore pressure, associated with sample dilation. The final excess pore pressures measured were in the range of negative 320 to 350 kPa that are in the range of the initial sample pore pressures. Greater negative pore pressures could have developed if the initial pore pressures were greater. The testing of very dense samples requires high initial pore pressures, and therefore high initial cell pressures, to allow for large negative excess pore pressure to develop. The physical limitations of the triaxial test cell used did not allow for significantly greater initial cell pressures to be safely developed.

4.3.3 DEVIATOR STRESS - MEAN EFFECTIVE PRESSURE STRESS PATHS

The stress paths for the triaxial tests are shown in Figures 4.14, 4.15 and 4.16. These plots show the deviator stress, q , versus mean effective pressure, p' , for the 5, 7.5 and 10 percent fines content tests respectively. Figures 4.17, 4.18 and 4.19 plot the p' - q diagram for only the loose samples for the 5, 7.5 and 10 percent fines content tests respectively. The loose samples typically show a slight increase in p' and q within the initial two percent strain, followed by a decrease in p accompanied by increasing q . A peak q value is reached between two to four percent strain, after which both the q and p' values both decrease to steady state values.

4.3.4 NORMALIZED DEVIATOR STRESS - NORMALIZED MEAN EFFECTIVE PRESSURE

Figures 4.14 to 4.19 provide an overall view of the stress path response of the triaxial tests. However, to compare the behavior across a wide range of stress levels a normalized approach is preferred. Figures 4.20, 4.21 and 4.22, representing the 5, 7.5 and 10 percent fines content tests, show the stress paths normalized by dividing both the q and p' values by the corresponding p'_{es} determined for that test. These figures provide a useful means of comparing the stress path behavior of dense and very loose samples tested at a wide range of confining stresses

4.3.5 VOID RATIO - MEAN EFFECTIVE PRESSURE

The changes in state during the triaxial test are shown on the void ratio - log mean effective pressure diagrams, Figures 4.23, 4.24 and 4.25. These figures show the changes in void ratio plotted against the log of mean effective pressure for the 5, 7.5 and 10 percent fines content test, respectively. Figures 4.26, 4.27, and 4.28 show the maximum, minimum and steady state lines determined for each level of fines content.

4.4 Shear Wave Velocity Results

Shear wave measurements were taken during the consolidation portion of six triaxial tests. The loosest and densest samples consolidated to an initial mean confining stress of 450 kPa at each of the 5, 7.5 and 10 percent fines were used for shear wave velocity measurements. The shear wave velocities measured and the associated void ratio and mean confining stress are presented in Table 4.7. Shear wave measurements were attempted at steady state conditions with little success. A typical shear wave plot is shown on Figure 4.29. Figure 4.30 shows the shear wave velocity plotted against void ratio for all test results.

The determination of the arrival time was carried out according to procedures outlined by Brignoli, *et al.* (1994). The majority of shear wave plots were well behaved and relatively straightforward to interpret. However the shear wave plots at higher mean confining stress had smaller amplitudes that were not amenable to magnification or signal processing making interpretation difficult and subject to personal judgment. This reduction in signal quality and clarity of interpretation makes the results of shear wave velocity measurements operator dependent. This observation is discussed in greater detail in Section 5.4.

**TABLE 4.1
REPRESENTATIVE SIEVE ANALYSIS RESULTS
OTTAWA SAND WITH KAOLINITE FINES**

Grain Size	Ottawa Sand % finer than	Kaolinite % finer than	5% fines		10% fines			7.5% Fines	
			Initial	Final with no paper	Initial	Final with no paper	With Filter paper	Initial	Final with no paper
0.84	100.00	100.00	100.00	100.00	100.00	100.00	100.00	100.00	100.00
0.52	71.00	100.00	72.45	72.15	73.90	73.40	73.85	73.18	72.78
0.25	21.00	100.00	24.95	24.65	28.90	28.40	28.85	26.93	26.53
0.148	3.00	100.00	7.85	7.55	12.70	12.20	12.65	10.28	9.88
0.074	0.00	100.00	5.00	4.70	10.00	9.50	9.95	7.50	7.10
0.025	0.00	100.00	5.00	4.70	10.00	9.50	9.95	7.50	7.10
0.015	0.00	98.00	4.90	4.60	9.80	9.30	9.75	7.35	6.95
0.009	0.00	91.00	4.55	4.25	9.10	8.60	9.05	6.83	6.43
0.005	0.00	80.00	4.00	3.70	8.00	7.50	7.95	6.00	5.60
0.0008	0.00	42.50	2.13	1.83	4.25	3.75	4.20	3.19	2.79

**TABLE 4.2
D₁₀, D₆₀ AND c_u RESULTS
OTTAWA SAND WITH KAOLINITE FINES**

	Ottawa Sand	Kaolinite	5% Fines		7.5% Fines		10% Fines		
			Initial	Final with no paper	Initial	Final with no paper	Initial	Final with no paper	With paper
D ₁₀ (mm)	0.22	na	0.17	0.18	0.10	0.12	0.07	0.08	0.08
D ₆₀ (mm)	0.45	na	0.43	0.44	0.42	0.43	0.41	0.41	0.42
C _u	2.05	na	2.52	2.50	4.42	3.70	5.56	4.91	5.57

TABLE 4.3
VOID RATIO CALCULATIONS
OTTAWA SAND WITH ADDED KAOLINITE FINES

Test No.	% Kaolinite	Void Ratio		
		Initial Set up	After Saturation	After Final Consolidation
r7	0	0.762	0.740	0.719
r8	0	0.898	0.898	0.819
r9	0	0.925	0.914	0.807
r13	5	0.701	0.679	0.623
r14	5	0.761	0.761	0.725
r15	5	0.754	0.746	0.705
r23	5	0.838	0.787	0.700
r26	5	0.518	0.510	0.457
r16	7.5	0.699	0.695	0.654
r17	7.5	0.603	0.606	0.583
r18	7.5	0.642	0.640	0.599
r27	7.5	0.810	0.805	0.617
r28	7.5	0.492	0.490	0.448
r10	10	0.580	0.581	0.479
r11	10	0.605	0.609	0.541
r12	10	0.651	0.649	0.627
r22	10	0.812	0.802	0.501
r25	10	0.470	0.469	0.422
r19	20	0.771	0.592	0.549

TABLE 4.4
SUMMARY OF VOID RATIO SHOWING LOOSEST
AND DENSEST STATE ATTAINED
OTTAWA SAND WITH ADDED KAOLINITE FINES

Percentage of Kaolinite Fines Added	Void Ratio		
	Loosest		Densest
	Initial	Final	
0	0.925	0.819	na
5	0.838	0.725	0.457
7.5	0.810	0.654	0.448
10	0.812	0.627	0.422
20	0.771	0.549	na

TABLE 4.5
SUMMARY OF TEST CONDITIONS
OTTAWA SAND WITH ADDED KAOLINITE FINES

Test No.	Percentage Kaolinite Fines Added	Initial Cell Pressure (kPa)	Initial Back Pressure (kPa)	σ'_{3c} (kPa)	Initial Pore Pressure (kPa)	Initial \bar{e} Value
r7	0	600	250	350	260	1.00
r8	0	800	450	350	460	0.99
r9	0	700	350	350	347	1.01
r13	5	600	250	350	250	0.97
r14	5	900	650	250	625	0.97
r15	5	900	750	150	708	0.96
r23	5	1100	650	450	633	0.96
r26	5	800	350	450	339	0.96
r16	7.5	1000	650	350	629	0.97
r17	7.5	900	650	250	630	1.03
r18	7.5	800	650	150	626	1.01
r27	7.5	1100	650	450	631	0.96
r28	7.5	800	350	450	327	0.96
r10	10	600	250	350	249	0.97
r11	10	700	450	250	446	0.97
r12	10	400	250	150	248	0.98
r22	10	1100	650	450	634	0.96
r25	10	900	450	450	433	0.98
r19	20	600	450	150	466	0.96

**TABLE 4.6
EXCESS PORE PRESSURES DEVELOPED DURING TRIAXIAL TESTING
OTTAWA SAND WITH ADDED KAOLINITE FINES**

Test No.	% Kaolinite	Excess Pore Pressure—u		
		At 5% strain (kPa)	At steady state (kPa)	$= \frac{u}{P'_{initial}}$
r7	0	na	na	na
r8	0	0	0	0
r9	0	308	317	0.91
r13	5	117	57	0.16
r14	5	225	232	0.93
r15	5	124	131	0.87
r23	5	420	422	0.94
r26 [~]	5	-390	-385	-0.85
r16	7.5	306	320	0.91
r17	7.5	184	195	0.78
r18	7.5	89	80	0.53
r27	7.5	404	417	0.93
r28	7.5	-204	-323	-0.72
r10	10	278	299	0.85
r11	10	213	222	0.89
r12	10	131	136	0.91
r22	10	392	408	0.91
r25	10	-437	-437	-0.97
r19	20	113	120	0.80

- drained test ~ - limited due to low initial pore pressure and transducer limitations

**TABLE 4.7
SHEAR WAVE VELOCITY MEASUREMENTS
OTTAWA SAND WITH FINES**

Sample	% Fines	Mean Confining Pressure p' (kPa)	Void Ratio e	V_s (m/s)
r23	5	20	0.813	120
		50	0.787	161
		150	0.743	215
		250	0.725	274
		350	0.711	303
		450	0.700	330
r26	5	50	0.510	205
		150	0.509	277
		250	0.476	331
		350	0.469	369
		450	0.457	403
r27	7.5	50	0.805	148
		150	0.715	205
		250	0.673	266
		350	0.636	321
		450	0.617	356
r28	7.5	50	0.490	205
		150	0.476	278
		250	0.467	324
		350	0.457	359
		450	0.448	391
r22	10	50	0.802	145
		150	0.675	235
		250	0.596	281
		350	0.548	305
		450	0.501	360
r24	10	50	0.797	150
		150	0.767	171
		250	0.731	189
		350	0.702	234
		450	0.689	315

FIGURE 4.1 GRAIN SIZE DISTRIBUTION FOR SELECTED SAMPLES

Ottawa Sand with Varying Kaolinite Fines Content

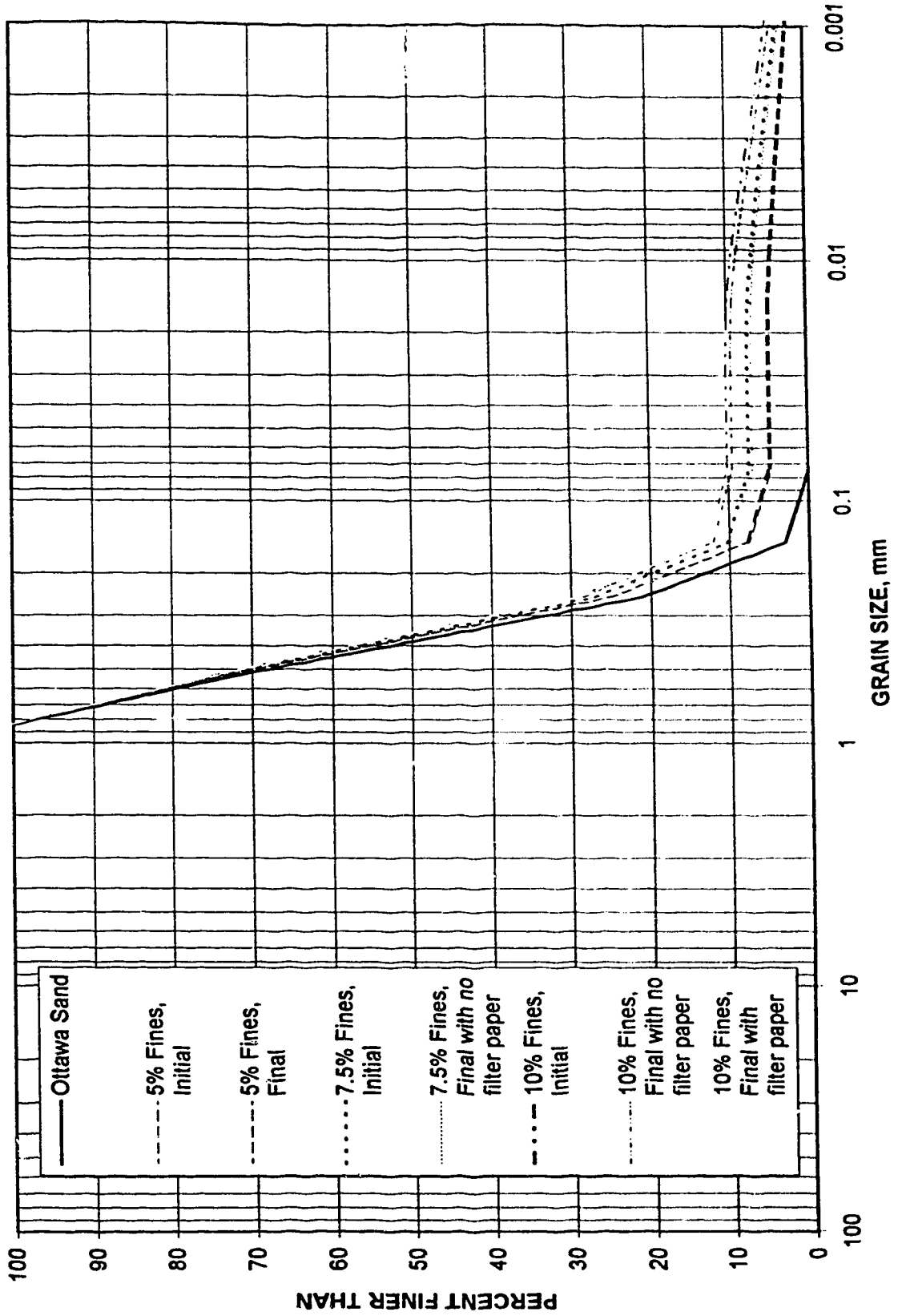


FIGURE 4.2 DEVIATOR STRESS versus STRAIN
Ottawa Sand with 5% Kaolinite

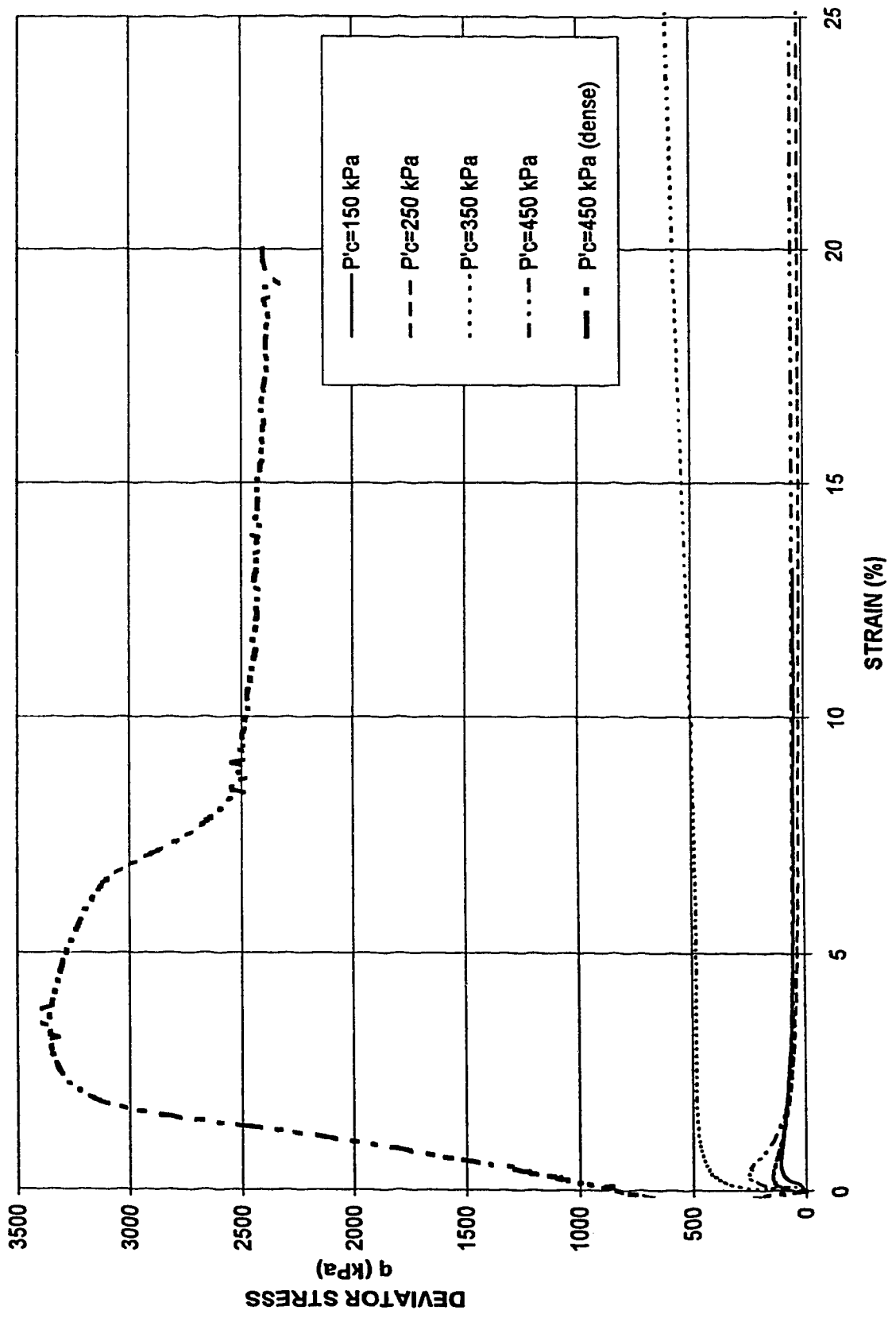
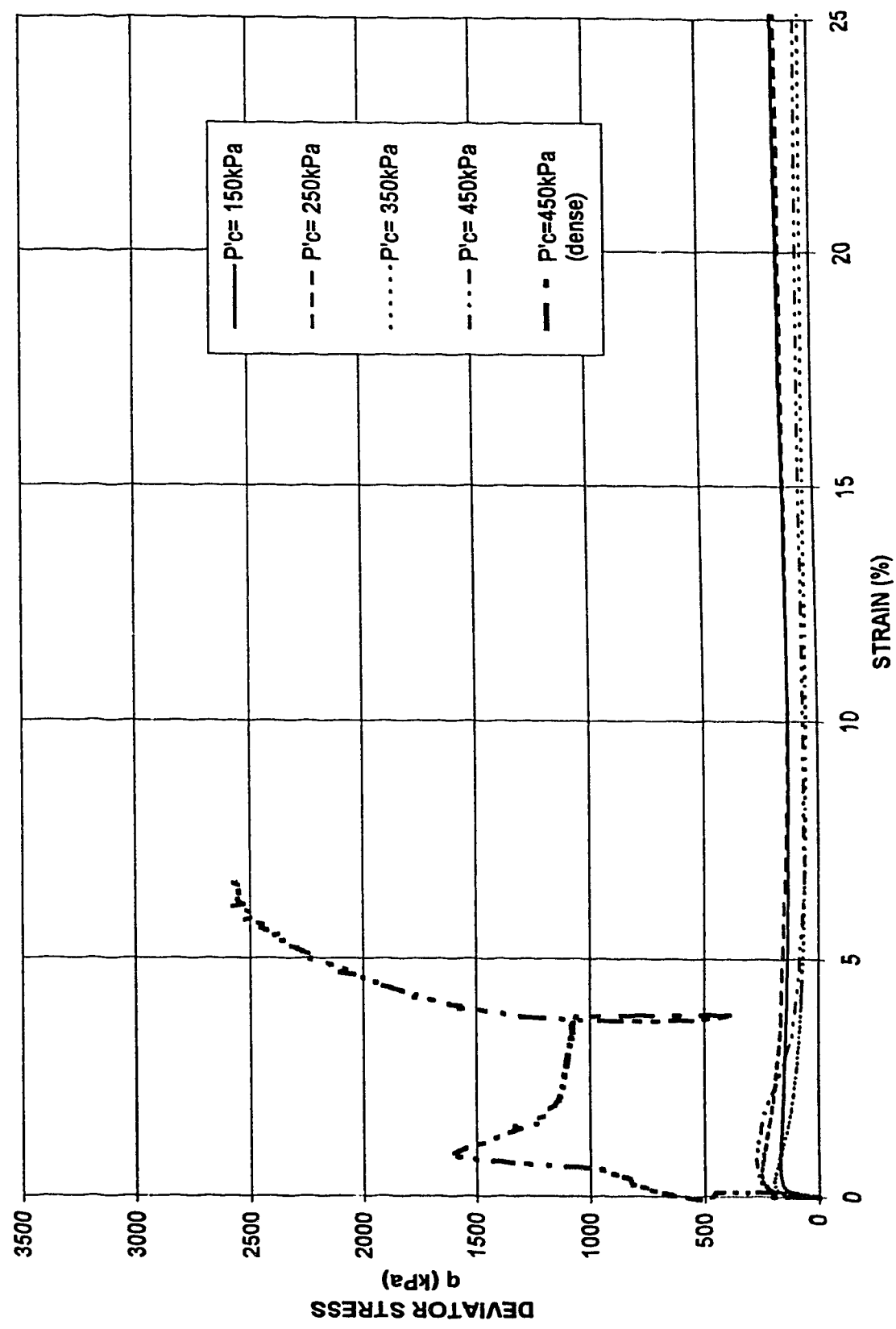
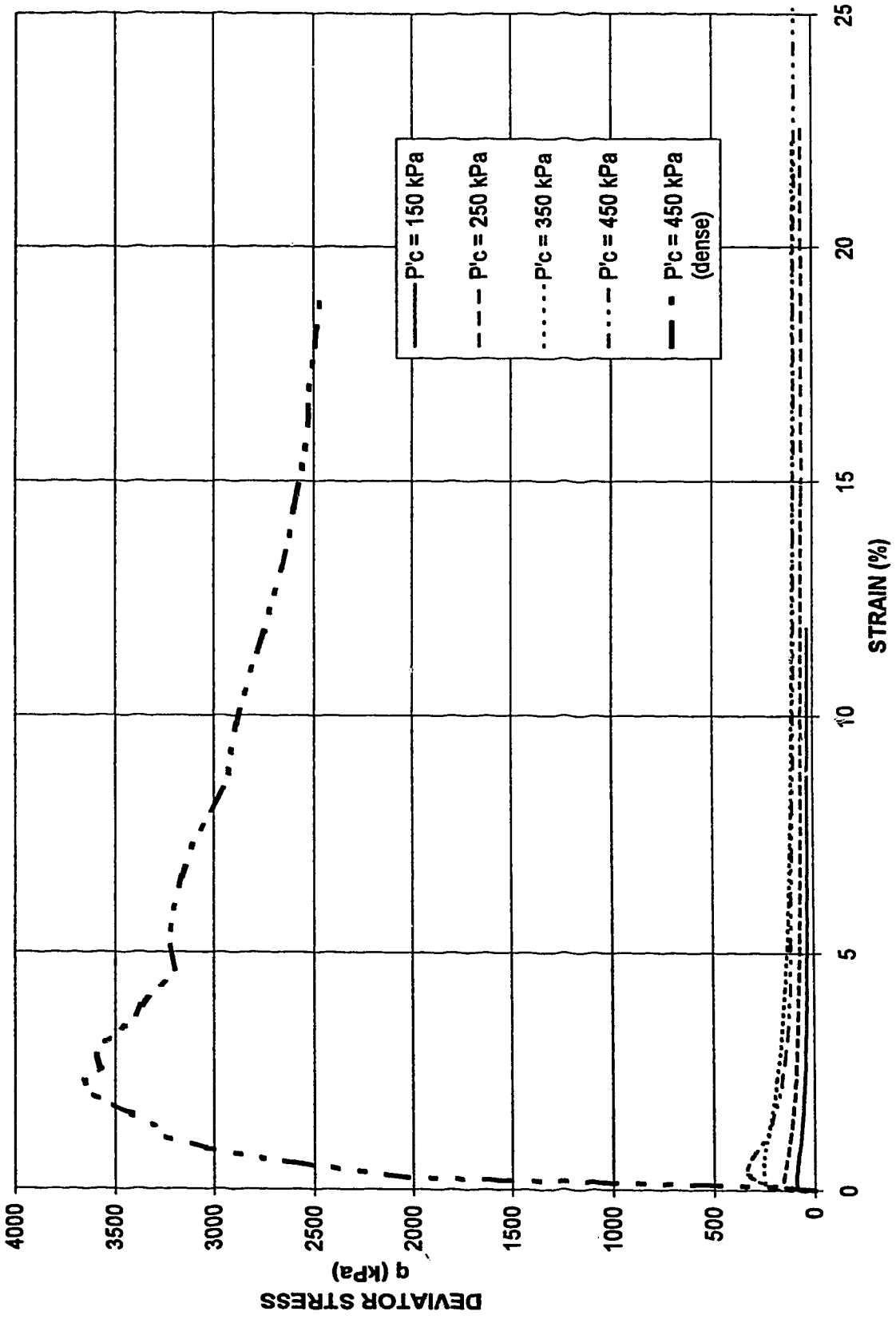


FIGURE 4.3 DEVIATOR STRESS versus STRAIN
Ottawa Sand with 7.5% Kaolinite



**FIGURE 4.4 DEVIATOR STRESS versus STRAIN
Ottawa Sand with 10% Kaolinite**



**FIGURE 4.5 DEVIATOR STRESS versus STRAIN
Ottawa Sand with 5% Kaolinite**

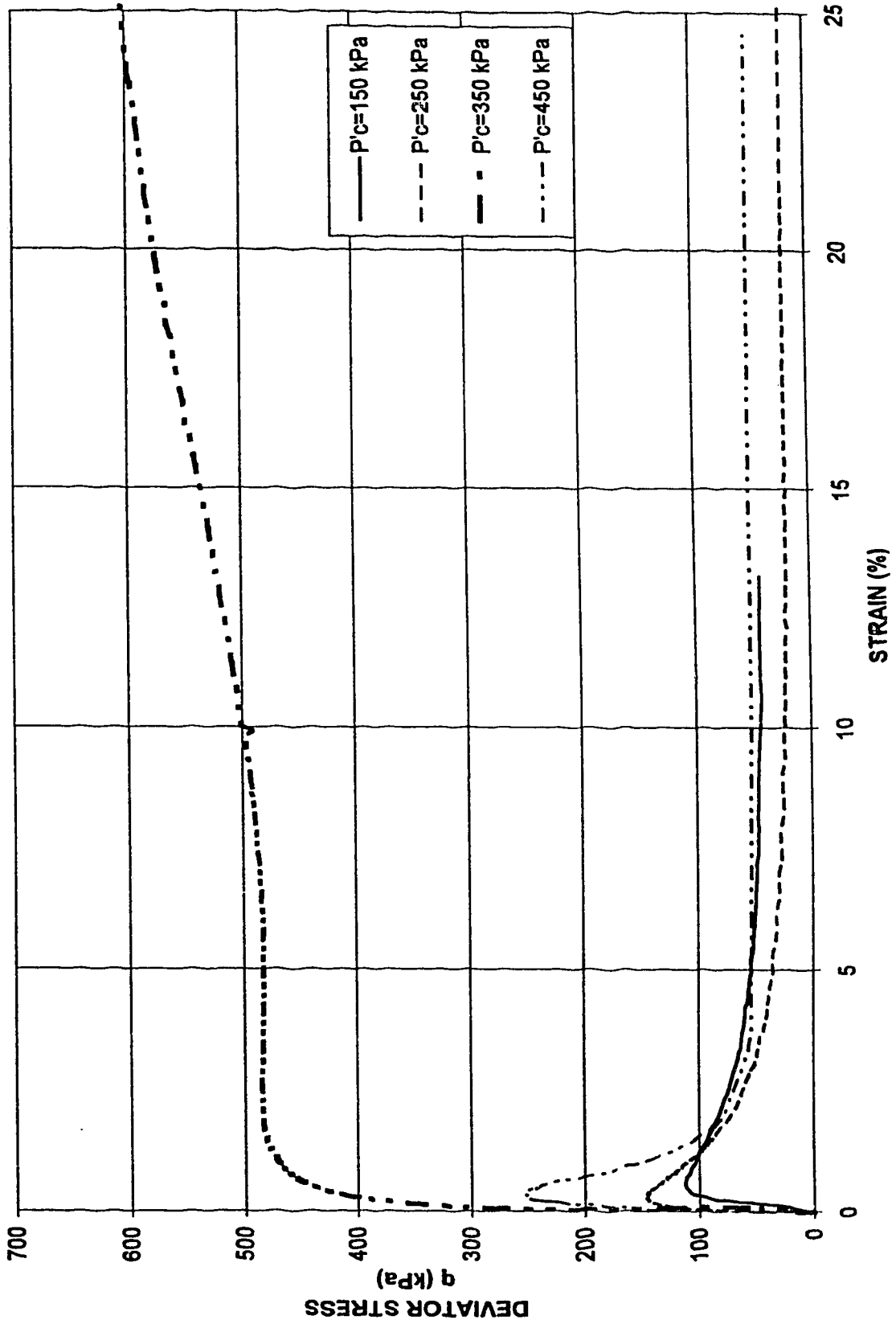


**FIGURE 4.6 DEVIATOR STRESS versus STRAIN
Ottawa Sand with 7.5% Kaolinite**

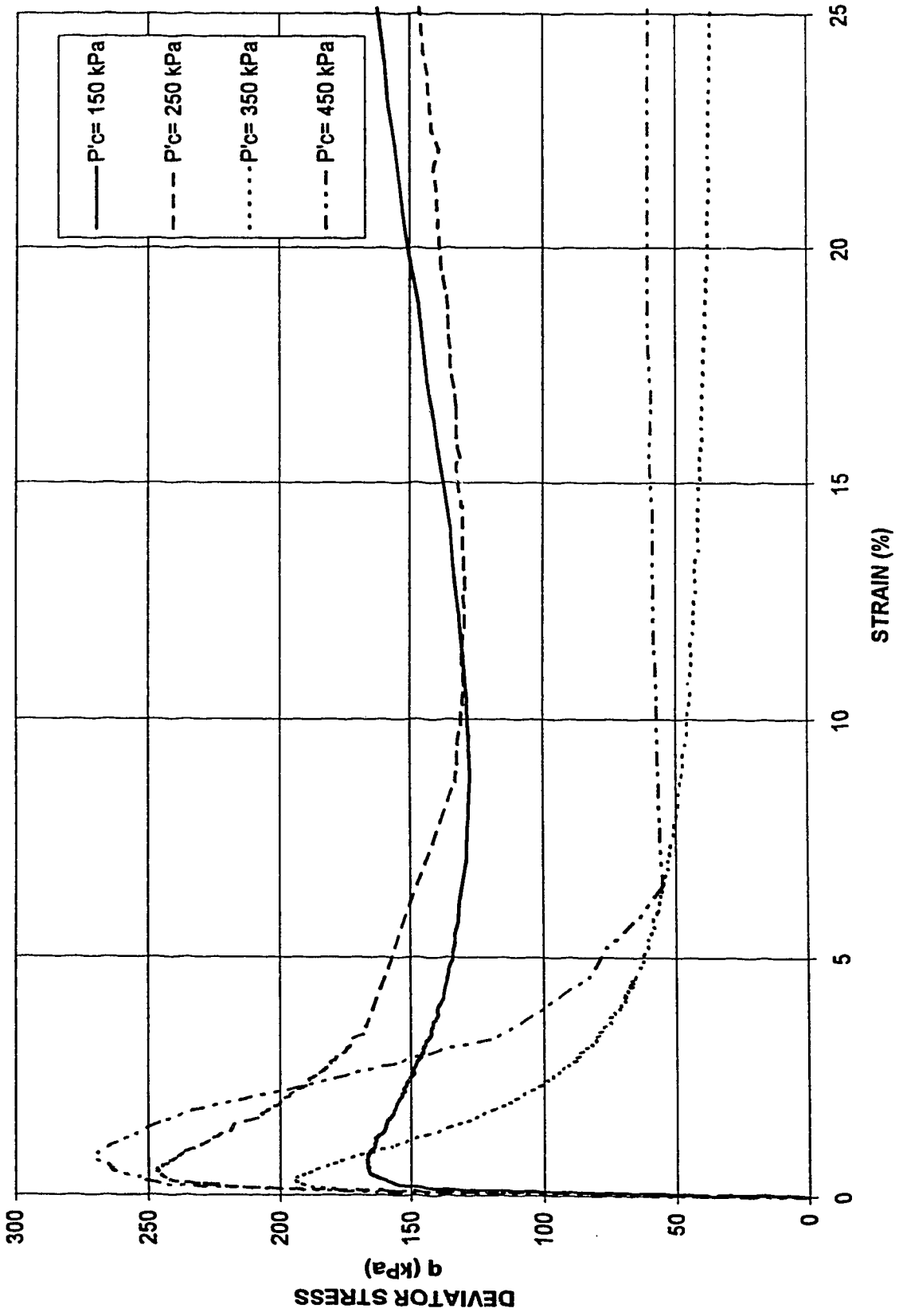


**FIGURE 4.7 DEVIATOR STRESS versus STRAIN
Ottawa Sand with 10% Kaolinite**

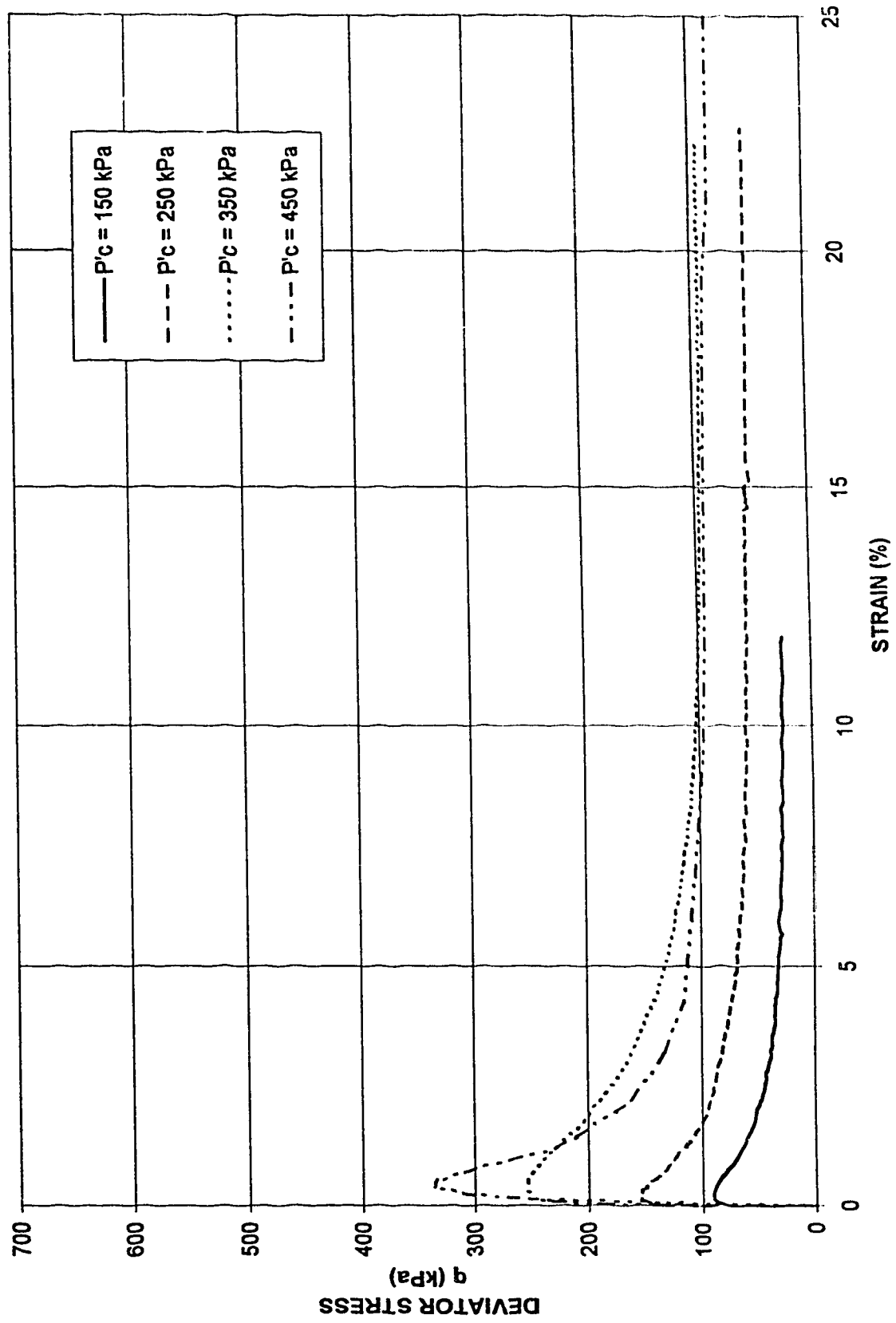
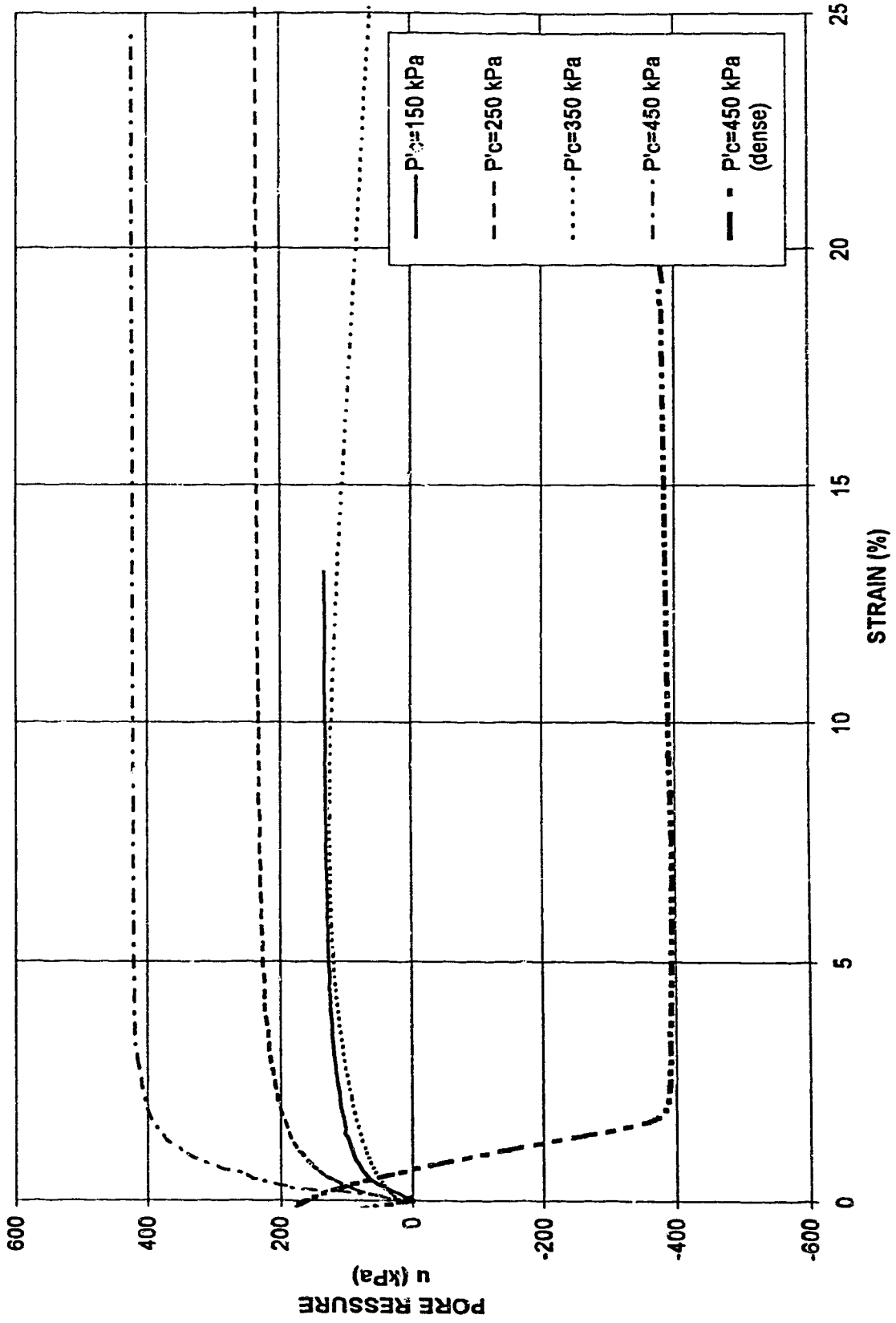


FIGURE 4.8 PORE PRESSURE versus STRAIN
Ottawa Sand with 5% Kaolinite



**FIGURE 4.9 PORE PRESSURE versus STRAIN
Ottawa Sand with 7.5% Kaolinite**

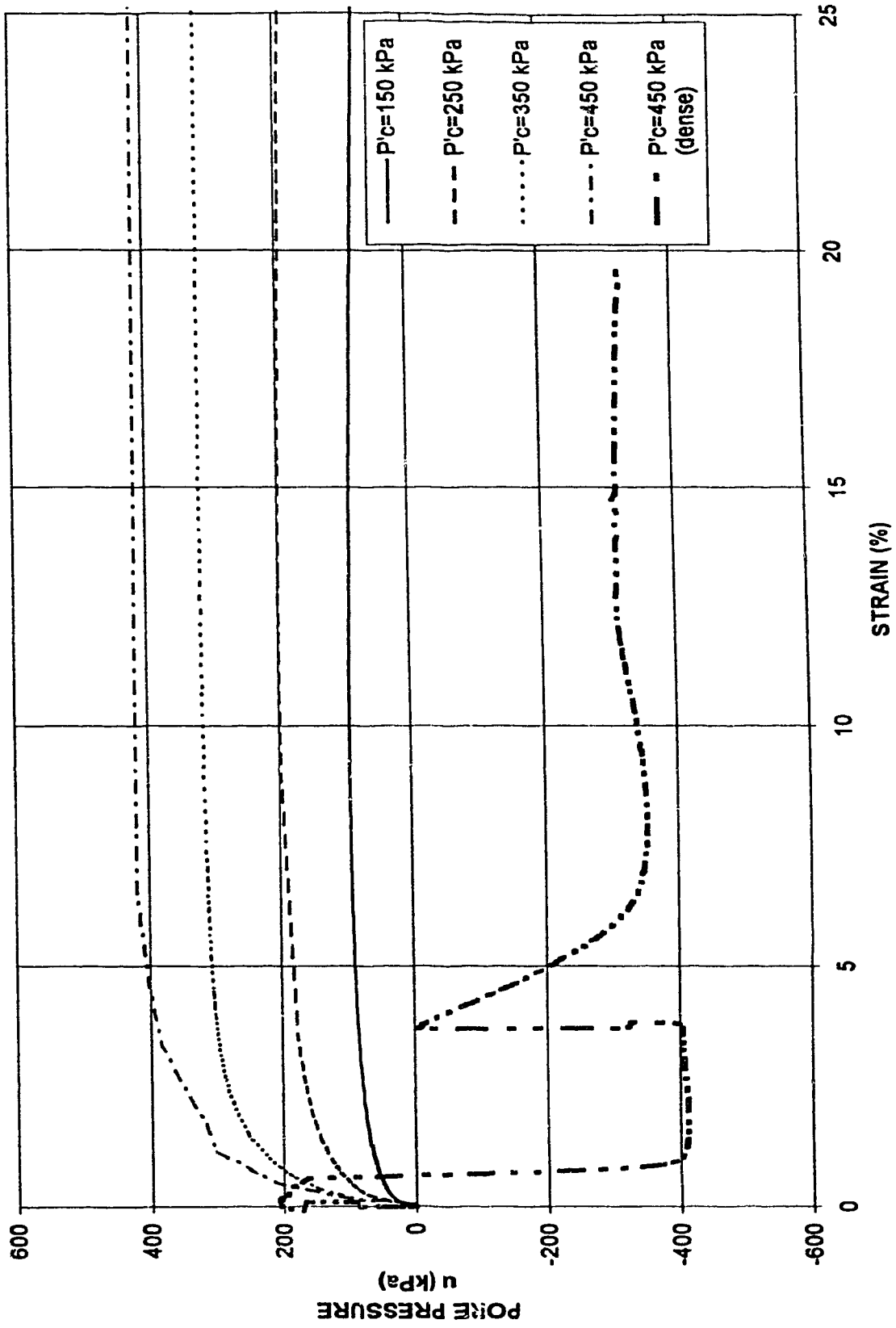
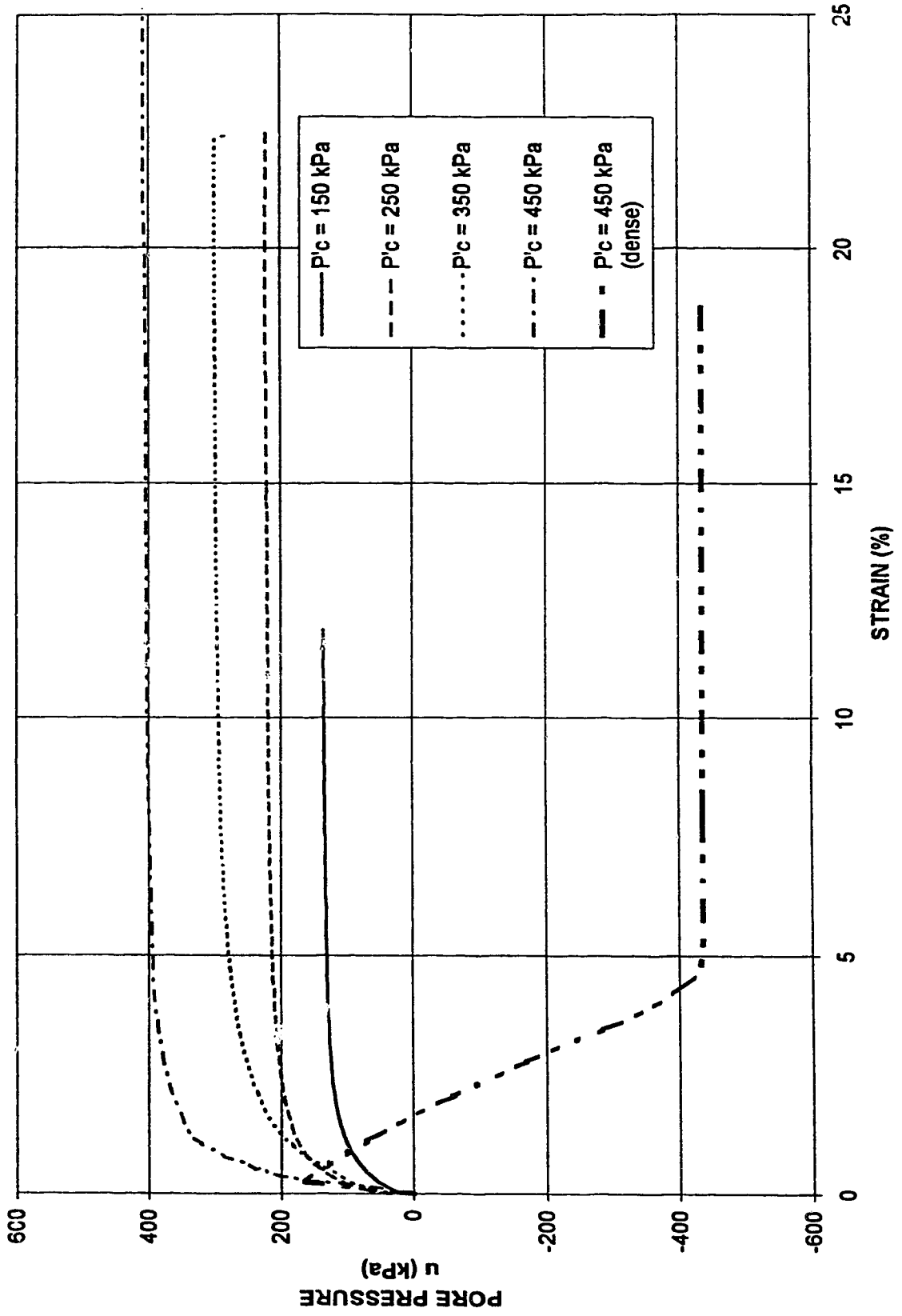
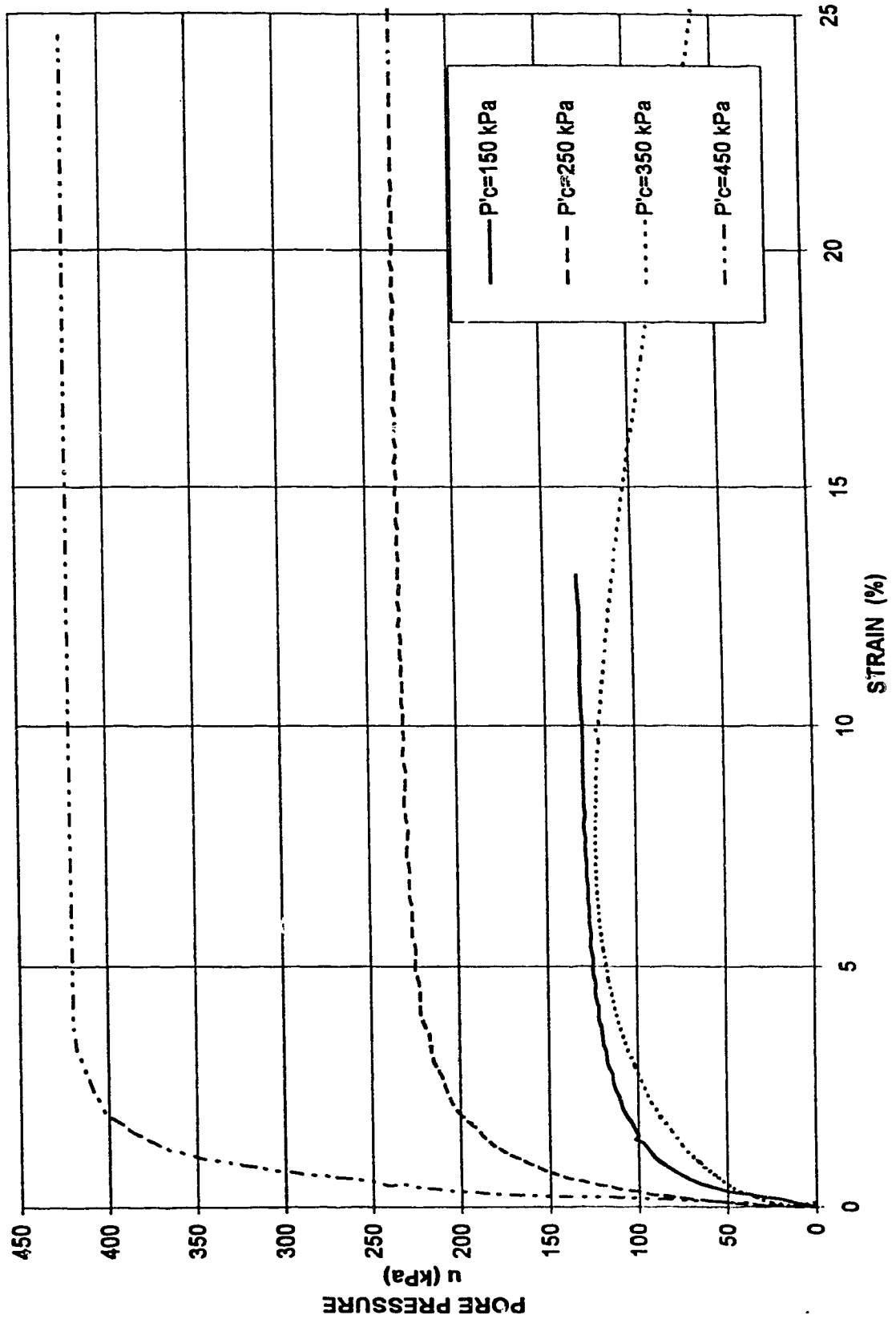


FIGURE 4.10 PORE PRESSURE versus STRAIN
Ottawa Sand with 10% Kaolinite



**FIGURE 4.11 PORE PRESSURE versus STRAIN
Ottawa Sand with 5% Kaolinite**



**FIGURE 4.12 PORE PRESSURE versus STRAIN
Ottawa Sand with 7.5% Kaolinite**

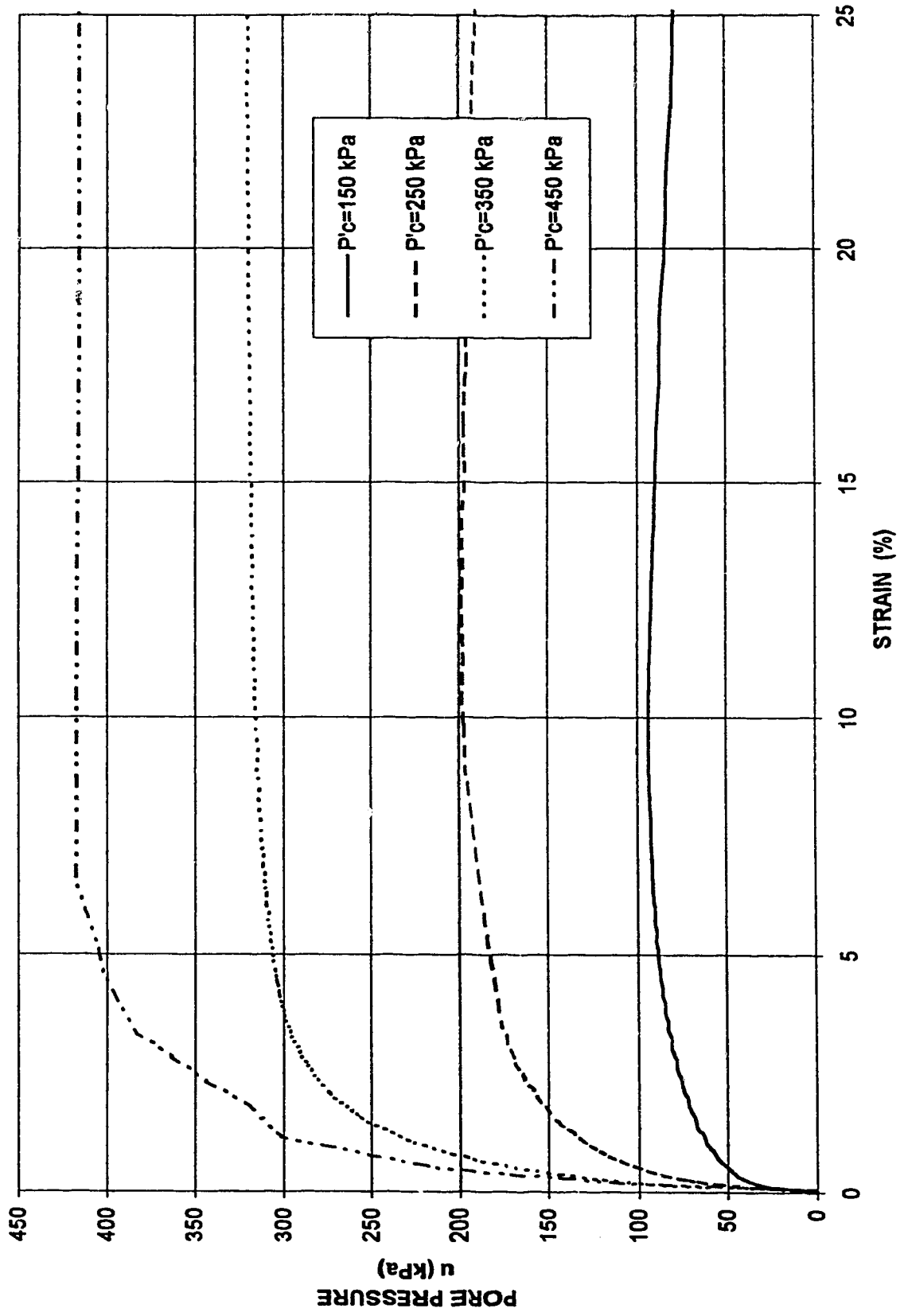


**FIGURE 4.13 PORE PRESSURE versus STRAIN
Ottawa Sand with 10% Kaolinite**

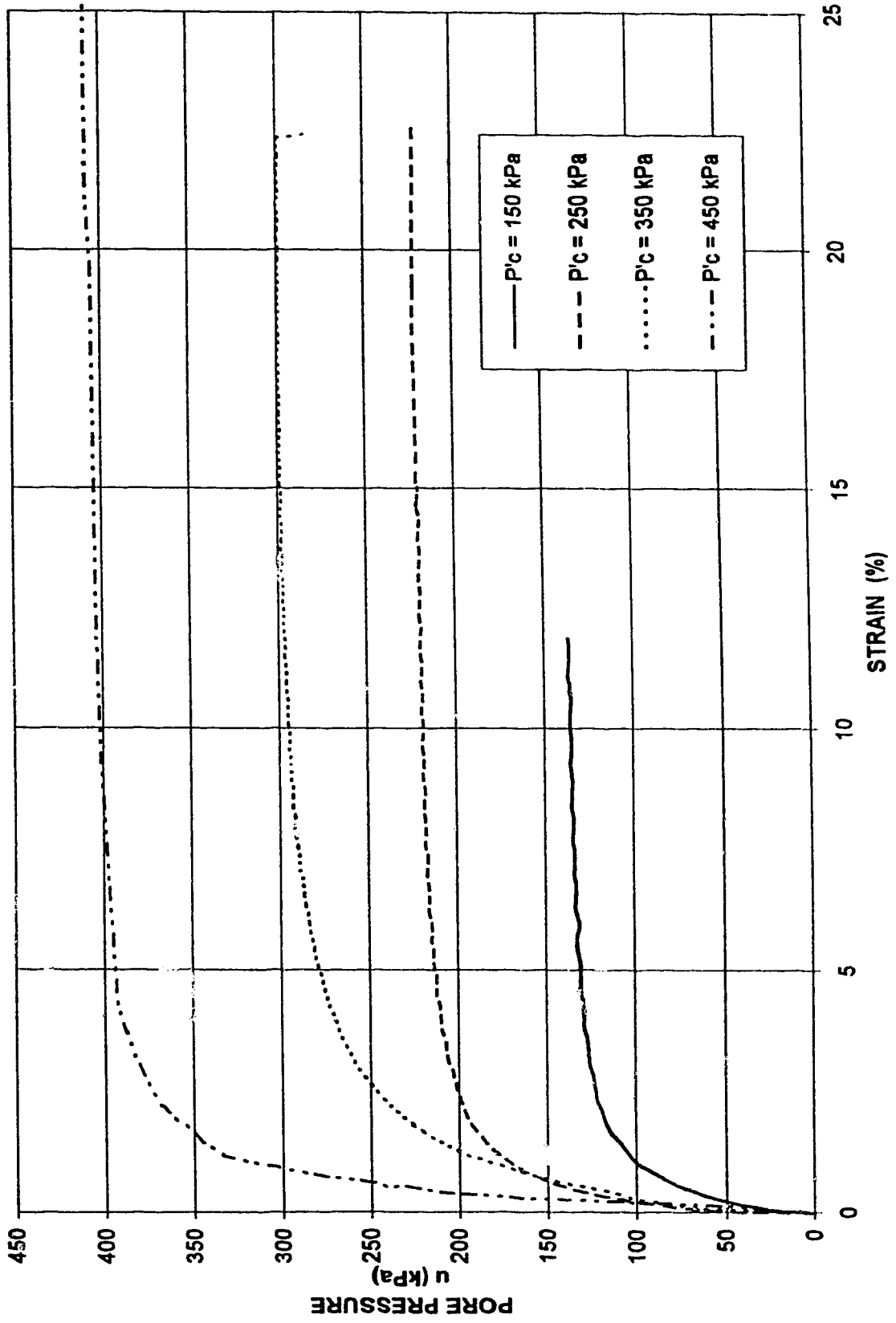


FIGURE 4.14 p' - q DIAGRAM
Ottawa Sand with 5% Kaolinite

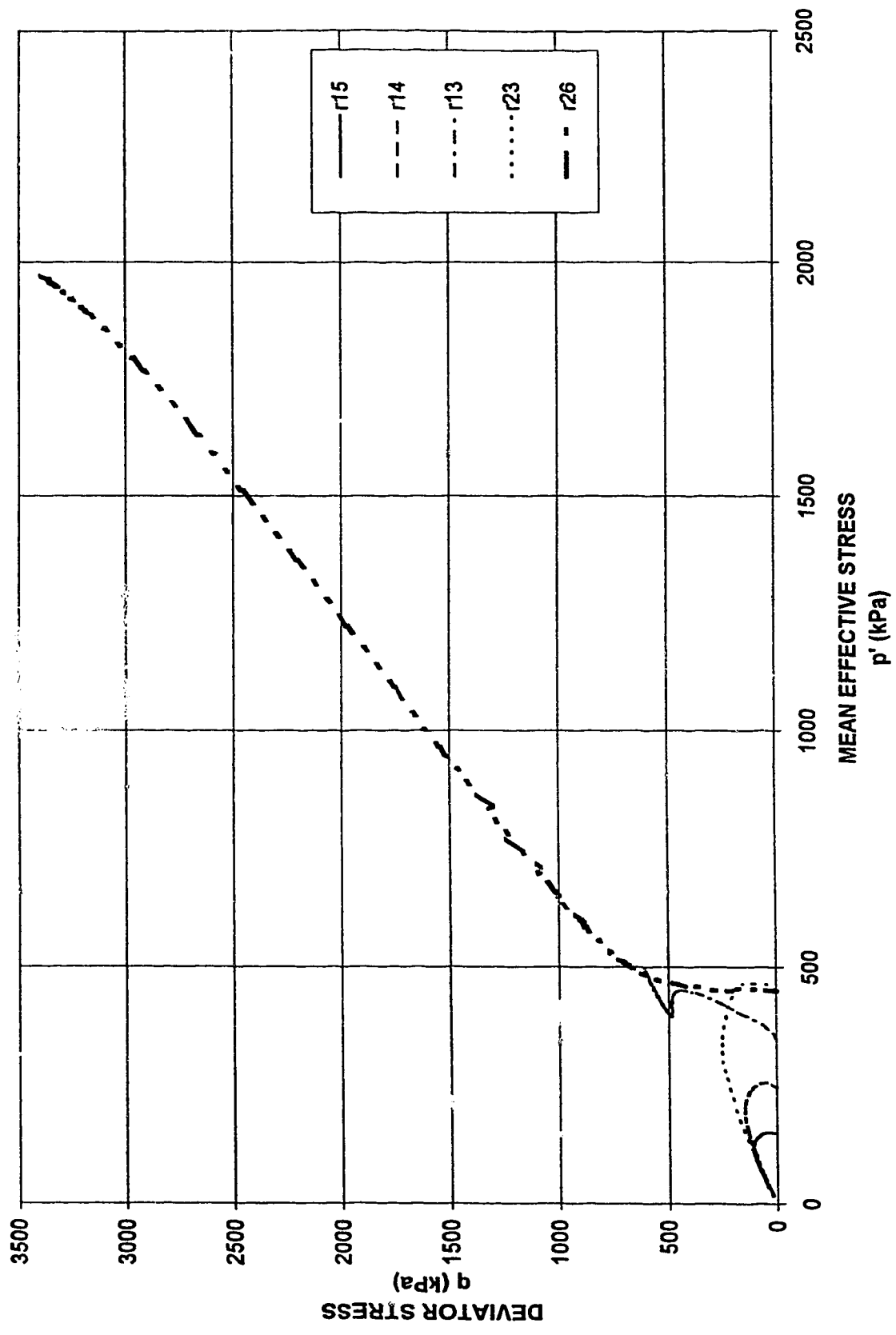


FIGURE 4.15 $p' - q$ DIAGRAM
 Ottawa Sand with 7.5% Kaolinite

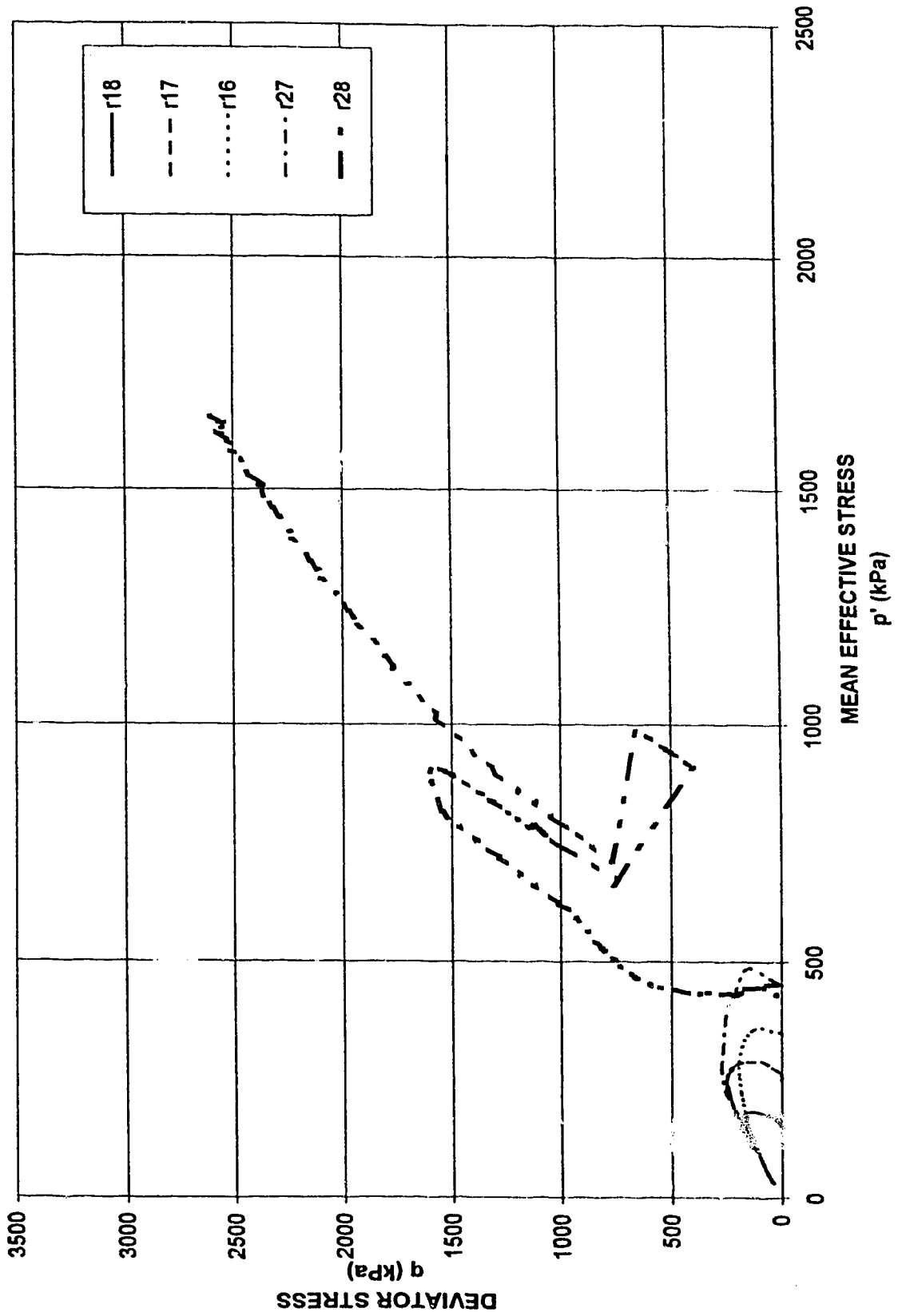


FIGURE 4.16 p' - q Diagram
 Ottawa Sand with 10% Kaolinite

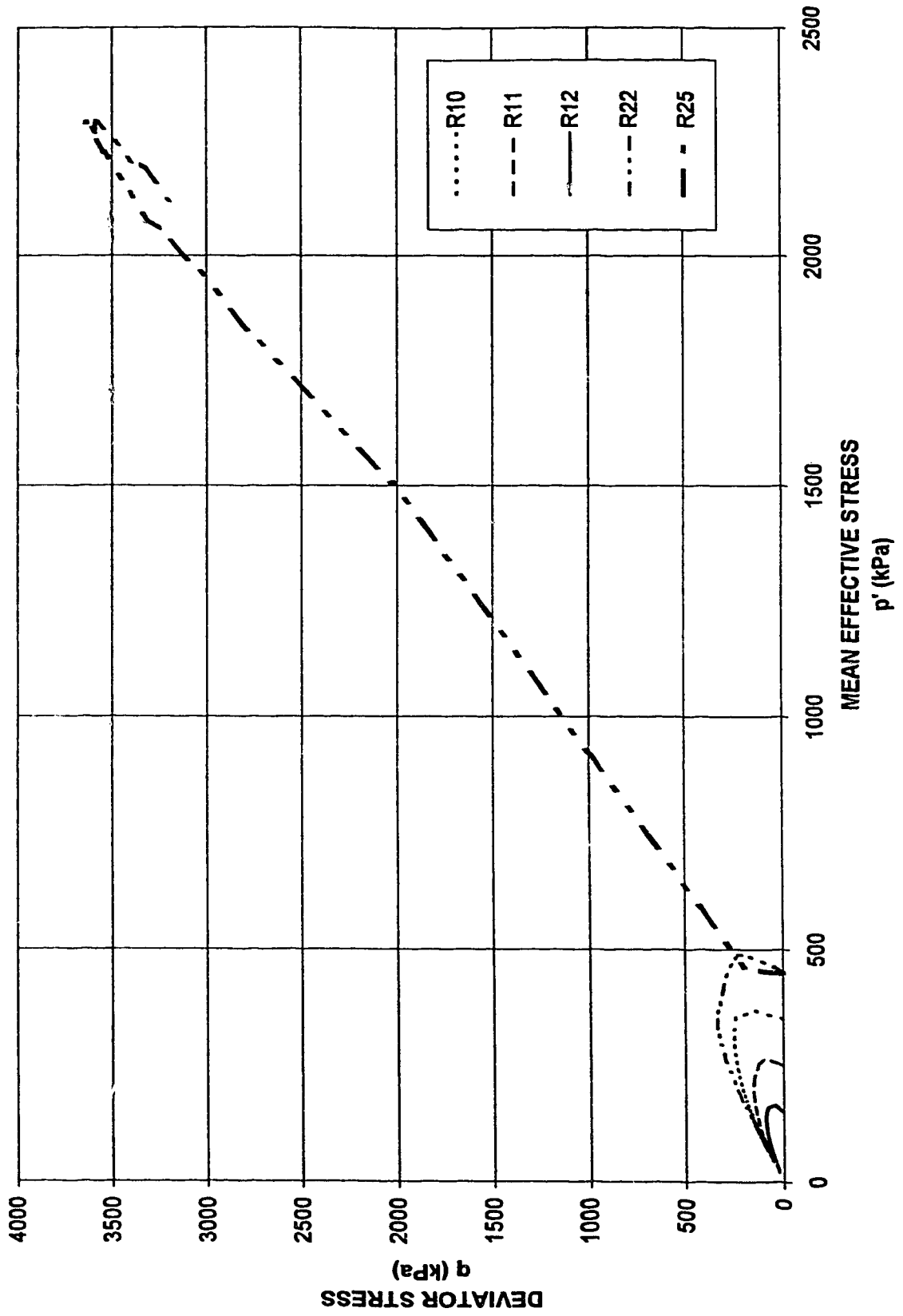
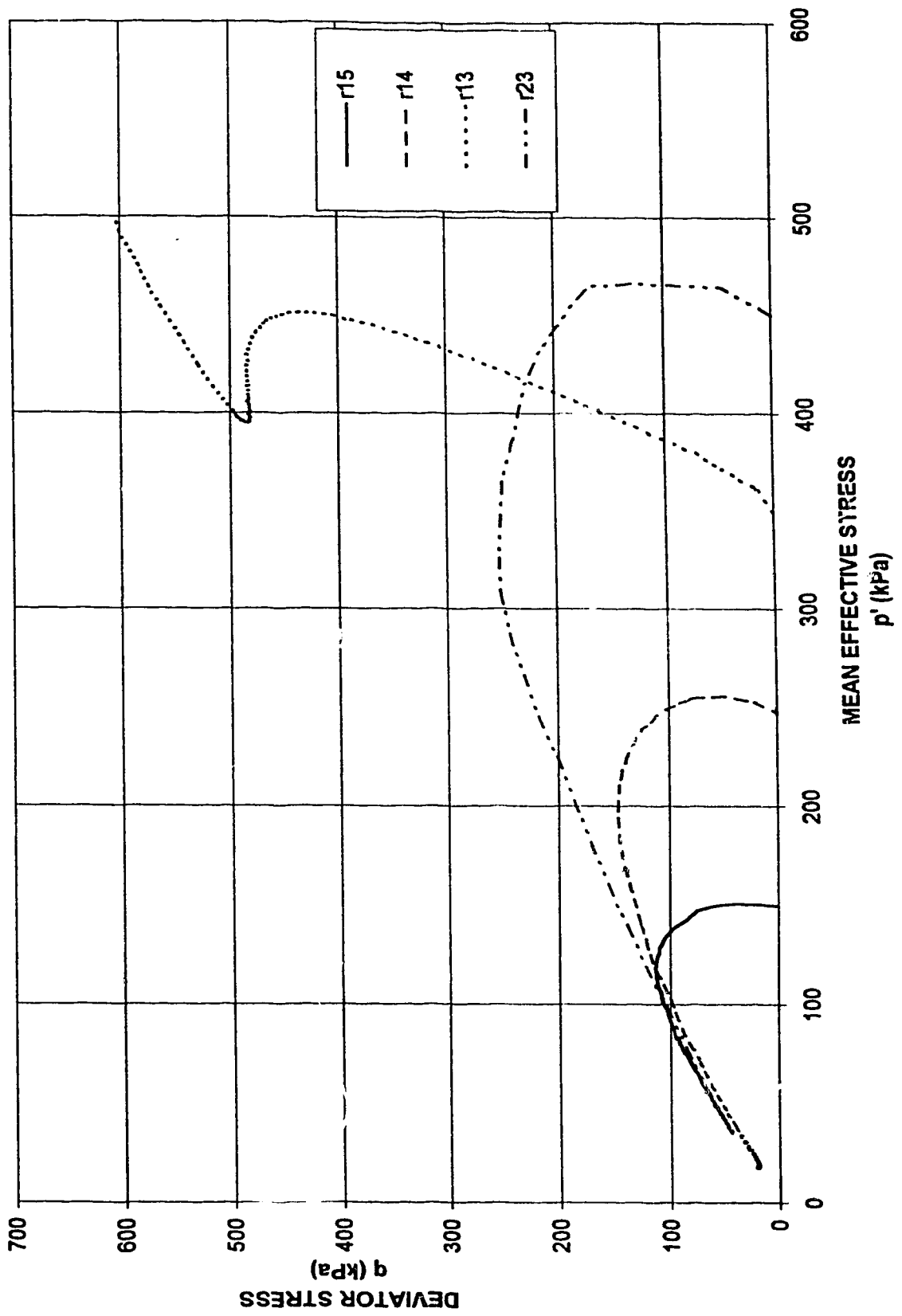


FIGURE 4.17 p' - q DIAGRAM
 Ottawa Sand with 5% Kaolinite



**FIGURE 4.18 p' - q DIAGRAM
Ottawa Sand with 7.5% Kaolinite**

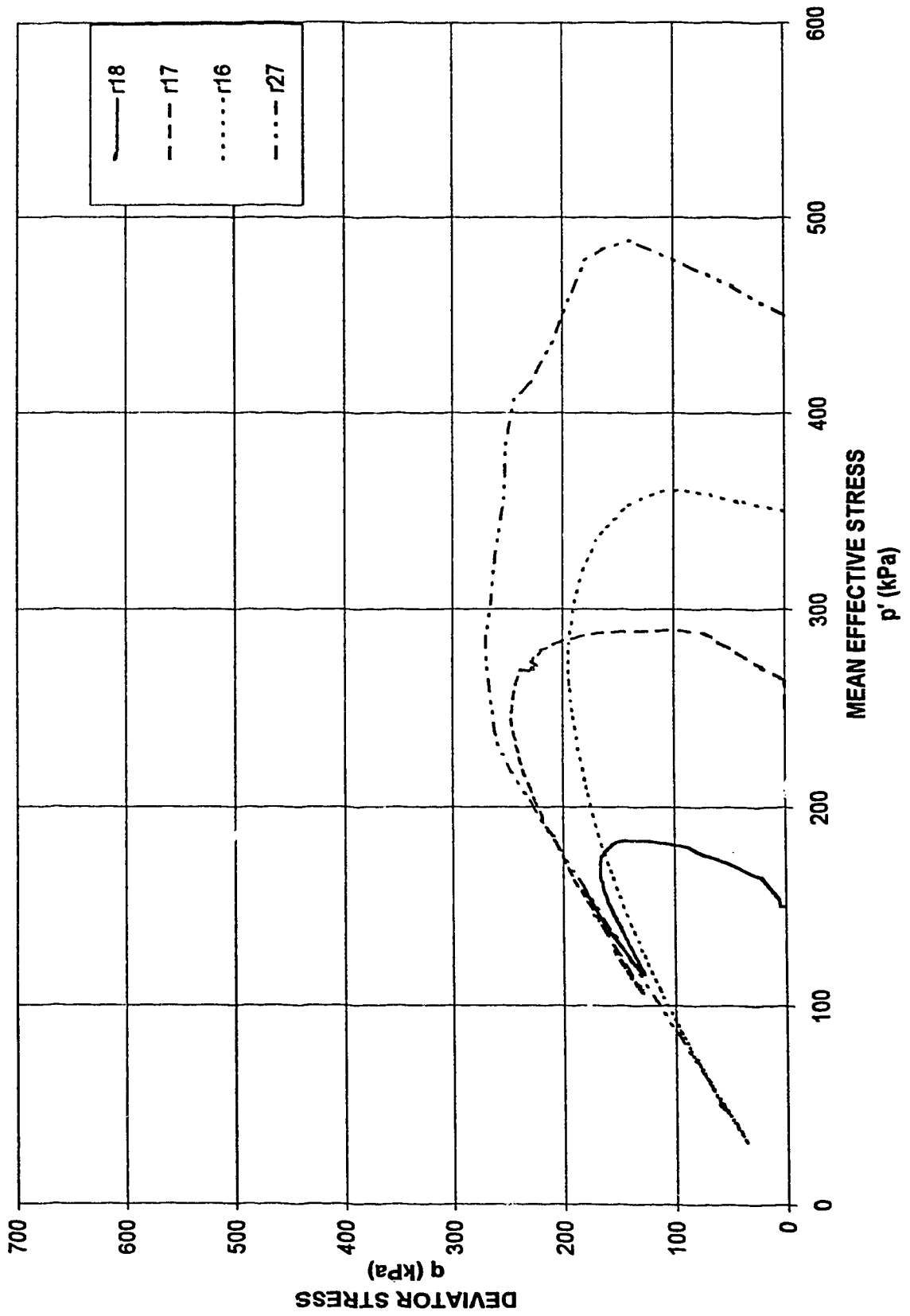


FIGURE 4.19 p' - q DIAGRAM
 Ottawa Sand with 10% Kaolinite

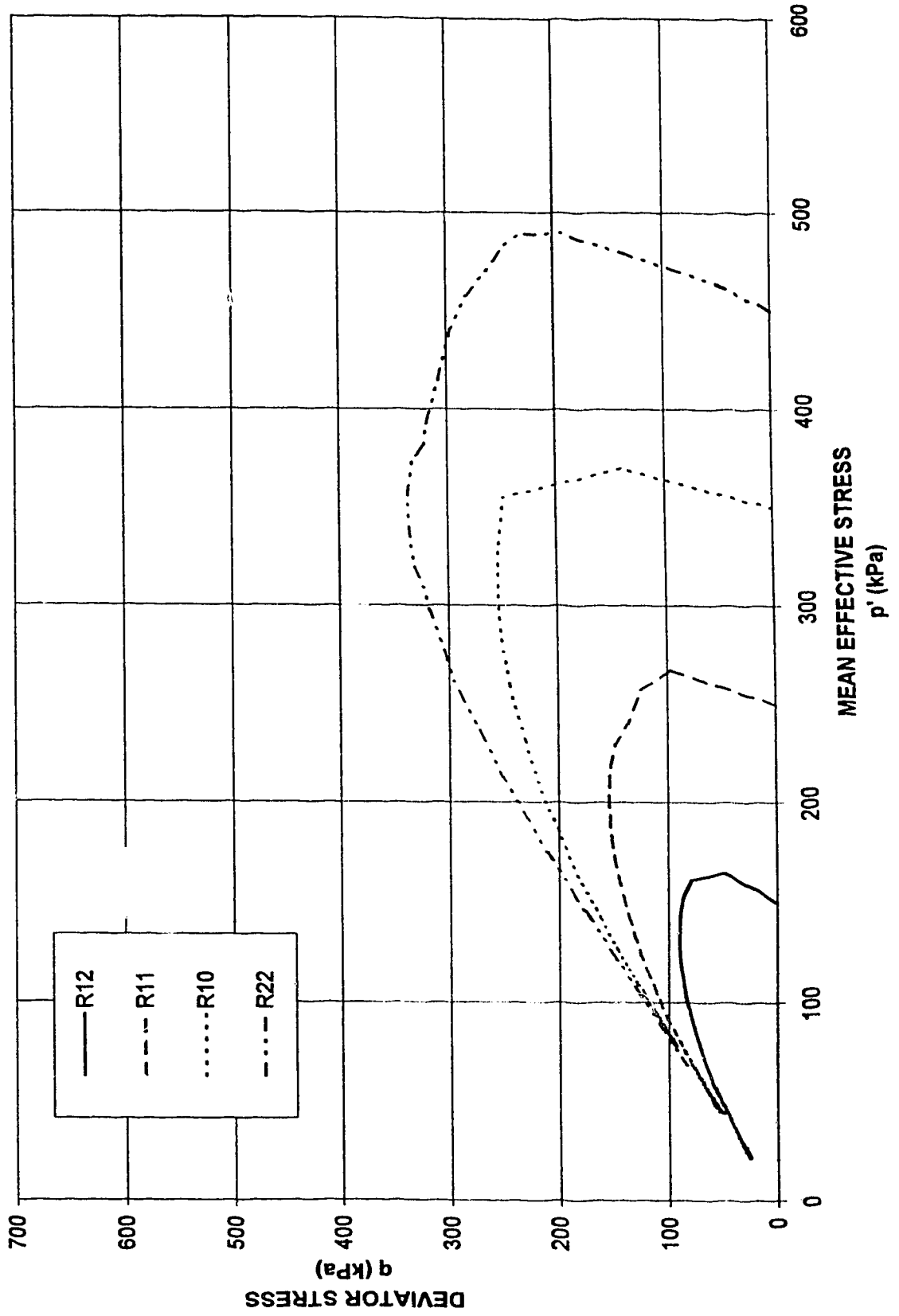


FIGURE 4.20 **NORMALIZED p'-q DIAGRAM**
Ottawa Sand with 5% Kaolinite

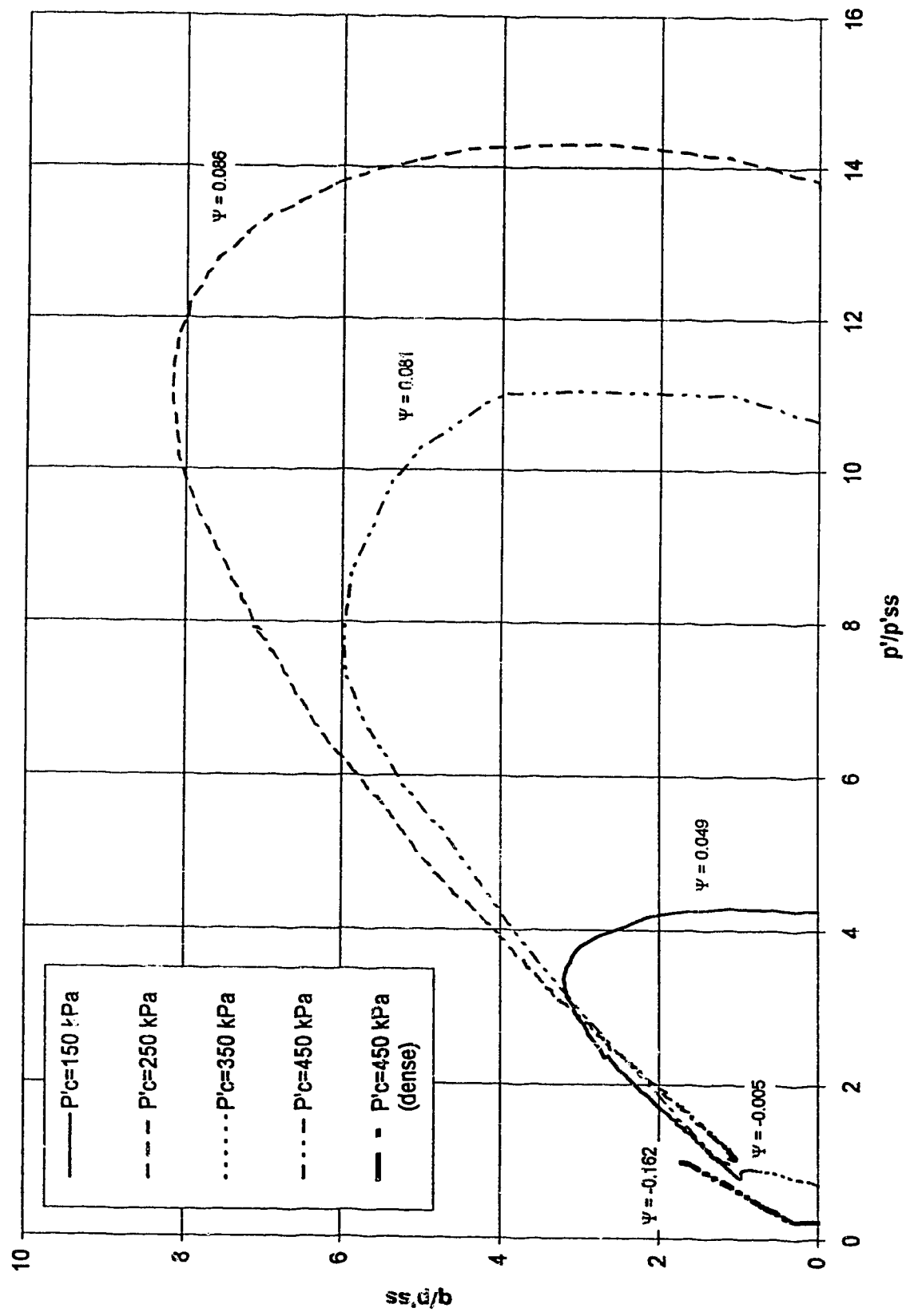


FIGURE 4.21 **NORMALIZED p'-q DIAGRAM**
Ottawa Sand with 7.5% Kaolinite

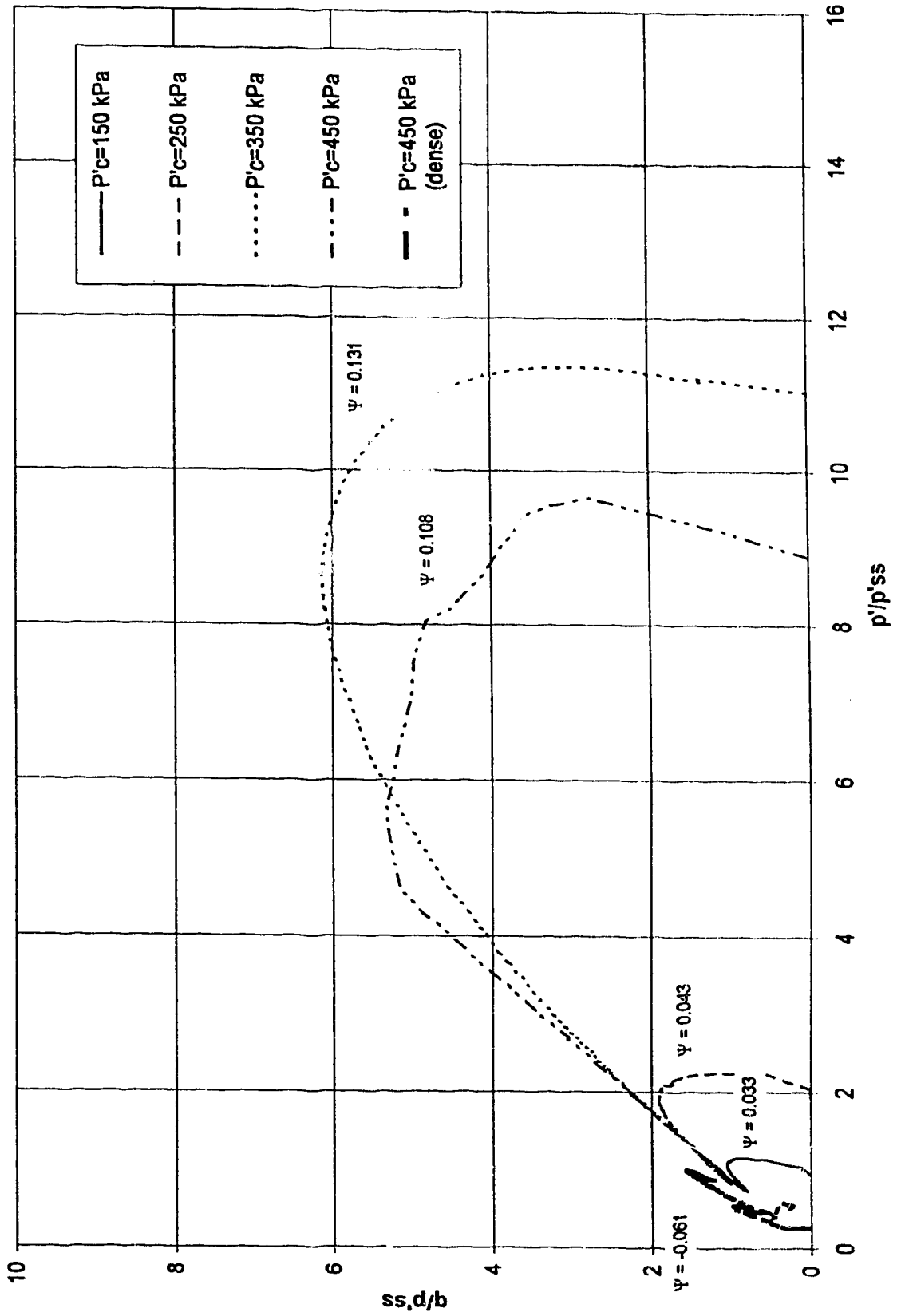


FIGURE 4.22 **NORMALIZED p'-q DIAGRAM**
Ottawa Sand with 10% Kaolinite

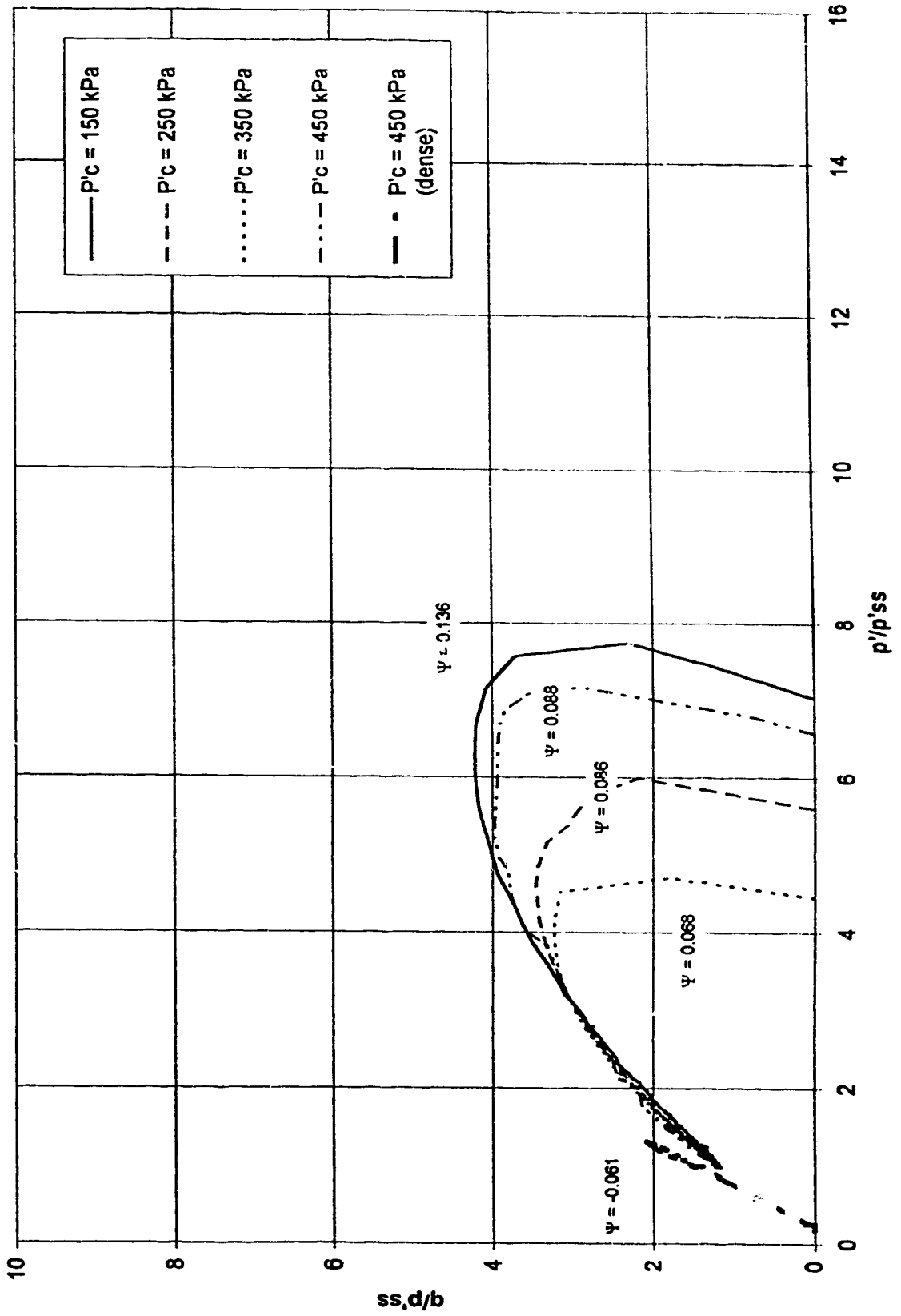


FIGURE 4.23 $e - \log(p')$
 Ottawa Sand with 5% Kaolinite

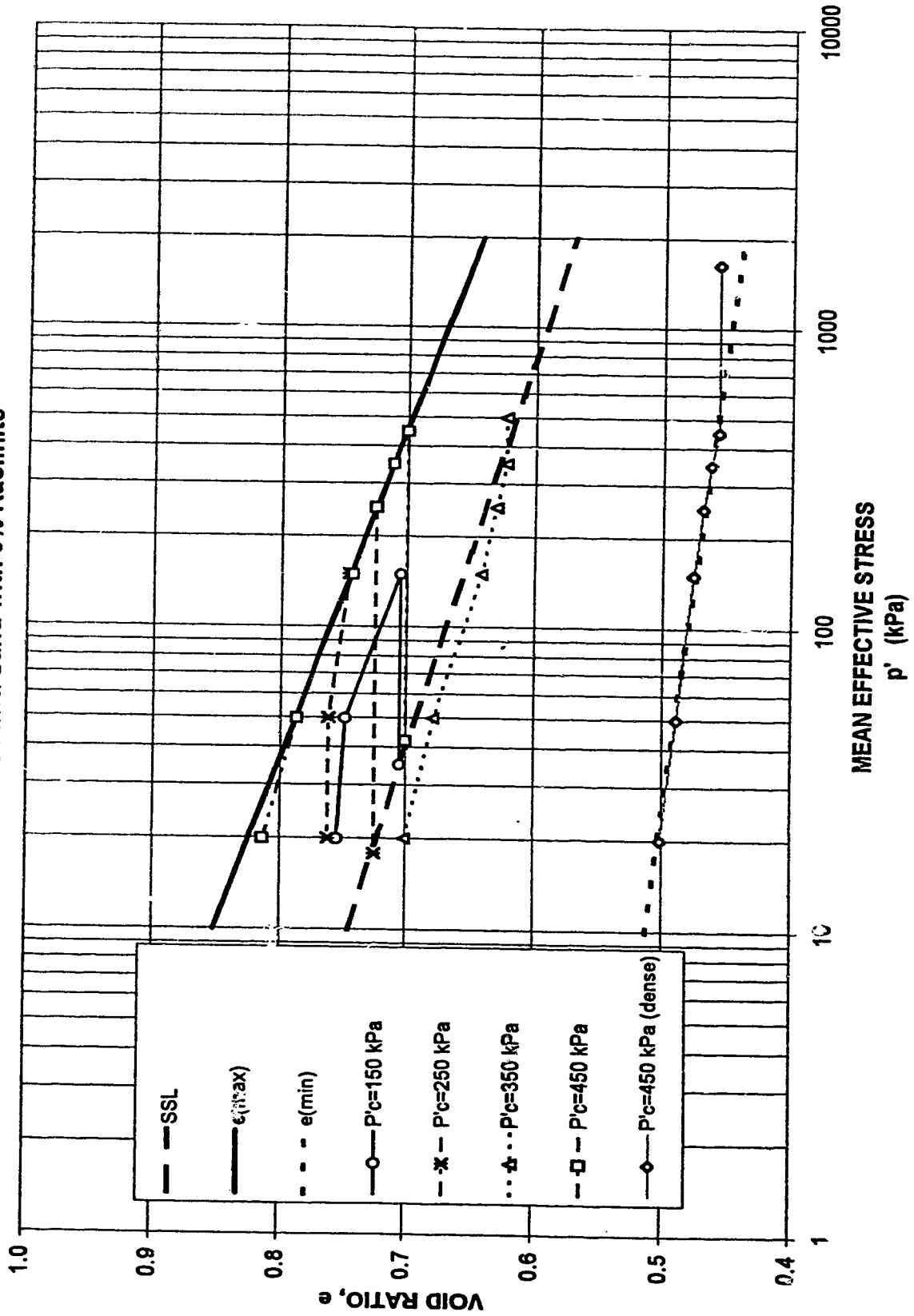


FIGURE 4.24 $e - \log(p')$
 Ottawa Sand with 7.5% Kaolinite

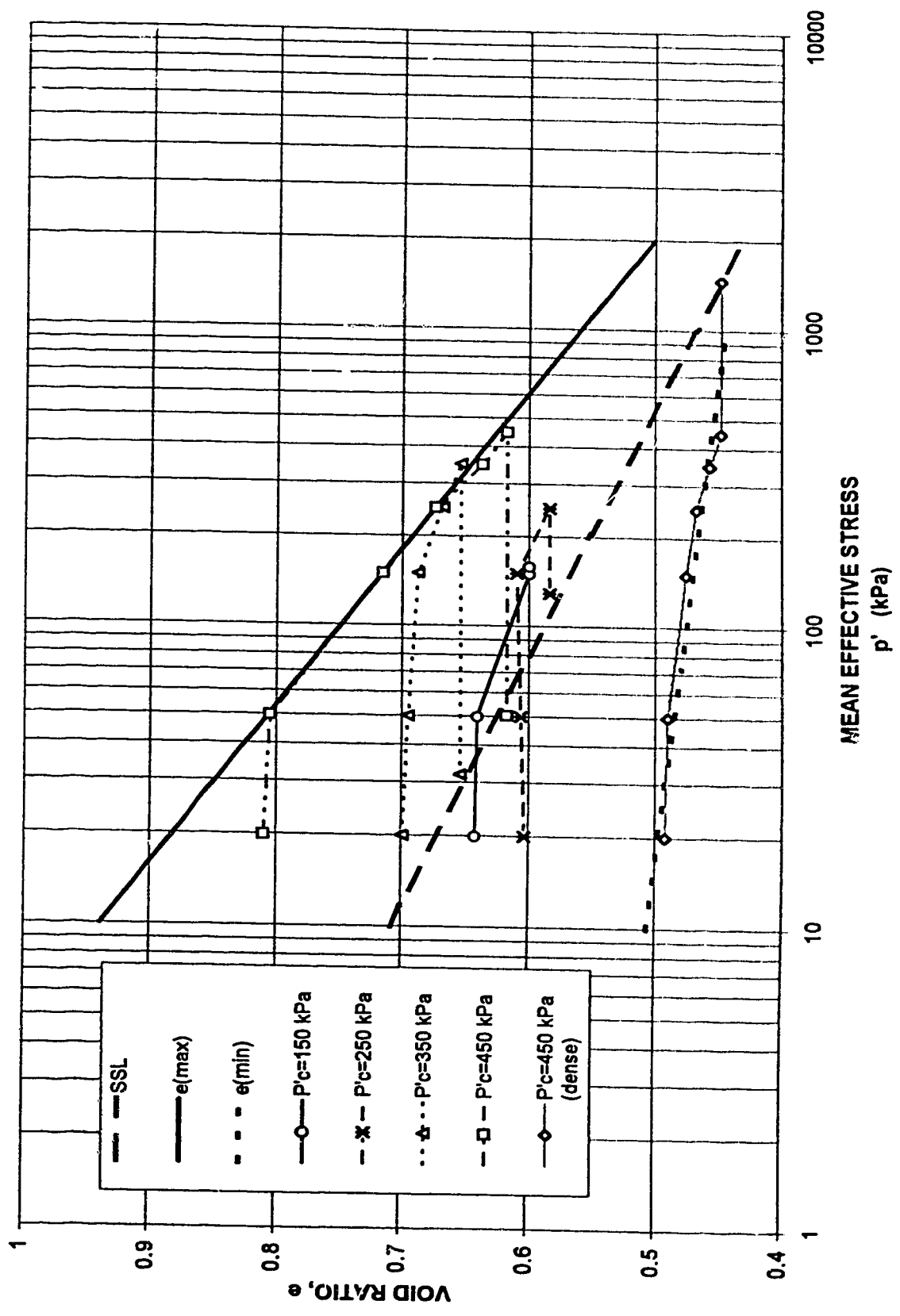


FIGURE 4.25 $e - \log(p')$
Ottawa Sand with 10% Kaolinite

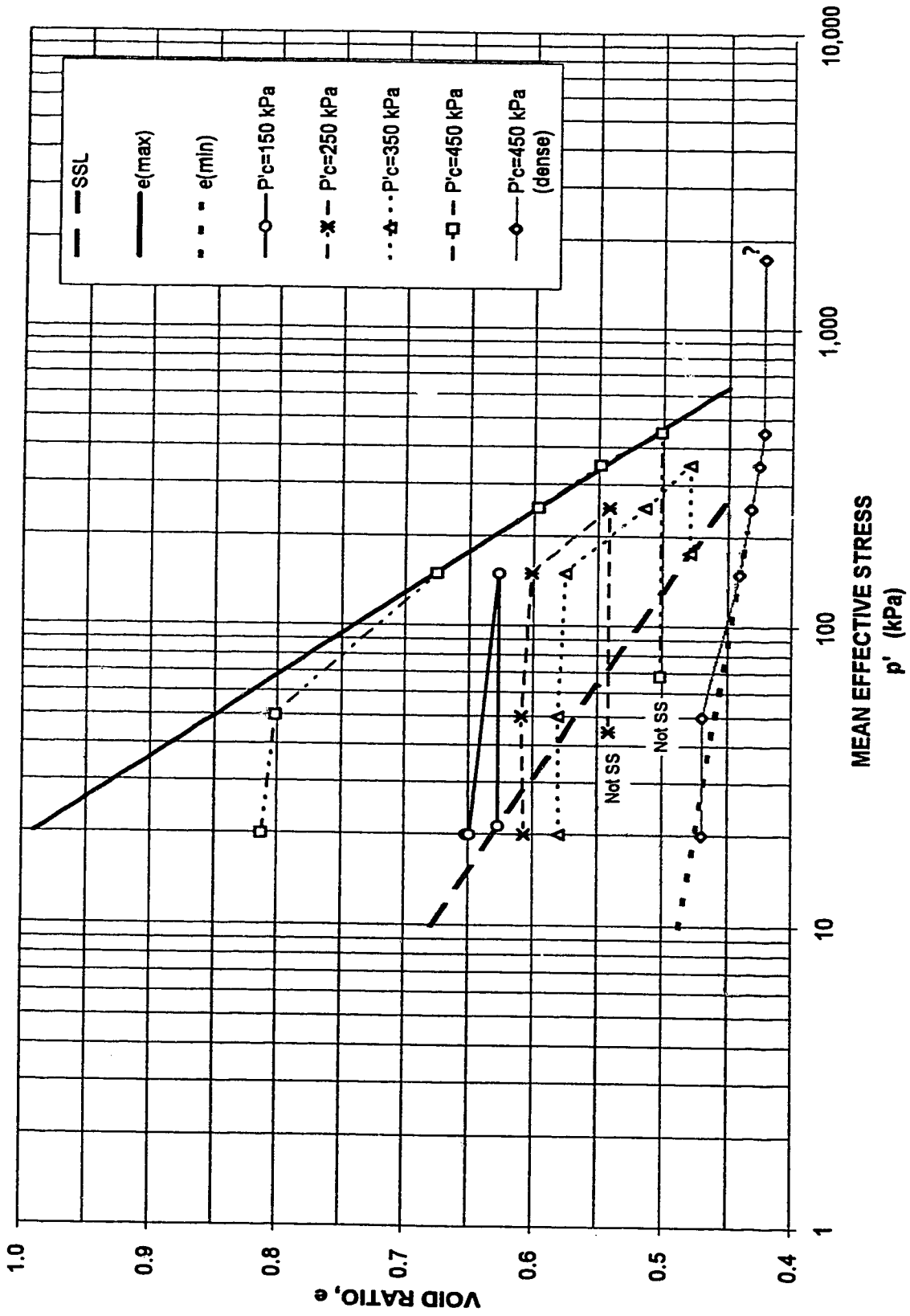


FIGURE 4.26 $e - \log(p')$
Ottawa Sand with 5% Kaolinite

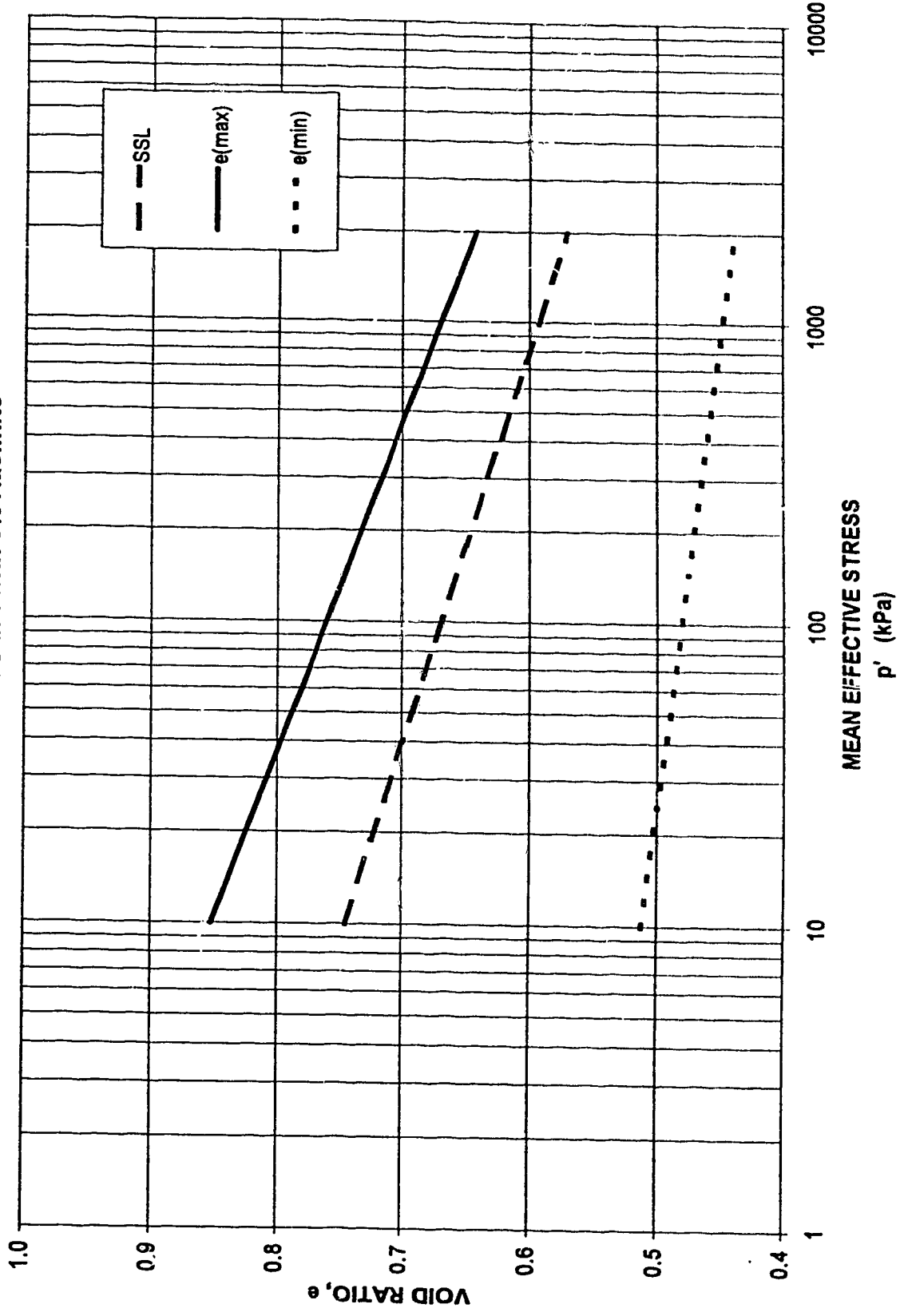


FIGURE 4.27 $e - \log(p')$
Ottawa Sand with 7.5% Kaolinite

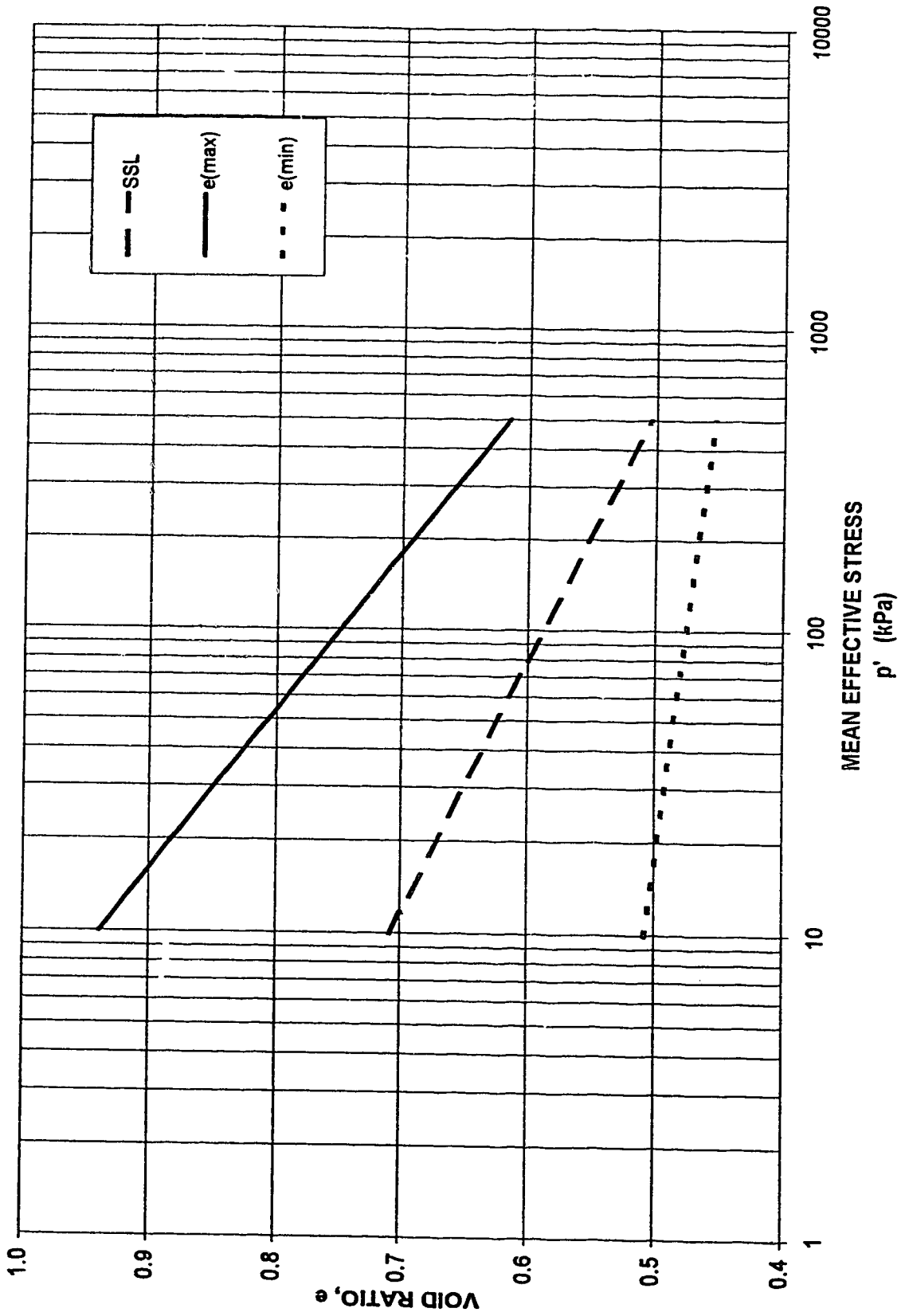
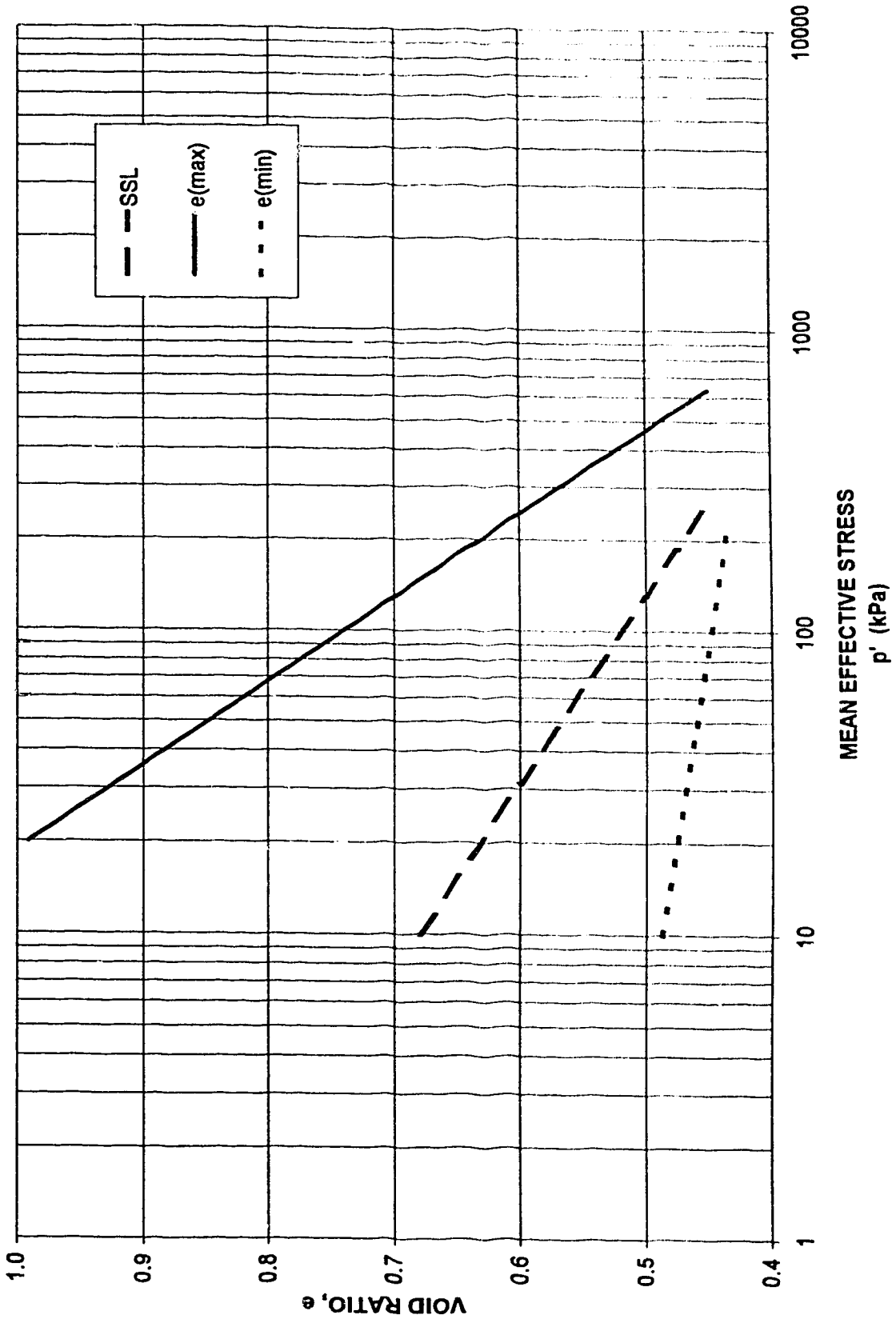


FIGURE 4.28 $e - \log(p')$
Ottawa Sand with 10% Kaolinite



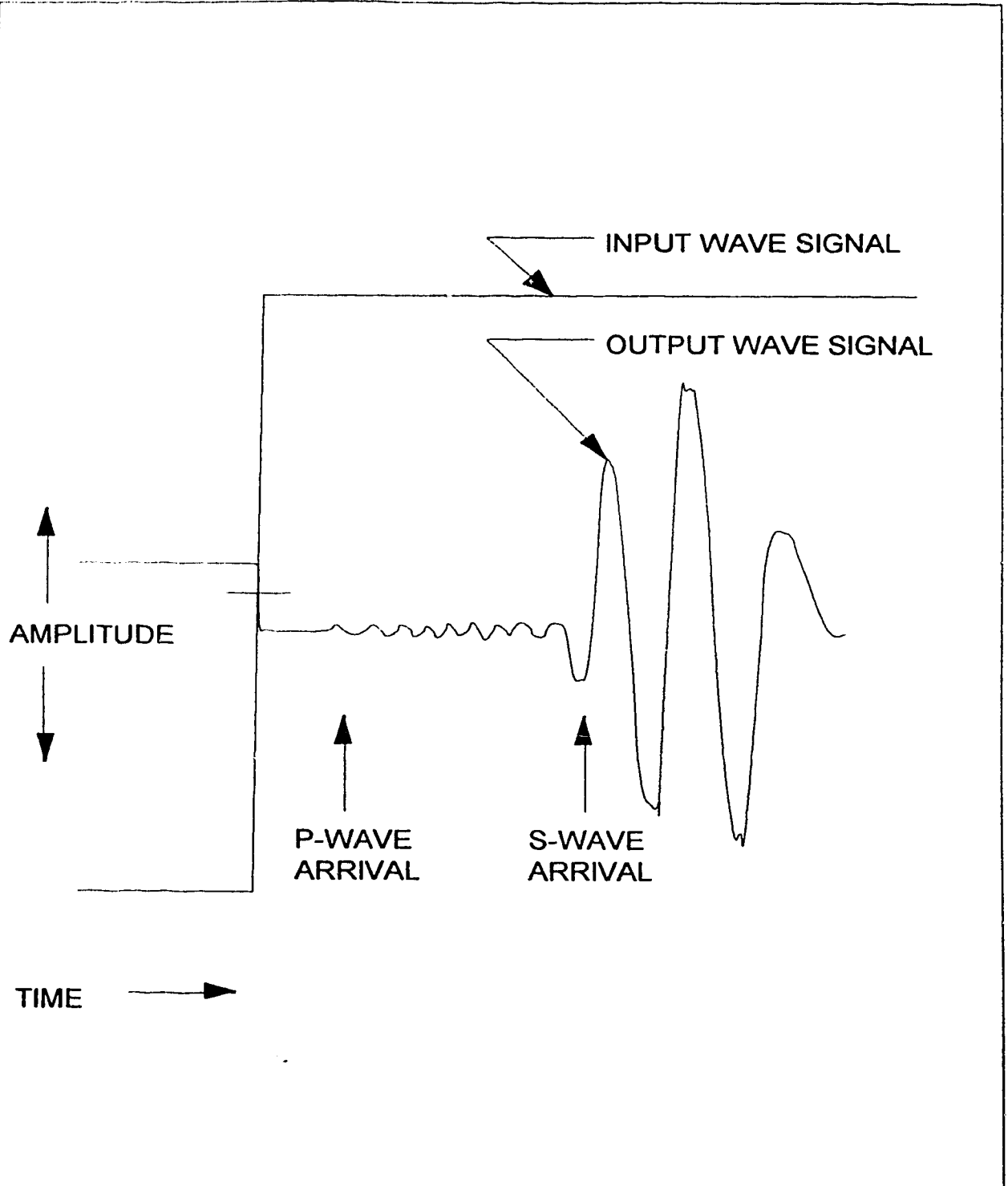


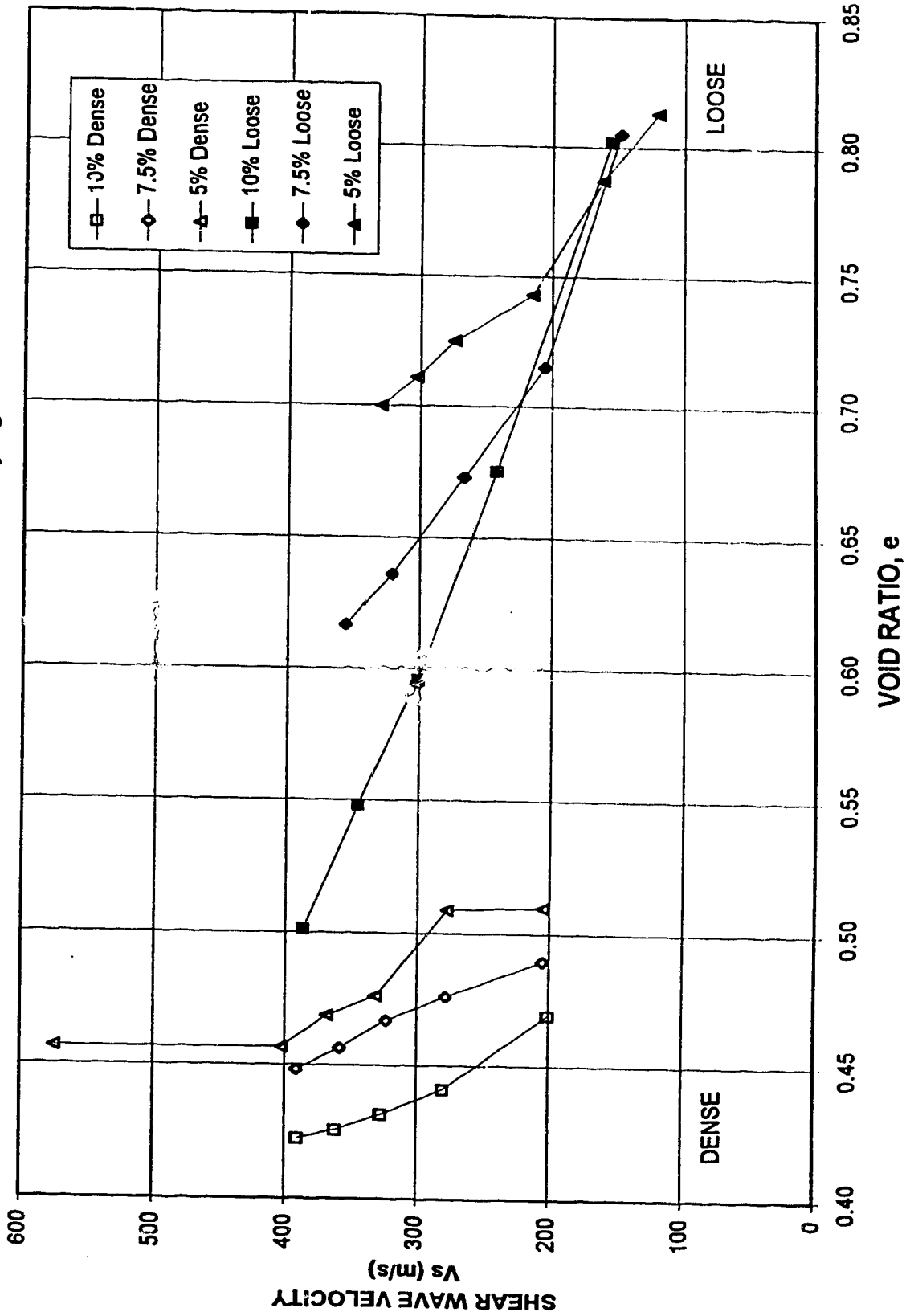
FIGURE 4.29

TYPICAL SHEAR WAVE PLOT

SEPTEMBER 1995

REVISION 2

FIGURE 4.30 SHEAR WAVE VELOCITY versus VOID RATIO
Ottawa Sand with Varying Kaolinite Content



5. DISCUSSION

5.1 Sieve Analysis

Review of the sieve analysis in Table 4.1 and 4.2 shows that the C_u values decreased if filter paper was not used, even at the 5 percent fines content level. Insertion of filter paper effectively minimized the loss of fines and maintained initial C_u value. Inspection of the filter paper upon completion of the tests did not reveal a noticeable scrim of fines on the paper. Based on this observation it was assumed that the internal stability of the sample was maintained through the use of filter paper. The amount of fines lost, in the absence of filter paper, did increase in conjunction with greater initial fines content. It is clearly beneficial to use filter papers during the triaxial testing to maintain the sample grain size distribution, and thereby provide some level of restriction of migration of fines and segregation of the samples. Use of filter paper did not appear to inhibit consolidation of the samples.

Seed *et al* (1976) grain size distribution boundaries for liquefiable soil are shown on Figure 5.1, as are several of the sands discussed in this thesis. The figure clearly shows that the grain size distributions for all the soils lie within the boundaries for most likely liquefiable soil. This provides some assurance if the Seed boundaries are used as a preliminary screening for liquefaction potential. The concept of soil compressibility is discussed in the following sections as it involves the grain size distribution and void ratio.

5.2 Void Ratio

5.2.1 INTERGRANULAR VOID RATIO

Pitman (1993) showed that the void ratio at steady state decreased as the percentage of fines increased until about 20% fines were present. He also showed that at greater fines contents the void ratio increased. However, all of his tests were conducted at a mean effective pressure of 350 kPa. Pitman also calculated an intergranular void ratio to determine a void ratio based on the sand, or granular, portion of the sample only. The intergranular void ratio was intended to differentiate between granular soil with similar void ratios but different fines content. There are several issues related to the used of an "intergranular" void ratio as a means of comparison between granular soils. The equation used by Pitman to determine the intergranular void ratio may be rewritten as Equation 5.1.

$$e_i = \frac{V_v + V_f}{V_s} = e + \frac{V_f}{V_s}(1+e) \quad [5.1]$$

where V_t , V_s , and V_f are the total volume, volume of sand and volume of fines respectively.

If the specific density of the fines and granular portions are approximately the same Equation 5.1 can be rewritten in terms of mass as shown below.

$$e_i = e + \frac{W_f}{W_s} (1 + e) = e + \frac{\%fines}{(100 - \%fines)} (1 + e) \quad (5.2)$$

A practical limitation to the use of the intergranular void ratio is shown on Figure 5.2. This figure shows the intergranular void ratio versus fines content for various initial "clean" samples with varying void ratios. The figure shows that the intergranular void ratio increases as the fines content increases, eventually reaching unrealistic, large values of intergranular void ratio. A sample with a void ratio of less than unity may have an intergranular void ratio greater than two at fines content of 40 percent. There does not appear to be any rational to define a boundary that shows where the intergranular void ratio is appropriate for use. It would certainly not be possible to compare the state lines with moderate Kaolinite content against the state line for pure Kaolinite on an intergranular void ratio basis. For these reasons the use of intergranular void ratio was not applied as a means of comparing the behavior of Ottawa sand with varying Kaolinite content, and the conventional definition of void ratio was used.

5.2.2 MINIMUM VOID RATIO (DENSEST STATE ATTAINED)

The void ratio along the densest state lines for the 5, 7.5 and 10 percent fines did not change by more than ± 0.04 within the mean effective pressure range of 10 to 450 kPa. The lines defining the minimum void ratio versus mean effective pressure for each level of fines content are shown on Figure 5.3. The lines show a small but measured decrease in void ratio as the fines level increased. The minimum void ratio attained during this study was 0.422 for a fines content of 10%.

Figure 5.12 shows interpreted state lines from this study, including state lines extrapolated for 30% and 40% Kaolinite fines content, based on results from Pitman. The figure shows a consistent rotation of the state line, which may be extrapolated to the very low void ratio region probed by Pitman. It is unclear how Pitman (1993) achieved a minimum void ratio of about 0.17 for a fines content of 20% and a consolidation pressure of 350 kPa. The minimum void ratio obtained in trials by this author was 0.415 for a fines content of 20% and a consolidation pressure of 450 kPa.

5.2.3 MAXIMUM VOID RATIO (LOOSEST STATE ATTAINED)

The void ratio along the loosest state lines for the 5, 7.5 and 10 percent fines varied considerably. Below a mean effective stress level of about 85 kPa the void ratio lines, in order from loosest to densest was 10, 7.5 and 5%. Above 85 kPa the order was reversed, as shown on Figure 5.3 The slope of the maximum voids ratio line was determined by approximating a line along the loosest consolidation lines at the varying fines content.

5.2.4 COMPRESSIBILITY

As discussed in Chapter 2, the compressibility of a given soil sample is affected by the amount of fines, all other variables held constant. A measure of the sample compressibility can be made by comparing the maximum and minimum void ratio lines determined for each level of fines. Figure 5.5 shows the $(e_{\max} - e_{\min})$ versus mean effective stress for various percent fines. The values of e_{\max} and e_{\min} are those determined from the triaxial samples, as discussed above, and not by ASTM methods.

Both the maximum and minimum void ratio lines decreased as the mean effective stress increased. The decrease in void ratio may be interpreted simply as infilling of the voids between granular particles. It is likely that at some level of fines content the granular particles would be inhibited from making point to point contact and compressibility would increase. This is shown on Figure 5.5 at low mean effective stresses. At low mean effective stresses the compressibility lines in order of greater possible decrease in void ratio are the 10%, the 7.5%, and the 5% fines content compressibility lines. At higher mean effective stresses the order is reversed. This is a reflection of the difficulty in making loose samples at high confining pressure and with high fines content.

The differences between the e_{\min} and e_{\max} lines for all fines content levels tends to decrease as mean effective stresses increases. This is predictable since the slope of the consolidation line for loose samples is much steeper and will converge to the consolidation lines for dense samples as consolidation occurs. At some level of mean effective stress and void ratio the loose and dense consolidation lines are expected to become tangential if not identical.

5.3 Triaxial Test

Twenty-five triaxial tests were undertaken. Nineteen of these tests produced results that could be interpreted. Six tests were terminated due to difficulties met with during the test. Shear wave measurements were taken during the consolidation portion of six triaxial tests that were consolidated to 450 kPa.

The test conditions are summarized in Table 4.5. The triaxial tests were isotropically consolidated to the initial mean confining pressures shown on Table 4.5. The minimum B_{bar} was 0.96, with an average B_{bar} value of 0.98. To reach the desired B_{bar} level it was necessary to undertake back pressure saturation cycles to 250 to 750 kPa. The percentage of fines does not appear to have had a significant affect on the level of back saturation pressure required to achieve a B_{bar} value in excess of 0.96.

5.3.1 DEVIATOR STRESS - STRAIN

5.3.1.1 Comparison of Deviator Stress versus Strain curves

Figures 4.2, 4.3, 4.4 show the deviator stress plotted against percentage strain for the series of tests done at 5%, 7.5%, and 10% fines, respectively. Figures 4.5, 4.6, and 4.7 show the deviator stress plotted against percentage strain for the loose test only, and exclude the single dense samples at each fines content level.

A comparison of the post-peak deviator stress behavior between 5, 7.5 and 10% fines content tests shows a steeper deviator stress - strain slope at lower fines content than at higher fines content. This indicates that although flow liquefaction occurred in samples at all fines content, the rate at which shear strain was lost is different. A samples with higher fines content takes a gentler path to residual strength than does a clean sand sample. It is considered that the resistance to redistribution of the sand particles related to fabric effects and the generation of pore pressures explains this phenomenon.

5.3.1.2 Use of Brittleness Index to Compare Deviator Stress - Strain Responses

The brittleness index provides an indication of the severity of the loss of deviator stress between the peak and steady state values. This provides useful information for soils that exhibit a well-defined steady state stress level. However, the brittleness index does not provide information related to the strain corresponding to the stress levels used in the calculation of the I_B , which may be termed the rapidity of failure. The rapidity of failure may be useful in FEM analysis of deformations and stability assessments for earthworks constructed from liquefiable soils. A soil that collapses to some moderate undrained shear strength value under 1 or 2 % strain may have a greater role in determining the progressive instability of an embankment than a soil that collapses to a very low undrained shear strength but under 10% strain.

For comparison sake the brittleness index was calculated at three strains, 5% (I_B^5), 10% (I_B^{10}) and at steady state, about 20% (I_B^{ss}) and ratios relating the I_B at 5 and at 10% strain to that determined at steady state (I_B^5/I_B^{ss} and I_B^{10}/I_B^{ss}). The results of these calculations are

provided in Table 5.1. For all calculations the peak deviator stress used refers to the initial peak, usually reached within the first 2 to 4% strain.

The ratios of I_B^5/I_B^{ss} (A) and I_B^{10}/I_B^{ss} (B) show the degree to which the deviator stress had collapsed at 5 and 10% strain. If (A) and (B) are similar than the sample has experienced a rapid and permanent collapse. By denoting the product of I_B^5 and I_B^{10} as B_R some additional insight into the severity and rate of collapse may be discussed. This term is suggested as a means of relating the severity of the collapse in term of deviator stress and strain. B_R varies between 0 and 1. A B_R value of 1 indicates a complete and rapid loss of deviator stress while a value of zero could indicate either a strain hardening material or a material that shows no loss in deviator stress post peak until a complete collapse occurs after 5% strain. The latter condition is unlikely and as such a B_R of zero would indicate strain hardening. Other normalizations are possible, each with specific advantages and limitations for assisting in interpretation of the test results.

The maximum B_R value for a sample with 5% fines content was 0.66 (test r14). This sample experienced a rapid and substantial loss of strength. Maximum B_R values of 0.56 (test r27) and 0.48 (test r22) were recorded for 7.5% and 10% fines content. For these tests the samples collapsed within 5% strain but the severity of the collapse was not as marked as for the 5% sample. Minimum B_R values of near zero were obtained, indicating strain hardening conditions.

For strain softening samples, the ratio of I_B^5/I_B^{ss} ranged from 0.75 to 0.98 indicating that the sample collapse, in terms of deviator stress, was substantially complete within the first 5% strain. The ratio of I_B^{10}/I_B^{ss} ranged from 0.94 to 1.00 indicating that sample collapse was nearly complete by 10% strain.

Previous studies by Pitman (1993) and Georgiannou (1988) predict a decrease in brittleness with increased fines content. The results from my study are inconclusive in this regard, due to the inconsistencies in comparing samples prepared at different initial void ratios and consolidation pressures. Figure 5.11 shows the change in I_B with increased fines content for Pitman, Georgiannou and this study. Figure 5.12 shows only the I_B for this study.

5.3.2 PORE PRESSURE - STRAIN

5.3.2.1 Comparison of Pore Pressure - Strain Curves

Figures 4.8, 4.9 and 4.10 show the excess pore pressure developed during the shearing portion of the triaxial test plotted against percentage strain. Figures 4.11, 4.12 and 4.13 show the excess pore pressure developed during testing of very loose samples only. The

pore pressure plots were similar for most tests and showed a rapid increase in pore pressure during the first five percent strain after which little change in pore pressures developed. The pore pressure at five percent strain and the maximum excess pore pressure developed are summarized in Table 4.6. For the loose samples the excess pore pressures developed were in the range of 85 to 95% of the initial p' value.

The pore pressure plots for the very dense tests showed an initial increase in pore pressure followed by a rapid decrease in pore pressure, associated with sample dilation. The final excess pore pressures measured were in the range of negative 120 to 350 kPa that are in the range of the initial sample pore pressures. Greater negative pore pressures could have developed if greater initial pore pressures were set up. The testing of very dense samples requires high initial pore pressures, and therefore high initial cell pressures, to allow for large negative excess pore pressure to develop. The physical limitations of the triaxial test cell used did not allow for significantly greater initial cell pressures to be safely developed.

5.3.3 DEVIATOR STRESS - MEAN EFFECTIVE PRESSURE

5.3.3.1 Comparison of Deviator Stress - Mean Effective Pressure Curves

The stress paths in q - p' space for the triaxial tests are shown in Figures 4.14, 4.15 and 4.16. These plots show the deviator stress, q , versus mean effective pressure, p' , for the 5, 7.5 and 10 percent fines content tests respectively. Figure 4.17, 4.18 and 4.19 plots the p' - q diagram for the loose samples only for the 5, 7.5 and 10 percent fines content tests respectively. The loose samples typically show a slight increase in p' and q within the initial two percent strain, followed by a decrease in p' accompanied by increasing q . A peak q value is reached between two to four percent strain, after which both the q and p' values both decrease to steady state values. The shape of the stress path is characteristically initially semi circular before the peak q , and becomes tangential to a common steady state surface defined by the angle of friction, ϕ' by equation 5.3:

$$\phi = \arcsin\left(\frac{3(q / p')}{6 + (q / p')}\right) \quad [5.3]$$

At steady state the slope of the line through the origin and the steady state point in p' - q space is defined as M , as denoted in equation 5.4:

$$M = q / p'_{ss} \quad [5.4]$$

Therefore M and ϕ_{ss} are related as such:

$$\phi_{ss} = \arcsin\left(\frac{3M}{6+M}\right) \quad [5.5]$$

Figures 4.17 to 4.19 show the test results for loose samples only and provide greater detail. The q-p' curves approach a common tangency but do not all terminate along this tangency or reach the same final conditions of p'_{ss} and q'_{ss} . Since the void ratios were not consistent between different fines content for a given starting p' value it is not prudent to make comparisons of final p' , peak q or q'_{ss} values.

5.3.3.2 Comparison of Normalized Deviator Stress - Mean Effective Pressure Curves

Figures 4.14 to 4.19 provide an overall view of the stress path response. However, to compare the behavior across a wide range of stress levels a normalized approach is preferred. Figures 4.20, 4.21 and 4.22, representing the 5, 7.5 and 10 percent fines content tests, show the stress paths normalized by dividing both the q and p' values by the corresponding p'_{ss} determined for that test. The figures provide a useful means of comparing the stress path behavior of very loose samples tested at a wide range of confining stresses and the stress path behavior of dense samples which shear at very high stresses. The normalized p/p'_{ss} value can be compared to the horizontal distance on the void ratio - $\log p$ diagram. The horizontal measure is related as noted in equation 5.6:

$$\text{Horizontal distance} = \log(p') - \log(p'_{ss}) = \log\left(\frac{p'}{p'_{ss}}\right) \quad [5.6]$$

The maximum value of p'/p'_{ss} as shown on Figures 4.20 to 4.22 decreases from 14 to 11 to 7 as the fines content increases from 5 to 7.5 to 10%. Maximum p/p'_{ss} values of about 20 were determined by Sasitharan (1994) and Cuning (1994) for clean Ottawa Sand. The decrease in p/p'_{ss} values is an indication of the decrease in brittleness of the samples as the fines content increases. It is also an indication that it becomes increasingly difficult to make very loose samples and the fines content increases. Figure 5.6 shows the calculated I_B values versus p'/p'_{ss} . A natural logarithmic trendline through the data points predicts the following relationship:

$$I_B = 0.168 \ln\left(\frac{P'_o}{P'_{ss}}\right) + 0.38 \quad (5.7)$$

with a correlation coefficient, R^2 , of 0.82

Close inspection of the data on Figure 5.6 also shows the decrease in brittleness of the samples as the fines content increases. Boundaries have been placed on the figure to show

the upper bound that each level of fines content reaches. The relationship between I_B and p'/p'_{ss} is also shown on Figure 5.7 with data from other researchers superimposed. A similar curved relationship is evident, however, the data points approach the $I_B = 1$ line at much lower p'/p'_{ss} values (less than 7 versus > 20 for this study). The steeper slope may be due to test methods, resulting in an inability to make very loose samples that are highly collapsible, or due to material differences. The superimposed data are from Hird and Hassona (1990) for Leighton Buzzard Sand, and from Been and Jefferies (1985) and Sladen *et al* (1985) for Kogyuk Sand. The apparent difference in $I_B - p'/p'_{ss}$ curves may simply indicate that different materials have unique $I_B - p'/p'_{ss}$ relationships.

Figures 5.8, 5.9 and 5.10 show the normalized $p'-q$ diagrams with the interpreted M , s and β lines. These lines represent lines through the final or ultimate state and origin (M), tangent to the collapse surface (s) and through the peak deviator stress and ultimate state points (β). The interpreted values are summarized on Table 5.2. The slope of the collapse surface, the line through the peak deviator stress and the line through the steady state point all tend to decrease as fines content increases.

5.3.4 VOID RATIO - MEAN EFFECTIVE PRESSURE

The changes in state during the consolidation stage of the triaxial test are shown on the void ratio - log mean effective pressure diagrams, Figures 4.23, 4.24 and 4.25. These figures show the void ratio plotted against the log of mean effective pressure for the 5, 7.5 and 10 percent fines content tests, respectively. The maximum and minimum void ratio state lines and the steady state line are shown on each figure. These lines were derived from the consolidation lines of the loose and dense samples respectively.

5.3.5 STEADY STATE CONDITIONS

5.3.5.1 Steady State Conditions - This Study

The steady state parameters, as derived from Figures 4.23, 4.24 and 4.25 are summarized on Table 5.3. The terms Γ , λ refer to the void ratio at $p'=1$ and the slope of the steady state line, respectively. The results show that as the percent fines increases, λ increases and the steady state lines tend to rotate about the $p'=1$ and $e=0.8$ coordinates. The $p'=1$ void ratio dropped as the fines content increased from zero to five percent, and increased thereafter. The intercept would be expected to increase as further fines content increased until the intercept matched the 100 percent Kaolinite content intercept. The slope of the steady state line increased steadily as Kaolinite content increased. This is indicative of the increase in compressibility of the samples. Figure 5.13 shows the rotation of the steady state lines as fines

content are increased. The slope of the SSL for 20% fines content is based on data from Pitman (1993) and this study. Based on additional testing by Pitman on Ottawa sand samples with 30 and 40% fines, a further increase in the slope is anticipated such that the SSL for Ottawa sand with 40% would approach the SSL for Kaolinite. Hypothetical steady state lines for 30 and 40% fines are shown on Figure 5.13.

Figure 5.14 shows the SSL, e_{min} and e_{max} lines for various Kaolinite fines content. The slope of the e_{max} line was steeper than the corresponding SSL at all fines contents. This is an important finding because a common assumption in steady state design is that the consolidation line and SSL are parallel. This study shows that the consolidation line and the SSL are not parallel at fines contents as low as 5%. The deviation from parallel increases with fines content. As the percentage of fines increased the $p'=1$ void ratio intercept and slope increased for the loosest state, or consolidation, line. In all cases the consolidation line state parameters λ_d and Γ_d were greater than the steady state line parameters.

The slope of the densest line, λ_d marginally increased as the percentage of fines increased. The value of Γ_d decreased marginally as the fines content increased. It should be noted that the state parameters for the dense samples are based on limited test results.

The initial state parameter, Ψ , was determined for all samples based on the steady state parameters listed in Table 5.3. The initial state parameters are presented in Table 5.4, and are also shown on the normalized p' - q diagrams, Figures 4.20, 4.21 and 4.22.

5.3.5.2 Steady State Conditions - Other Studies

The rotation of the SSL due to increased fines has been investigated by Been and Jefferies (1985), and Hird and Hassona (1990), among others. Figure 5.15 shows the SSL's for Kogyuk sand with varying levels of mica as reported by Been and Jefferies. The rotation of the SSL was observed with the addition of as little as 2% mica to the Kogyuk sand. The SSL appears to rotate about a mean effective stress point of about 50 kPa.

Figure 5.16 shows a similar phenomena for Leighton Buzzard Sand (LBS) described by Hird and Hassona (1990). In this case the rotation of the SSL continued as the content of mica fines was increased to 30%. The change in the slope and intercept of the SSL was not constant for a given change in fines content between the Kogyuk, LBS, or Ottawa sand used in this study. This suggests that a unique relationship between the position and slope of the SSL is likely for a given sand and a given type and percent of fines content. For comparison purposes the SSL of Ottawa sand, LBS and Kogyuk sand with 10% fines content are plotted on Figure 5.17. A more comprehensive grouping of SSL's is shown on Figure 5.18.

Figure 5.19 shows the steady state line determined by Robertson and Skirrow (1994) for Hong Kong Pearl River Sand. The steady state line was probed using undrained and drained isotropically consolidated triaxial compression tests. The figure shows that a unique steady state line results from test done in both drained and undrained conditions. Undrained triaxial tests are generally considered simpler to run, and eliminate the need to track the void ratio during shear. However, the testing of very dense samples may be more appropriately done using drained tests. The present study had difficulty in achieving steady state conditions for very dense samples tested in an undrained state. Figure 5.19 shows the undrained and drained loading paths in $e - \log p'$ space.

5.3.6 STATE PARAMETER, ψ

5.3.6.1 State Parameter Related to Mean Effective Stress

The state parameter is a useful parameter for describing the state of a soil sample relative to the steady state condition. Table 5.4 presents a summary of ψ values for all tests. The value of ψ may be positive or negative. A positive ψ value may be interpreted as a condition of potential contraction and strain softening behavior. A negative ψ value may be interpreted as a condition of potential dilation and strain hardening.

The value of ψ was found to increase at lower mean effective pressures and decrease with higher mean effective pressures. This is due to the steepness of the consolidation lines in relation to the SSL. The change in ψ with mean effective stress is shown on Figure 5.20. This figure is an alternative method of showing the increased compressibility with increased fines, as also shown in Figure 5.5. It is also evident from Figure 5.20 that samples cannot be made at combinations of void ratio and mean effective stress above the positive ψ line or below the negative ψ line, assuming that these lines represent the loosest and densest possible states, respectively.

Calculated values of ψ have been indicated on Figures 4.20, 4.21 and 4.22. Based on the general shape and location of the p' - q plots on these figures, a comparison was made of p' - q plots at arbitrary ψ values of 0.05 and 0.1. Figure 5.21 shows this comparison. At a given ψ value the maximum p/p'_{ss} and q/p'_{ss} are found to decrease as fines content increases. The undrained behavior of a sand is therefore dependent not only on the amount of fines, but also on the initial state conditions.

5.3.6.2 State Parameter Related to Brittleness Index

Figure 5.21 may be reinterpreted to show the change in brittleness as ψ changes. This is shown in Figure 5.22. The brittleness is shown to decrease as fines content is increased and also as the ψ value is decreased. A unique relationship appears to related ψ and I_B at each level of fines content. This observation holds for 5, 7.5 and 10% fines content levels and is expected to hold at least to the 20% fines content level, as shown by the single data point at 20% fines content on Figure 5.22. Another interpretation of this figure is that a given level of brittleness may be achieved at any fines content level provided the value of ψ sufficient to produce the required I_B is possible.

5.3.6.3 State Parameter Related to Unconfined Shear Stress

The minimum (residual) shear strength (s_u) of liquefied deposits is of interest for slope stability design considerations for tailings dams and other earthworks. Figure 5.23 shows the ratio of s_u/p'_o plotted against the ψ value for all contractive samples. This figure generally shows that as the state parameter is increased the available post liquefaction shear strength, as a ratio of the initial p' condition, decreases. Since the value of s_u/p'_o is related to I_B , this finding was anticipated. Figure 5.24 extends these findings for the dense samples, i.e. the samples that dilated. A best fit line was determined, as given by Equation 5.8 with a correlation coefficient of 0.70:

$$\frac{S_{u@USS}}{p'_o} = 0.527 \exp^{-14.46\psi} \quad (5.8)$$

The relationship between ψ and RSR is given by:

$$RSR = \ln\left(\frac{p'_o}{p'_{ss}}\right) = \frac{\psi}{\lambda_{ln}} \quad (5.9)$$

The theoretical relationship between s_u/p'_o and ψ may be therefore be determined by combining Equations 5.4, 5.6 and 5.9 to produce:

$$\frac{S_{u@ss}}{p'_o} = \left(\frac{M}{2}\right) \exp\left(\frac{-\psi}{\lambda}\right) \quad (5.10)$$

The undrained shear strength at steady state may therefore be predicted once the state parameter and slope of the state line are known. Figure 5.23 shows measured values of s_u/p'_o , annotated with the associated fines content, with curves of s_u/p'_o versus ψ for each level

of fines content, based on the associated state parameters. The measured values plot very near the predicted curves in most instances.

Figure 5.24 indicates that substantial strain hardening occurs at ψ values less than about -0.04. It also shows that for the predicted undrained shear strength for negative values of ψ will be higher for a clean sand than for a silty sand, which is the reverse condition for positive values of ψ . The wide scatter of data in the negative ψ range is partly a result of the termination of the undrained triaxial tests on dense samples prior to achieving steady state conditions. The scatter also suggests that it may be inappropriate to use a "best fit" line to predict the undrained shear strength. This observation holds for both the negative and positive values of ψ .

5.4 Shear Wave Velocity Results

Shear wave measurements were taken during the consolidation portion of six triaxial tests. The loosest and densest samples consolidated to an initial mean confining stress of 450 kPa at each of the 5, 7.5 and 10 percent fines were used for shear wave velocity measurements. The shear wave velocities measured and the associated void ratio and mean confining stress are presented in Table 4.7. Shear wave measurements were attempted at steady state conditions with little success.

5.4.1 SHEAR WAVE VELOCITY - VOID RATIO

Figure 4.30 shows the shear wave velocity plotted against void ratio. There is a wide scatter of data in this plot but the general trend is for a reduction in shear wave velocity as void ratio increases. The wide range in shear wave velocities can be narrowed through normalization using the confining mean effective stress as described below.

5.4.2 NORMALIZED SHEAR WAVE VELOCITY - VOID RATIO

Figure 5.25 shows the normalized shear wave velocity plotted against void ratio. The normalization was accomplished using the following relationship:

$$V_s' = V_s \left(\frac{p_c'}{p_a} \right)^{0.266} \quad (5.11)$$

where: $p_a = 100$ kPa

The scatter in data using this normalization is reduced to a band width of ± 30 m/s.

5.4.3 SHEAR WAVE - VOID RATIO - MEAN EFFECTIVE STRESS RELATIONSHIP

Research on the shear wave velocity - void ratio - mean effective pressure relationship was carried out on Ottawa sand by Sasitharan (1993). Sasitharan developed procedures for measuring shear wave velocity using bender element technology and it was his testing equipment that was used for the most of this work. Sasitharan gave a relationship between V_s - e - p' , based on Hardin and Richart (1963) as;

$$V_s = (100.2 - 57.3e)p'^{0.25} \quad (5.12)$$

The measured shear wave velocities versus mean effective stress are shown on Figure 5.26. The upper and lower bounds were using:

$$V_s = (109 - 72e)p'^{0.266} \quad (5.13)$$

The values of 109 and 72, representing " m_1 " and " m_2 " in the Hardin and Richart equation (Table 2.1), were determined to produce the best fit to the actual data. Figure 5.26 shows that the maximum shear wave velocities increase as the mean effective stress increases and that denser sands will produce higher shear wave velocities than looser sands at a given effective stress. It is also evident that there is a practical upper bound to the measured shear wave velocities.

5.4.3.1 Shear Wave Velocity Contours

Contours of shear wave velocity may be superimposed onto void ratio - mean effective stress plot using V_s - e - p' relationships derived from Table 4.7. Equation 5.13 was rewritten as shown in Equation 5.14 and was used to develop the shear wave contour shown on Figure 5.28 and Figure 5.29.

$$p' = \left[\frac{V_s}{(109 - 72e)} \right]^{1/0.266} \quad (5.14)$$

By keeping V_s constant and varying the void ratio, values of p' were determined, thereby producing coordinates in e - p' space of constant V_s . Figure 5.28 shows only the V_s contours superimposed on an e - $\log p'$ graph. The contours have been bounded to the zone between the e_{min} and e_{max} lines. Figure 5.29 further superimposes the measured V_s values. The measured V_s values plot within the appropriate contours with few discrepancies.

The use of linear equations such as Equation 5.13 to produce contours of shear wave velocity is valid over a limited range of void ratios since this type of equation predicts a shear

wave velocity equal to zero as the void ratio approaches A/B (about 1.5). Reilly (1995) proposed a best fit exponential relationship between V_{s1} and e given by;

$$V_{s1} = (139.54e^{-0.9019})K_o^{0.125} \quad (5.15)$$

Shear wave velocity contours may be plotted using this exponential relationship. Within the void ratio range from 0.5 to 1.0 there is a close agreement between the linear and exponential equations. Equation 5.15 provides a useful means of interpreting shear wave measurements for higher void ratio conditions, perhaps for highly angular sands of open slightly cemented sands. Within the void ratio range determined for Ottawa Sand, with less than 20% fines, Equation 5.14 is considered more appropriate.

Shear wave velocity contour plots were also developed by Cunning (1994) for Ottawa sand, Alaska Tailings Sand and Syncrude Tailings Sand, and by Robertson and Skirrow (1994) for Hong Kong Pearl River Sand. The values of m_1 , m_2 and n in Roesler's equation (Table 2.1) vary between given soils. It is therefore necessary to produce contour plots for each soil. The use of V_s contours provides a useful means of checking the validity of V_s data and an easy means of estimating state.

5.4.4 MEAN EFFECTIVE STRESS - VOID RATIO - SHEAR WAVE VELOCITY RELATIONSHIP FOR OTHER SANDS

Figure 5.30 plots the normalized V_s against void ratio for a wide variety of sands. The $V_s - e$ data from highly compressible sands, such as the Alaska Tailings Sand (Thane sand), and incompressible sands, such as Ottawa Sand, all plot within a reasonably narrow band. The band width is about ± 25 m/s. Moderately calcareous, uncemented Pearl River sand was also found to plot within this band. The V_{s1} decreases with increased void ratio for all sand types. A generalized relationship given by Equation 5.16 was developed to describe the trendline of the Ottawa sand data obtained from this study, and also from Cunning (1994) and Sasitharan (1994):

$$V_{s1} = 373 - 245e \quad (5.16)$$

The values of 373 and 245 represent the "A" and "B" constants in Robertson's equation (1992) shown in Table 2.1. Other $V_{s1} - e$ relationships are summarized in Table 2.3, $V_{s1} - e$ relationships determined from this study are summarized on Table 5.6. An additional relationship was determined for all data;

$$V_{s1} = 355 - 228e \quad (5.17)$$

There is clearly some difference between the relationship developed by Sasitharan for Ottawa sand and that determined for all sands and shown in Equation 5.17. Figure 5.27 shows a plot of Vs backcalculated using Vs1 - Vs relationships against the measured Vs values for this study. The correlation coefficients for Equation 5.16 and Equation 5.17, were determined to be 0.97 and 0.98, respectively, indicating a very good correlation for both equations.

The difference between these two equation is minor, as shown on Figure 5.30. Equation 5.17 provides a reasonable approximation of the Vs1 - e relationship for all sands. The A and B parameters determined for Equations 5.16 and 5.17 are biased towards the sand with the greatest number of data points, clean Ottawa Sand. If a given sand is known to be relatively compressible or incompressible some refinement may be done to better approximate the Vs1 - e.

5.4.5 SHEAR WAVE VELOCITY - VERTICAL EFFECTIVE STRESS

Using Equation 5.18 (Sasitharan, 1994), a plot of shear wave velocity against effective vertical stress can be made for a given value of Ko and ψ.

$$V_s = \left[\psi - \left(\frac{A}{B} - \Gamma \right) - \lambda_{in} \ln \left(\frac{\sigma_v}{3} (1 + 2K_o) \right) \right] \left[\frac{B(\sigma_v)^{na+nb} K_o^{na}}{P_a^{na+nb}} \right] \quad (5.18)$$

Figure 5.31 shows the results of Equation 5.18 for an assumed Ko value of 0.4, at a ψ value of 0, representing steady state conditions. The plot of Vs - σv at ψ = 0 represents the boundary between contractive and dilative behavior. As fines content increases the boundary shifts to the right on Figure 5.31. The direction of the shift is not what would be expected, and there may be some question regarding the validity of this methodology. It should be noted that the prediction of the contractive/dilative boundary is based purely on the e and p' values determined through laboratory testing, and the general Vs equation developed for all sands. Application of the same methodology to Hird and Hassona's (1990) steady state results for Leighton Buzzard Sand produces Figure 5.32. The boundary between contractive and dilatent behavior shifts to the left in Figure 5.32 as the fines content is increased, which is a more conventional assessment. The methodology is therefore applicable and the direction of the boundary shift is therefore related to the input parameters Extending this methodology to Ottawa Sand at a higher ψ and Ko level shows the same direction of shift, as shown in Figure 5.33. The Vs - σv lines on Figure 5.33 do not indicate the contractive/dilative boundary but would be an indication of the degree or severity of collapse, as discussed earlier. A further increase in Ko to 1.0 again shows a shift in the lines to the right, as shown in Figure 5.34.

Figure 5.35 compares the $V_s - \sigma_v$ lines for clean and 10% Kaolinite Ottawa sand at corresponding K_o values of 0.4 and 1.0, at steady state. The $V_s - \sigma_v$ lines shift to the right as K_o increases, as well as when the percentage fines increases. There is a slightly larger shift to the right between the $K_o = 0.4$ and $K_o = 1.0$ lines at 10% Kaolinite than for the shift for clean sand. The same conditions are shown on Figure 5.36, for a ψ value of 0.1.

5.4.6 SPT RELATIONSHIPS

One of the most practical application of shear wave velocity measurements is the development of a contractive-dilatant boundary based on conventional SPT or CPT soundings for a given soil deposit. Once a boundary has been established field conditions can be rapidly assessed using accepted field test methods that most practitioners have a high level of comfort with. Yoshida *et. al.* (1988) developed an equation to estimate the Standard Penetration Test blow count, corrected to 60% efficiency, N_{60} . This equation is given as:

$$N_{60} = \left[\left(\frac{V_s}{89.8} \right) \left(\frac{100}{\sigma'_v} \right)^{0.14} \right]^4 \quad (5.19)$$

Using Equation 5.18 and 5.19 it is possible to determine a contractive/dilatant boundary in terms of N_{60} plotted against the vertical effective stress, σ'_v at varying fines content. Figure 5.37 shows the results of this analysis for a K_o value of 0.4, at steady state conditions. The shift in the contractive boundary to the right, as fines are added, implies that the use of a single N_{60} line for a given deposit may lead to incorrect prediction of contractive/dilatant behavior. Data points that may plot on the dilative side of a $N_{60} - \sigma_v$ line for clean sand may plot on dilative side of a 5% fines line.

It should be noted that although the potential for contractive undrained behavior increases as fines content increased, the severity of the "collapse" decreases. Additionally, it becomes difficult to make loose, contractive, samples as fines content increases. This phenomena would likely produce higher N_{60} as the vertical effective stress increase in-situ, thereby producing N_{60} data points on the dilative side of the boundary.

Figure 5.38 shows the application of Equation 5.19 to the shear wave velocity curves shown in Figure 5.32 for Leighton Buzzard Sand. The shift in the boundary is to the left and the magnitude of the shift is reduced. This figure indicates that the shift in the boundary depends on the steady state parameters, in particular the location of the point about which the steady state lines "pivot" in $e - \ln p'$ space.

Figure 5.39 shows for Ottawa Sand the shift in the $N_{60} - \sigma_v$ lines as fines content increases, for steady state and $K_o = 1.0$ conditions. Figure 5.40 plots the increase in N_{60} as fines content increases for steady state conditions. The increase in N_{60} becomes larger as the effective vertical stress increases.

5.4.7 CPT RELATIONSHIPS

The change in N_{60} with increased fines content is mirrored in cone penetration analysis. Based on Robertson *et al.* (1992) the following equation was used to plot curves of q_c versus effective vertical stress:

$$V_s = 102q_c^{0.23} \left(\frac{\sigma'_v}{P_s} \right)^{0.135} \quad (5.20)$$

Figure 5.41 and 5.43 show the change in the $q_c - \sigma_v$ lines at steady state conditions for $K_o = 0.4$ and 1.0 respectively. The q_c was found to increase fourfold between the clean sand and 10% fines content lines at $K_o = 0.4$. An even greater increase was noted at $K_o = 1.0$. This observation implies that without due regard for the fines content of a deposit, even very high q_c values may be indicative of contractive behavior. Figure 5.42 shows the $q_c - \sigma_v$ lines for Leighton Buzzard Sand. Figure 5.44 shows the net increase in q_c values as fines content increases, plotted against effective vertical stress.

5.5 Testing Limitations

The testing undertaken for this study was limited mainly to loose sand samples and the collection of V_s data during the consolidation portion of testing on dense samples. Shear testing of dense samples generally did not reach steady state conditions due to limitations created by the generation of large negative excess pore pressures during shear, a result of the sample dilation. Data scatter in this study is considered to be due to a combination of laboratory constraints, minor non-uniformity in the samples, such as thin looser zones or zones of higher fines content, the use of an average void ratio for the entire sample (rather than for the failure zone) and fabric discontinuities.

The application of laboratory test results to a real soil must be used with caution and with a full awareness that real soil may exhibit a structure that is not reproducible using reconstituted techniques, whether moist tamped, pluviated or whichever. This fabric effect may take many forms. Thin layers of clay within a sandy strata would likely govern the undrained behavior of a sample. Segregated, recently deposited sand may be expected also exhibit a preferred slip surface inconsistent with homogeneous laboratory samples. The fabric of

samples sheared to steady state is considered to be the same, irrespective of initial fabric, as stated by Oda (1972). However, the initial constituents need to be well matched in the first place.

Been and Jefferies (1985) noted that thin loose zones are created between layers during and that denser samples were more uniform. Void ratio variations of ± 0.011 may be expected. Thin zones are horizontal and would therefore have little effect on the triaxial test results. They assumed that the use of an average void ratio would be simpler to study and check. The scatter due to fabric effects was thought to be small since most fabric is altered to more or less the same conditions at steady state.

Martin *et al.* (1975) note that triaxial test results are difficult to interpret if $S < 1$. The small variation in B_{bar} values may account for some data scatter. Hird and Hassona (1990) estimated a margin of error of ± 0.015 for Ψ . This value is considered applicable to the present study. Depending on the value of λ a deviation in ψ of 0.015 may result in a deviation in p'_{ss} of 10 to 100 kPa.

5.5.1 REPEATABILITY

Initial triaxial testing was undertaken to reproduce results achieved by Sasitharan (1994). These trials produced steady state conditions consistent with those determined by Sasitharan, implying that the test procedures outlined by Sasitharan were adequate to produce high quality consistent samples. The author spent many hours making samples with differing compaction efforts, height of lifts, vacuum pressure, etc. It is possible to make very loose test specimens at a consistent initial void ratio, at fines content up to at least 10%.

**TABLE 5.1
VOID RATIO CALCULATIONS
OTTAWA SAND WITH ADDED KAOLINITE FINES**

Test No.	% Kaolinite	Brittleness Index and Brittleness Ratios					
		I_B^5 (A)	I_B^{10} (B)	I_B^{SS}	I_B^5/I_B^{SS}	I_B^{10}/I_B^{SS}	B_R (A)*(B)
r7	0	na	na	na	na	na	na
r8	0	na	na	na	na	na	na
r9	0	0.56	0.62	0.70	0.80	0.89	0.35
r13	5	0.01	0.01	na	na	na	0.00
r14	5	0.78	0.85	0.87	0.90	0.98	0.66
r15	5	0.52	0.61	0.62	0.84	0.98	0.32
r23	5	0.78	0.79	0.80	0.98	0.99	0.62
r26	5	na	na	na	na	na	na
r16	7.5	0.68	0.77	0.81	0.84	0.95	0.52
r17	7.5	0.36	0.47	0.48	0.75	0.98	0.17
r18	7.5	0.20	0.23	0.24	0.83	0.96	0.05
r27	7.5	0.71	0.79	0.80	0.89	0.99	0.56
r28	7.5	na	na	na	na	na	na
r10	10	0.39	0.40	0.41	0.95	0.98	0.16
r11	10	0.56	0.62	0.66	0.85	0.94	0.35
r12	10	0.64	0.71	0.72	0.89	0.99	0.45
r22	10	0.67	0.72	0.75	0.89	0.96	0.48
r25	10	na	na	na	na	na	na
r19	20	0.52	0.56	0.56	0.93	1.00	0.29

**TABLE 5.2
SUMMARY OF NORMALIZED p'-q PARAMETERS**

Fines Content (%)	Ultimate State Slope		Collapse Surface Slope	Peak Deviator Slope
	M	ϕ'	s	β
5	1.21	30.2	1.09	0.71
7.5	1.16	29.0	0.98	0.67
10	1.20	29.9	0.94	0.60

**TABLE 5.3
STEADY STATE PARAMETERS
OTTAWA SAND WITH FINES**

FINES CONTENT (%)	STEADY STATE PARAMETERS			
	Line	Γ	λ	p' RANGE (kPa)
0	Consolidation or loosest	na	na	na 10-1000 na
	Steady State	0.926	0.032	
	Densest	na	na	
5	Consolidation or loosest	0.942	0.039	
	Steady State	0.823	0.033	
	Densest	0.545	0.014	
7.5	Consolidation or loosest	1.129	0.083	
	Steady State	0.829	0.052	
	Densest	0.539	0.015	
10	Consolidation or loosest	1.458	0.156	
	Steady State	0.840	0.070	
	Densest	0.526	0.017	
20	Consolidation or loosest	na	na	na na
	Steady State	0.977	0.120	
	Densest	na	na	
100	Steady State	1.850	0.260	

**TABLE 5.4
INITIAL STATE PARAMETERS
OTTAWA SAND WITH FINES**

% Kaolinite Fines and State Parameters	INITIAL STATE					
	Test No.	e	e _{ss}	Ψ	$\frac{\Psi}{\lambda}$	$\frac{p'_o}{p'_{ss}}$
0 Γ=0.926 λ _{in} =0.0324	r8	0.819	0.754	0.0825	2.55	0.60
	r9	0.807	0.807	0.0705	2.18	7.32
5 Γ=0.823 λ _{in} =0.0334	r13	0.623	0.623	-0.005	-0.14	0.70
	r14	0.725	0.725	0.086	2.58	13.98
	r15	0.705	0.705	0.049	1.47	4.26
	r23	0.700	0.700	0.081	2.42	10.65
	r26	0.457	0.457	-0.162	-4.87	0.28
7.5 Γ=0.829 λ _{in} =0.052	r16	0.654	0.654	0.131	2.51	10.94
	r17	0.583	0.583	0.043	0.83	1.94
	r18	0.599	0.599	0.033	0.63	0.95
	r27	0.617	0.617	0.108	2.06	8.89
	r28	0.448	0.448	-0.061	-1.17	0.31
10 Γ=0.840 λ _{in} =0.070	r10	0.479	0.479	0.048	0.69	4.46
	r11	0.541	0.541	0.086	1.24	5.62
	r12	0.627	0.627	0.136	1.95	7.03
	r22	0.501	0.501	0.088	1.25	6.57
	r25	0.422	0.422	0.008	0.12	0.26
20 Γ=0.977 λ _{in} =0.120	r19	0.549	0.549	0.171	2.45	3.52

* - Based on measured p'_{ss}, not p'_{ss} determined from steady state line.

TABLE 5.5
SHEAR WAVE AND STEADY STATE PARAMETERS

Material	A	B	n	Γ	$\lambda \ln$
Ottawa (Clean)	381	259	0.266	0.926	0.0324
Ottawa (5% Kaolinite)	368	221	0.266	0.823	0.0334
Ottawa (7.5% Kaolinite)	362	227	0.266	0.829	0.0523
Ottawa (10% Kaolinite)	337	178	0.266	0.840	0.0698
Ottawa (20% Kaolinite)	na	na	0.266	0.977	0.12

FIGURE 5.1 GRAIN SIZE DISTRIBUTION FOR SEVERAL SANDS
with LIQUEFACTION POTENTIAL LINES
(Seed et al., 1976)

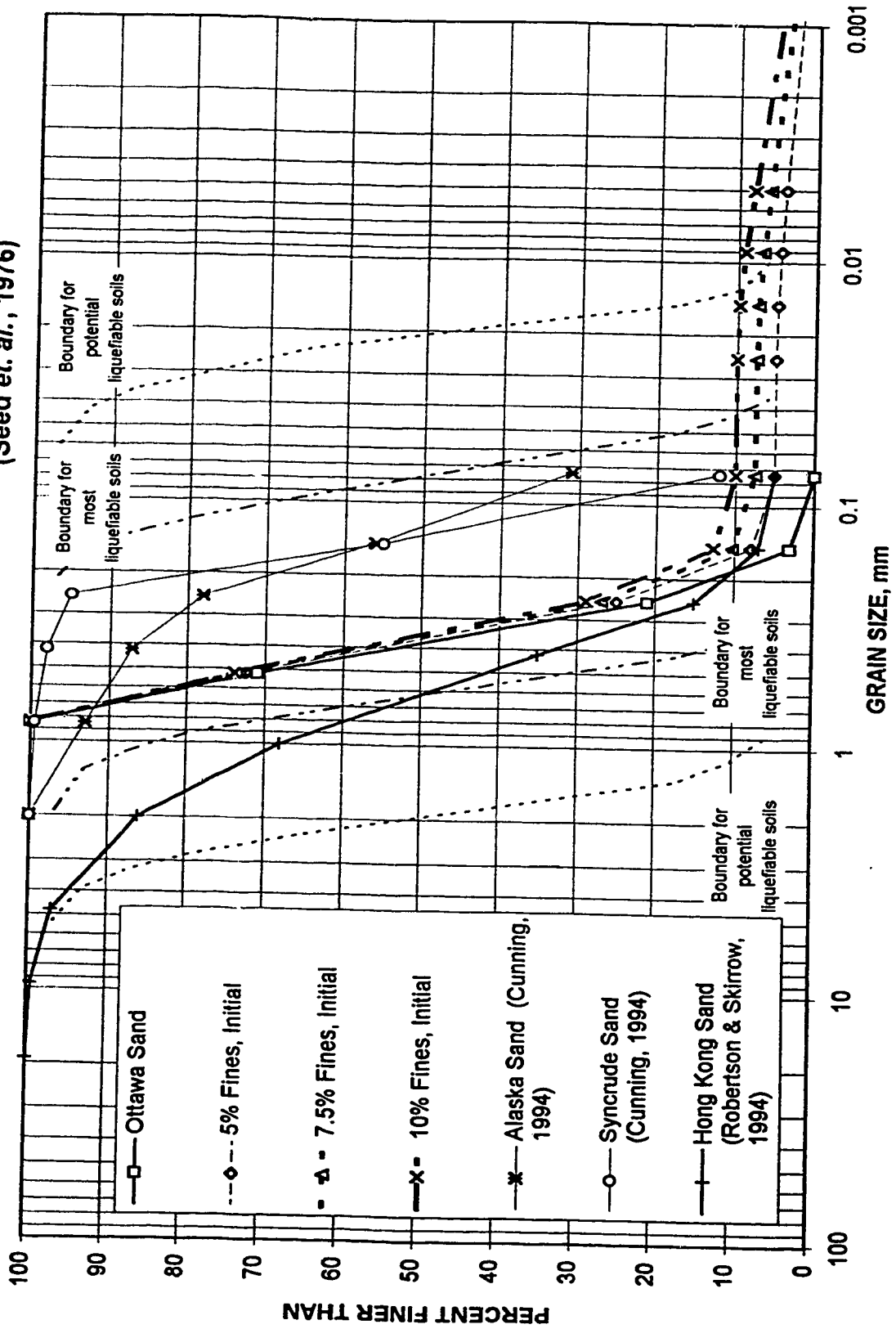


FIGURE 5.2 CHANGE IN INTERGRANULAR VOID RATIO WITH INCREASING FINES CONTENT

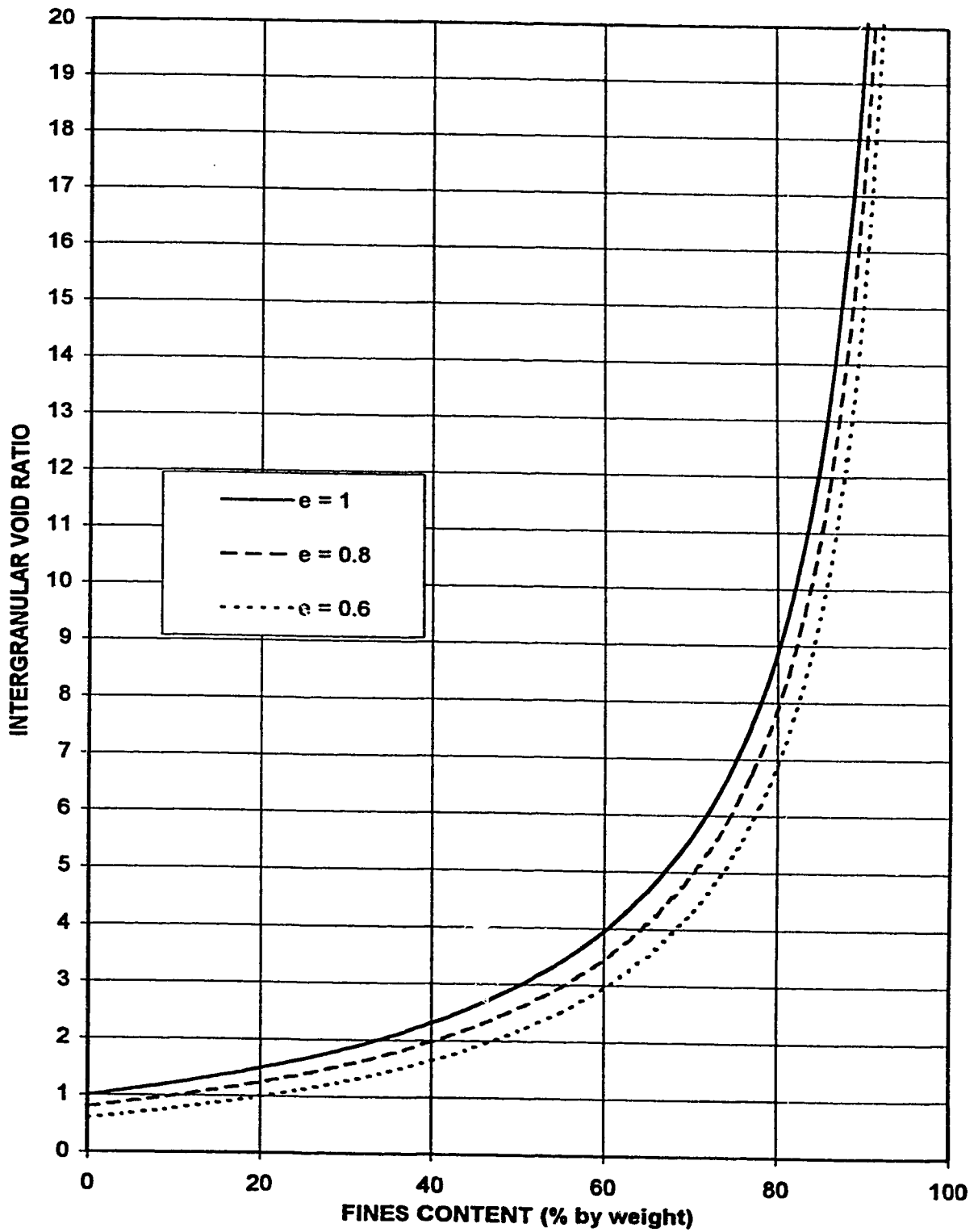


FIGURE 5.3 MINIMUM VOID RATIO versus MEAN EFFECTIVE STRESS
Ottawa Sand With Varying Kaolinite Content

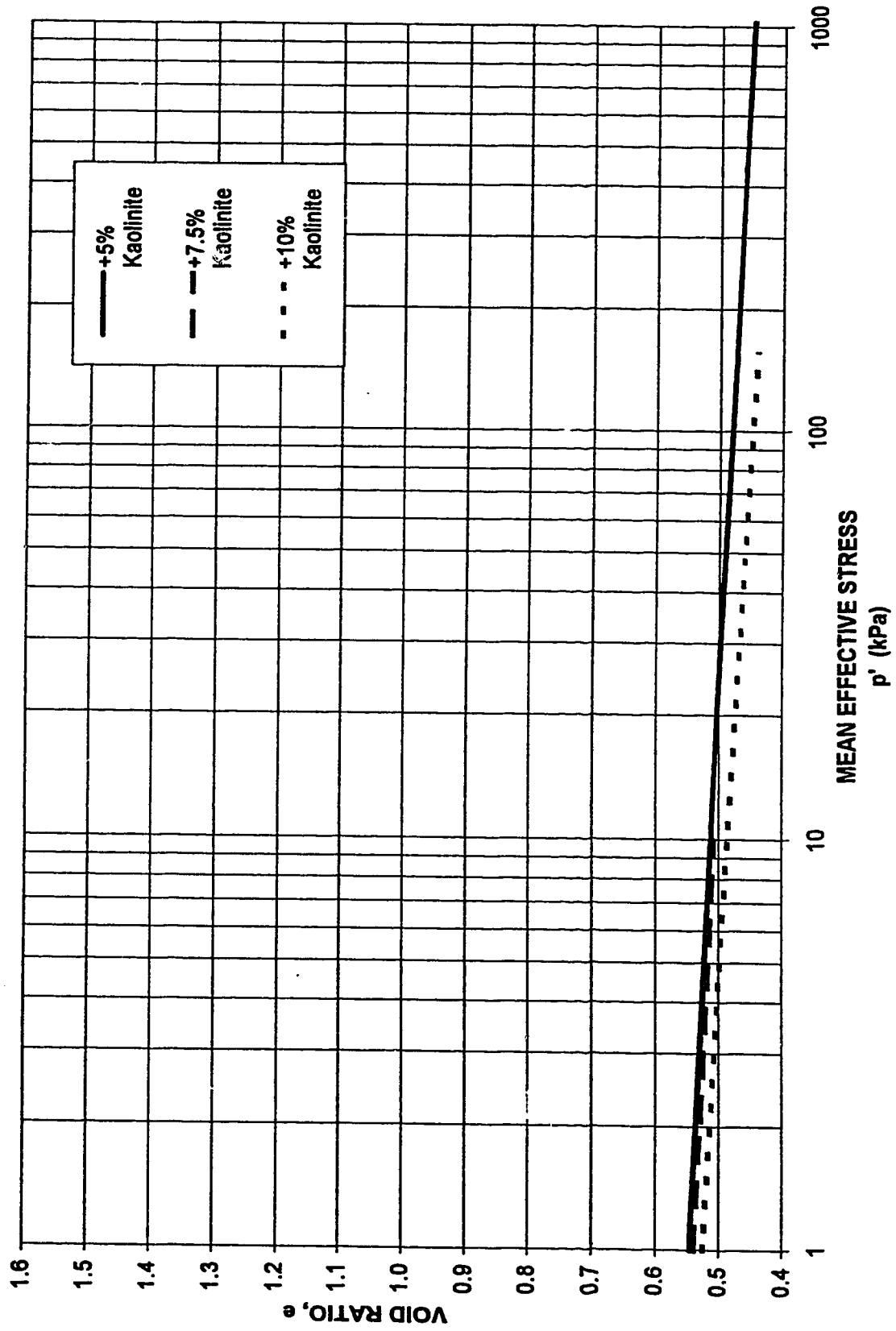


FIGURE 5.4 MAXIMUM VOID RATIO versus MEAN EFFECTIVE STRESS
Ottawa Sand With Varying Kaolinite Content

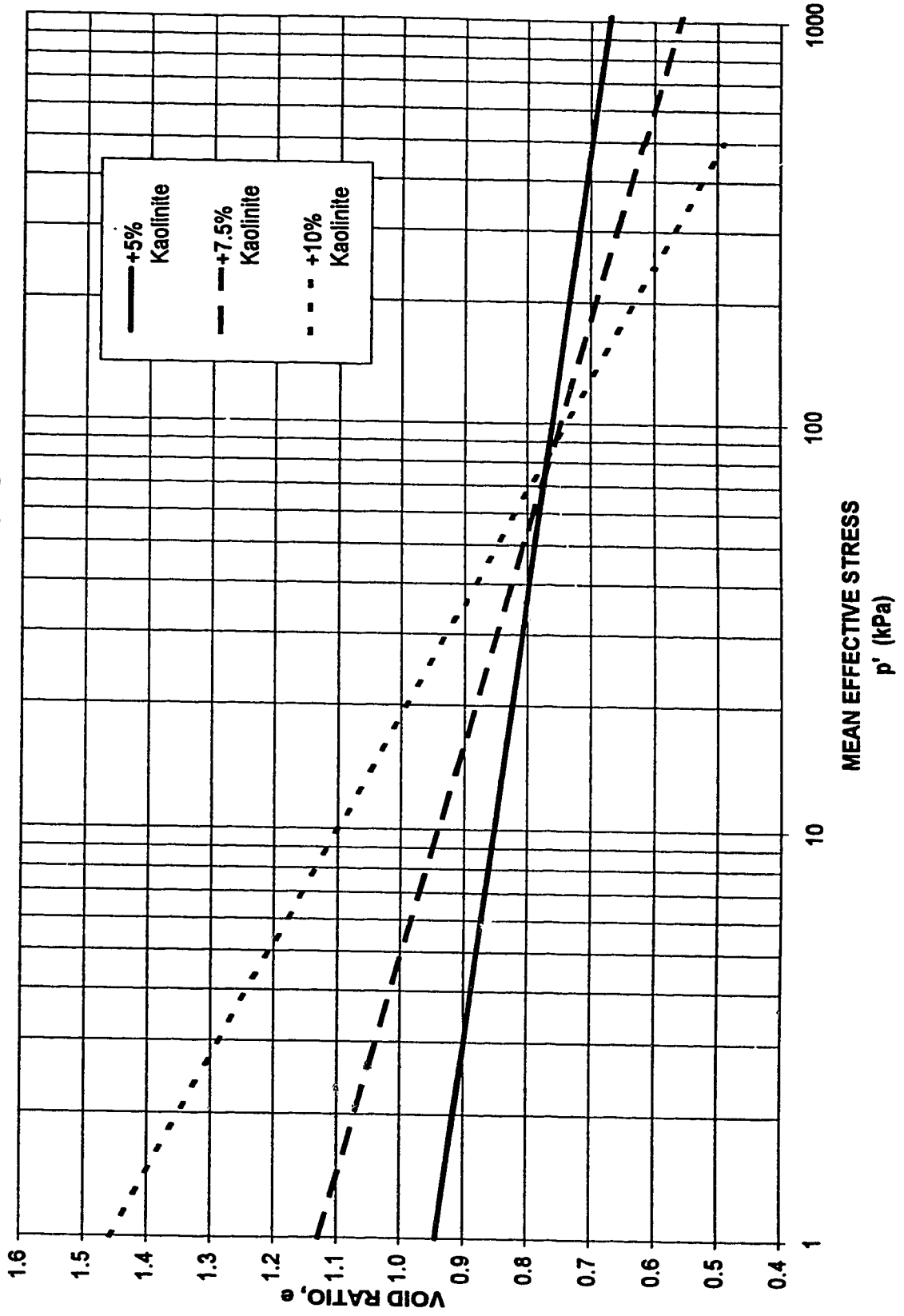


FIGURE 5.5 COMPRESSIBILITY versus MEAN EFFECTIVE STRESS
Ottawa Sand with Varying Kaolinite Content

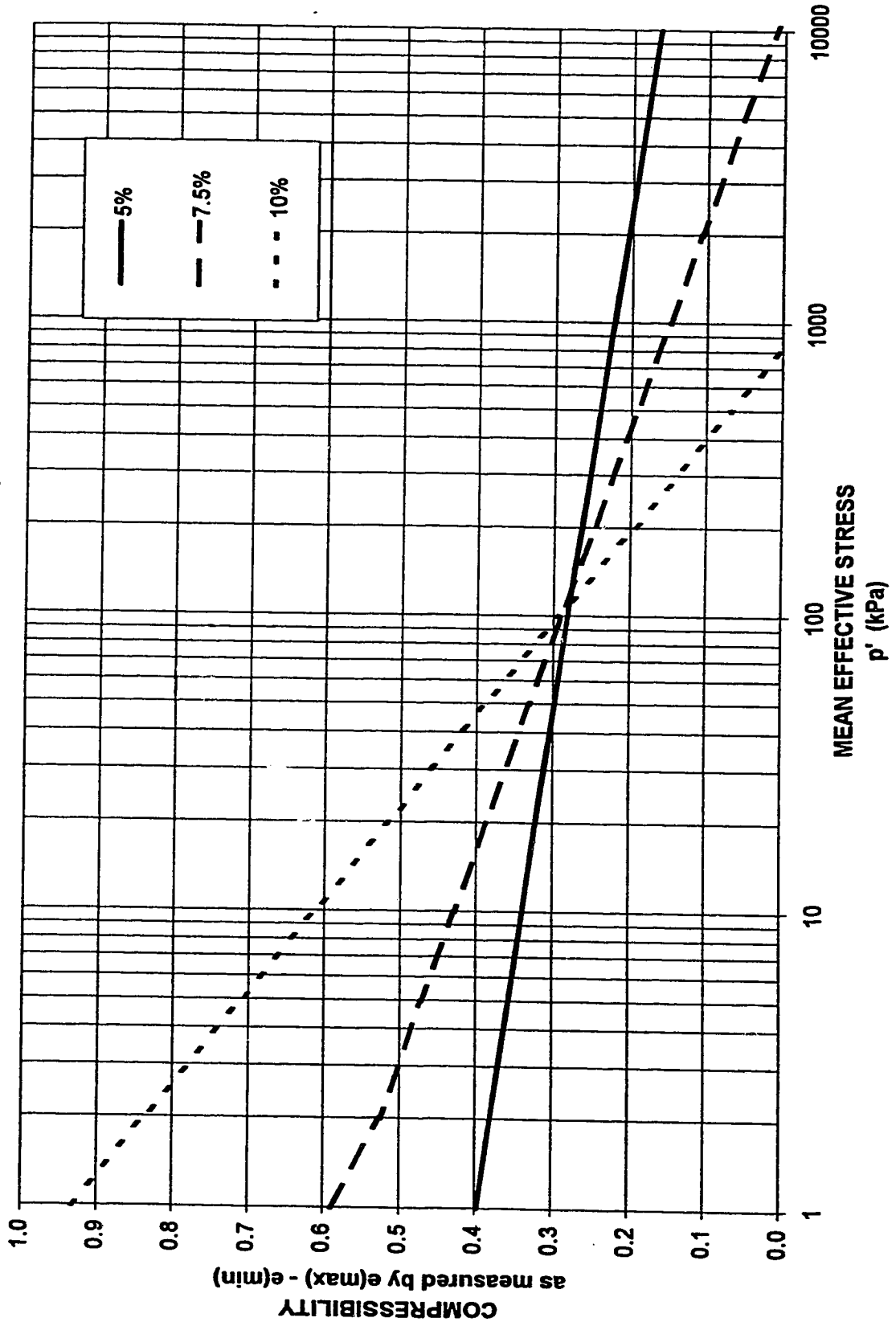


FIGURE 5.6 BRITTLINESS INDEX versus p'/p'_{ss}

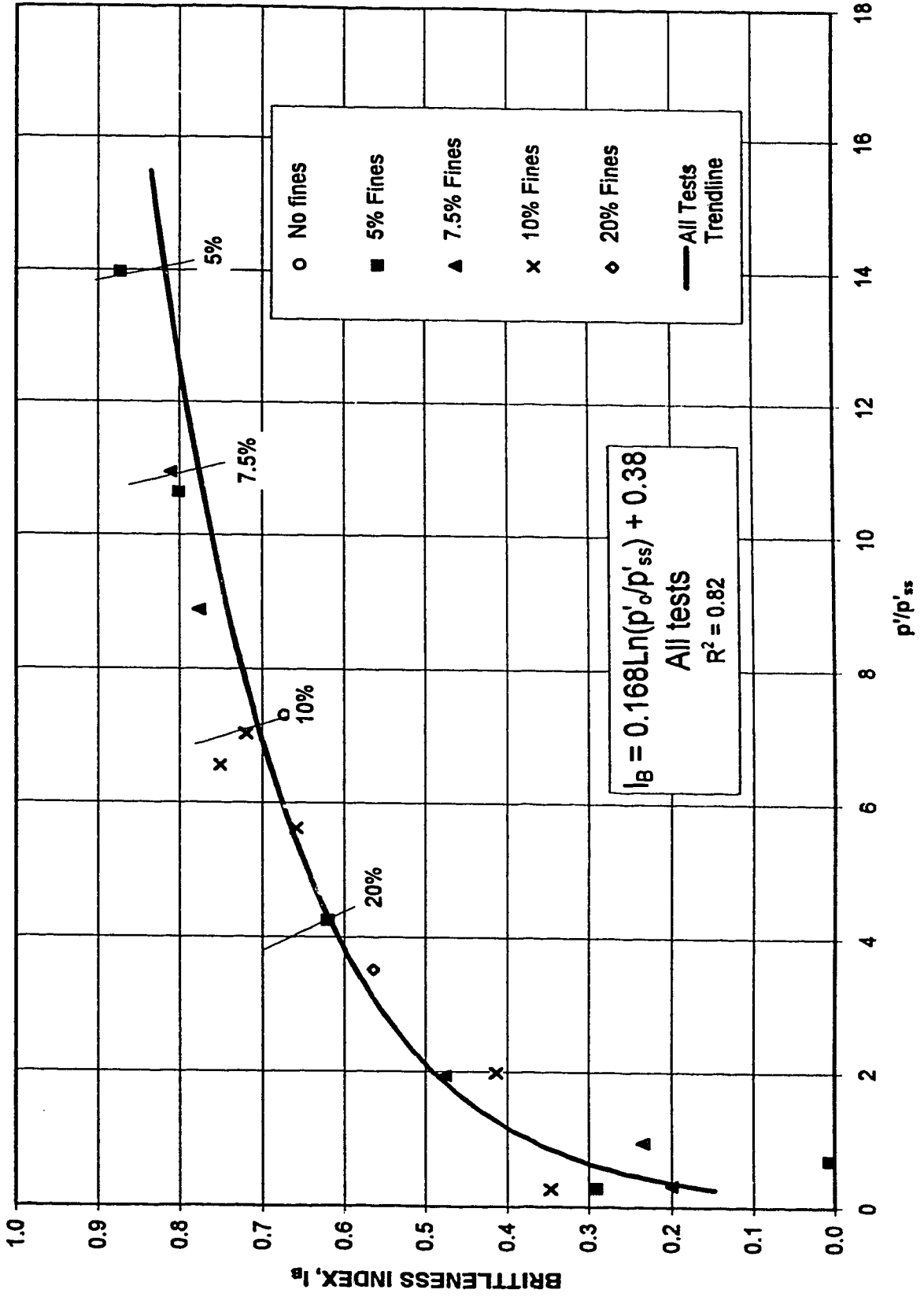


FIGURE 5.7 BRITTLENESS INDEX versus p'/p'_{ss}
 with data from Hird and Hassona (1990), Sladen et al (1985)
 and Been and Jefferies (1985)

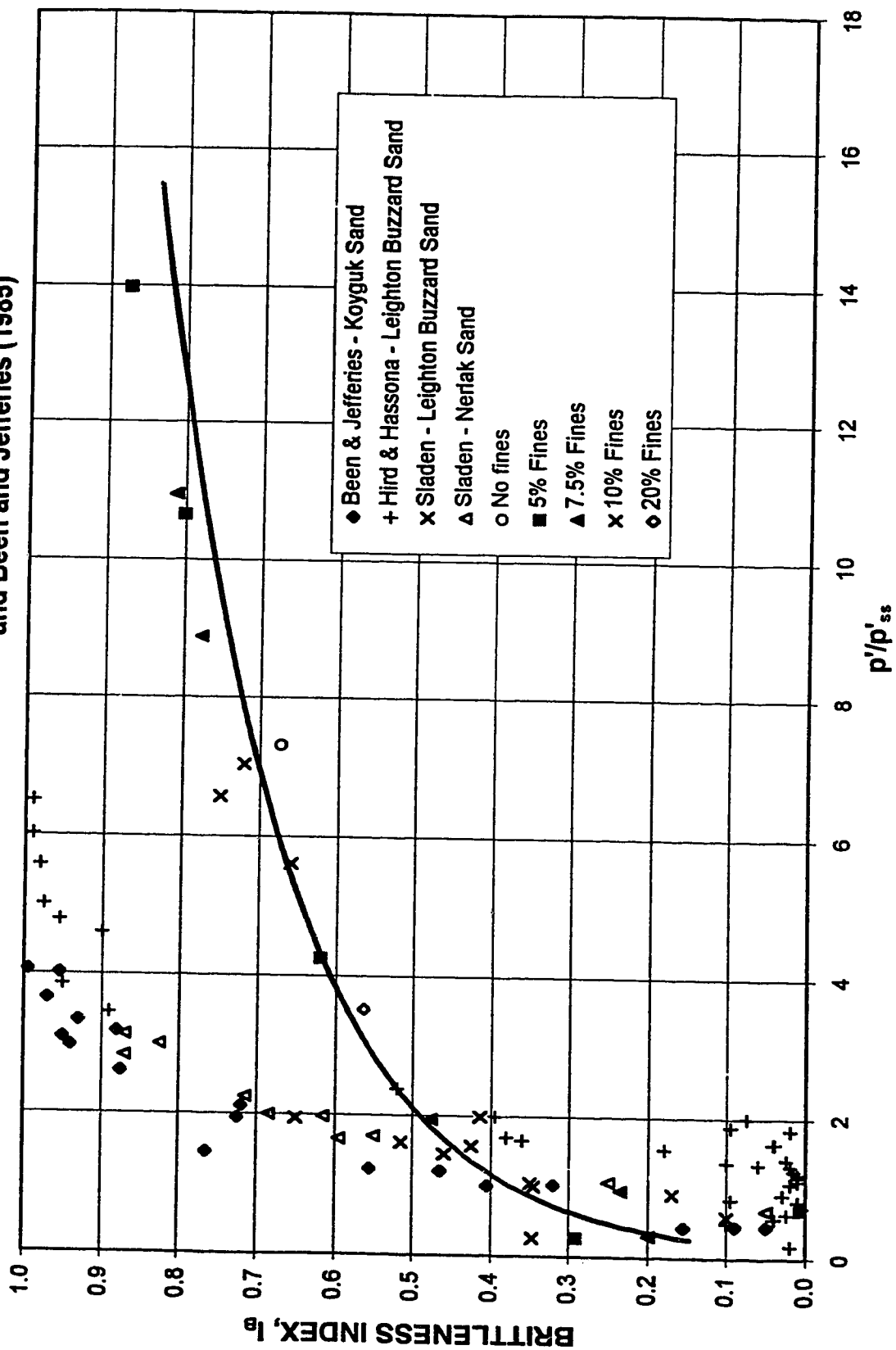


FIGURE 5.8 NORMALIZED p' - q DIAGRAM
 Ottawa Sand with 5% Kaolinite

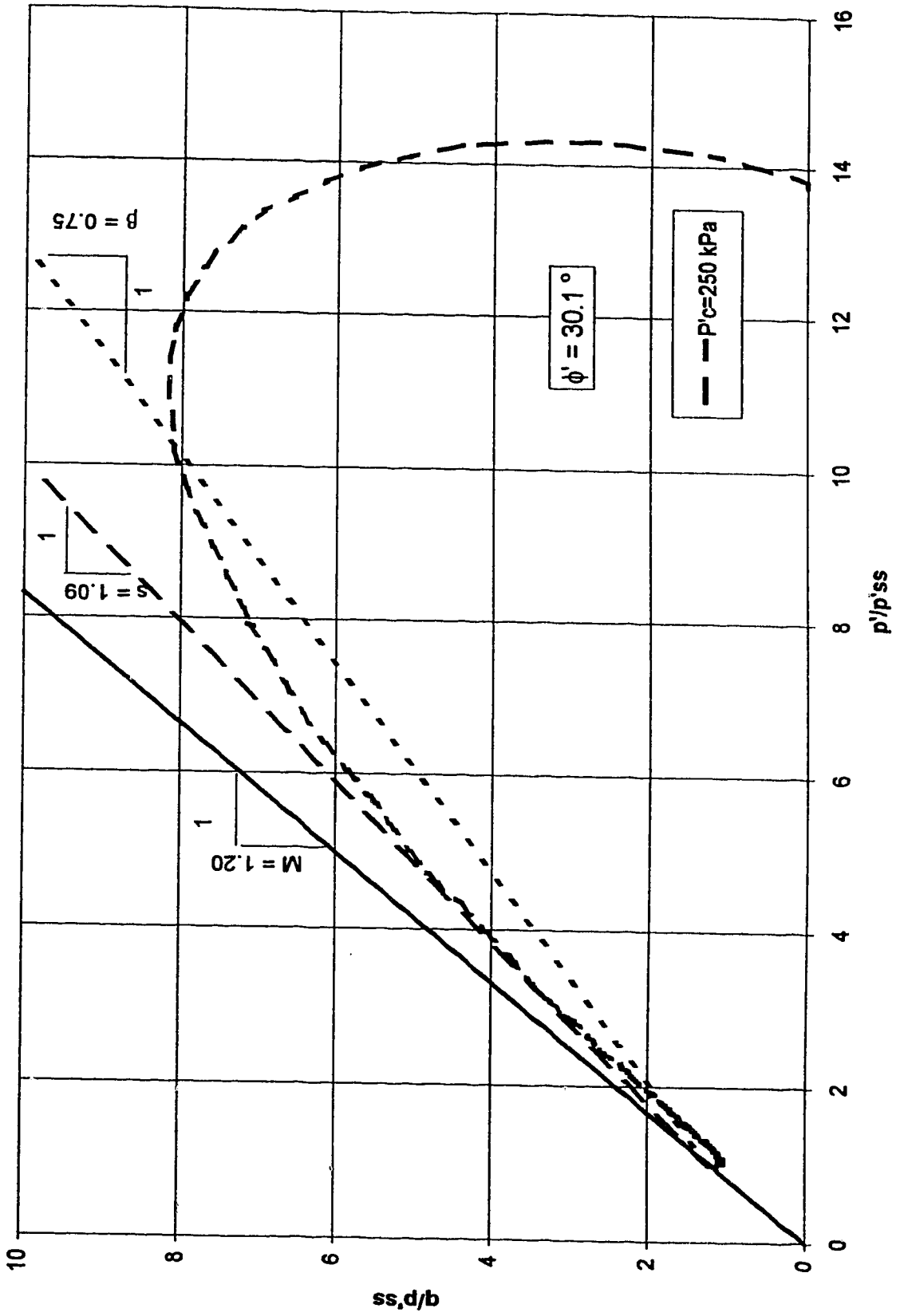


FIGURE 5.9 NORMALIZED p' - q DIAGRAM
 Ottawa Sand with 7.5% Kaolinite

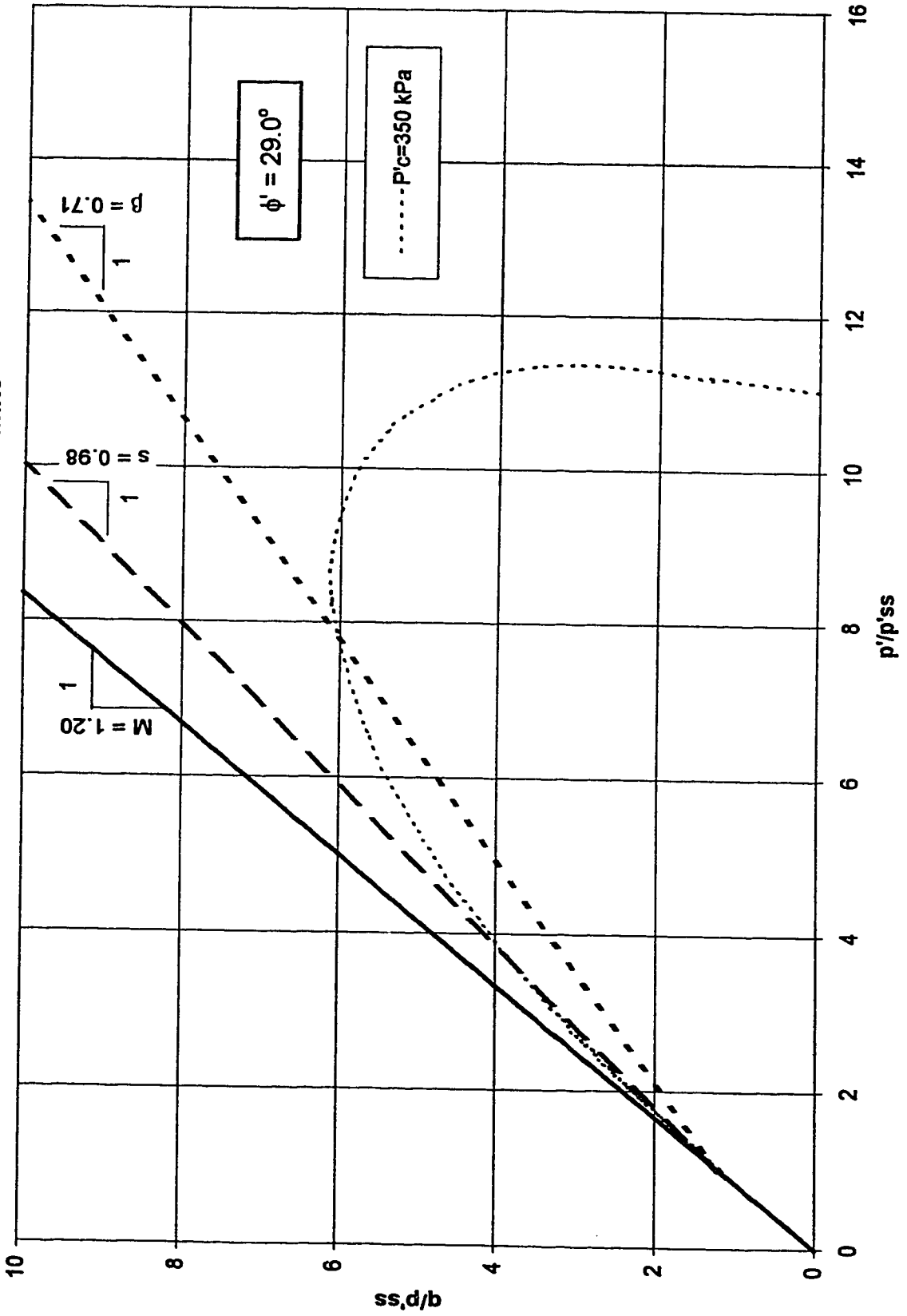
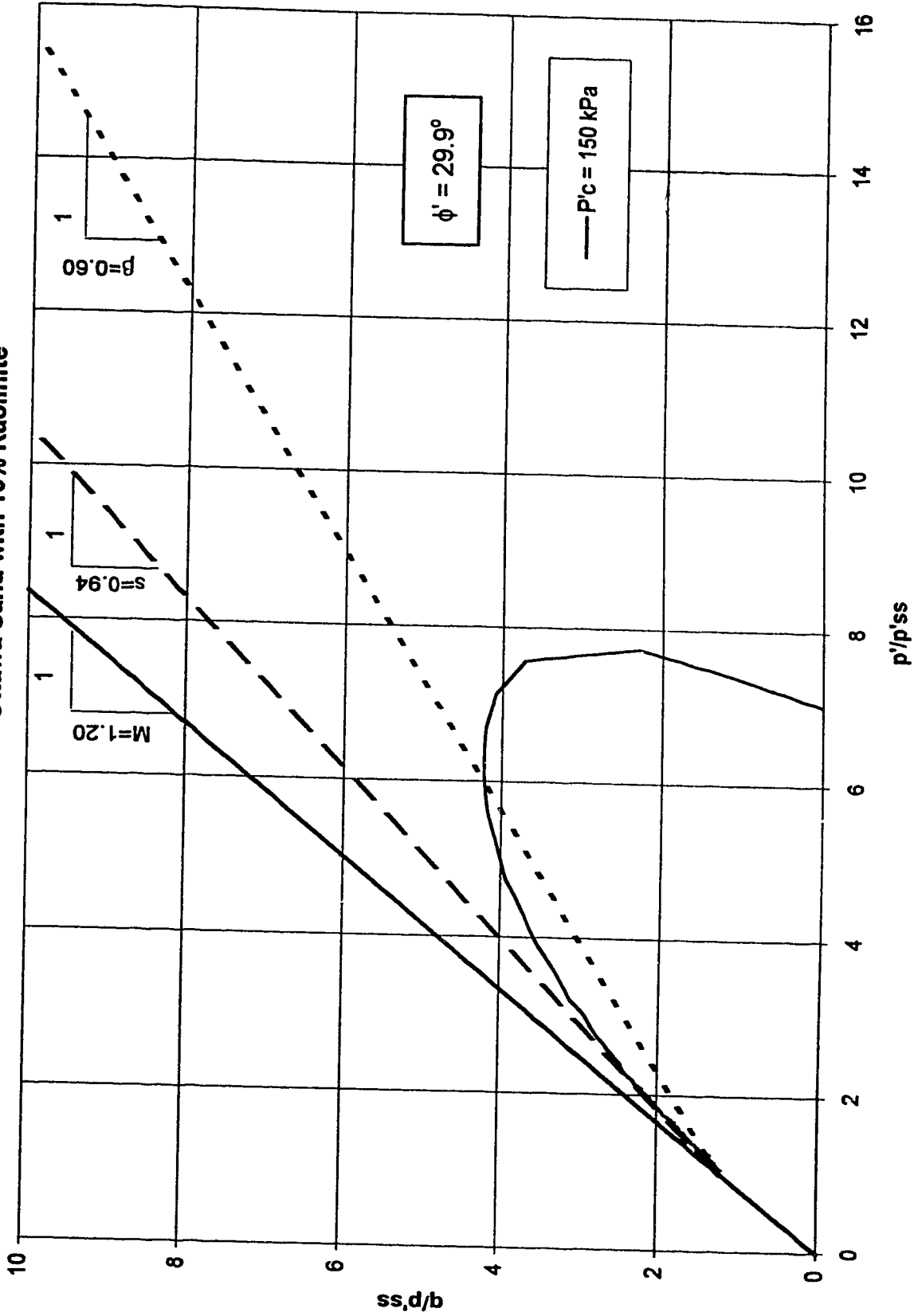


FIGURE 5.10 NORMALIZED p' - q DIAGRAM
 Ottawa Sand with 10% Kaolinite



**FIGURE 5.11 BRITTLENESS INDEX versus PERCENT FINES
For Various Consolidation Pressures**

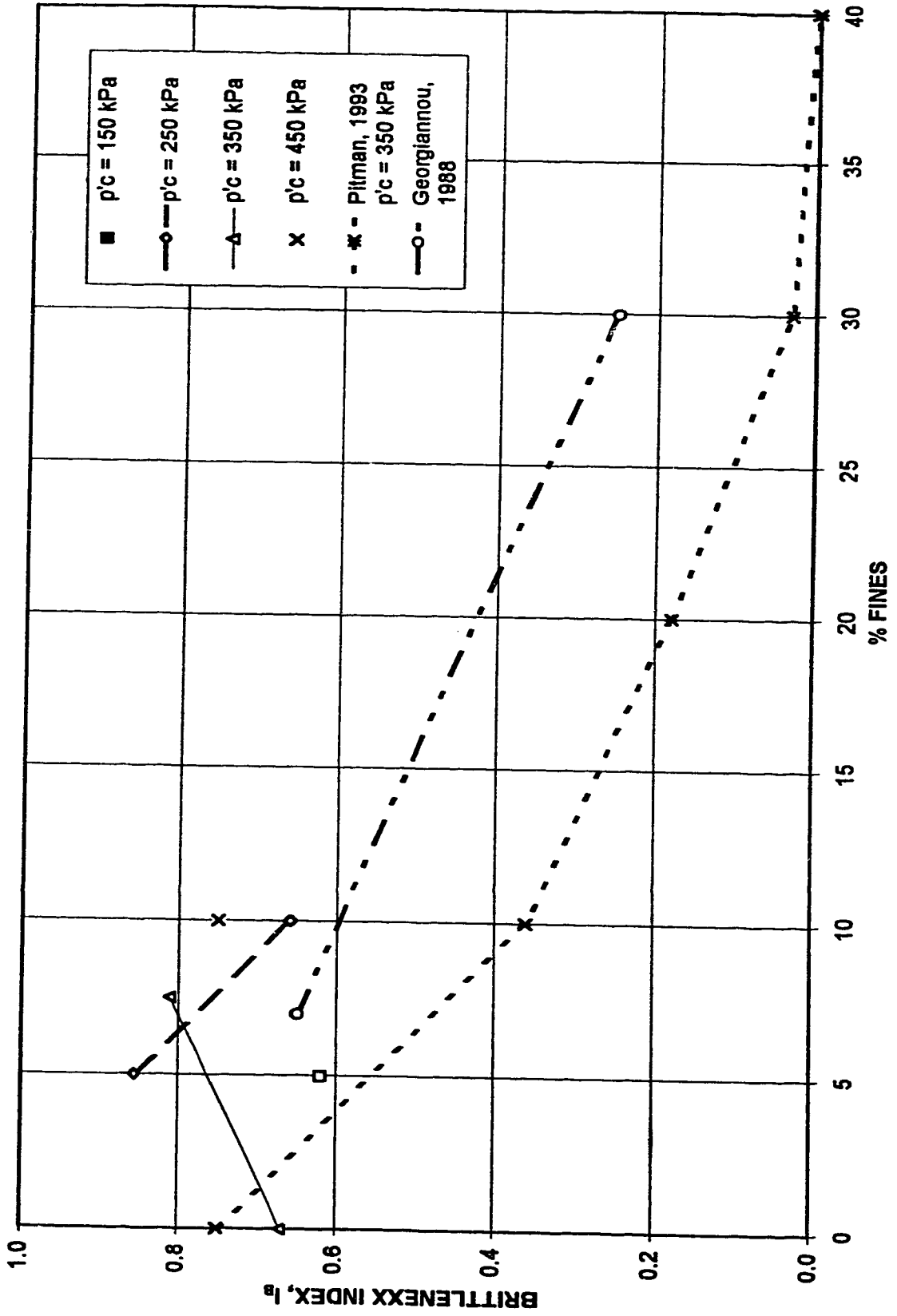
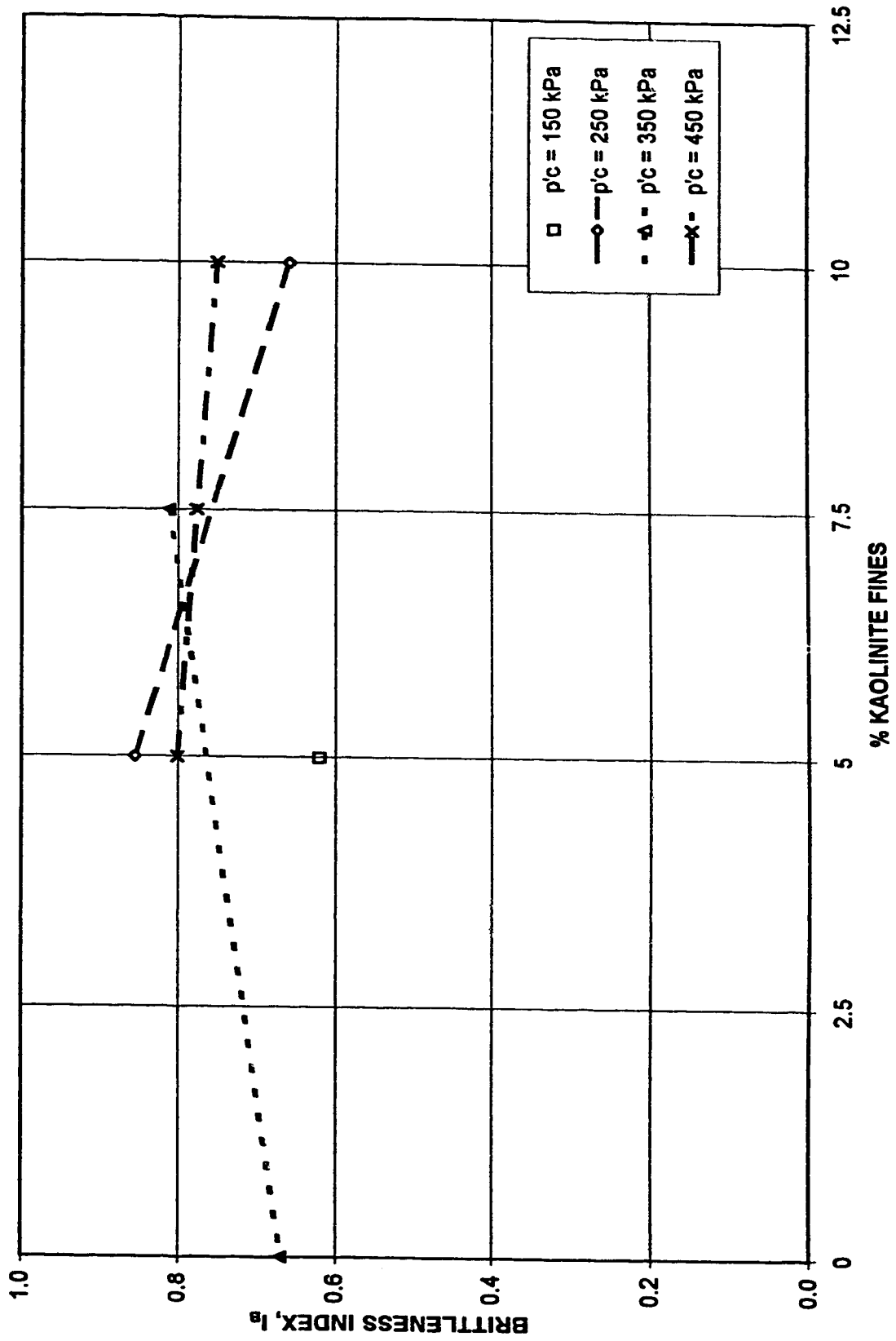


FIGURE 5.12 BRITTLINESS INDEX versus PERCENT FINES
Various Consolidation Pressures, This Study Only



**FIGURE 5.13 STEADY STATE LINES
Ottawa Sand With Varying Kaolinite Content**

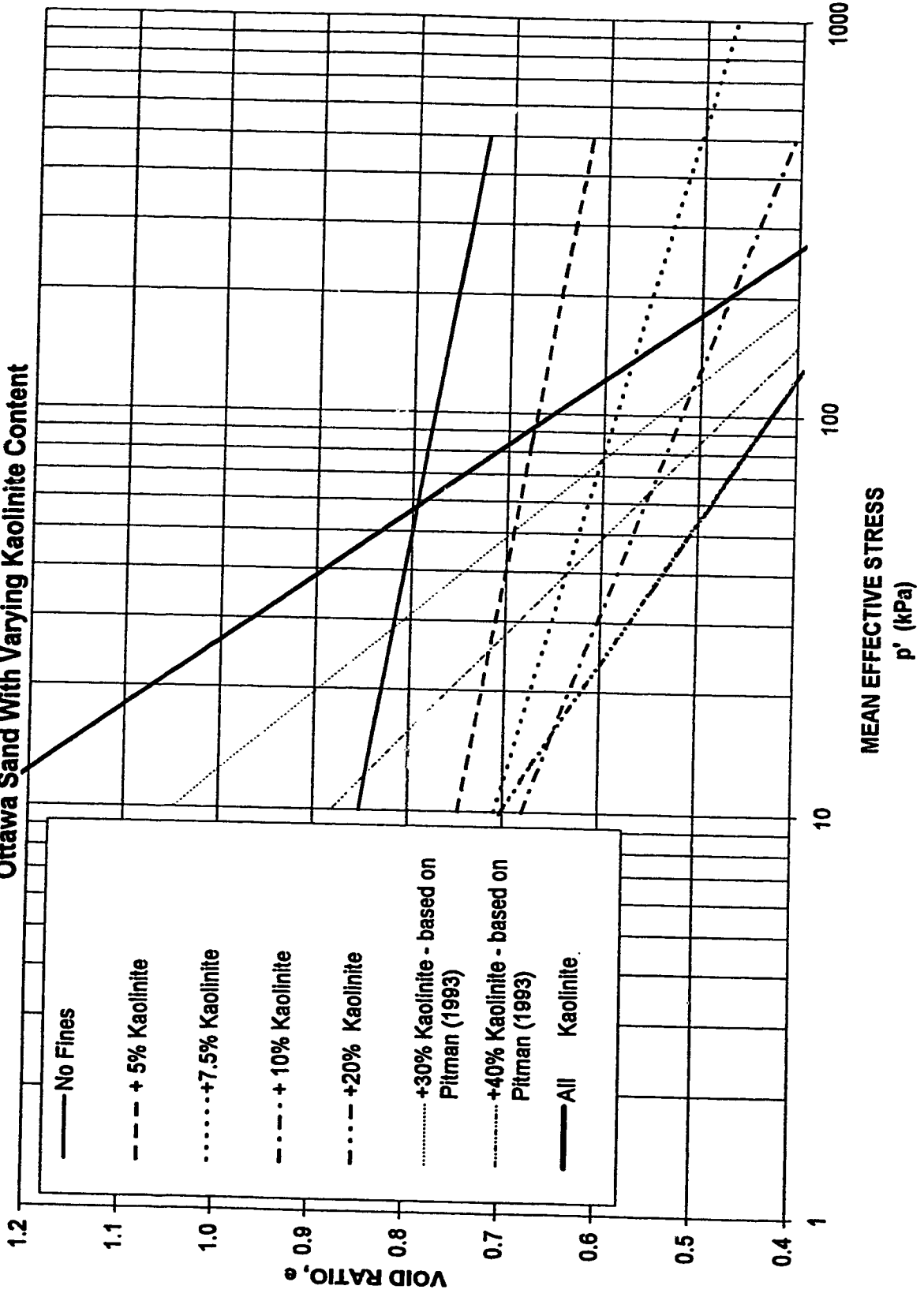


FIGURE 5.14 $e - \log(p')$
Ottawa Sand with Kaolinite

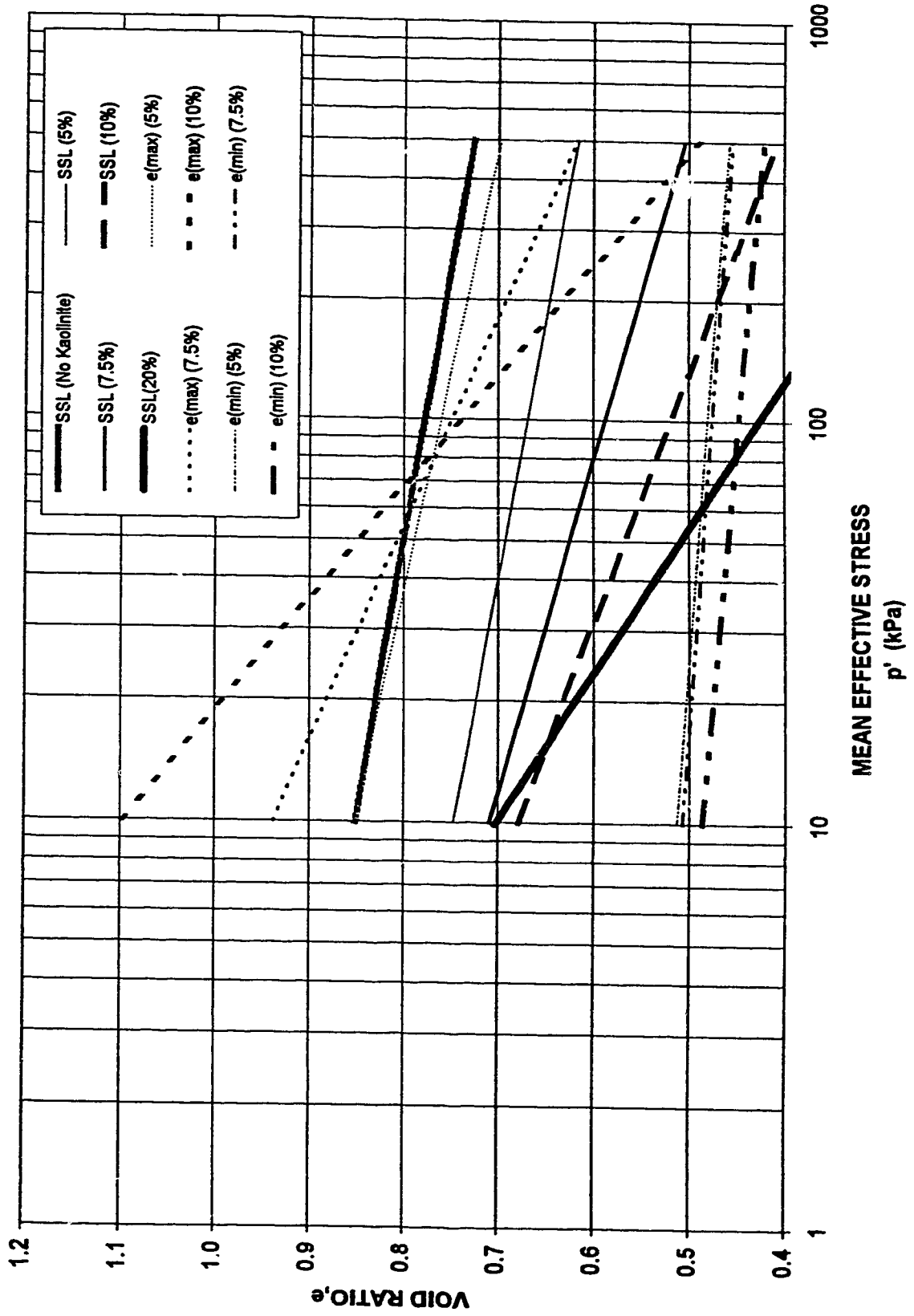


FIGURE 5.15 **STEADY STATE LINES**
Kogyuk Sand With Varying Mica Content
 (Been and Jefferies, 1985)

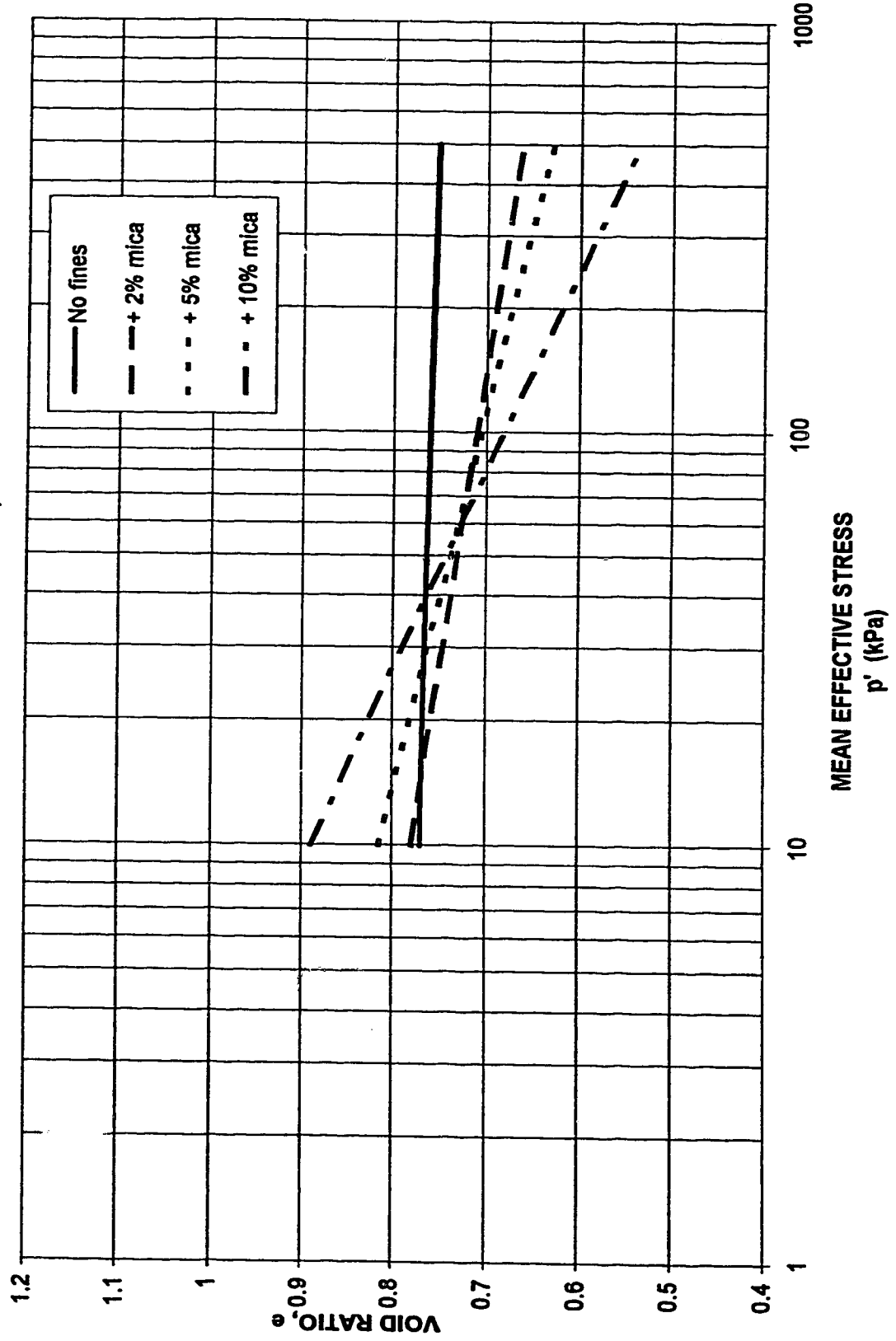


FIGURE 5.16 **STEADY STATE LINES**
Leighton Buzzard Sand With Varying Mica Content
(Hird and Hassona, 1990)

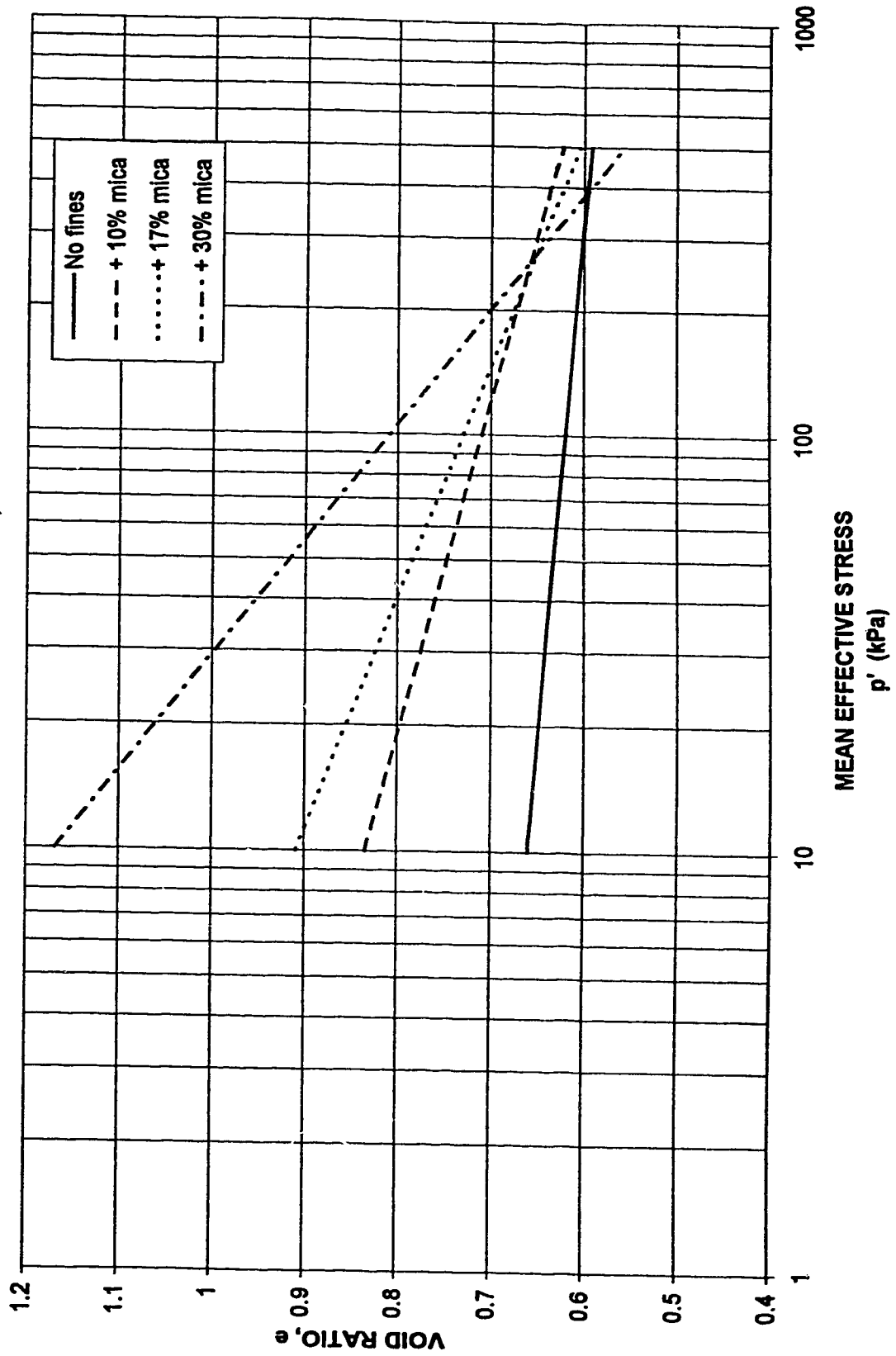
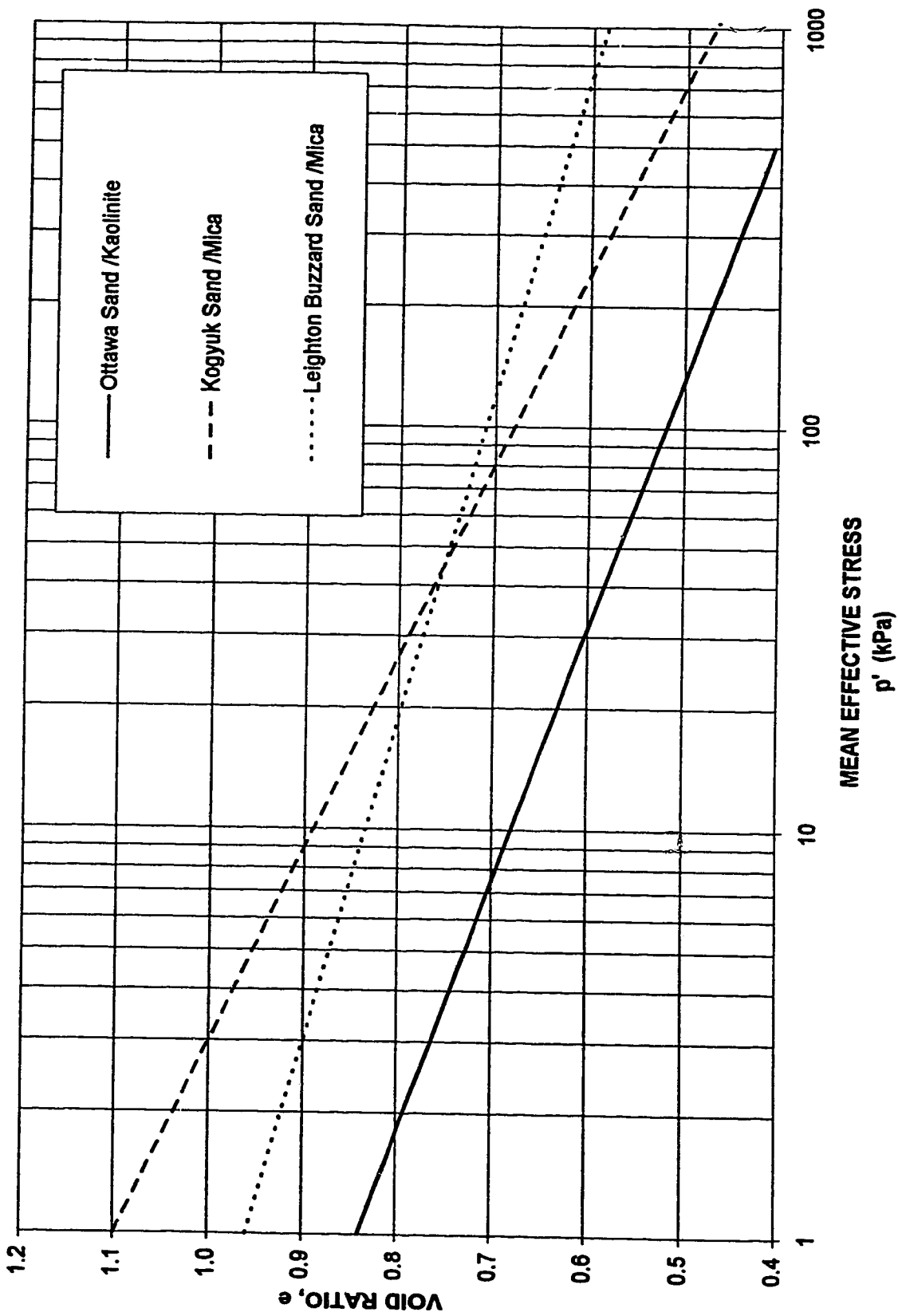


FIGURE 5.17 STEADY STATE LINES
Different Sands with 10% Fines Content



**FIGURE 5.18 STEADY STATE LINES
SSL's of Various Sands with Added Fines**

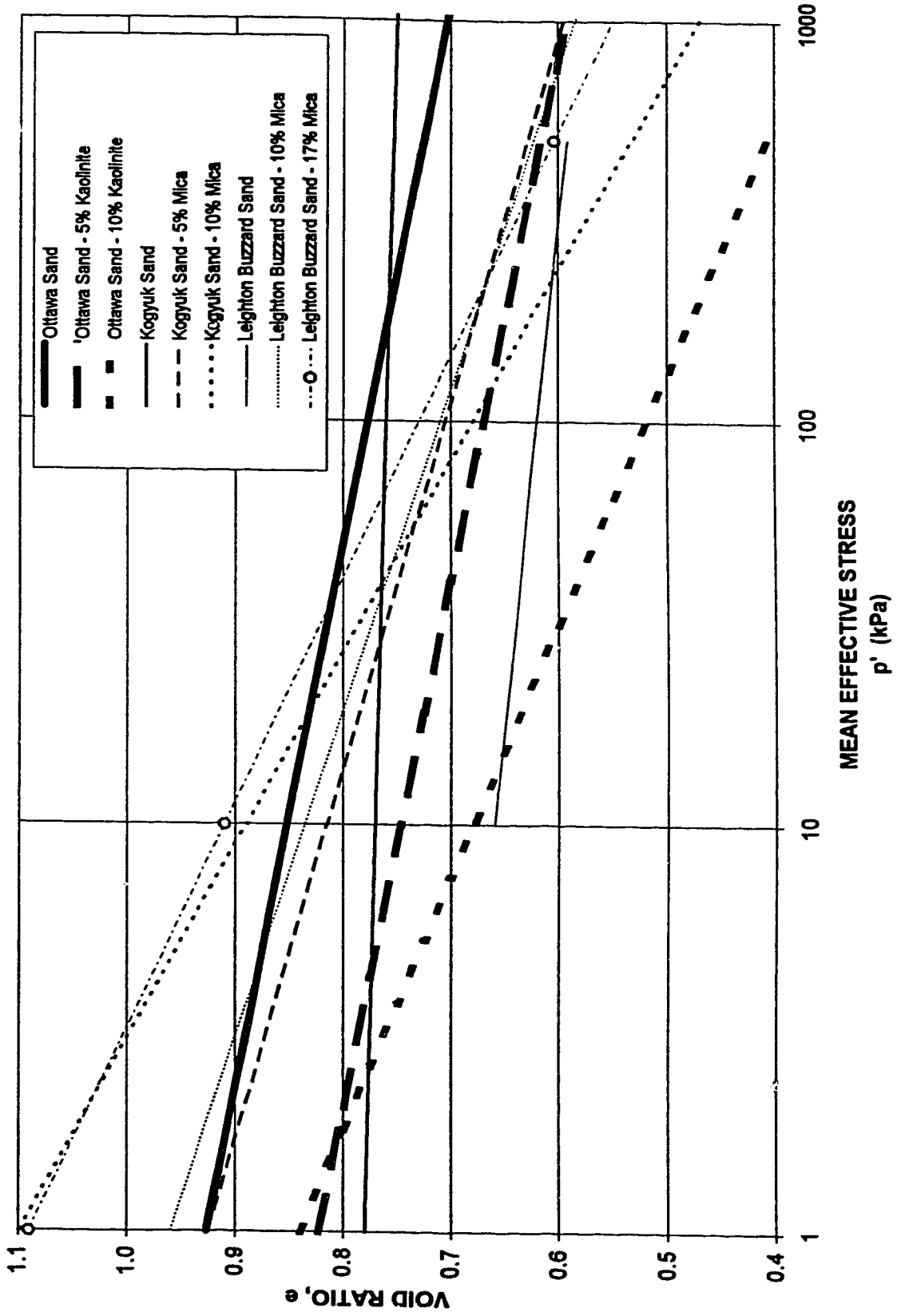


FIGURE 5.19 STEADY STATE LINE FOR HONG KONG PEARL RIVER SAND SHOWING TEST CONDITIONS

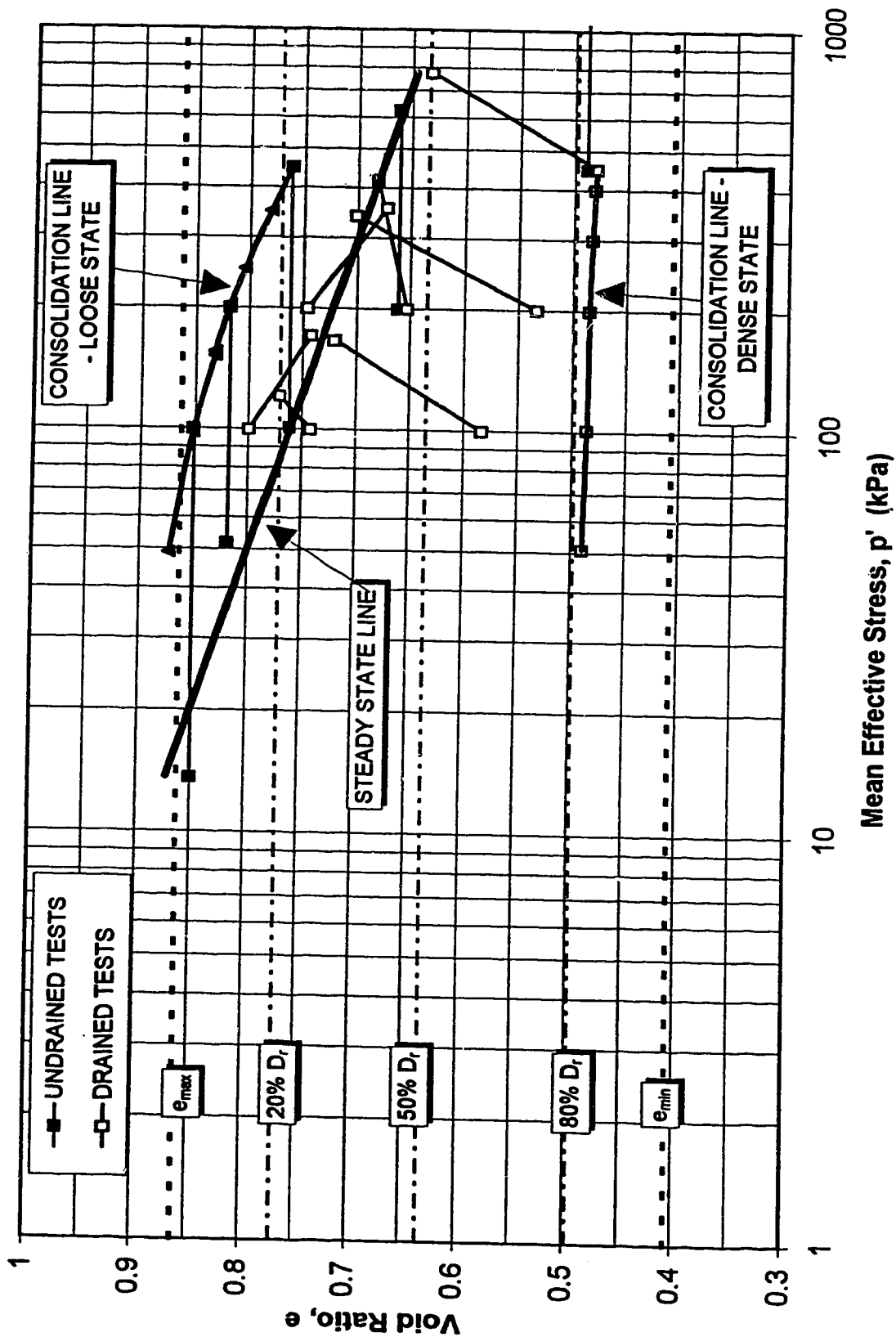


FIGURE 5.20
 ψ versus p'
Ottawa Sand with Varying Kaolinite Content

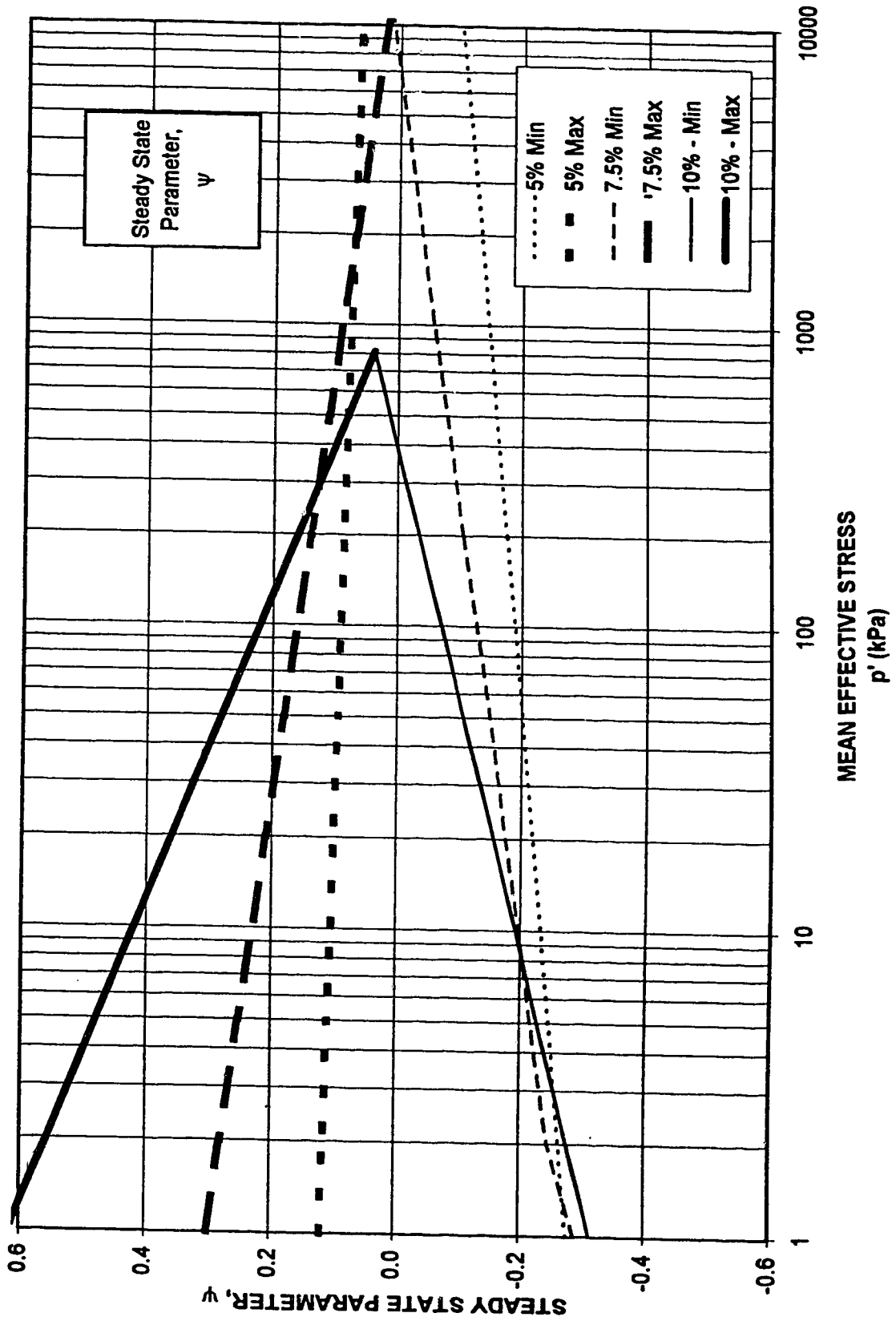


FIGURE 5.21 NORMALIZED p'-q Diagram SHOWING STATE PARAMETER RELATIONSHIPS Ottawa Sand with Added Kaolinite

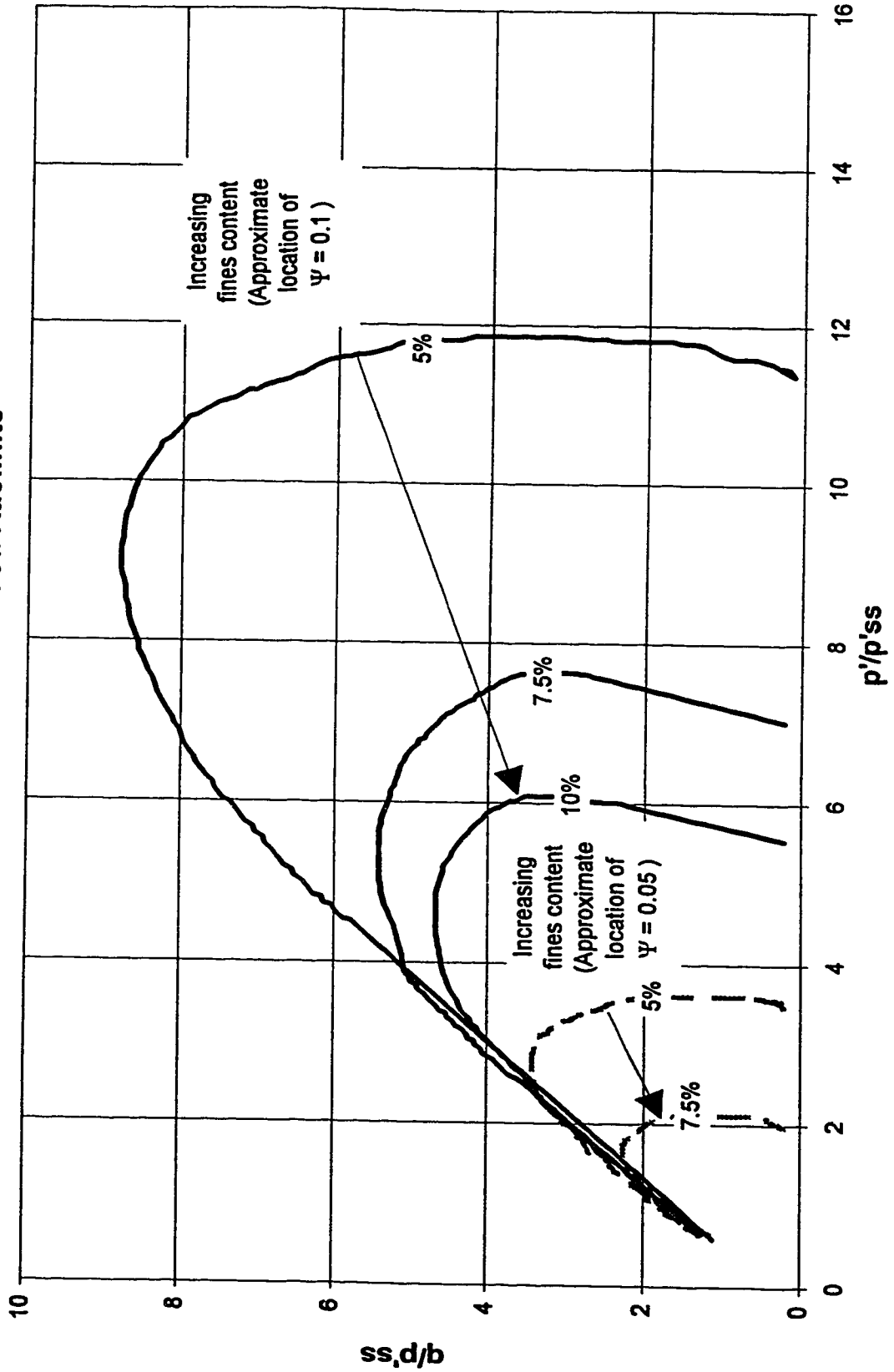


FIGURE 5.22 BRITTLINESS INDEX versus STATE PARAMETER
Ottawa Sand with Varying Kaolinite Fines

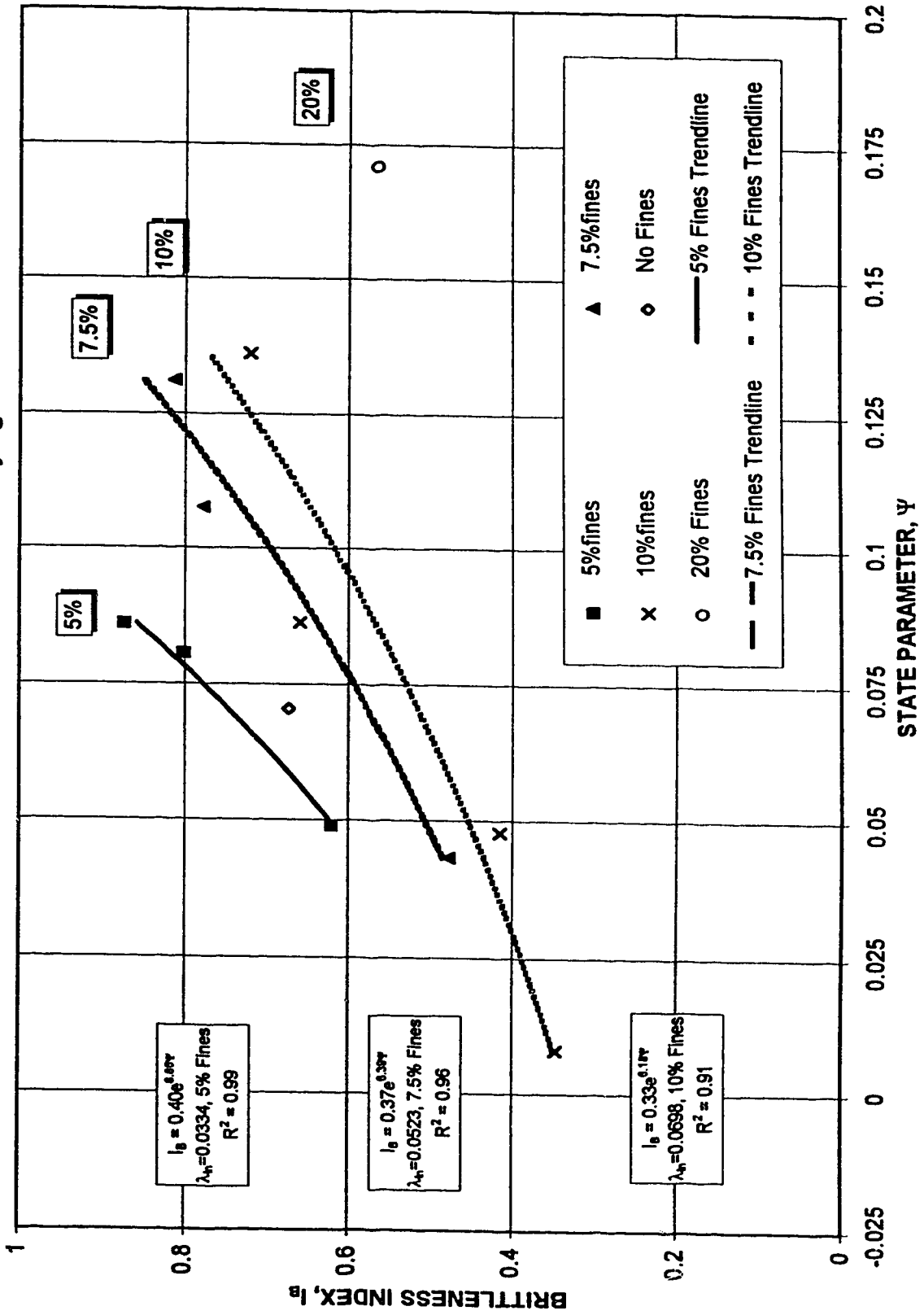


FIGURE 5.23 **NORMALIZED S_u/p'_o versus STATE PARAMETER**
Ottawa Sand with Varying Fines Content, Positive ψ Values Only

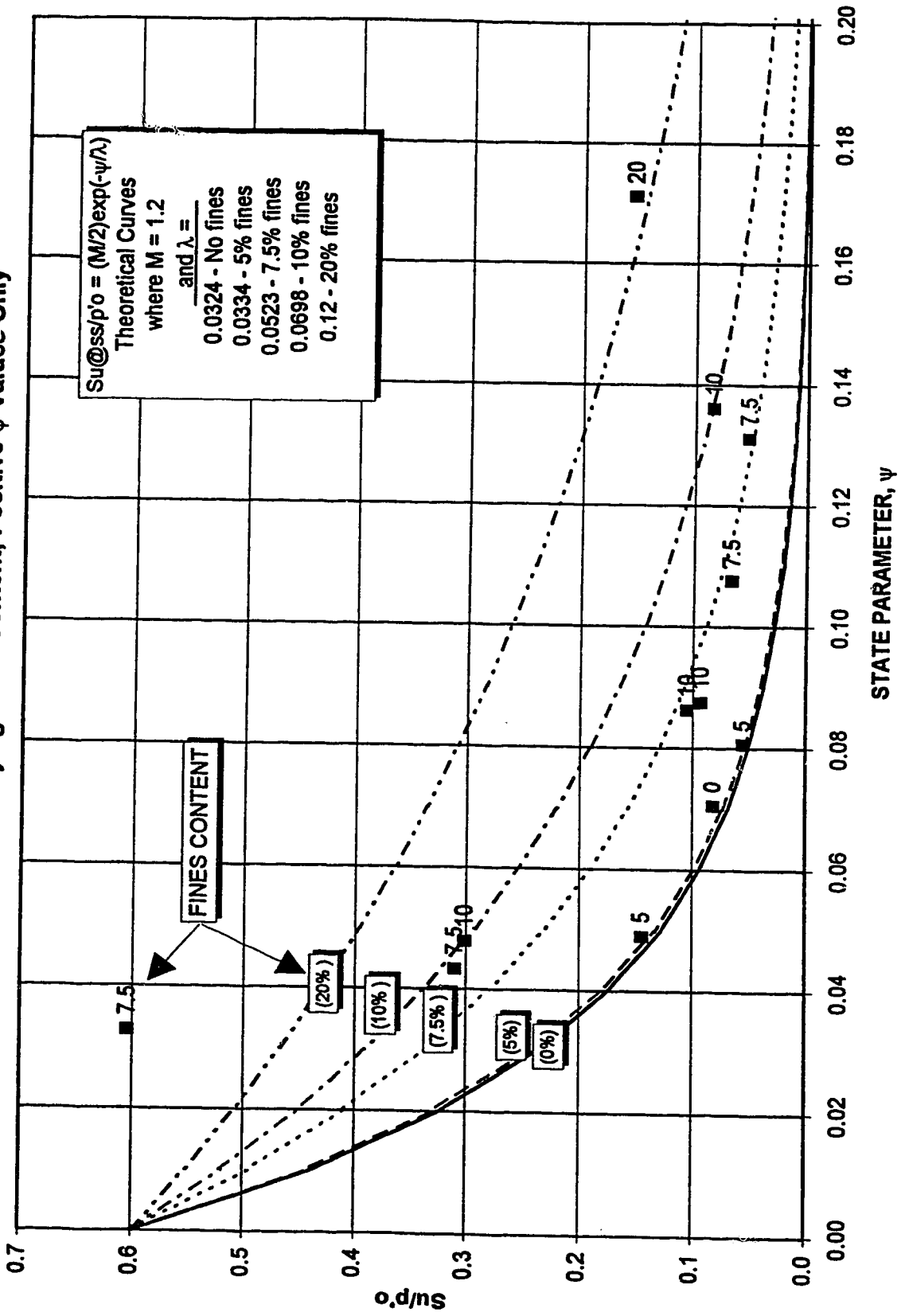


FIGURE 5.24 NORMALIZED S_u/p'_o versus STATE PARAMETER
 Ottawa Sand with Varying Kaolinite Content, All Data

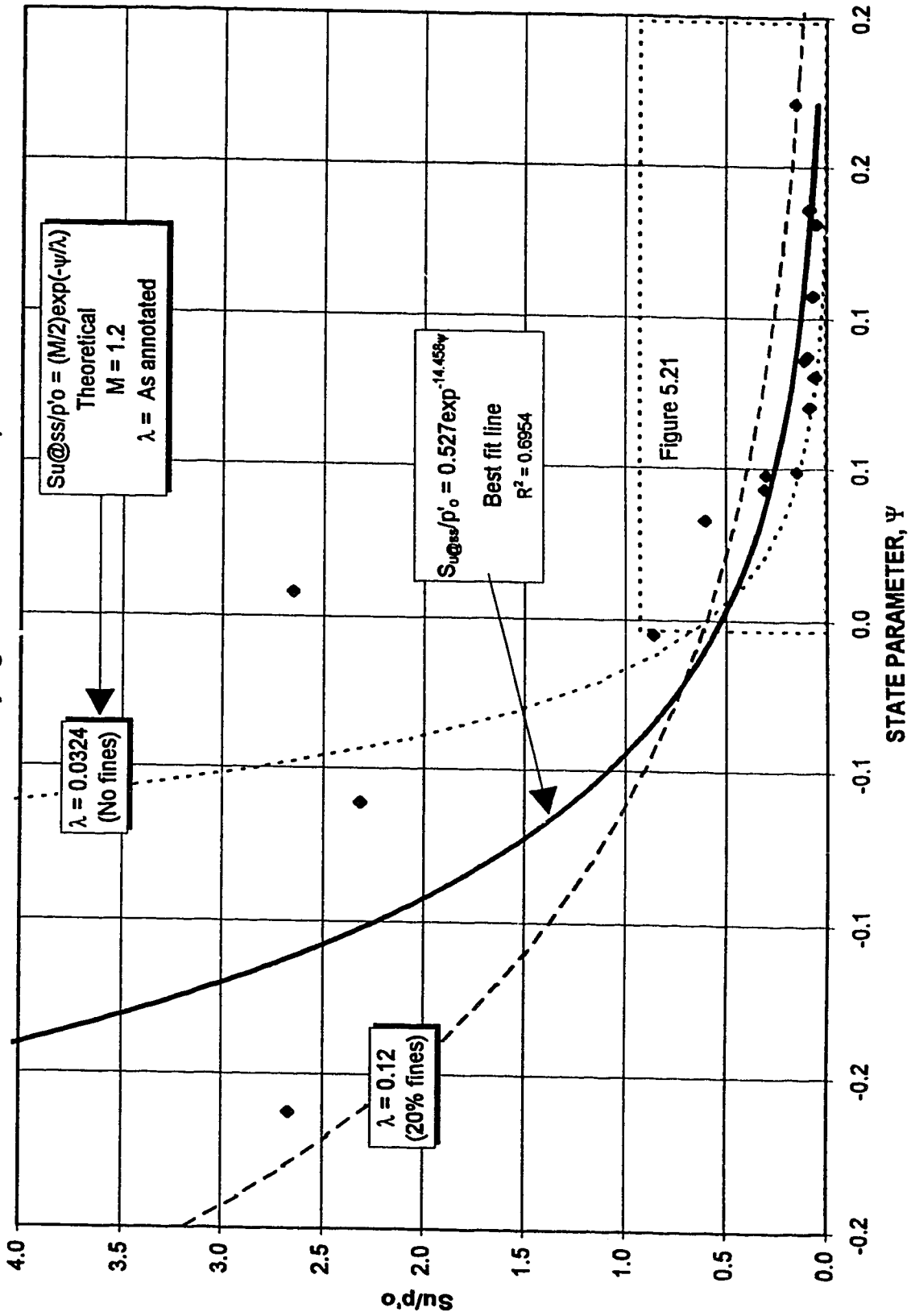


FIGURE 5.25 **NORMALIZED SHEAR WAVE VELOCITY**
versus VOID RATIO
Ottawa Sand with Varying Kaolinite Content

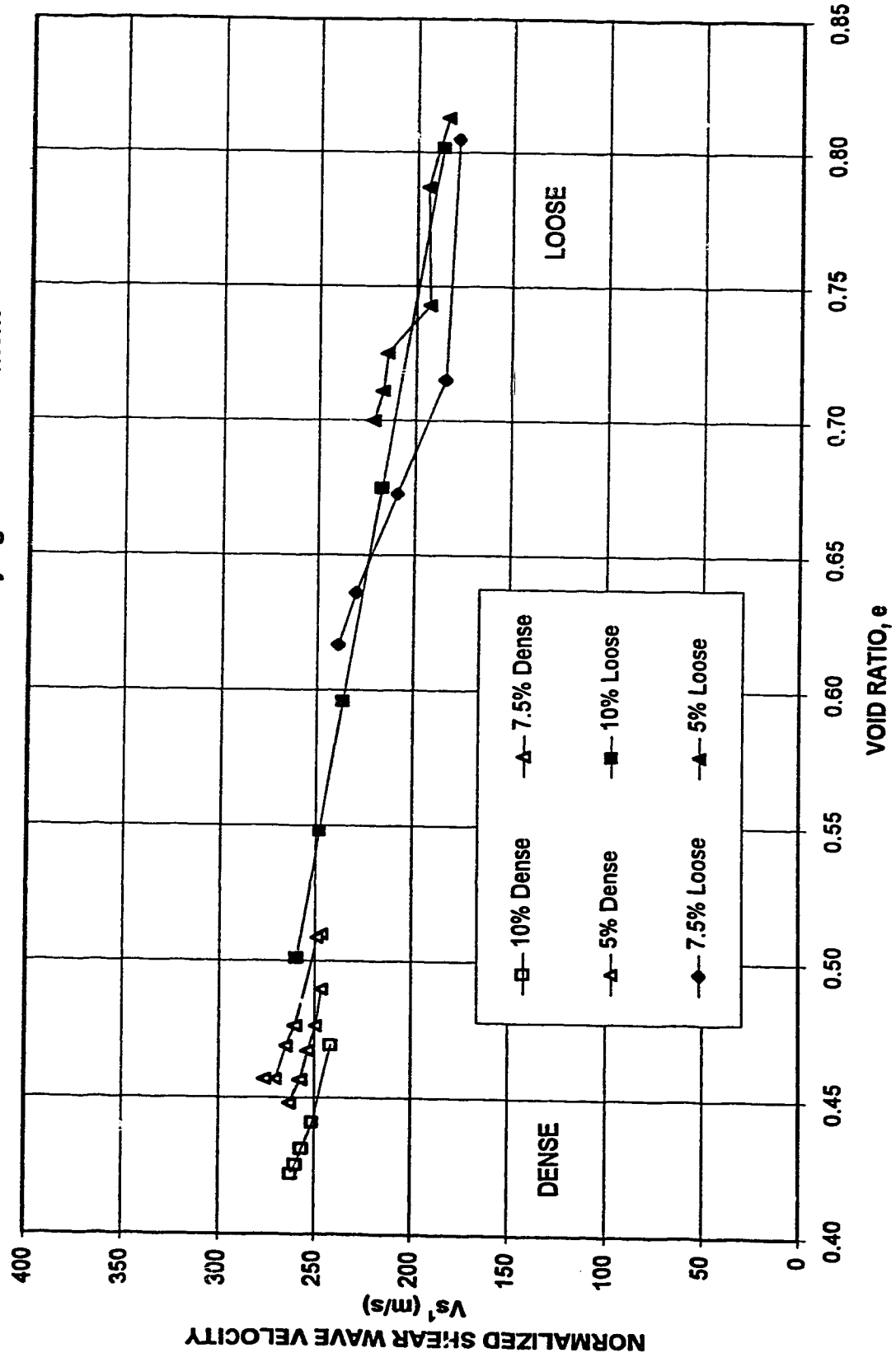


FIGURE 5.26 SHEAR WAVE VELOCITY versus MEAN EFFECTIVE STRESS
Ottawa Sand with Varying Kaolinite Content, During Consolidation

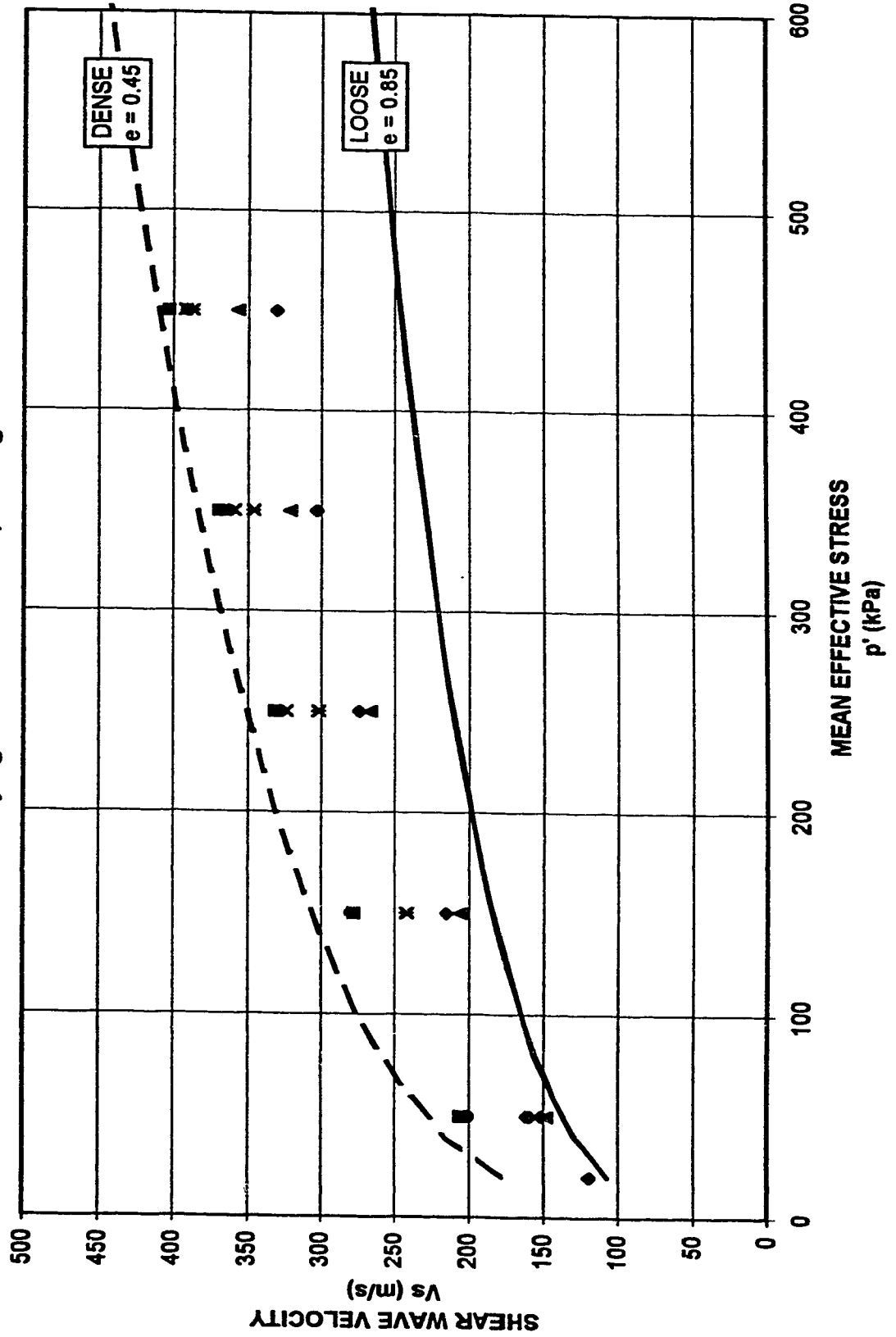


FIGURE 5.27 CALCULATED versus MEASURED SHEAR WAVE VELOCITY FOR ALL OTTAWA SAND

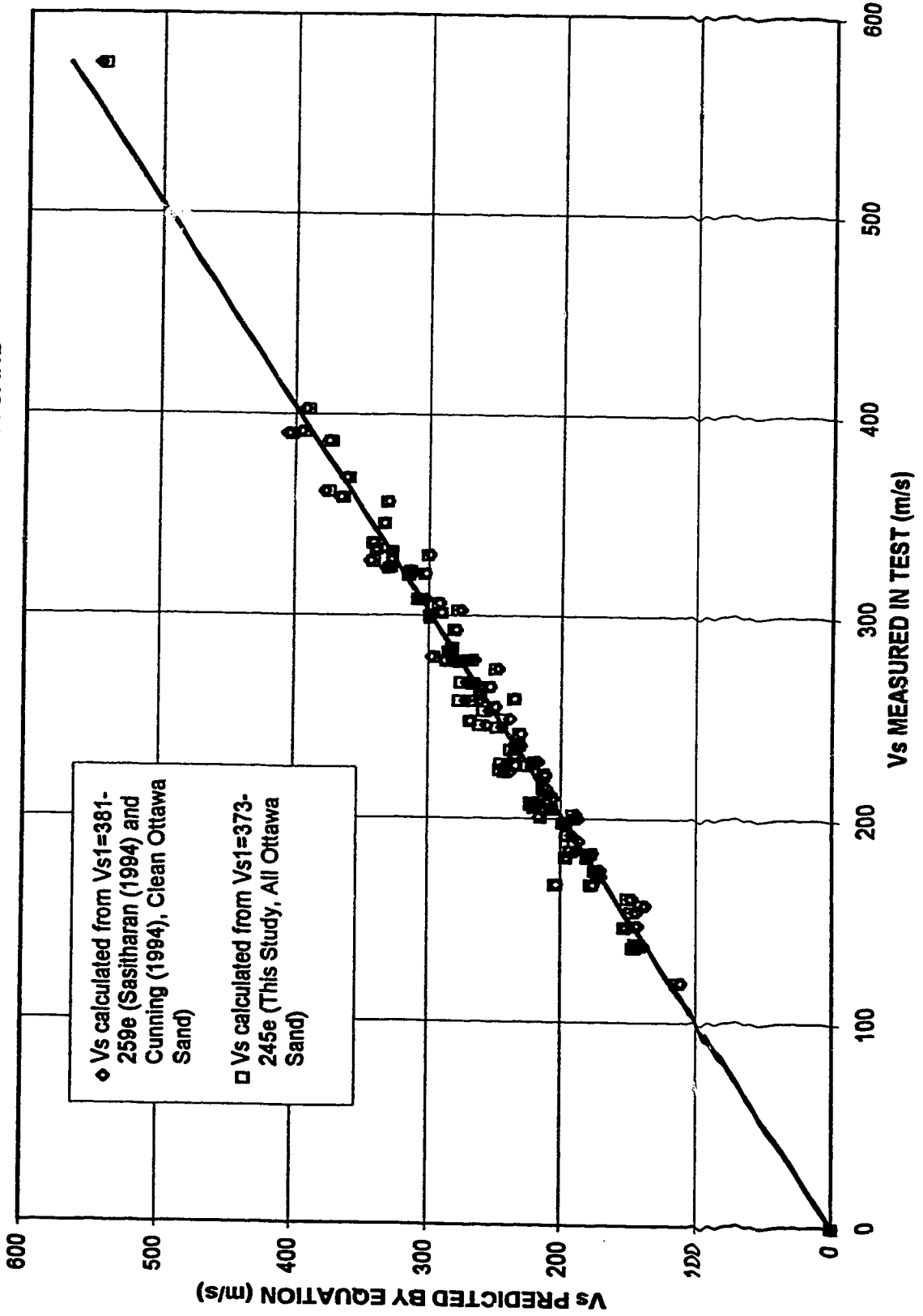


FIGURE 5.28 VOID RATIO versus MEAN EFFECTIVE STRESS
 Showing Contours of Shear Wave Velocity

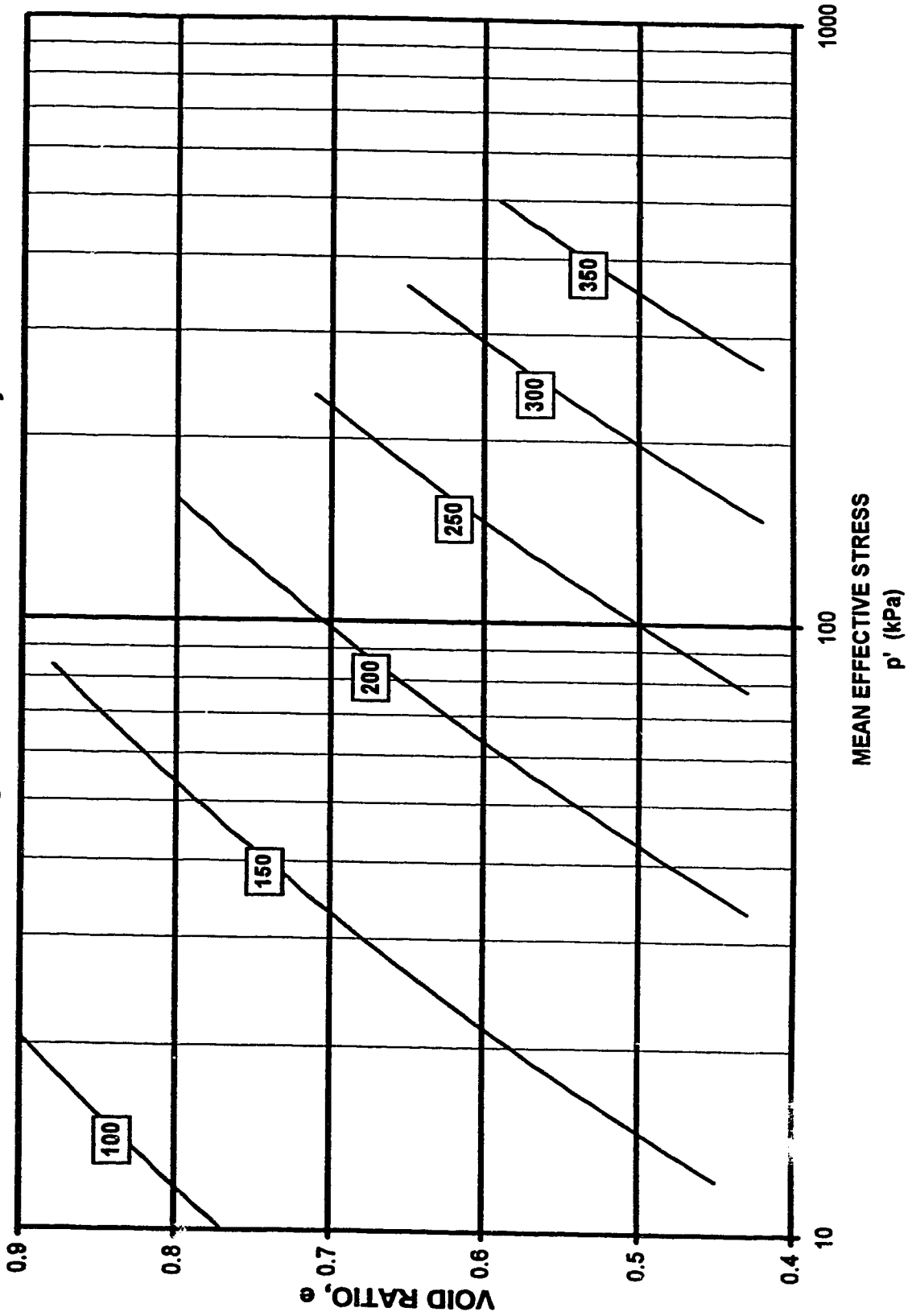


FIGURE 5.29 VOID RATIO versus MEAN EFFECTIVE STRESS
Showing Contours of Shear Wave Velocity
With Test Results Superimposed
Ottawa Sand with Varying Kaolinite Content

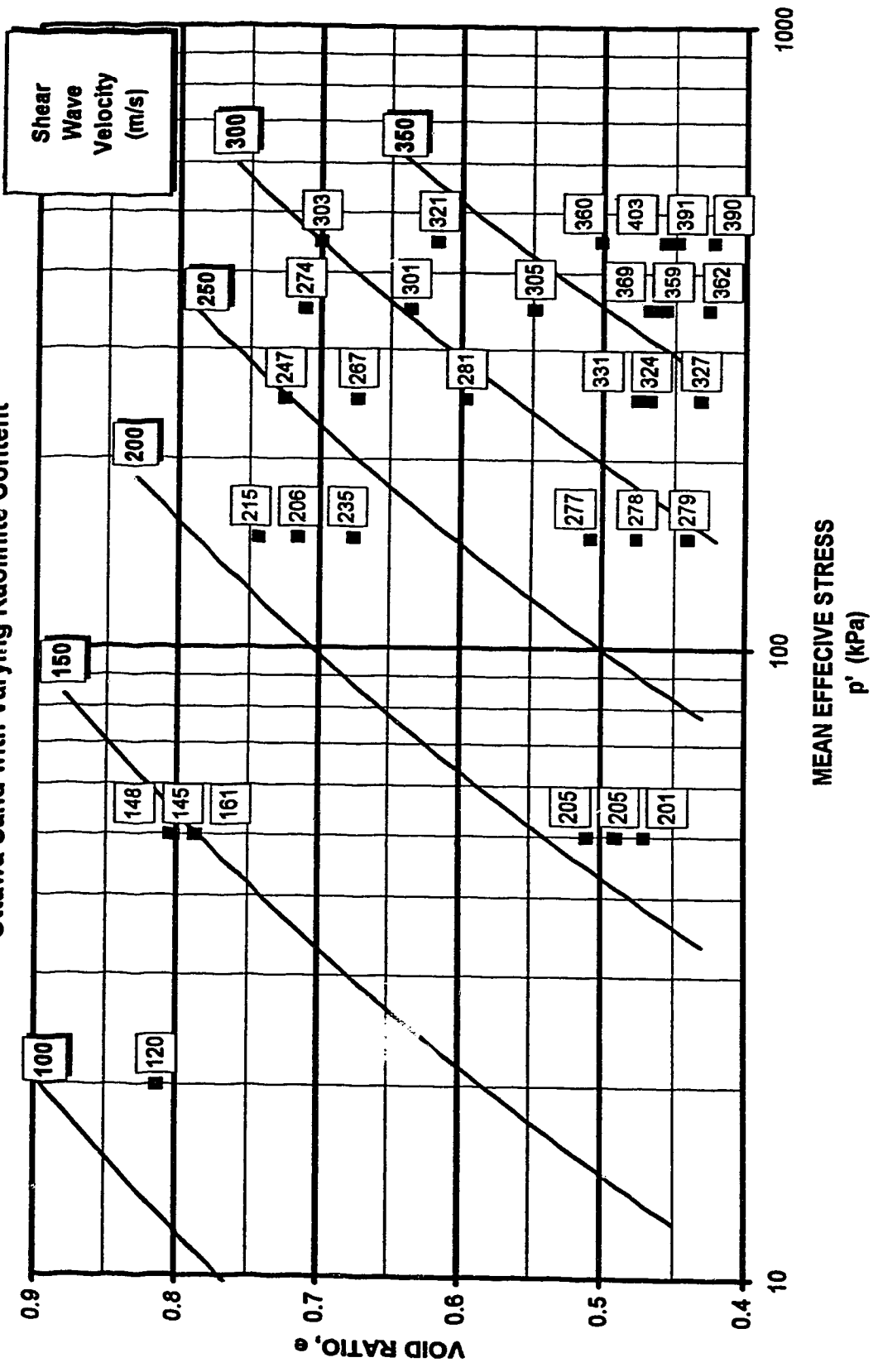


FIGURE 5.30 **NORMALIZED SHEAR WAVE VELOCITY**
versus VOID RATIO FOR VARIOUS SANDS

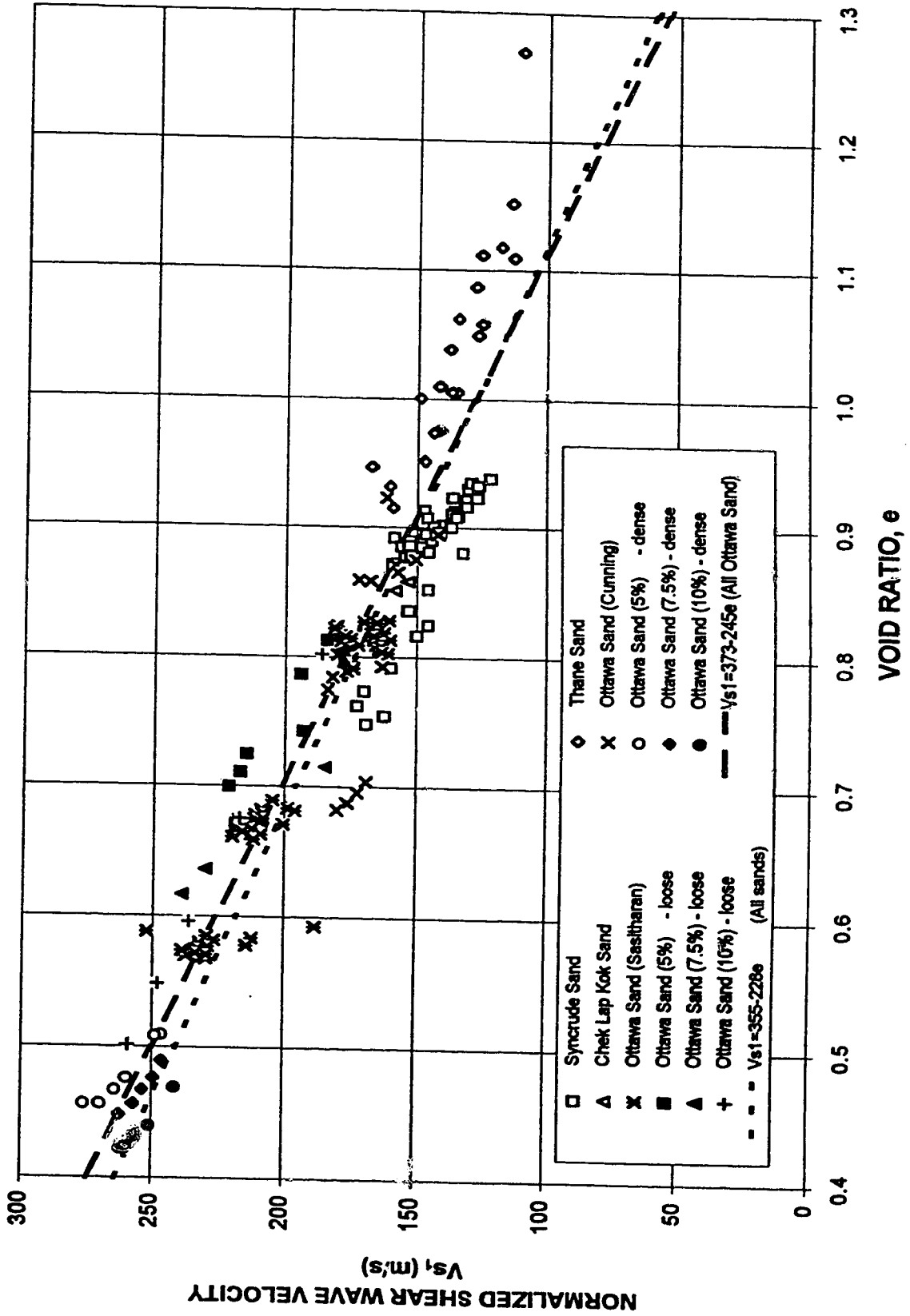
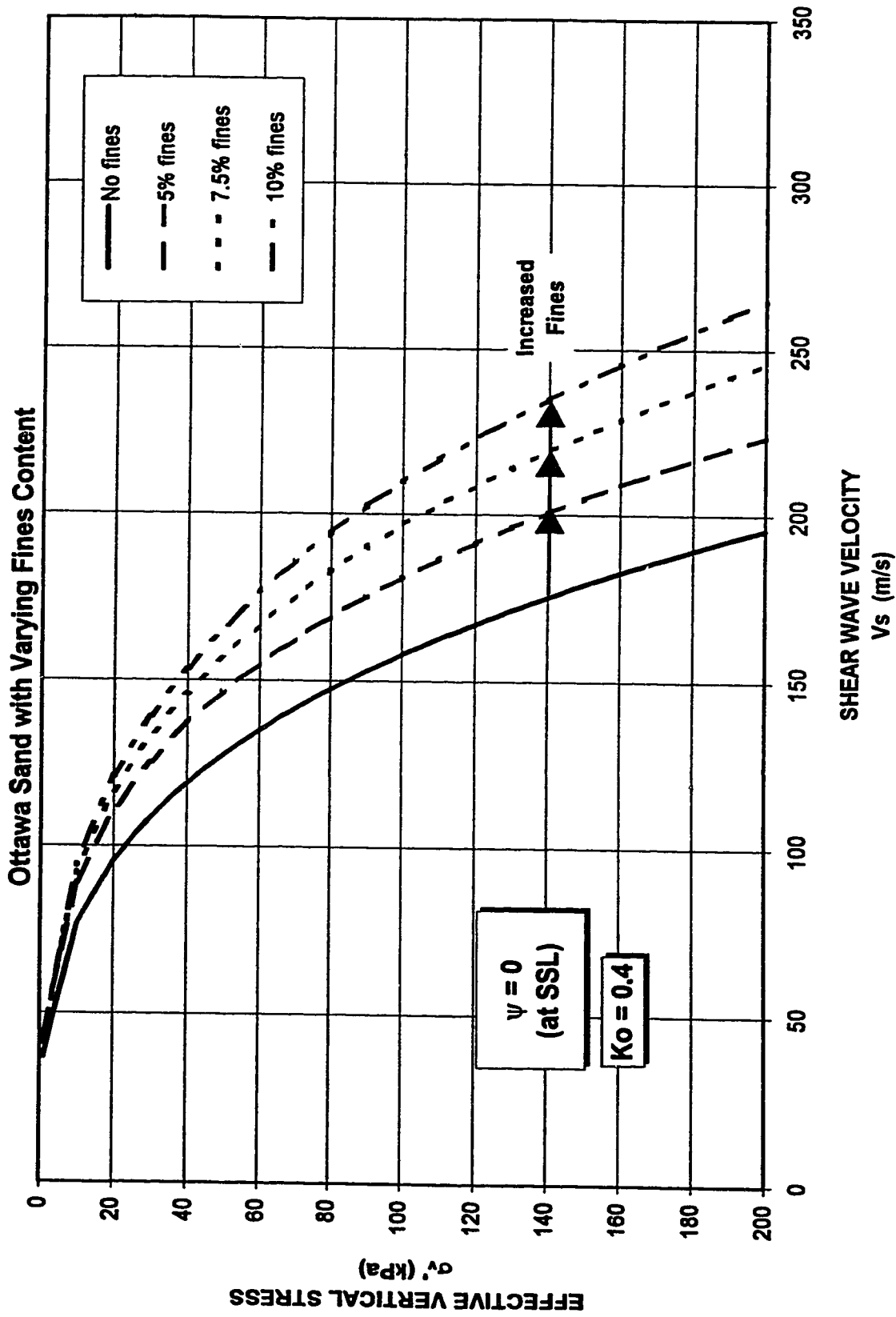


FIGURE 5.31 SHEAR WAVE VELOCITY versus EFFECTIVE VERTICAL STRESS
Ottawa Sand with Varying Fines Content



**FIGURE 5.32 SHEAR WAVE VELOCITY versus
EFFECTIVE VERTICAL STRESS**
Leighton Buzzard Sand with Varying Mica Fines Content

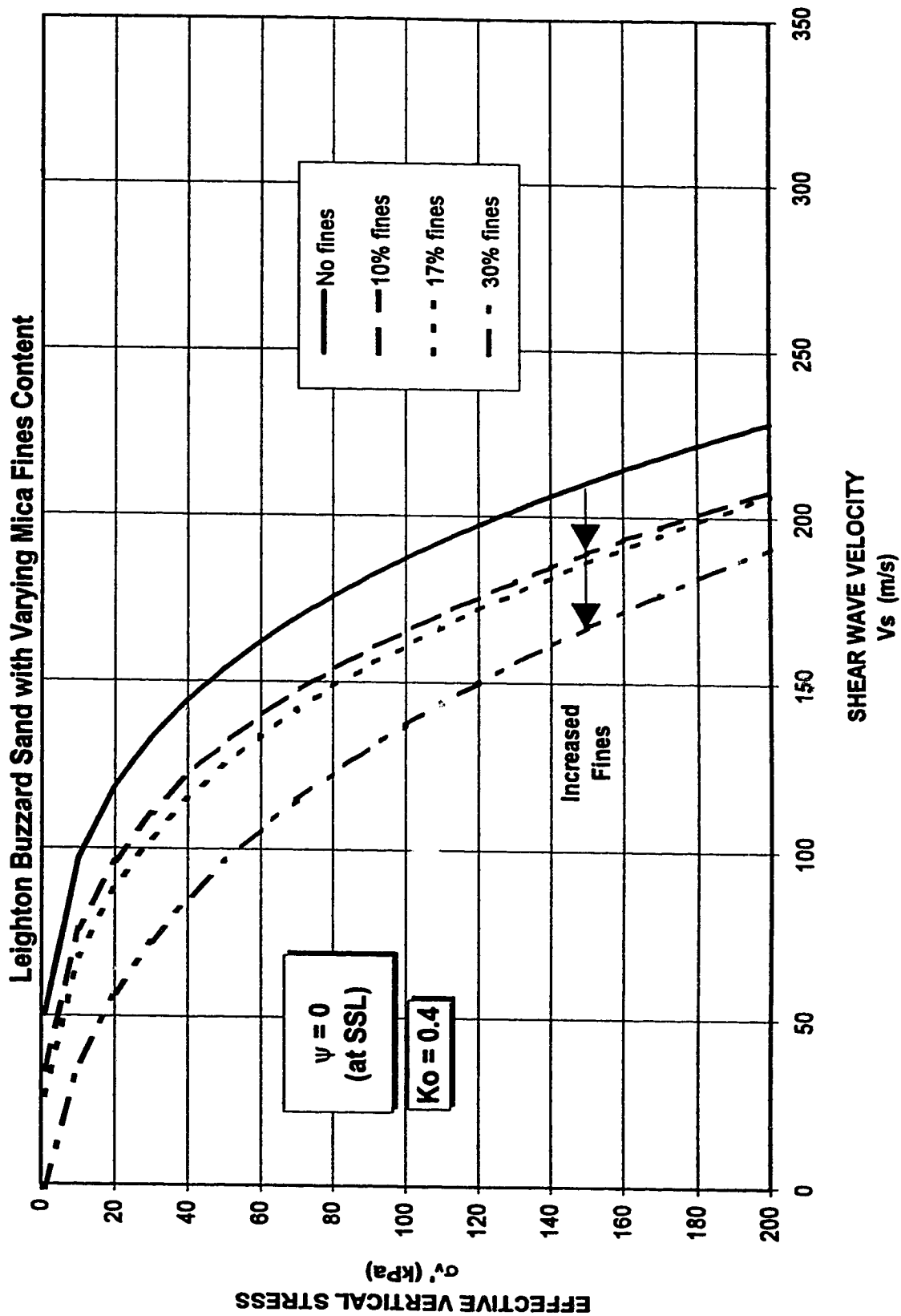
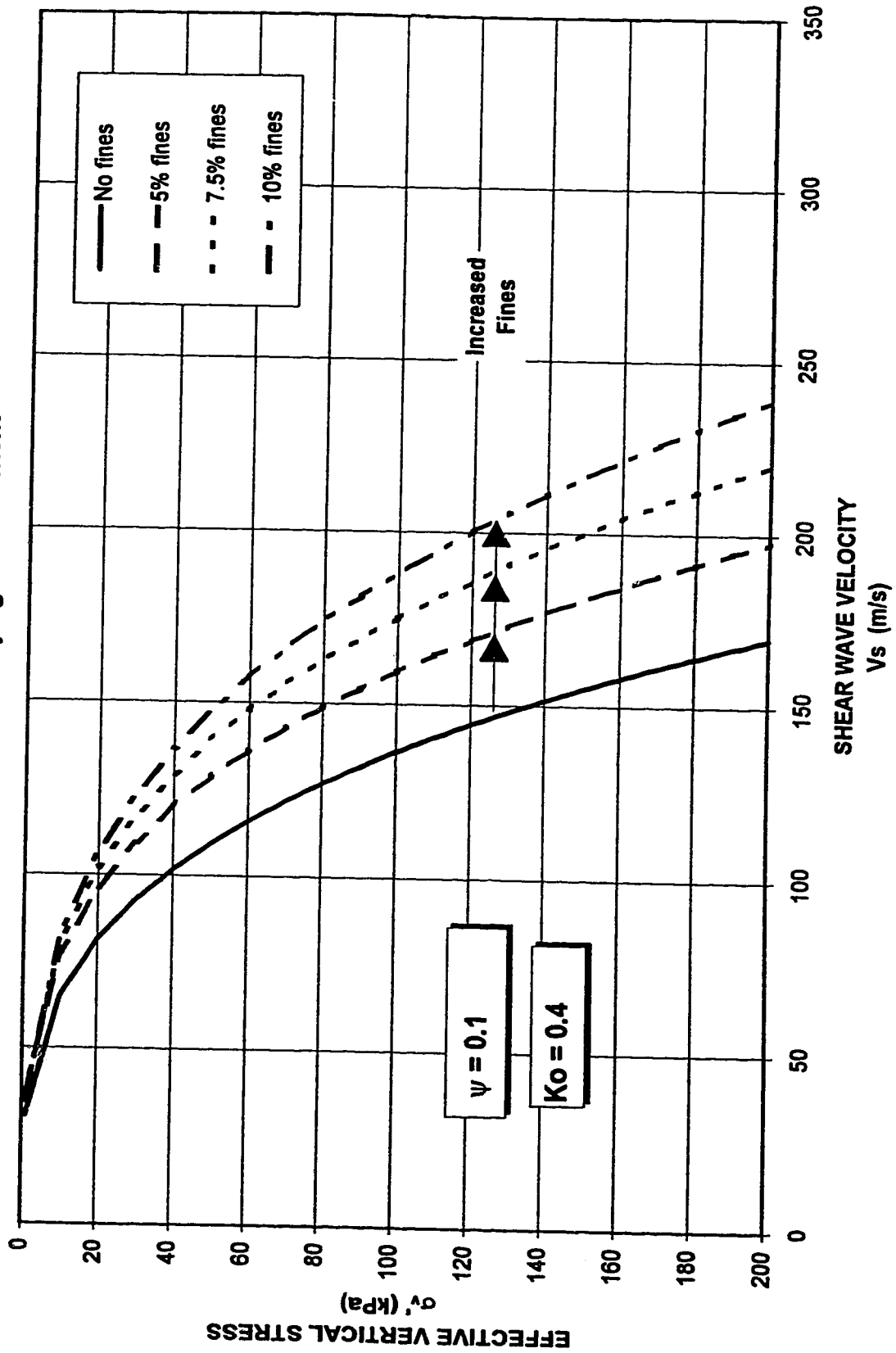
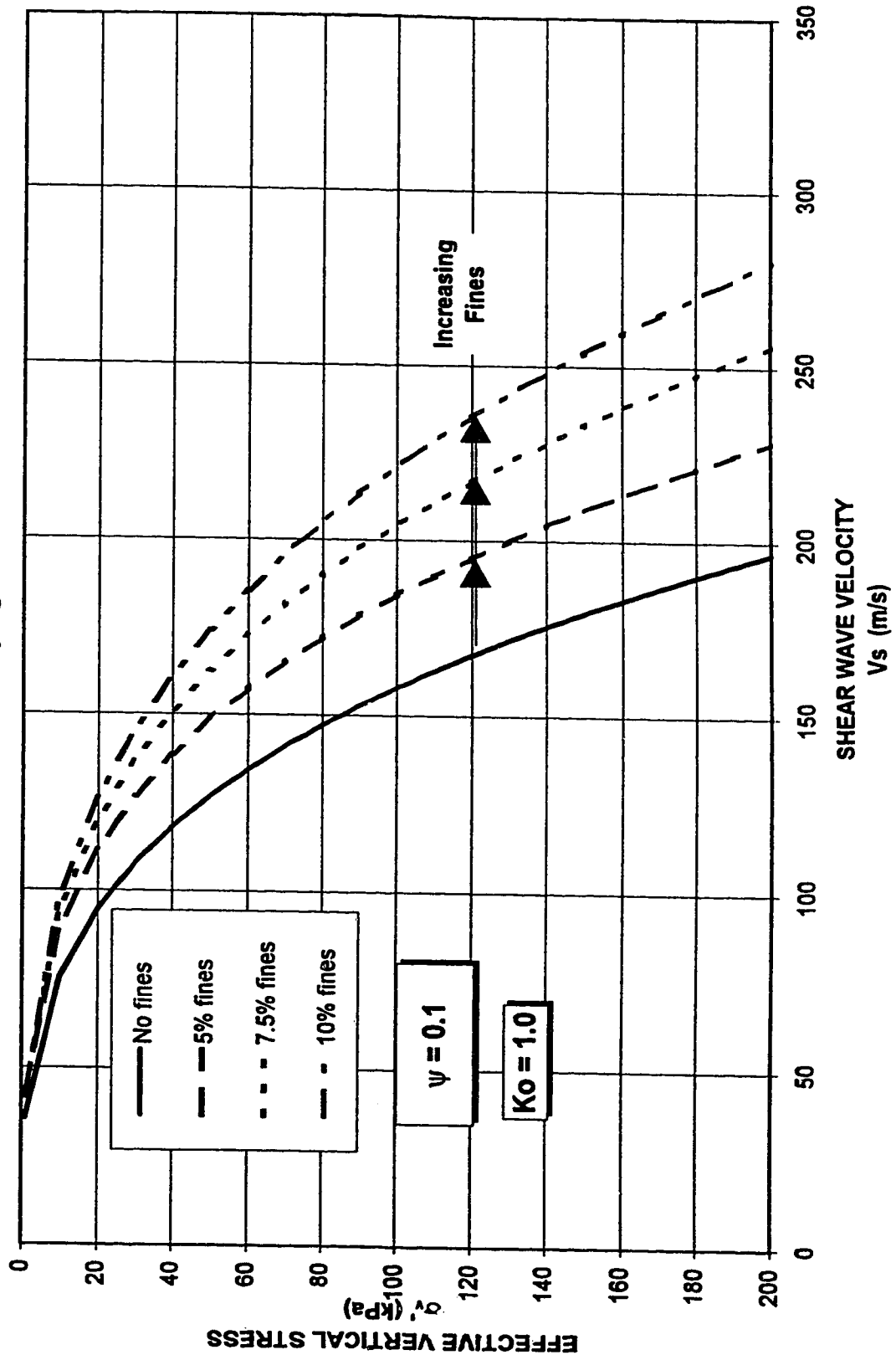


FIGURE 5.33 SHEAR WAVE VELOCITY versus EFFECTIVE VERTICAL STRESS
Ottawa Sand with Varying Fines Content



**FIGURE 5.34 SHEAR WAVE VELOCITY versus
EFFECTIVE VERTICAL STRESS
Ottawa Sand with Varying Fines Content**



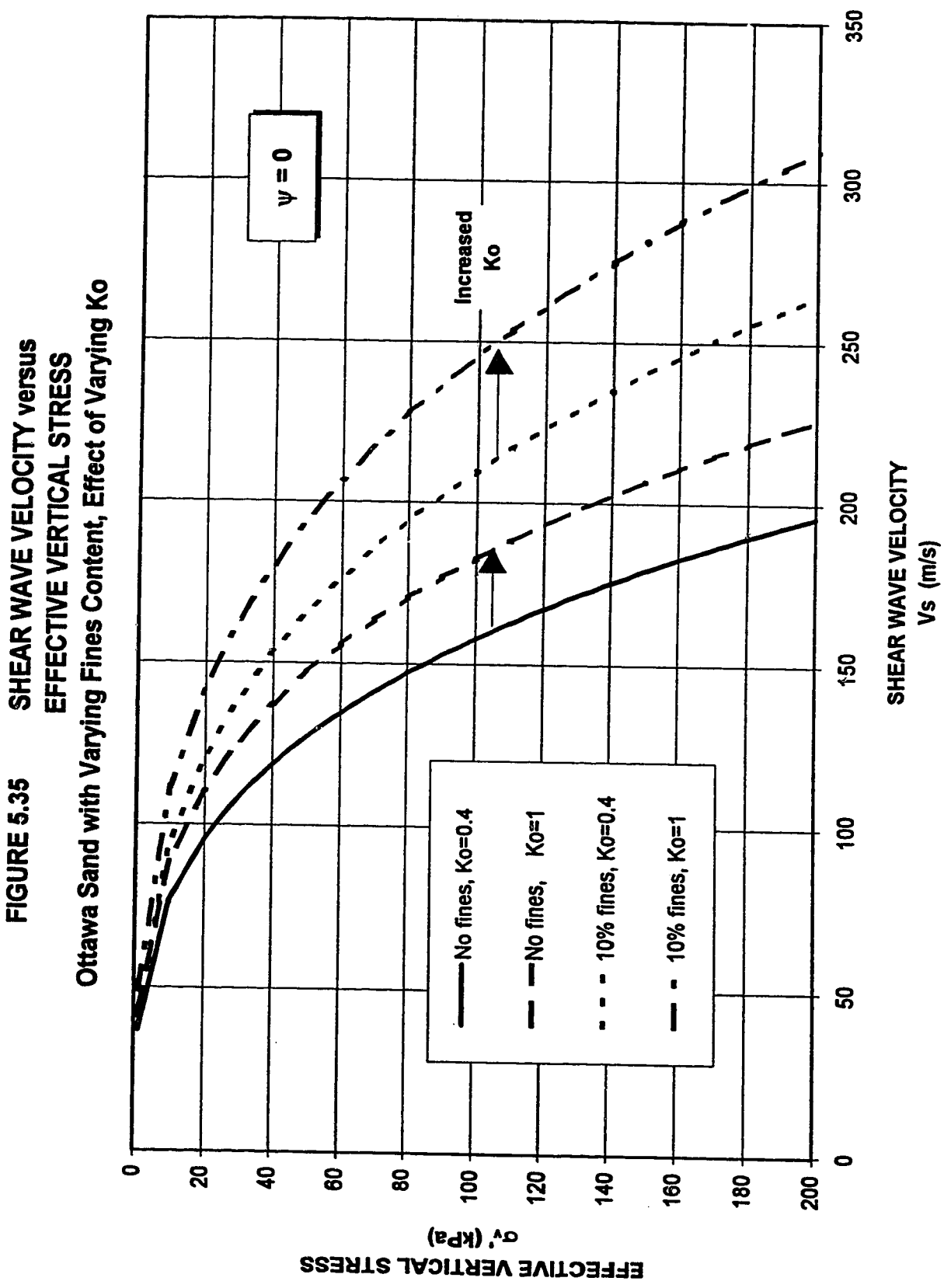


FIGURE 5.36 SHEAR WAVE VELOCITY versus EFFECTIVE VERTICAL STRESS
Ottawa Sand with Varying Fines Content, Effect of Varying K_0

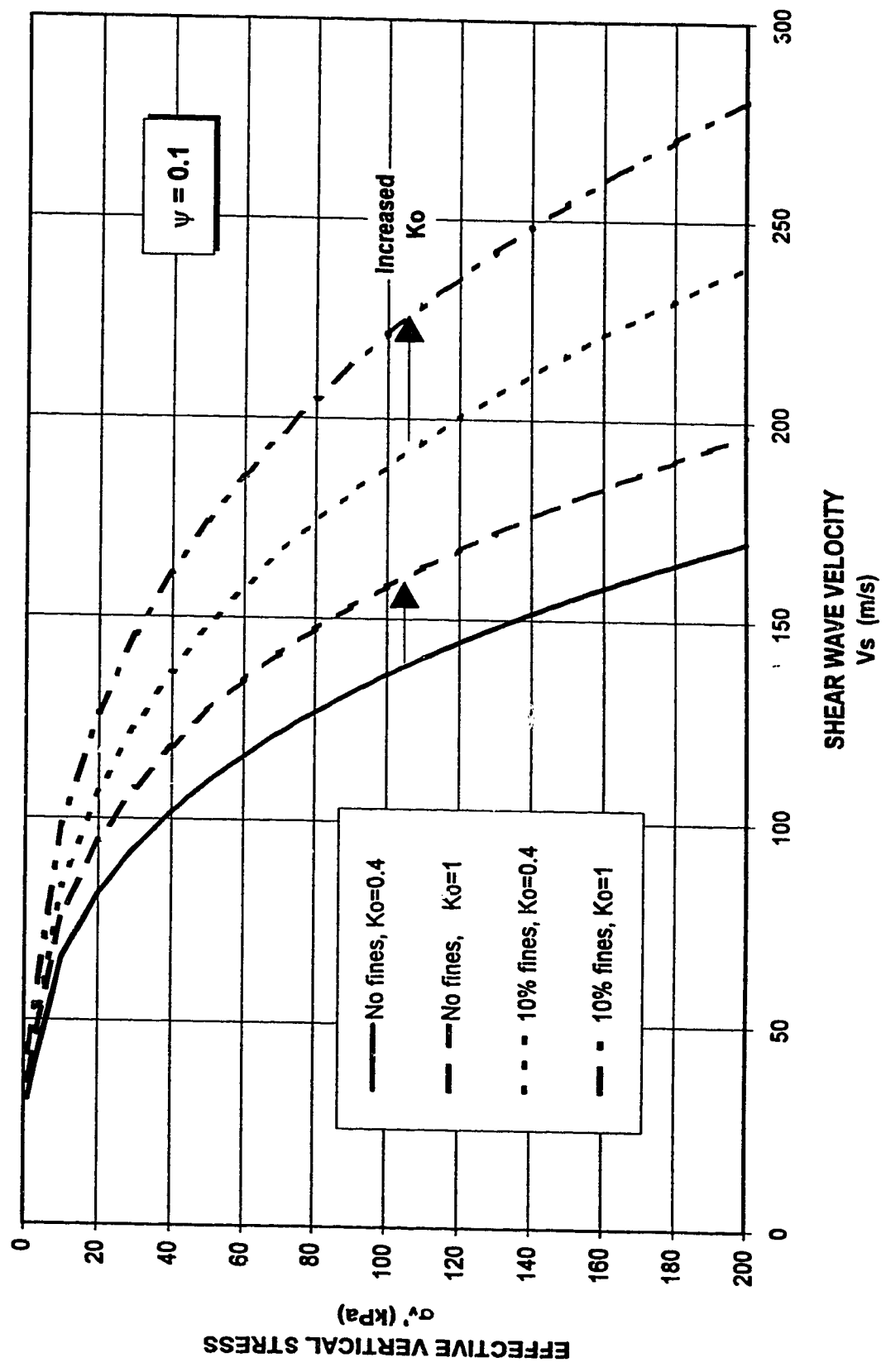


FIGURE 5.37 SPT N(60) versus EFFECTIVE VERTICAL STRESS
Ottawa Sand with Varying Kaolinite Content

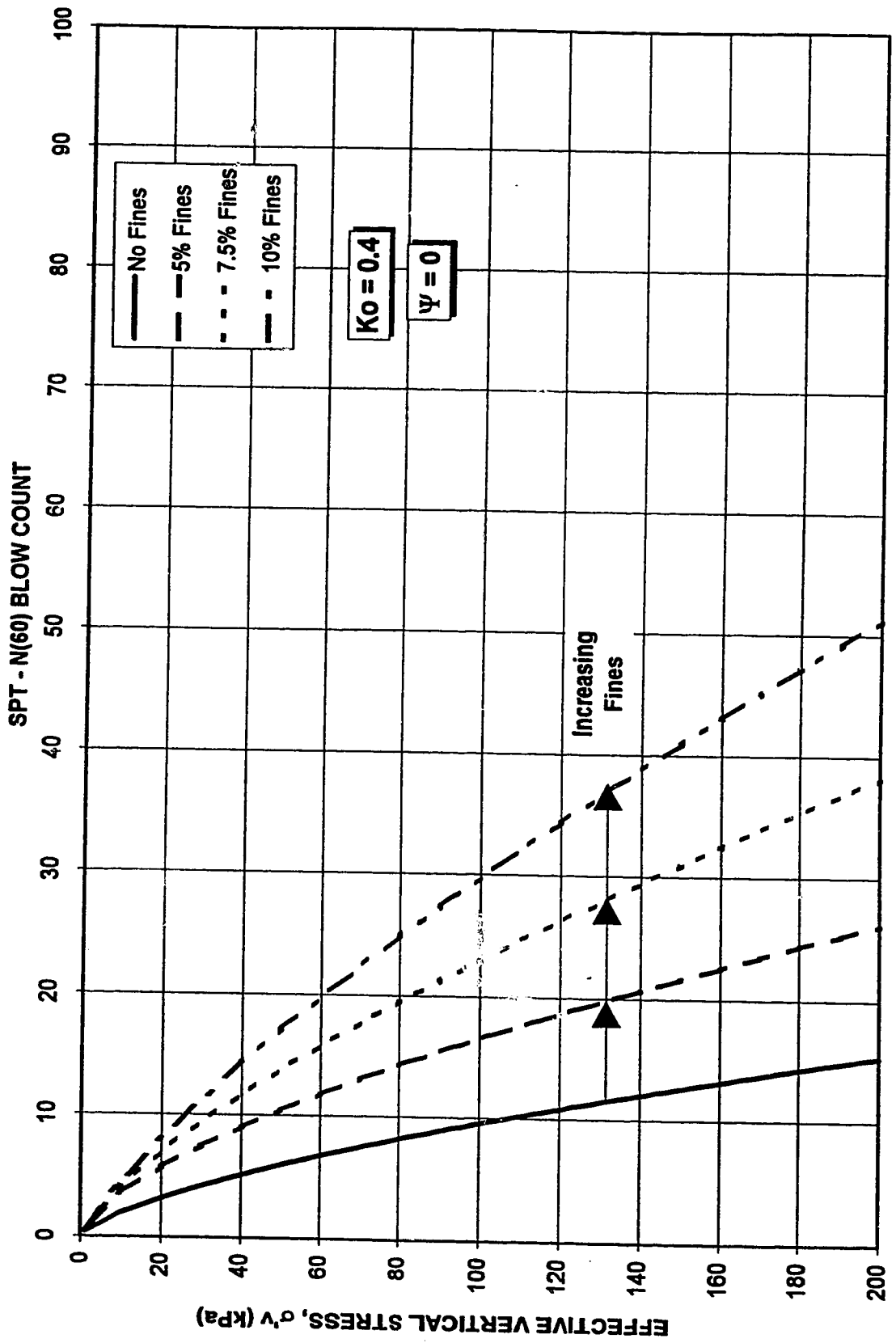


FIGURE 5.38 SPT N(60) versus EFFECTIVE VERTICAL STRESS
Leighton Buzzard Sand with Varying Mica Content

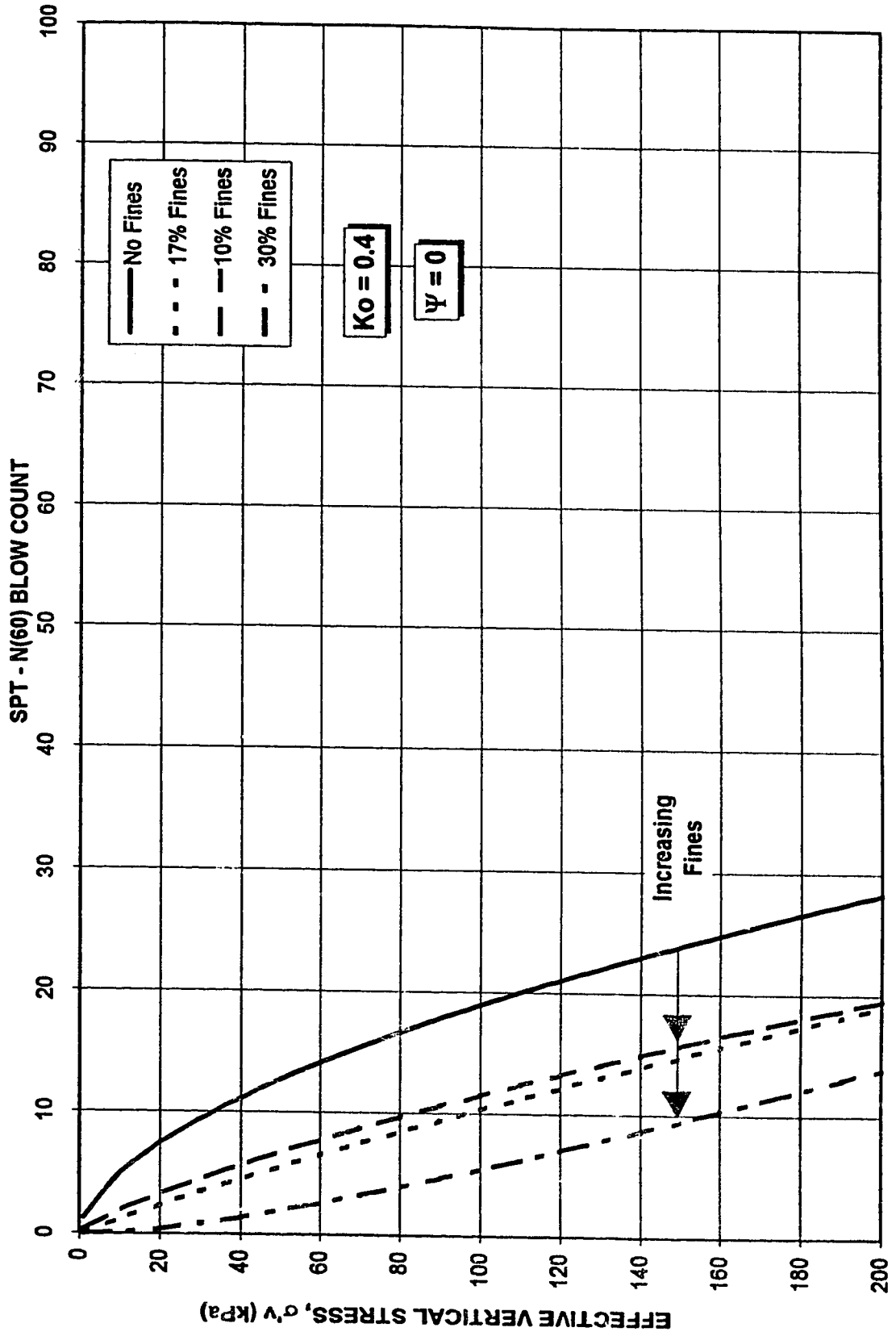


FIGURE 5.39 SPT N(60) versus VERTICAL EFFECTIVE STRESS
Ottawa Sand with Varying Kaolinite Content

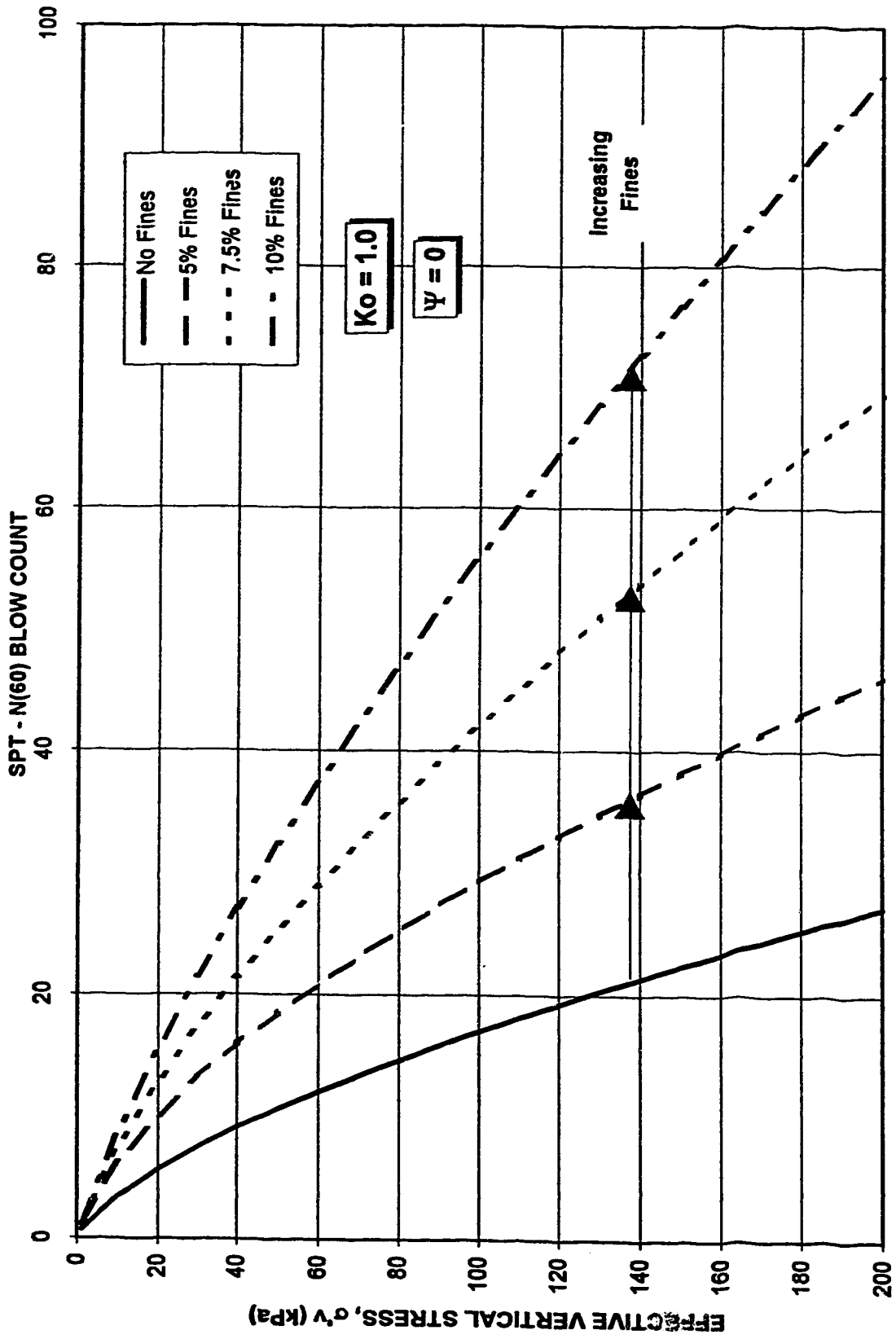
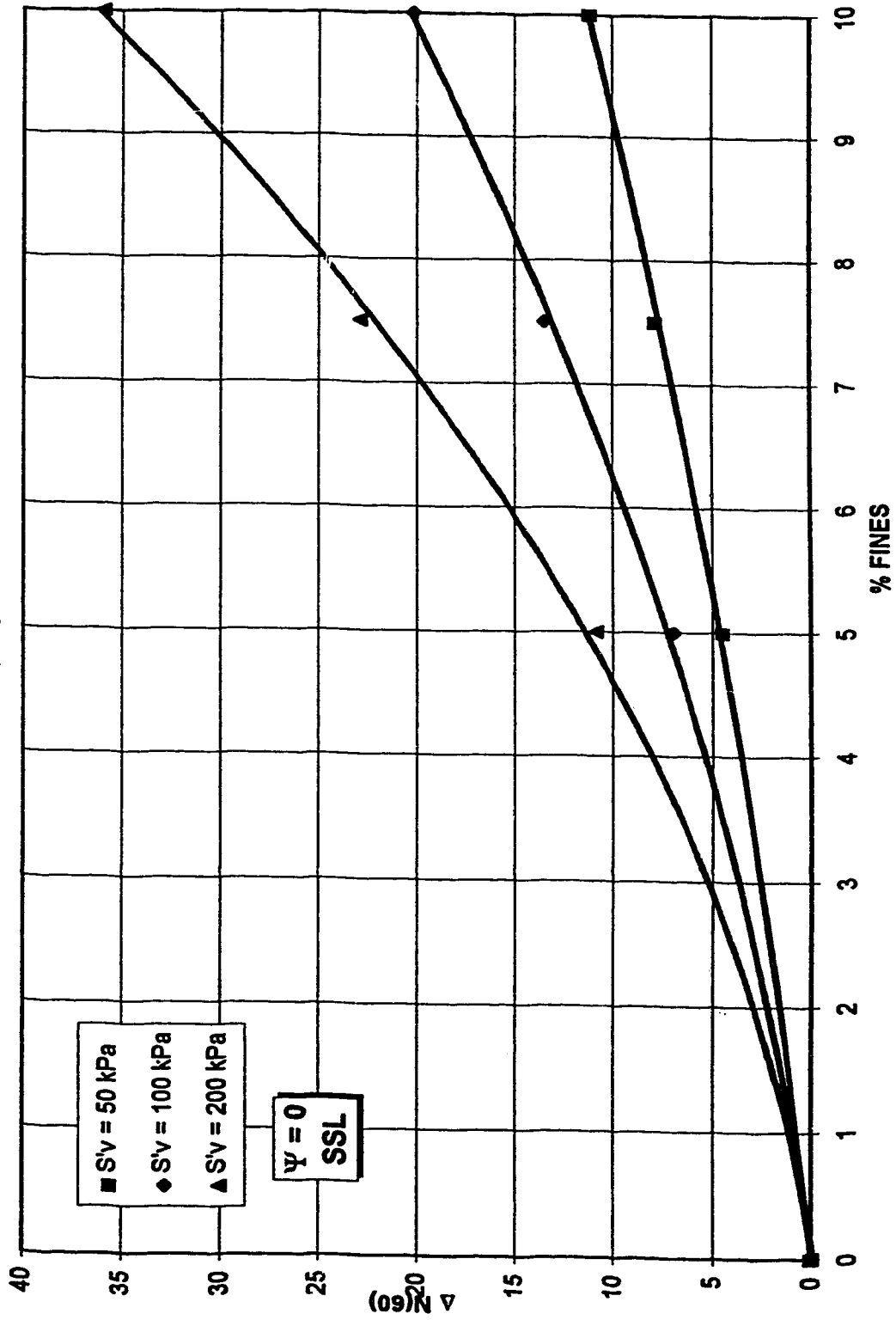


FIGURE 5.40 CHANGE IN SPT N(60) versus % FINES CONTENT
 Ottawa Sand with Varying Kaolinite Fines



**FIGURE 5.41 CPT q_c versus EFFECTIVE VERTICAL STRESS
Ottawa Sand with Varying Kaolinite Fines Content**

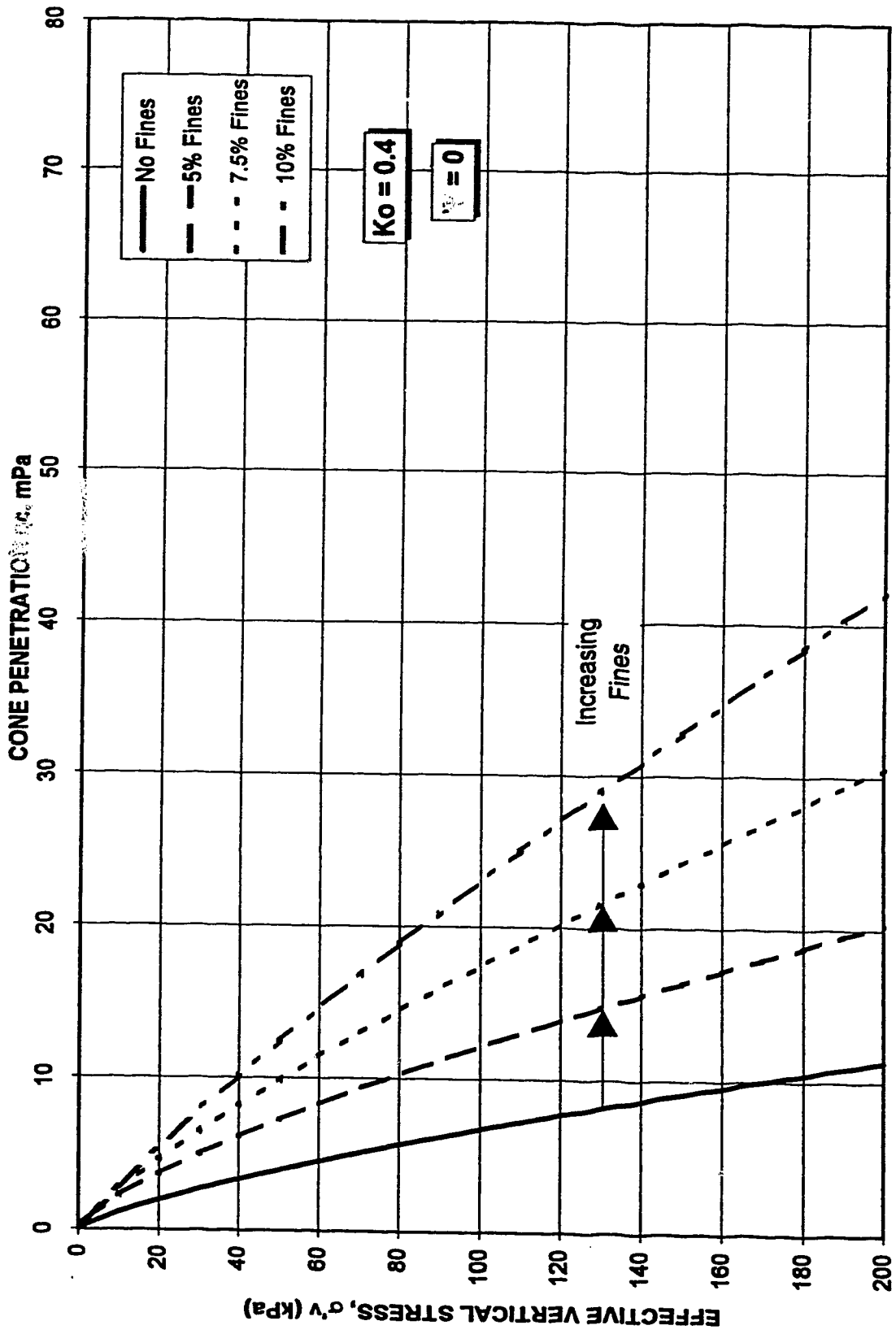


FIGURE 5.42 CPT q_c versus EFFECTIVE VERTICAL STRESS
Leighton Buzzard Sand with Varying Mica Fines Content

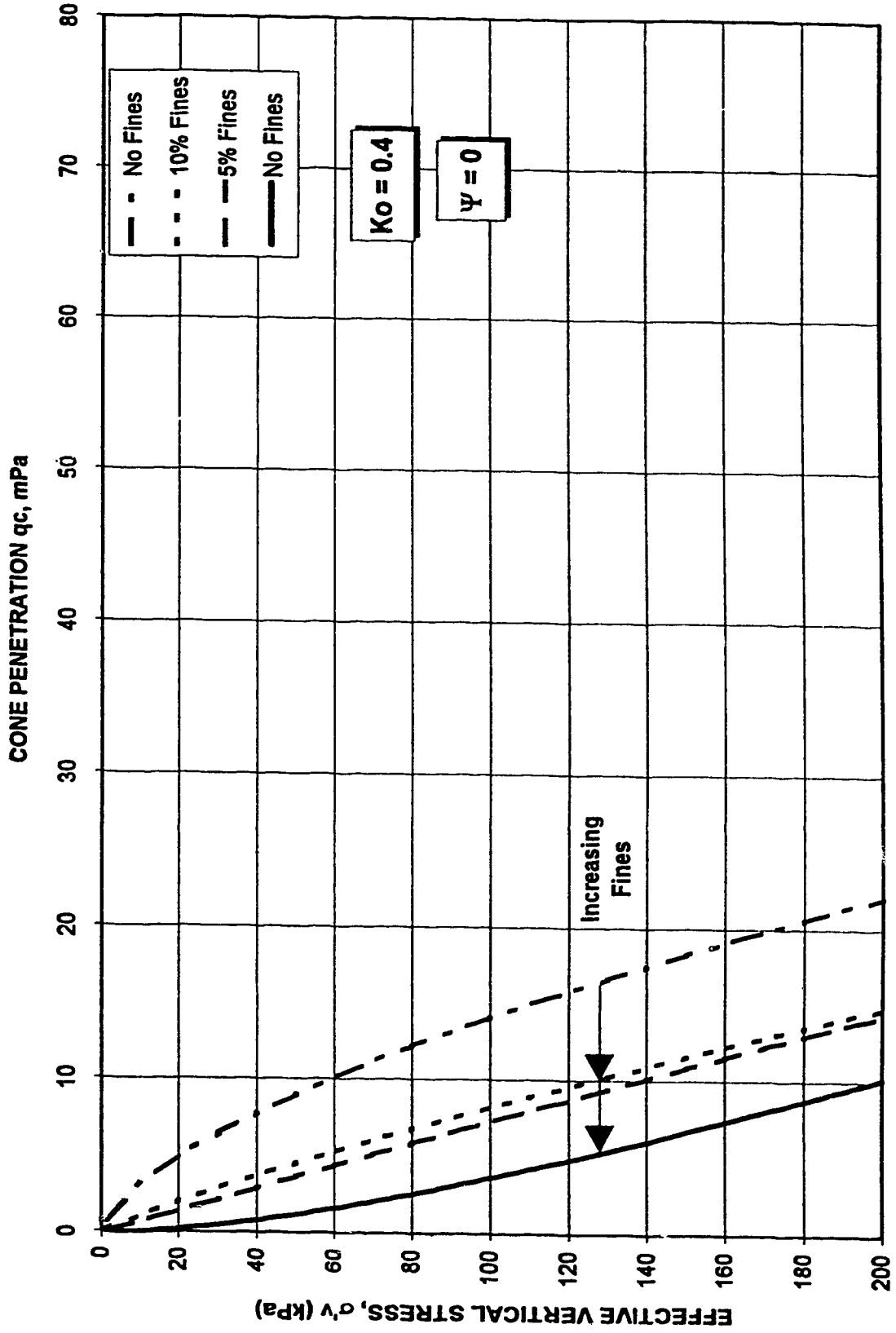


FIGURE 5.43 CPT qc versus EFFECTIVE VERTICAL STRESS
Ottawa Sand with Varying Kaolinifite Content

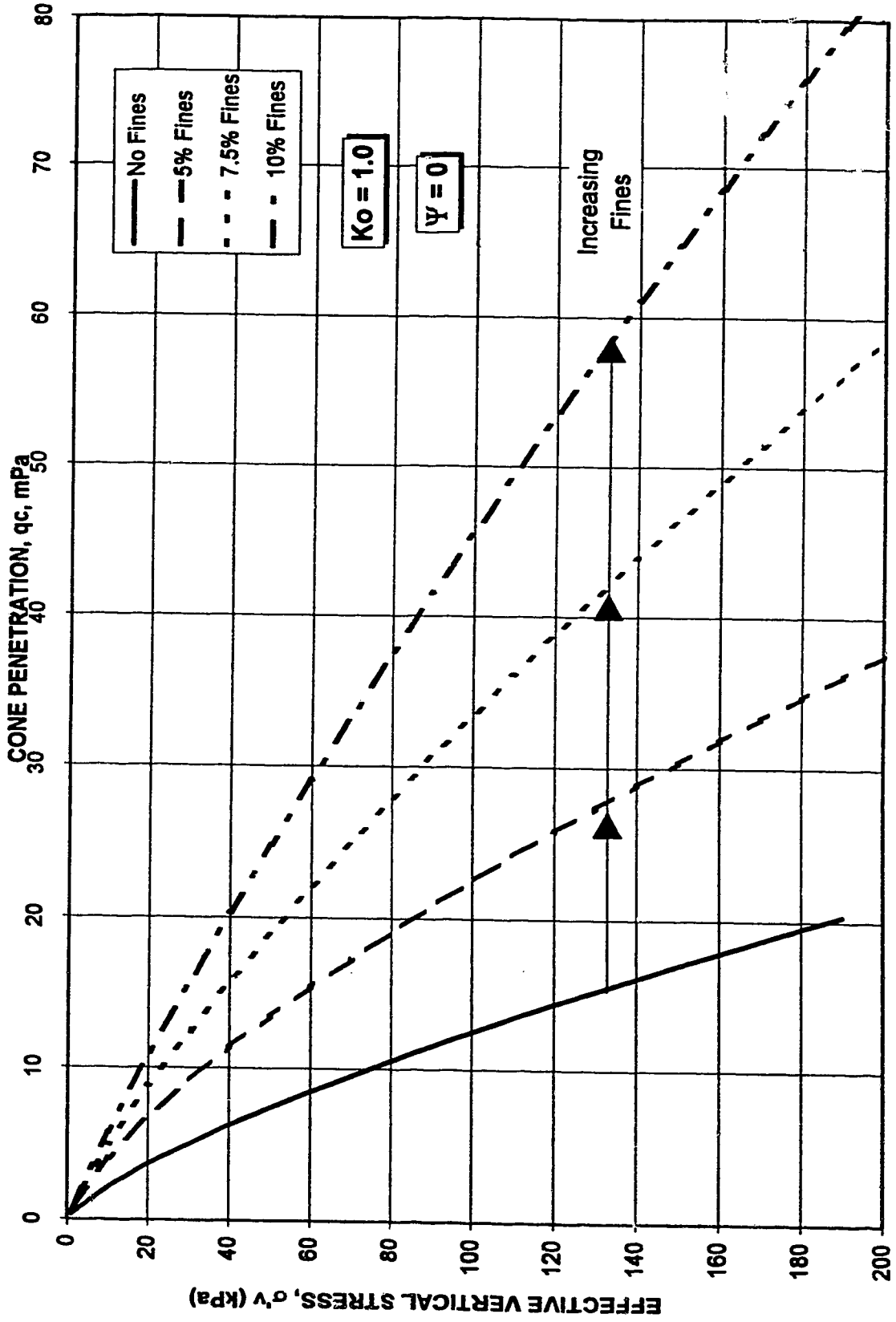
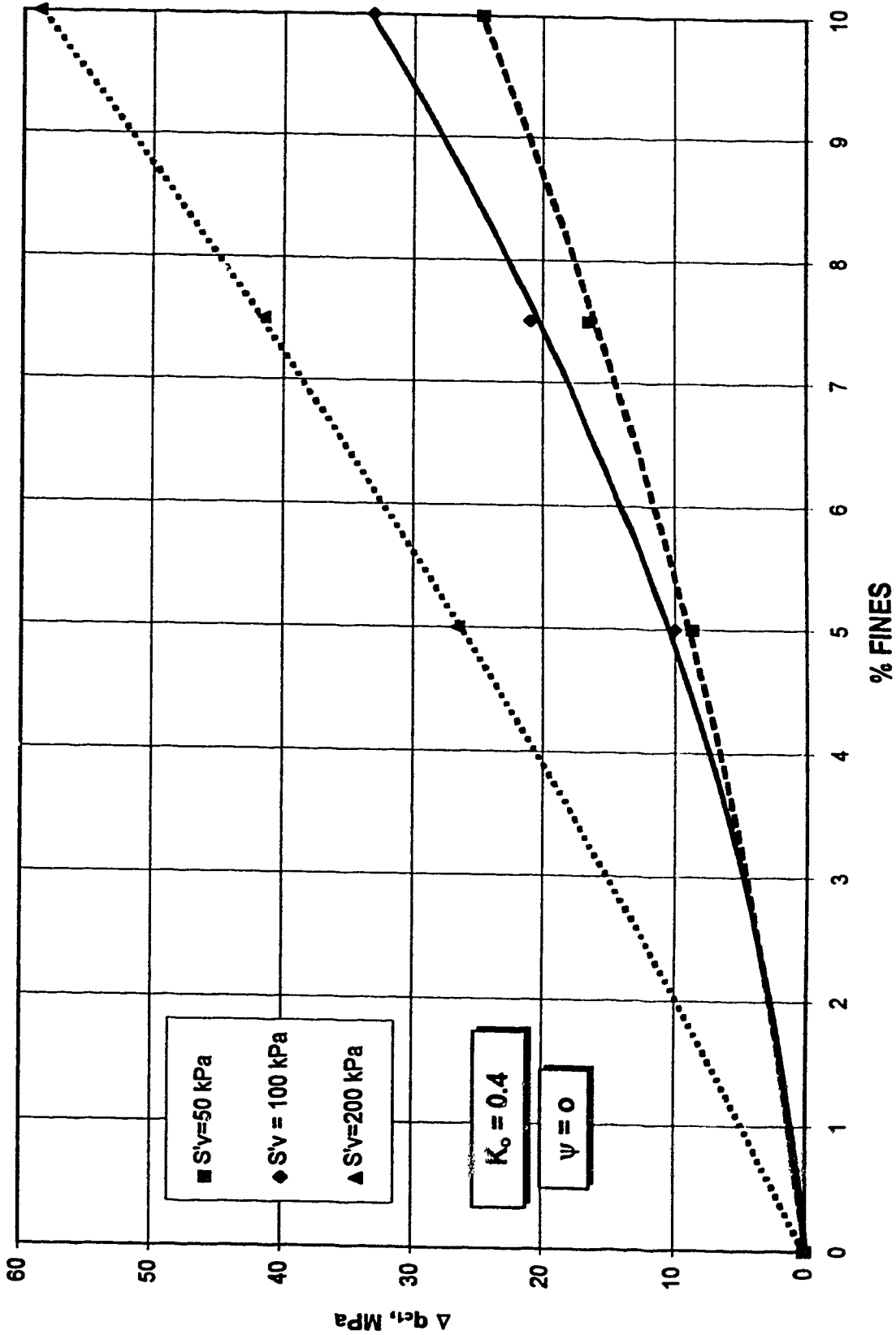


FIGURE 5.44 CHANGE IN CPT q_{c1} versus FINES CONTENT
Ottawa Sand with Varying Fines Content



6. SUMMARY AND CONCLUSIONS

6.1 Undrained Monotonic Triaxial Compression Tests

Monotonic undrained triaxial compression tests were undertaken on samples of Ottawa sand mixed with varying amounts of Kaolinite fines. Samples at each level of fines content were isotropically consolidated to varying initial mean effective stress prior to shearing. Prior work by Pitman (1993) provided data on monotonic undrained triaxial testing at several levels of fines content, but at only one confining pressure.

Protruding bender elements were incorporated into the triaxial test apparatus to facilitate measurement of shear wave velocities. Shear wave velocities were measured during the consolidation phase of the triaxial test on six samples, consisting of loose and dense samples at three levels of fines content. Prior work by Sasitharan (1994) and Cuning (1994) provided data for shear wave velocity measurements at 0% fines.

The results of the triaxial tests on reconstituted samples of Ottawa sand and Kaolinite were used to develop a framework for the evaluation or estimation of in-situ state. The SSL's at 0, 5, 7.5, 10 and 20% fines were found to rotate and shift position. The SSL steepened as fines content was increased. It was anticipated that the SSL would approach that of pure Kaolinite at some point above 40% fines content, based on work by Pitman (1993). Been and Jefferies (1985), investigating Kogyuk sand with mica fines, and Hird and Hassona (1990), investigating Leighton Buzzard sand with mica fines, both showed a similar response of the SSL to the presence of added fines. It appears that this rotation is a common feature to the undrained behavior of sands as plastic fines are added.

The slope of the isotropic consolidation (ICL) line for the loosest samples was determined to be not parallel to the SSL. The consolidation line was in all cases steeper than the SSL, with the higher fines content showing a greater deviation in slope angles. The difference between the ICL and the line defining the minimum void ratio attained was used as a measure of potential sample compressibility. Samples with higher fines content showed a greater potential compressibility than lower fines content at low mean effective stress, however, the situation was reversed at higher mean effective stress. The higher the fines content the more difficult it was to make loose samples at high stresses.

The brittleness Index was used describe the severity of the sample collapse. The RSR value could be used as well for this purpose. The I_b was found to decrease as fines content increased indicating the severity of strength loss was less for high fines content samples than for clean sand. The state parameter, ψ , was used to describe the initial state of the sample

relative to the steady state line. The envelope described by plotting the difference between the e_{min} and the SSL and the e_{max} line to the SSL describes the possible state of a given sand with a given fines content. This envelope was found to be widest at high fines content and low mean effective stress, but also narrowed the quickest for higher fines content. This is also a confirmation of the difficulty in making very loose samples of high fines content samples at high mean effective stress levels. The relative position of normalized $p' - q$ curves at comparable ψ values clearly shows the reduction in collapse severity as fines content is increased.

The brittleness index was found to increase as the state parameter increase. In addition the higher the fines content, the higher the state parameter for a given I_B value. a strain hardening response was observed for all dense samples. For samples prepared at ψ values less than about -0.4 the value of s_v/p'_o were in excess of 1, indicative of strain hardening conditions.

6.2 Shear Wave Velocity Relationships

The measured shear wave arrival times were used to calculate shear wave velocities. Some experience is required to interpret the arrival time of the "s" wave, the paper by Brignoli (1994) is useful in this regard. With the accumulation of V_s , e and p' data it is possible to develop relationships to plot contours of constant shear wave velocity on void ratio - mean effective stress charts. A plot of shear wave results from several researchers was developed, including highly compressible sand, angular sands, sands with calcareous inclusions, and incompressible sands with varying fines content. A single equation was used to show the $V_s - e$ relationship for these sand with reasonable accuracy, ± 30 m/s at a given e .

Contractive/dilative boundaries may be produced in effective vertical stress - V_s , SPT and CPT space. For all cases the location of the contractive boundary was noted to shift to the right as fines content was increased. The shift in the contractive boundary of the SPT and CPT samples implies that the interpretation of N_{60} or q_u data must account for the presence of fines.

6.3 Practical Application

The methodology used in this study to determine the state parameters and shear wave velocity relationships may be used by practitioners to predict the behavior of cohesionless soils subjected to drained or undrained loading. The suggested interaction between field characterizations and in-situ response as predicted by laboratory testing was shown through the development of steady state lines for Ottawa sand and the coupling of these lines to field behavior through the use of shear wave velocity measurements.

A typical liquefaction assessment may involve the following stages:

- (1) In-situ measurements of shear wave velocity using SASW or SCPT means, in addition to conventional SPT or CPT profiling. Pressuremeter and geophysical means may also be incorporated if better estimates of the in-situ state are required.**
- (2) Sampling of in-situ soils for laboratory testing. Frozen core undisturbed sampling techniques or bulk disturbed sampling may be undertaken depending on the nature, scope and available budget.**
- (3) Undertake sieve analysis to determine the distribution of fines content throughout the profile of the deposit.**
- (3) Determination of the steady state conditions using drained or undrained triaxial testing of reconstituted samples or thawed undisturbed samples. Addition of fines to reconstituted samples should be undertaken to match the range of fines content determined for the deposit.**
- (4) The shear wave velocity - void ratio relationship presented in Equation 5.17 may be used as a preliminary guideline to estimate the boundary between contractive and dilatant response in $V_s - \sigma'_v$ space. If a greater level of detail is required, or the soil is of an unusual nature, shear wave measurements should be taken during the triaxial testing, and a site and soil specific, unique $V_s - e$ relationship determined.**
- (5) The $V_s - \sigma'_v$ relationship may then be converted to a CPT or SPT basis. Plotting of the field CPT and SPT values on a CPT "qc" - σ'_v or SPT "N" - σ'_v curve readily shows whether the soil, under the in-situ conditions, has a contractive response and presents a liquefaction concern.**
- (6) The stability of earthworks may then be assessed using steady state undrained shear strength values as determined using Equation 5.10. Depending on type of earthworks involved, the issue of whether the soil is liquefiable or not may not be of prime concern. A parametric risk assessment of the stability would likely require evaluation of the stability under liquefaction conditions, regardless of however improbable these conditions might be.**

The application of the above methodology is considered applicable to a wide range of sand fabric ranging from angular to well rounded, very loose to tightly packed cohesionless sands with fines content up to at least 20%. Application of the above methodology to aged, cemented sands should be undertaken using steady state parameters determined from undisturbed samples only, and should be undertaken with due caution. The $V_s - e$ relationship

appears to be applicable within a void range of about 0.5 to 1.5, however Reilly (1995) and others have shown the $V_s - e$ relationship to be exponential if higher void ratio results are to be interpreted.

6.4 Further Study

Additional research into the behavior of silty sands at fines content in excess of 20% and at fines content less than 5% would provide a more complete picture of the undrained response. Further refinement in the bender element methodology, such as that pursued by Cunning (1994), and use of bender elements on retrieved samples with improved correlation to field shear wave measurements, either from SCPT, SASW or other means will provide a useful means of assessing in-situ state and in the prediction of the undrained behavior of in-situ soils, such as pursued by Reilly (1995).

The cost of a liquefaction assessment based on present techniques is substantial, particularly if undisturbed frozen core sampling is carried out, and is only justified if there is a significant risk to people or property associated with potential liquefaction failures. Until the cost of such detailed investigations drops significantly, the current practice, using charts for liquefaction potential developed based on case histories, will likely continue to be used for smaller projects and where there is a strong historical success and confidence with site specific conditions. Further investigations using shear wave velocity measurements and steady state testing will no doubt be incorporated into the empirical database, further refining the charts already in use.

There continues to be a great deal of research on shear wave velocity measurement related to soil response. The methods by which SCPT and SASW techniques can be applied to evaluate in-situ state are reasonably well defined, and these field methods will likely become even more widely used and accepted for site characterization.

The application of steady state testing should be extended to aged and cemented sands. The loading response of tailings sand, ash, coke and other such deposits is expected to be affected by the degree of aging and cementation.

REFERENCES

- Alarcon-Guzman, A., Leonards, G. A., and Chameau, J. L. 1988. Undrained monotonic and cyclic strength of sands. *Journal of Geotechnical Engineering, American Society of Civil Engineering*, 114(10): 1089-1109
- Arthur, J. R. F., and Menzies, B. K. 1972. Inherent anisotropy in a sand. *Geotechnique*, 22(1): 115-128
- Atkinson, J. H., Richardson, D., and Robinson, P. J. 1987. Compression and extension of Ko normally consolidated Kaolin clay. *Journal of Geotechnical Engineering, American Society of Civil Engineering*, 113(2): 1468-1481
- Bardet, J. P., and Kapuskar, M. 1993. Liquefaction sand boils in San Francisco during 1989 Loma Prieta earthquake. *Journal of Geotechnical Engineering, American Society of Civil Engineering*, 119(3): 543-562
- Bates, C. P. 1989. Dynamic soil property measurements during triaxial testing. *Geotechnique*, 39(4): 721-726
- Been, K., and Jefferies, M. G. 1985. A state parameter for sands. *Geotechnique*, 35(2): 99-112
- Been, K., Jefferies, M. G., and Hachey, J. 1991. The critical state of sand. *Geotechnique*, 41(3): 365-381
- Brignoli, G. M., Gotti, M., and Stokoe, K. H. 1994. Measurement of shear waves in laboratory specimens by means of piezoelectric transducers. Preprint copy
- Castro, G. 1975. Liquefaction and cyclic mobility of saturated sands. *Geotechnical Engineering Division, American Society of Civil Engineering*, 101(GT6): 551-569
- Chapuis, R. P. 1981. Discussion on the steady state of deformation. *Geotechnical Engineering Division, American Society of Civil Engineering*, 107(GT8): 1085-1091
- Cunning, J.C.. 1994. Shear wave velocity measurements of cohesionless soils for evaluation of state. M.Sc. Thesis, University of Alberta, Edmonton, Alberta
- De Alba, D. A., Seed, H. B., Retamal, E., and Seed, R. B. 1988. Analysis of dam failures in 1985 Chilean earthquake. *Journal of Geotechnical Engineering, American Society of Civil Engineering*, 114(12): 1414-1434
- DeGregorio, V. B. 1990. Loading systems, sample preparation, and liquefaction. *Journal of Geotechnical Engineering, American Society of Civil Engineering*, 116(5): 805-821
- De Matos, M. 1988. Mobility of soil and rock avalanches. Ph.D. Thesis, Department of Civil Engineering, University of Alberta, Alberta
- Dobry, R., and Alvarez, L. 1967. Seismic failures of Chilean tailings dams.

- Donovan, N. C. 1968. Analysis of soil liquefaction; Niigata earthquake - Discussion Journal of Soil Mechanics and Foundation Division, American Society of Civil Engineering, 92(SM2): 582-583
- Dyvik, R., and Madshus, C. 1985. Lab measurements of Gmax using bender elements. Proceedings, Advances in the Art of Testing Soils under Cyclic Conditions, American Society of Civil Engineering Annual Convention, Detroit Michigan, October 1985: 186-196
- Eckersly, D. 1990. Instrumented laboratory flow slides. Geotechnique, 40(3): 489-502
- Georgiannou, V.N. 1988. Behavior of clayey sands under monotonic and cyclic loading. Ph.D. Thesis, Department of Civil Engineering, Imperial College of Science, Technology and Medicine, London, England
- Gu, W. H., Morgenstern, N. R., and Robertson, P. K. 1993. Progressive failure of lower San Fernando Dam. Journal of Geotechnical Engineering, American Society of Civil Engineering, 119(2): 333 - 349
- Hamilton, E.L. 1976 Shear wave velocity versus depth in marine sediments---a review. Geophysics, 41: 985
- Hardin, B. O. And Dmievich, V. P. 1972. Shear modulus and damping in soils; measurement and parameter effects. Journal of Soil Mechanics and Foundation Division, American Society of Civil Engineering, 98(SM6): 603-624
- Hardin, B.O., and Richart, F.E. Jr. 1963. Elastic wave velocities in granular soils. American Society of Civil Engineering, Journal of Soil Mechanics and Foundation Division, 89(SM1): 33-65
- Hird, C. C., and Hassona, F. A. K. 1990. Some factors affecting the liquefaction flow of saturated sands in laboratory tests. Engineering Geology, 28: 149-170
- Hom, I.W. 1980. Some laboratory experiments on shear wave propagation in unconsolidated sands. Marine Geotechnology, 4(1): 31-54
- Idriss, I.M. and Seed, H.B. 1967. Response to earth banks during earthquakes, American Society of Civil Engineers, Journal of the Soil Mechanics and Foundation Division, 93(SM3): 61-82
- Ishihara, K. 1993. Liquefaction and flow failure during earthquakes. Geotechnique, 43(3): 355-415
- Ishihara, K., Troncoso, J., Kawase, Y. And Takahashi, Y. 1980. Cyclic strength characteristics of tailings materials. American Society of Civil Engineering, Journal of Geotechnical Engineering Division, 116(6): 932-947
- Ishihara, K., Verdugo, R., and Acacio, A.A. 1991. Characterization of cyclic behavior of sand and post seismic stability analysis. Proceeding of the Asian Regional Conference on Soil Mechanics and Foundation Engineering. Bangkok, Thailand, 2: 45-68
- Jefferies, M. G. 1993. Nor-Sand: a simple critical state model for sand. Geotechnique, 43(1): 91-103

- Kallstenius, T., and Bergau, W. 1961. Research on the texture of granular masses. Proceedings of 5th International Conference on Soil Mechanics and Foundation Engineering. 1: 165-170
- Konrad, J. M. 1990. Minimum undrained strength versus steady state strength of sands. Journal of Geotechnical Engineering, American Society of Civil Engineering, 116(6): 948-963
- Kuerbis, R.H. 1989. The effect of gradation and fines content on the undrained loading response of sand. M.Sc. Thesis. Department of Civil Engineering, University of British Columbia, Vancouver, British Columbia
- Kuerbis, R., and Vaid, Y. P. 1988. Sand sample preparation - the slurry deposition method. Soils and Foundation, Japanese Society of Soil Mechanics and Foundation Engineering, 28(4): 107-118
- Leps, T. M. 1968. Seismic failures of Chilean tailings dam - discussion. Journal of Soil Mechanics and Foundation Division, American Society of Civil Engineering, 94(SM3): 809-810
- Luo, D., MacLeod, J. E. S., Leng, X., and Smart, P. 1992. Automatic orientation analysis of particles of soil microstructures. Geotechnique, 42(1): 97-107
- Martin, G. R., Finn, W. D. L., and Seed, H. B. 1975. Fundamentals of liquefaction under cyclic loading. Geotechnical Engineering Division, American Society of Civil Engineering, 101(GT5): 423-438
- McGown, A., Marsland, A., Radwin, A. M., and Gabr, A. W. A. 1980. Recording and interpreting soil macrofabric data. Geotechnique, 30(4): 417-447
- Mulilis, J. D., Seed, H. B., Chan, C. K., Mitchell, J. K., and Arulanandan, K. 1977. Effects of sample preparation on sand liquefaction. Geotechnical Engineering Division, American Society of Civil Engineering, 103(GT2): 91-108
- Ng, T., and Dobry, R. 1994. Numerical simulations of monotonic and cyclic loading of granular soil. Journal of Geotechnical Engineering, American Society of Civil Engineering, 120(2): 388-403
- Oda, M. 1972. The mechanism of fabric changes during compressional deformation of sand. Soils and Foundation, Japanese Society of Soil Mechanics and Foundation Engineering, 12(2): 1-18
- Oda, M. 1981. Anisotropic strength of cohesionless sands. Geotechnical Engineering Division, American Society of Civil Engineering, 107(GT9): 1219-1230
- Pastor, M. 1991. Modeling of anisotropic sand behavior. Computers and Geotechnics, 11, 173-208
- Pitman, T. 1993. Effects of fines on collapse surface of loose sands. M.Sc. Thesis, University of Alberta, Edmonton, Alberta
- Poulos, S. J. 1981. The steady state of deformation Geotechnical Engineering Division, American Society of Civil Engineering, 107(GT5): 553-561

- Reilly, S.T. 1995. Flow liquefaction analysis of a slope failure in coal ash tailings. M.Sc. Thesis, University of Alberta, Edmonton, Alberta
- Robertson, P. K., Campanile, R. G., Gillespie, D., and Rice, A. 1986. Seismic CPT to measure in situ shear wave velocity. *Journal of Geotechnical Engineering, American Society of Civil Engineering*, 112(8): 791-803
- Robertson, P. K., Woeller, D. J., and Finn, E. D. L. 1992¹. Seismic cone penetration test for evaluating liquefaction potential under cyclic loading. *Canadian Geotechnical Journal*, 29(4): 686-695
- Robertson, P.K., Woeller, D.J., Kokan, M., Hunter, J., and Lutemauer, J. 1992². Seismic techniques to evaluate liquefaction potential. 45th Canadian Geotechnical Conference, Toronto, Ontario, October 26-28, 1992, 5: 1-9
- Robertson, P. K. 1993. Design considerations for liquefaction. U.S. - Japan Workshop, 1993
- Robertson, P.K. and Skirrow, R.K. 1994. Report on the liquefaction behavior of Hong Kong Chek Lap Kok Airport Replacement Sand.
- Robertson, P.K. and Fear, C. 1995. Liquefaction of sands and its evaluation. First International Conference on Earthquake Engineering, IS Tokyo '95, Japan, Tokyo
- Roesler, S.K. 1979. Anisotropic shear modulus due to stress anisotropy. *American Society of Civil Engineering Journal of Geotechnical Engineering Division*, 105(GT7): 871-880
- Roscoe, K.H., Schofield, A.N. and Wroth, C.P. 1958. On the yielding of soils. *Geotechnique*, 8: 22-53
- Rothenburg, L., Bathurst, R. J., and Matyas, E. L. 1986. Mechanisms of fabric evolution in granular media. XIth International Conference on Soil Mechanics and Foundation Engineering, Rio De Janeiro, 1: 753-756
- Rowe, P. W. 1972. The relevance of soil fabric to site investigation practice. *Geotechnique*, 22(2): 195-300
- Sasitharan, S. 1994. Collapse behavior of very loose sand. M.Sc. Thesis, University of Alberta, Edmonton, Alberta, Canada
- Sasitharan, S., Robertson, P. K., and Segoo, D. C. 1992. Sample disturbance from shear wave velocity measurements. 45th Canadian Geotechnical Conference, Toronto. 23:1-23:7.
- Schultheiss, P.J. 1981. Simultaneous measurement of P & S wave velocities during conventional laboratory soil testing procedures. *Marine Geotechnology*, 4(4): 343-367
- Seed, H.B., Martin, P.P. and Lysmer, J. 1976 Pore pressure changes during soil liquefactions. *Journal of Geotechnical Engineering Division, American Society of Civil Engineering*, 102(4). 323-346
- Seed, H. B., and Silver, M. 1972. Settlement of dry sands during earthquakes. *Geotechnical Engineering Division, American Society of Civil Engineering*, 98(GT2): 207
- Shirley, D.J. 1978. An improved shear wave transducer. *Journal of the Acoustical Society of America*, 63(5): 1643-1645

- Shirley, D.J., and Hampton, L.D. 1978. Shear wave measurements in laboratory sediments. *Journal of the Acoustical Society of America*, 63(2): 607-613
- Sladen, J. A., D'Houander, R. D., and Krahn, J. 1985. The liquefaction of sands, a collapse surface approach. *Canadian Geotechnical Journal*, 22: 564-579
- Sladen, J. A., and Handford, G. 1987. A potential systematic error in laboratory testing of very loose sands. *Canadian Geotechnical Journal*, 24(3): 462-466
- Stokoe II, R.H., and Naxarian, S. 1985. Use of rayleigh waves in liquefaction studies. Measurement and use of shear wave velocity for evaluating dynamic soil properties. Edited by R.D. Woods. *American Society of Civil Engineering*, New York
- Strachan, P. 1981. An investigation of the correlation between geophysical and dynamic properties of sand. *Proceedings, Oceans 1981*: 388-403
- Tokimatsu, K., and Hosaka, Y. 1986. Effects of sample disturbance on dynamic properties of sand. *Soils and Foundation*, Japanese Society of Soil Mechanics and Foundation Engineering, 26(1): 53-64
- Tokimatsu, K., and Uchida, A. 1990. Correlation between liquefaction resistance and shear wave velocity. *Soils and Foundation*, Japanese Society of Soil Mechanics and Foundation Engineering, 30(2): 53-64
- Tokimatsu, K., Yamazaki, T., and Yoshimi, Y. 1986. Soil liquefaction evaluations by elastic shear moduli. *Soils and Foundations*, Japanese Society of Soil Mechanics and Foundation Engineering, 26(1): 25-35
- Vaid, Y.P., and Chern, J.C. 1985. Cyclic and monotonic undrained response of saturated sand. *Advances in the Art of Testing Soils under Cyclic Loading*, American Society of Civil Engineering National Convention, Detroit, Michigan, U.S.A., October 1985: 120-147
- Vaid, Y. P., and Negussey, D. 1984. Relative density of pluviated sand samples. *Soils and Foundation*, Japanese Society of Soil Mechanics and Foundation Engineering, 24(2): 101-105
- Vaid, Y.P., and Negussey, D. 1984. A critical assessment of membrane penetration in the triaxial test. *Geotechnical Testing Journal*, 7(2): 70-76
- Yoshimi, Y., Hatanaka, M., and Oh-oka, H. 1978. Undisturbed sampling of saturated sands by freezing. *Soils and Foundation*, Japanese Society of Soil Mechanics and Foundation Engineering, 18(3): 59-73
- Yoshimi, Y., Tokimatsu, K., and Hosaka, Y. 1989. Evaluation of liquefaction resistance of clean sands based on high quality undisturbed samples. *Soils and Foundation*, Japanese Society of Soil Mechanics and Foundation Engineering, 29(1): 93-104
- Yoshimi, Y., Tokimatsu, K., Kaneko, O., and Makiyara, Y. 1984. Undrained cyclic shear strength of a dense Niigata sand. *Soils and Foundation*, Japanese Society of Soil Mechanics and Foundation Engineering, 24(4): 131-145
- Youd, T.L. 1977. Packing changes and liquefaction susceptibility. *Journal of the Geotechnical Engineering Division*, American Society of Civil Engineering, 103(GT8): 918-923

- Yu, P., and Richart, F.E. Jr. 1984. Stress ratio effects on shear modulus of dry sands. American Society of Civil Engineering, Journal of the Geotechnical Engineering Division, 110(3): 331-345**
- Yudhbir, and Abedinzadeh, R. 1991. Quantification of particle shape and angularity using the image analyzer. Geotechnical Testing Journal, 14(3): 296-30**